The Solar Cell RADIATION HANDBOOK

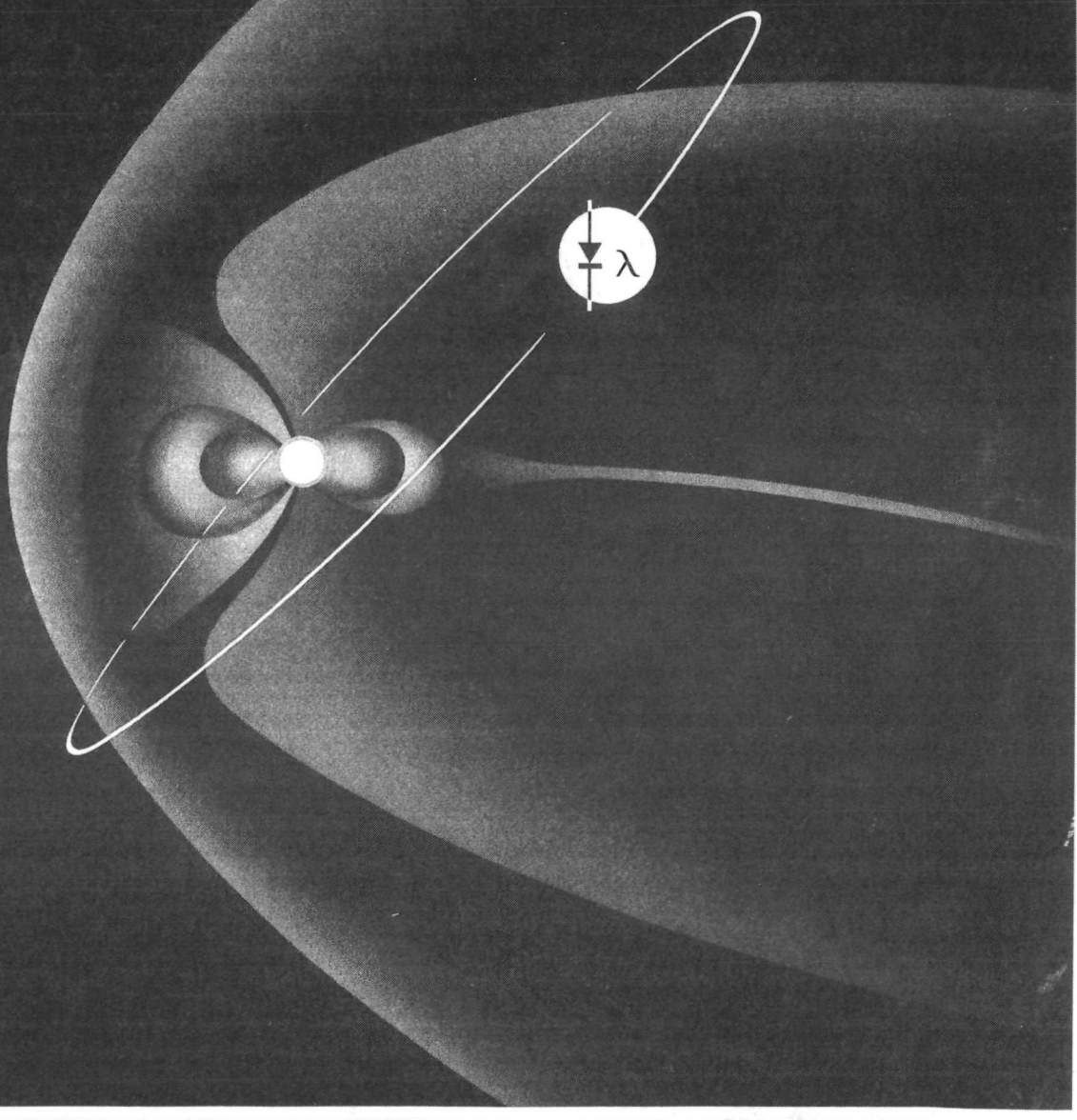

TRW
SYSTEMS GROUP

SOLAR CELL RADIATION HANDBOOK

28 June 1973

21945-6001-RU-00

Contract No. 953362

Jet Propulsion Laboratory
California Institute of Technology
Pasadena, California

Prepared by:

J. R. Carter, Jr.
H. Y. Tada

Approved by:

A. M. Liebschutz

TRW
SYSTEMS GROUP

ONE SPACE PARK • REDONDO BEACH CALIFORNIA 90278

This work was performed for the Jet Propulsion Laboratory, California Institute of Technology, as sponsored by the National Aeronautics and Space Administration under NAS 7-100.

ACKNOWLEDGEMENT

This document was conceived and supported by the Jet Propulsion Laboratory, California Institute of Technology. In this connection, the efforts of Dr. Bruce E. Anspaugh, project manager, and Mr. John V. Goldsmith are gratefully acknowledged.

The preparation of the document was done within the Vulnerability and Hardness Laboratory, TRW Systems. In this regard, the labors of many members of this organization are appreciated. In addition, Mr. Werner Luft, Space Vehicles Division, TRW Systems, provided essential unpublished data.

FOREWORD

The purpose of this document is to detail a method of predicting the degradation of a solar array in a space radiation environment. The text contains a discussion of solar cell technology which emphasizes the cell parameters which degrade in a radiation environment. The experimental techniques used in the evaluation of radiation effects are discussed. In Chapter 3, the theoretical aspects of radiation damage are discussed, and the experimental data, on which the concept of damage equivalent 1-MeV electron fluence is based, are presented. In Chapter 4, the methods of developing relative damage coefficients from the experimental data are detailed. In this regard, it was found necessary to institute two separate equivalent fluences to properly describe the changes of solar cell parameters under space proton irradiation.

Chapter 5 concerns the nature of the space radiation environment and contains predicted solar flare proton fluences for the twenty-first solar cycle based on a proposed model. In Chapter 6, the method of calculating equivalent fluence from electron and proton energy spectrums and relative damage coefficients is detailed. In addition, computer-calculated equivalent fluence contributions from trapped electrons and protons are tabulated for an extensive series of circular earth orbits. The estimated annual equivalent fluence contributions due to solar flare protons are tabulated for the remainder of the current solar cycle. The estimation of degraded solar cell output characteristics from equivalent fluence values is discussed. In Chapter 7, flight data from satellites is compared with estimated degradation.

TABLE OF CONTENTS

TABLE OF CONTENTS (Continued)

TABLES

TABLES (Continued)

TABLES (Continued)

Annex Tables

FIGURES

FIGURES (Continued)

FIGURES (Continued)

CHAPTER 1

1.0 THEORY OF THE SILICON SOLAR CELL

In this chapter some elementary concepts of semiconductor theory, which are useful in understanding solar cell operation, are described. The operation of the silicon solar cell is discussed in terms of an equivalent circuit, and the electrical characteristics of the equivalent circuit elements are explained in terms of physical quantities. In addition, the physical structure of a silicon solar cell is detailed.

1.1 Semiconductor Theory

1.1.1 Thermal Equilibrium Relationships and Excess Densities. Semiconductors are a class of materials which have electrical properties and physical characteristics intermediate between metals and dielectrics. An important characteristic of semiconductor materials is bipolar conduction, where charge transport may occur by conduction band electrons or through empty energy states in the valence band which behave electrically like positively-charged electrons and are referred to as holes. The equilibrium concentrations of conduction electrons and holes in silicon are determined from thermal considerations by the following expression:

$$n_o p_o = 1.5 \times 10^{33}\ T^3\ e^{-\frac{1.21(eV)}{kT}} \qquad (1.1.1)$$

$$= 2.2 \times 10^{20}\ cm^{-6},\ \text{for } T = 300\ K$$

where n_o = the equilibrium concentration of conduction electrons (cm^{-3})

p_o = the equilibrium concentration of holes (cm^{-3})

T = temperature (K)

k = Boltzmann constant (0.8618×10^{-4} eV/K)

For a highly purified semiconductor, the principal source of charge carriers is thermal excitation of electrons from the valence band to the conduction band, and the concentration of conduction electrons will equal the concentration of holes. This state, in which the electrical properties

of a semiconductor are not modified by impurities, may be referred to as intrinsic. The electron and hole concentrations in intrinsic silicon, for example, are equal to 1.5×10^{10} cm^{-3} at room temperature.

When elements from Column III and V of the periodic table occur in substitutional solid solution in silicon, they can be thermally ionized. In the case of Column V elements, such as phosphorus or arsenic, the ionization results in an electron in the conduction band and a positively-charged donor impurity atom in the silicon lattice. Impurities from Column III, such as boron, undergo ionization in silicon by accepting a thermally-ionized electron from the valence band. This process creates a hole in the valence band and a negatively-charged acceptor impurity ion. The activation energies for these donor and acceptor atoms in silicon are approximately 0.05 eV. For this reason, these equilibrium processes go to completion at temperatures near 300 K ($kT \sim 0.026$ eV), and the commonly-used Column III and V impurities in silicon can be considered to be completely ionized at room temperature.

If significant quantities of conduction electrons or holes are produced by the addition of impurities, as described above, the semiconductor may be classed as extrinsic. Extrinsic semiconductors are referred to as n-type (i.e., negative type) if the equilibrium concentration of conduction electrons exceeds the intrinsic carrier concentration. When the equilibrium concentration of holes exceeds the intrinsic carrier concentration of a semiconductor, it is referred to as a p-type (ie., positive type). The product of the equilibrium conduction electron and hole concentrations in extrinsic semiconductors remains constant as described by equation (1.1.1). Thus, boron-doped, p-type, extrinsic silicon with a resistivity of 10 ohm-cm and a hole concentration of 1.4×10^{15} cm^{-3} must also have a conduction electron concentration of 1.6×10^{5} cm^{-3}. In this case, the holes are referred to as majority carriers and the conduction electrons as minority carriers.

The concept of Fermi level may also be used to describe several aspects of semiconductor theory. The Fermi level of a material is defined

as that electron energy state at which the probability of occupancy is equal to 1/2. The Fermi level is at the center of the forbidden band when silicon is intrinsic. In an n-type semiconductor, the Fermi level is above the center of the forbidden band. In a p-type semiconductor the Fermi level is below the center of the forbidden band.

Concentrations of conduction electrons and holes in excess of thermal equilibrium values can be introduced in a semiconductor by electrical processes, by the absorption of electromagnetic radiation, or in the process of stopping high energy particulate radiation. The total instantaneous concentration of carriers during an excitation process can be expressed as follows:

$$p(t) = p_0 + p'(t) \tag{1.1.2}$$

$$n(t) = n_0 + n'(t) \tag{1.1.3}$$

where $p'(t)$ and $n'(t)$ are the instantaneous excess hole and electron concentrations, which in the general case will be functions of time. The absorption in a sample of silicon of electromagnetic radiation, referred to as the optical injection of carriers, is fundamental to the operation of the solar cell. In the absorption process, an electron-hole pair is created for each photon of light absorbed. The densities of excess electrons and holes created in this manner obey the following equations:

$$\frac{dp(t)}{dt} = g_{ext} + g_{th} - r, \tag{1.1.4}$$

$$\frac{dn(t)}{dt} = g_{ext} + g_{th} - r, \tag{1.1.5}$$

where g_{ext} represents the excitation rate per unit volume due to an external cause, g_{th} is the thermal generation rate, and r is the total recombination rate. If a net rate of recombination, u, is defined,

$$u = r - g_{th} , \tag{1.1.6}$$

then for the case of holes, for example,

$$\frac{dp(t)}{dt} = g_{ext} - u. \tag{1.1.7}$$

It has been found for semiconductors, for the case of small excess carrier densities, that is, $p(t) \ll p_o$, that a good approximation for u is,

$$u = (p_n - p_o)/\tau_p, \tag{1.1.8}$$

where p_n denotes the case of excess hole density in n-type, or electron-conducting material and τ_p is the lifetime of a hole. The implication of this can be seen if the above expression for the time derivative of p(t) is integrated, for the case of $g_{ext} = o$, with the initial condition $p_n(o) = p_{no}$. The result is,

$$p_n(t) = p_n(o)e^{-t/\tau_p}, \quad t > 0, \tag{1.1.9}$$

and the lifetime is now seen to be the decay time constant governing the return of excess holes in n-material if the external source is removed at $t = 0$.

An explicit expression for the lifetime, τ_p, has been developed by Hall and Shockley and Read; it is given by the expression, for holes,

$$\tau_p \propto (\sigma_p V_{th} N_t)^{-1}, \tag{1.1.10}$$

where σ_p is the cross-section for capture of a hole by what Shockley and Read have termed a recombination center, V_{th} is the thermal velocity of an excess carrier and is about 10^7cm/sec, and N_t is the density of the recombination centers. These centers, it has been determined, are responsible for the recombination of excess carriers, whether injected electrically or by electromagnetic, or particulate, radiation. Modification and the creation of additional centers of this type can result from the action of high energy radiation in producing lattice displacements and vacancies, as will be discussed in more detail below.

1.1.2 Carrier Transport. Current flow or charge transport can occur by either of two mechanisms in semiconductors. The drift of charged carriers in an electric field is observed in semiconductors as well as metals. Such a drift current for the case of holes in a p-type

semiconductor can be described as follows:

$$J_p = q\ p\ \mu_p\ E, \tag{1.1.11}$$

where J_p = hole current density (amperes/cm^2)

q = hole charge (coulomb)

p = hole concentration (cm^{-3})

μ_p = hole mobility (cm^2/volt sec)

E = electric field (volts/cm)

The coefficients of the electric field (E) in the above expression are related to the resistivity of the material in the following manner:

$$\rho\ (\text{ohm-cm}) = \frac{1}{q\ p\ \mu_p}\ . \tag{1.1.12}$$

Similar expressions can be written to describe conduction electron flow and combined expressions can be used if second carrier conduction is significant.

The second mechanism for charge transport in semiconductors is carrier diffusion. This process results from the random thermal movement of particles which exist in a concentration gradient. Such diffusion is analogous to flow of heat due to thermal gradients and the diffusion of atoms and molecules. When a gradient in the concentration of holes exists in a semiconductor, a hole flux will flow opposite to the gradient. The hole current, for a one-dimensional geometry, is shown in the following expression:

$$J_p = -q\ D_p\ \frac{dp}{dx}\ , \tag{1.1.13}$$

where J_p = hole current density (A/cm^2)

D_p = hole diffusion constant (cm^2/sec)

$\frac{dp}{dx}$ = gradient of hole concentration .

When both mechanisms contribute to the hole flow, the following equation describes the current:

$$J_p = q(p\,\mu_p\,E - D_p\,\frac{dp}{dx}) \quad . \tag{1.1.14}$$

A similar expression can be written for the conduction electron current as follows:

$$J_n = q\,(p\,\mu_n\,E + D_n\,\frac{dn}{dx}) \quad . \tag{1.1.15}$$

In some situations, an expression summing the hole and conduction electron current components may be necessary to describe the current.

The basic equation governing the behavior of charge carriers in time and space is the time-dependent continuity equation. This equation sums the effects of the divergence of current, carrier recombination, and carrier generation. For the non-equilibrium steady state case, the total carrier concentrations (n and p) remain constant, and $\frac{dn}{dt}$ and $\frac{dp}{dt}$ equal zero. In this case the one-dimensional continuity equations for electrons and holes are as follows:

$$g_{ext} - \frac{n - n_o}{\tau_n} - \frac{1}{q}\frac{d}{dx}J_n = 0 \tag{1.1.16}$$

$$g_{ext} - \frac{p - p_o}{\tau_p} - \frac{1}{q}\frac{d}{dx}J_p = 0, \tag{1.1.17}$$

where g_{ext}, introduced earlier, is the rate of generation of carriers per unit volume. If current flow occurs only by diffusion, equation (1.1.13) can be substituted into equation (1.1.17), and a similar substitution can be made in equation (1.1.16), leading to the following equations:

$$D_n\,\frac{d^2n}{dx^2} - \frac{n - n_o}{\tau_n} = -\,g_{ext} \quad , \tag{1.1.18}$$

$$D_p\,\frac{d^2p}{dx^2} - \frac{p - p_o}{\tau_p} = -\,g_{ext} \quad . \tag{1.1.19}$$

1.2 The P-N Junction

The current-voltage characteristic of a p-n junction is one of the factors which determine solar cell response. In this section, the general factors which determine diode characteristics will be discussed. The carrier concentrations found in a solar cell diode are shown graphically in Figure 1.1. The base or p-type region of the device has a majority carrier density (p_{po}) of approximately 10^{15} cm^{-3}. Because the product of the two carrier concentrations is roughly $10^{20} cm^{-6}$, the minority carrier concentration is 10^{5} cm^{-3}. The surface or diffused layer has a majority carrier concentration approaching 10^{20} cm^{-3}. Equilibrium considerations therefore require the minority carrier concentration of this region to be approximately unity. The concentrations of holes and conduction electrons differ greatly on different sides of the junction. This results in two effects. The minority carriers on either side of the junction tend to diffuse across the junction (i.e., create a diffusion current). In addition, the very large concentrations of conduction electrons existing in the n-type layer form an electrostatic potential barrier to oppose electron flow from this p-type region. As a result, all of the mobile charge carriers (holes and conduction electrons) are swept out of the interface region. The ionized impurity atoms form a dipole layer in the interface region. This layer is also referred to as a space charge layer. In a typical solar cell, the width of the n-type diffused layer is roughly 0.4 μm, and the width of the space charge region is very roughly 0.5 μm.

Equation (1.1.17) can be used to determine the behavior of excess carriers in the region of a junction. In the case of steady-state illumination,

$$D_n \frac{d^2 n_p}{dx^2} - \frac{n_p - n_{po}}{\tau_n} = -g_o \ , \quad x > 0 \ . \tag{1.2.1}$$

The solution of this equation for a semi-infinite semiconductor with the boundary condition, that at $x = 0$, $n_p = n_{po}$, is

$$n_p(x) = n_{po} + g_o \tau_n (1 - e^{-x/\sqrt{D_n \tau_n}}) \tag{1.2.2}$$

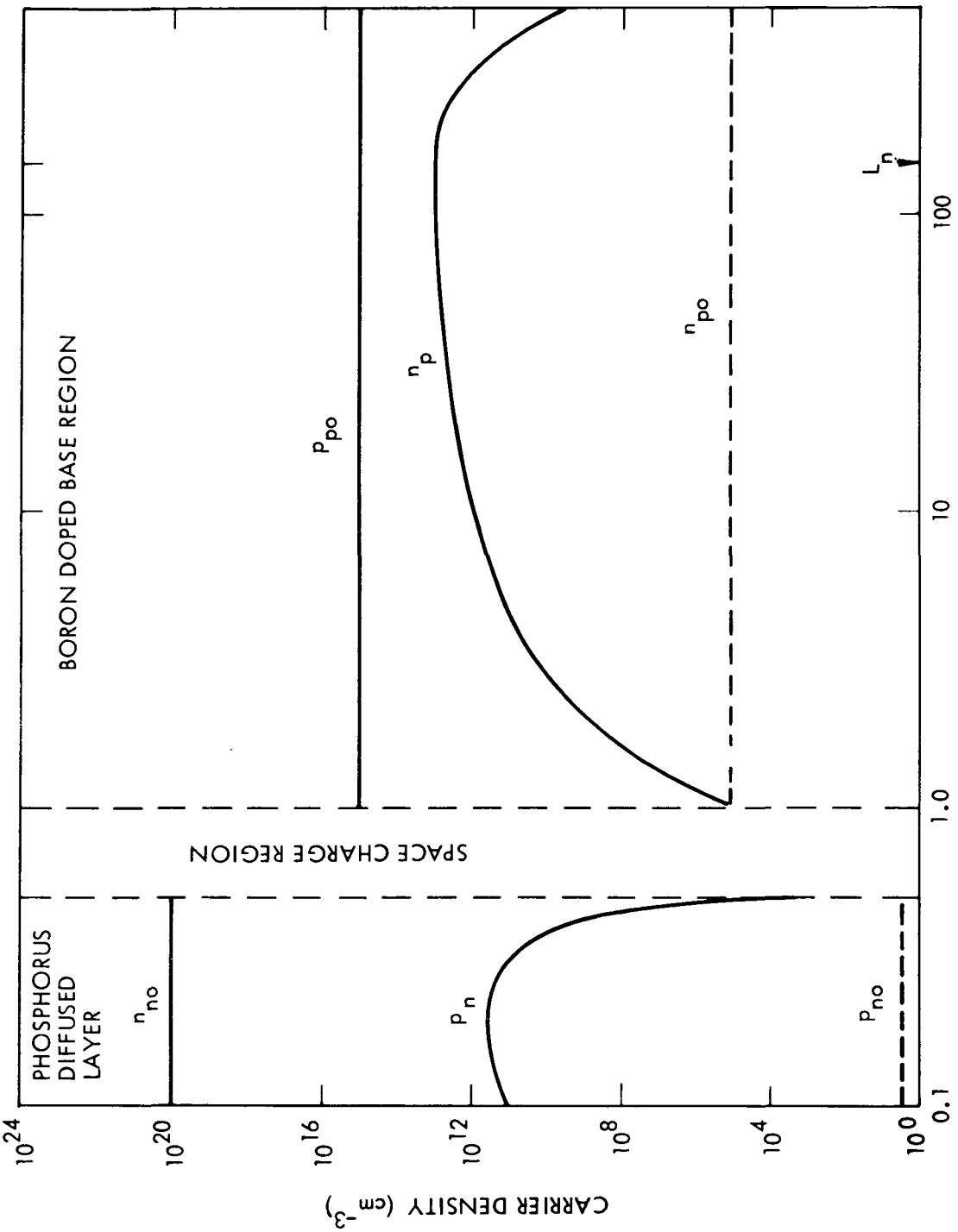

Figure 1.1 Carrier Concentrations in an Illuminated Solar Cell, Short Circuited

The quantity $\sqrt{D\tau}$ has the dimensions of length and is often referred to as the diffusion length (L). The above result indicates that at equilibrium the concentration of conduction electrons in the p-type region will approach zero at the junction and will increase exponentially with distance from the space charge region. This behavior is shown in Figure 1.1. At a distance of one diffusion length from the junction, the minority carrier concentration is 1/e that of the equilibrium bulk value. Actual diffusion lengths found in solar cells can be as large as 200 μm. This parameter is of primary importance in the determination of the efficiency of a solar cell.

The equation for the current flow as a function of bias is as follows for a p-n junction:

$$J = J_{01}(e^{qV/kT} - 1) \qquad (1.2.3)$$

In the case of a large forward bias ($V \gg 0$), $e^{qV/kT}$ is much larger than 1 and therefore,

$$J = J_{01}\, e^{qV/kT} \qquad (1.2.4)$$

When $V < 0$, $J = -J_{01}$. For this reason, J_{01} is also known as the saturation current. If the saturation current is assumed to be due to the diffusion of minority carriers into the junction, then:

$$J_{01} = \frac{q\, D_n\, n_{po}}{L_n} = q\, n_{po} \sqrt{\frac{D_n}{\tau_n}} \qquad (1.2.5)$$

Based on diffusion limited current, the calculated saturation current for an n-p 10 ohm-cm solar cell would be roughly 10^{-10} a/cm^2 at room temperature. The measured values of saturation currents found in such solar cells are considerably higher than the above value. The diffusion theory thus does not adequately explain the current voltage characteristics of a silicon junction diode. [1.1]

A second theory of the diode current voltage relationship involves carrier generation and recombination through defect centers located in the space charge region. The diode or rectifier equation predicted by this theory is as follows: [1.1]

$$J = J_{02}(e^{qV/2kT} - 1) \qquad (1.2.6)$$

The only difference between equations (1.2.3) and (1.2.6) is the factor of 1/2 which appears in the exponent and the form of J_{02}. The expression for J_{02} is:

$$J_{02} = \frac{q\, W\, n_i}{\tau_o} \qquad (1.2.7)$$

where W = width of space charge region

τ_o = carrier lifetime in space charge region

n_i = intrinsic carrier concentration ($\sim 1.5 \times 10^{10}$ cm^{-3})

Experimental studies have shown that the generation-recombination model and the diffusion model are necessary to describe the diode current flow at all voltages. An expression summing the currents of both models can be used to describe the current flow at all voltages.[1.1]

As a result of manufacturing variations, a solar cell junction is occasionally shunted by an ohmic resistance. When the value of this shunt resistance is less than 10^4 ohms, the shunt current will dominate the diode current at forward biases of slightly less than 0.2v. The symbol for shunt resistance is R_{sh}. As a result of resistive volume elements in current paths to the diode junction, the solar cell also has a finite resistance which appears in series with the diode. This series resistance (R_s) is usually less than one ohm and will dominate the current flow through the diode at large forward biases. A model summing both of the above elements is necessary to describe the forward voltage-current characteristic of a silicon solar cell in the most general case. Such a model is shown in Figure 1.2. In Figure 1.3, a generalized current-voltage characteristic is shown for a solar cell

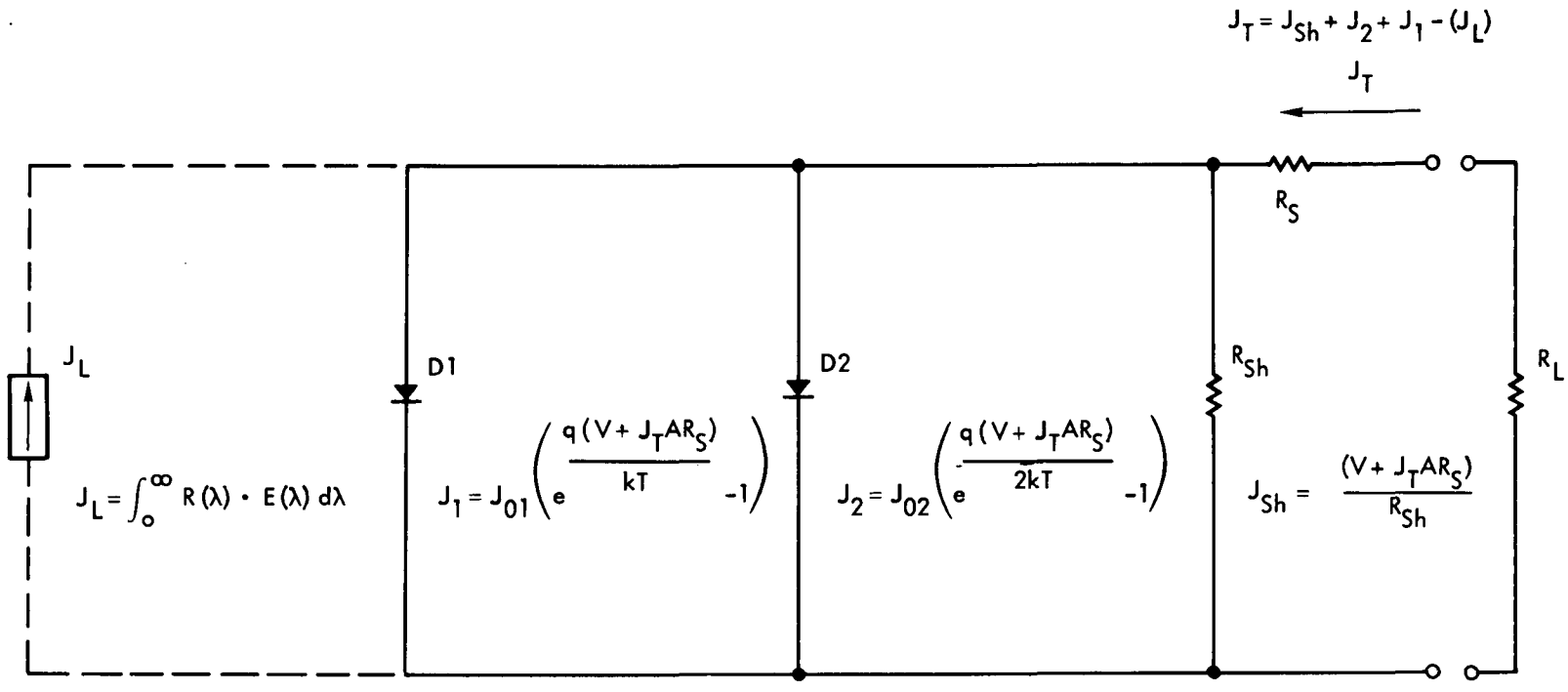

Figure 1.2 Solar Cell Equivalent Circuit Model

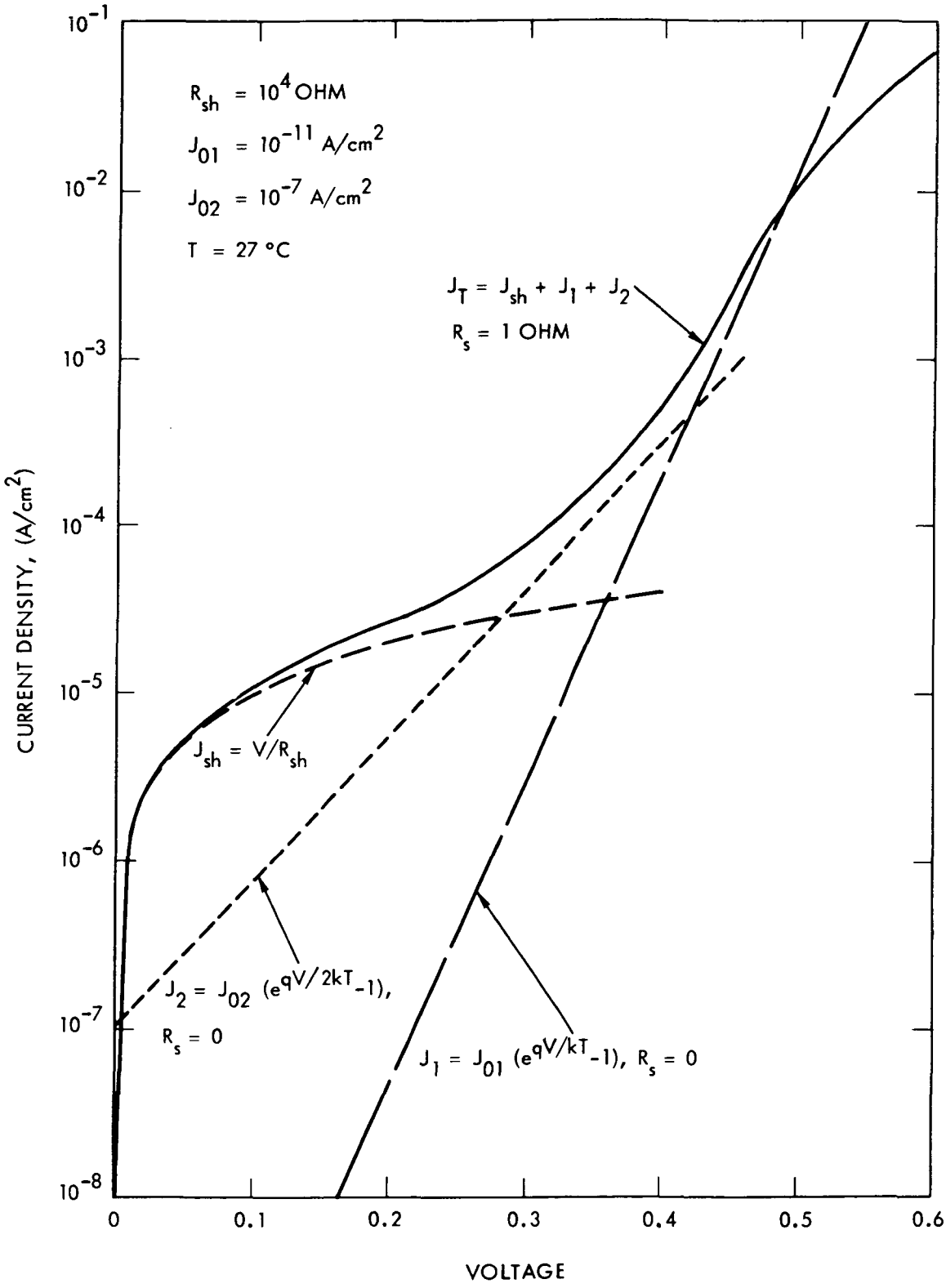

Figure 1.3 Typical Dark Solar Cell Current-Voltage Characteristic, Forward Bias

diode using the above model. Actual solar cells will have considerable variation in the shunt and series resistances.

The junction space charge region of a solar cell has an associated capacitance. The capacitance of a conventional solar cell is related to the width of the space charge region in the following manner:

$$C = \frac{\varepsilon A}{W} \tag{1.2.8}$$

where C is the capacitance, A is area, ε is the dielectric constant and W is the width of the space charge region. The acceptor density in the p-type region adjacent to the space charge region can be related to the capacitance per unit area by:

$$N_a = \frac{2(V_a + V_b)C^2}{q\varepsilon A^2} \tag{1.2.9}$$

where V_a is the applied voltage, and V_b is the barrier voltage (0.6 to 0.8v depending on resistivity of cell base). The above expression assumes an abrupt or step junction which is typical of conventional solar cells.

1.3 Silicon Solar Cell Theory

When a silicon p-n junction diode is exposed to ionizing radiation or light with a photon energy equal to or greater than the band gap of silicon, electron-hole pairs are produced in the silicon. Because of the gradient of conduction electrons (see Figure 1.1) which exists in the p-type region near the space charge region, the conduction electrons generated by the radiation diffuse to the junction. When these electrons reach the space charge region, they drift in the space charge region field to the opposite side of the junction. A similar behavior occurs for holes generated in the n-type regions of a solar cell. The diffusion flux of these generated carriers to the junction is the solar cell generated current. Several investigators have developed general

expressions for generation current.[1.2-1.8] These expressions are solutions of the continuity equations (1.1.18) and (1.1.19) for the case of optical carrier generation. The expression for electrons is as follows:

$$D_n \frac{d^2n}{dx^2} - \frac{D_n(n - n_o)}{L_n^2} + \alpha N_o(1 - R)\, e^{-\alpha d} = 0 \qquad (1.3.1)$$

where α = absorption coefficient for light of wavelength λ, (cm^{-1}) [1.9]

N_o = photon flux density

R = reflection loss

x = distance from the junction

d = distance from front surface

This equation can be solved to find the minority carrier concentration gradient at the edge of the space charge region. The current of carriers into the space charge region can be calculated by evaluating current at the edge of the space charge region by use of equation (1.1.15). Separate evaluations must be made for the diffused or surface layer and electron currents in the bulk response to monochromatic light as follows: [1.8]

Surface Layer:

$$J_p(\lambda) = \frac{q\ N_o\ (1 - R)\ \alpha L_p}{1 - \alpha^2 L_p^2} \frac{\left[\left(\alpha L_p + \frac{D_p}{S L_p}\right) \sinh \frac{a}{L_p} + \left(1 + \frac{\alpha D_p}{S}\right) \cosh \frac{a}{L_p}\right] e^{-\alpha a} - \left(1 + \frac{\alpha D_p}{S}\right)}{\sinh \frac{a}{L_p} + \frac{D_p}{S L_p} \cosh \frac{a}{L_p}} \qquad (1.3.3)$$

Bulk Response: (assuming $S = \infty$ at $d = b$)

$$J_n(\lambda) = \frac{q N_o (1 - R) \alpha L_n}{1 - \alpha^2 L_n^2} \frac{\left(\sinh \frac{b - a}{L_n} - \alpha L \cosh \frac{b - a}{L_n}\right) e^{-\alpha a} + \alpha L_n e^{-\alpha b}}{\cosh \frac{b - a}{L_n}} \qquad (1.3.4)$$

where a = junction depth (cm)

b = cell thickness (cm)

S = surface recombination velocity (cm/sec) .

Total Response:

$$J_L(\lambda) = J_n(\lambda) + J_p(\lambda) \qquad (1.3.5)$$

The above equations are written for the case of an n-p solar cell. It is also assumed that no significant drift fields are present. The cell response in A/cm^2 may be normalized to the photon flux density (N_o). In this way, the above equations describe the response of the cell in terms of amperes per photon/sec of incident light of a given wave length. Solar cell spectral response curves are routinely measured. In these experimental measurements, the response is usually normalized to the incident optical power density (watts cm^{-2}) rather than photon density rate. The calculated response of a typical solar cell in such terms is shown in Figure 1.4.

The previous equations illustrated the role of the minority carrier diffusion length in development of the light-generated current of a solar cell. These response equations can be folded with the solar spectral irradiance and integrated to yield the light-generated solar-cell current under solar illumination (see Figure 1.4).

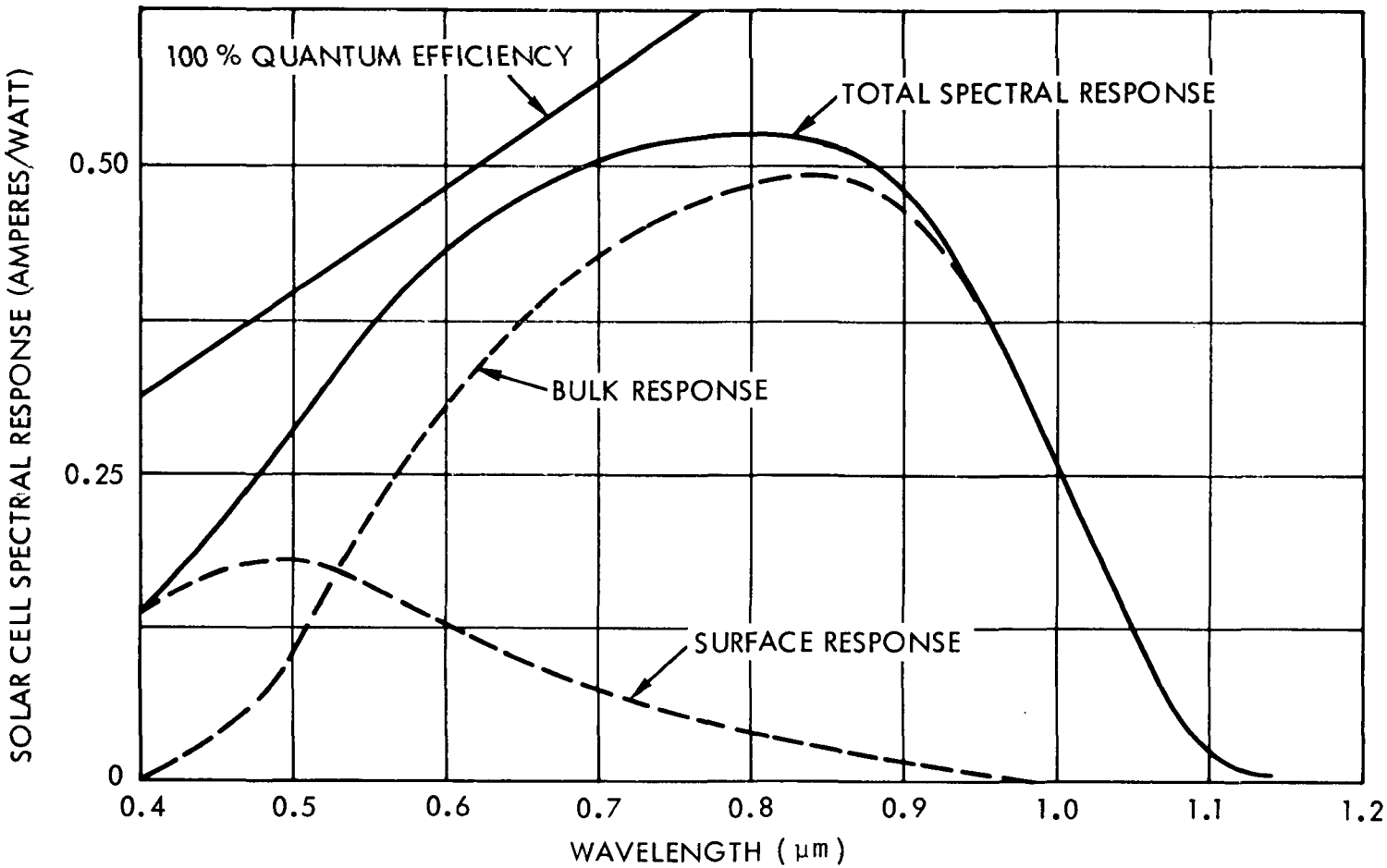

Figure 1.4 Calculated Silicon Solar Cell Spectral Response

The light generated current can be combined with previously discussed diode rectifier equations to determine the current-voltage characteristic of an illuminated solar cell. The model for an illuminated solar cell is the same as that shown in Figure 1.2 for a dark diode, with the addition of a current source.[1.10] The current source (shown dotted in Figure 1.2) represents the light generated current. On the basis of the above model, an equation can be written to describe the cell current into an external load:

$$I = I_L - I_{D1} - I_{D2} - I_{sh} \tag{1.3.6}$$

where I = cell current in external load

I_L = light generated current

I_{D1} = current in solar cell diode D1

I_{D2} = current in solar cell diode D2

I_{sh} = current in internal solar cell shunt (R_{sh})

Several observations can be made regarding the form of the above equation. The light generated current is independent of applied voltage and proportional to the intensity of the incident illumination. The development of the light generated current produces a forward bias on the solar cell diodes (D1 and D2). The light generated current (I_L) will divide between the parallel branches containing D1, D2, R_{sh} and $R_s + R_L$. The behavior of the illuminated solar cell current (I) and voltage (V) as R_L varies from zero to infinity is referred to as the I-V characteristic. This characteristic is the primary engineering tool used in evaluating solar cells. A general expression for the cell current to an external load can be obtained by substitution of equations (1.2.4) and (1.2.6) into equation (1.3.6). In the case of a good cell under 135 mW/cm^2 solar illumination, the current in R_{sh} can be neglected. It has been the practice to simplify the two diode currents with the following expression:

$$I_d = I_o \left[e^{q(V+IR_s)/nkT} - 1 \right] \tag{1.3.7}$$

where I_o is an apparent saturation current, and n is a constant, between 1 and 2 in value. The resulting expression is often used to describe solar cell I-V characteristics:

$$I = I_L - I_o \left[e^{q(V+IR_S)/nkT} - 1\right] \qquad (1.3.8)$$

The development of a solar cell I-V characteristic from the light generated current and dark diode characteristic is shown graphically in Figure 1.5. An I_L value of 35 mA/cm^2 is typical of solar cells under solar illumination of 135 mW/cm^2. This I_L value is shown in Figure 1.5. In addition, the dark diode or rectifier characteristics shown in Figure 1.3 are replotted in Figure 1.5. The diode characteristics are shown with and without the series resistance. The illuminated solar cell I-V characteristic for a hypothetical cell with $R_s = 0$ is obtained by subtracting the forward current flowing in D1, D2, and R_{sh} from the light generated current I_L. When R_s is some significant quantity, the dark diode characteristic is displaced an amount ΔV before subtraction from I_L. The quantity ΔV is the voltage drop across R_s when the solar cell diode conducts a forward current equal to $+I_L$.

It should be understood that this analysis is for a solar cell at 27°C under solar illumination of 135 mW/cm^2. The quantity I_L is proportional to the light intensity, a function of temperature, and also a function of the spectral content of the illumination. The dark diode currents I_{D1} and I_{D2} are strong functions of temperature. Under the assumed conditions of temperature and illumination, I_{D1} and R_s dominate the I-V characteristic of the solar cell. Under other conditions of temperature and illumination, the solar cell I-V characteristic may be influenced by other factors such as R_{sh} and I_{D2}.

A different set of parameters is used to describe the solar cell characteristic for engineering purposes. These are (a) short circuit current I_{sc}, (b) open circuit voltage V_{oc}, and (c) maximum power P_{max}. The short circuit current is that current produced by the cell when the load resistance (R_L) approaches zero. In good solar cells, this quantity is equal to the light generated current I_L or $J_L \cdot A$. In cells

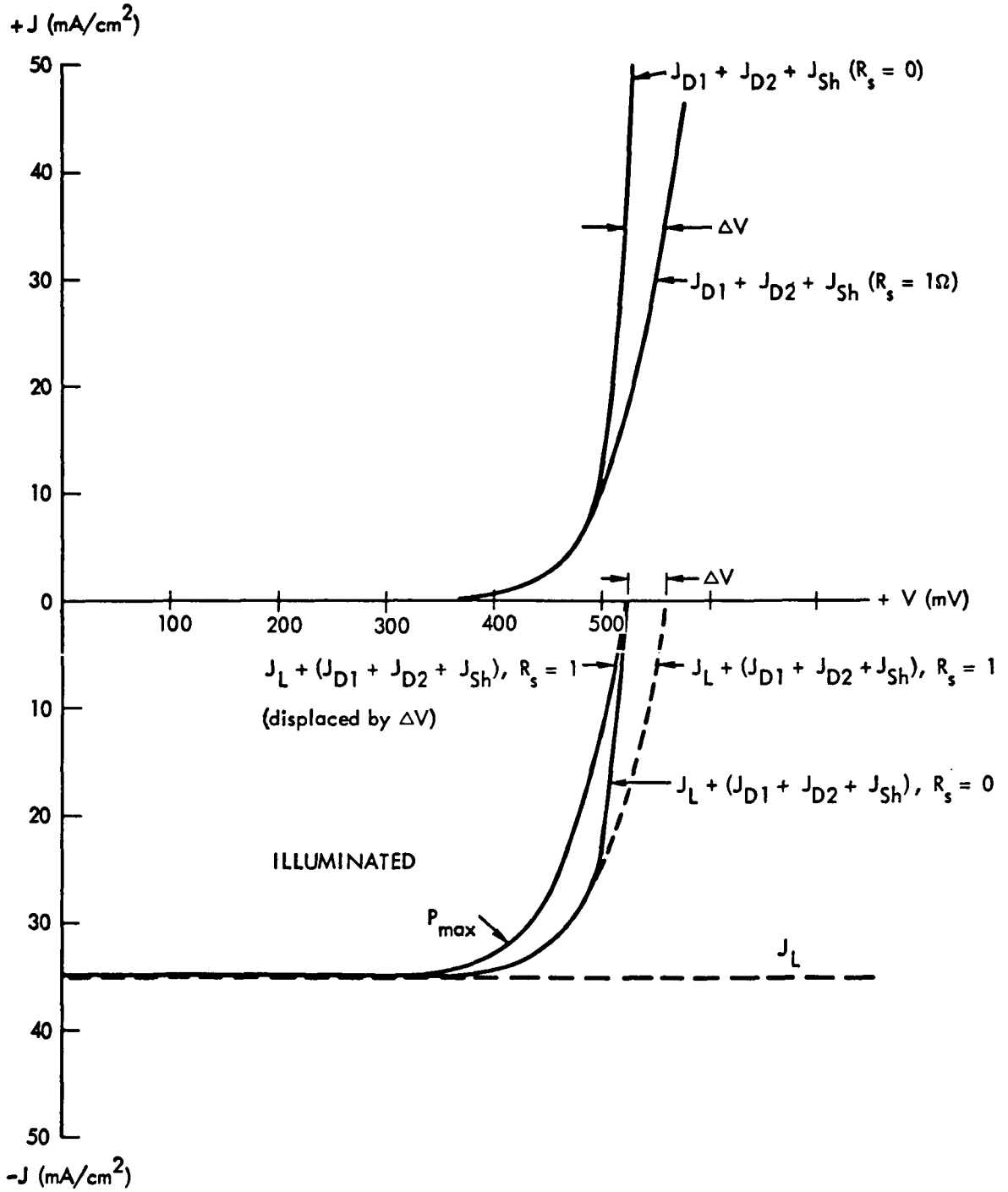

Figure 1.5 Development of a Current-Voltage Characteristic for an Illuminated Silicon Solar Cell

with high or excessive internal series resistance, or in good cells at higher illumination intensities, I_{sc} will be less than the light generated current. The open circuit voltage is the voltage produced by the cell when R_L is infinite. In this load condition, all of the light generated current is consumed in forward conduction of diodes D1 and D2.

$$V_{oc} = \frac{nkT}{q} \ln \frac{I_L}{I_o} \tag{1.3.9}$$

A maximum in the power delivered to the load resistance occurs at some point of the solar cell I-V characteristic. The power developed under such a load is called the maximum power (P_{max}). A method of determining an analytical expression for the I-V characteristic from parameters such as I_{sc}, V_{oc}, P_{max}, and V_{max} has been described in the literature.[1.11]

1.4 Solar Cell Coatings and Contacts

A silicon solar cell is a composite of several layers of material. The layers of n and p-type silicon form the basic cell structure in which the current is generated. Additional practical problems are involved in maximizing the light which enters the silicon and providing a low resistance path for the removal of the generated current from the solar cell. When the light passes from one medium to another medium which has a different index of fraction, some light is reflected. The amount of light reflected can be determined from the following relationship:

$$R = \left(\frac{n_2 - n_1}{n_2 + n_1}\right)^2 \tag{1.4.1}$$

where R = reflectivity (fraction of normal incidence light intensity reflected)

n_1 = index of refraction, medium 1

n_2 = index of refraction, medium 2

The above relationship holds only for normal incidence light. The more general case of light incident at an arbitrary angle θ from the normal is covered in a basic text on optics.[1.12]

The index of refraction for silicon in the solar cell response region varies between 3.5 and 4.0 in the optical region. For this reason, there are significant reflectance losses when light is incident on an air-silicon interface. The reflectance loss can be reduced by adding an intermediate layer. The optimum index of refraction for the intermediate layer is given by:

$$n_{op} = (n_1 \cdot n_2)^{1/2} \qquad (1.4.2)$$

The optimum index of refraction for an antireflection coating at an air-silicon interface is approximately 1.9 (Silicon monoxide, with an index of refraction in the range of 1.8 to 1.9, is used as an antireflection coating on solar cells.) Silicon solar cells used in the space environment are always covered by glass to shield against radiation and to raise the effective emissivity for better thermal control. Recently, efforts have been made to develop an antireflective coating optimizing the transmission from glass adhesive to the silicon. Since the adhesives have n values of approximately 1.4, the previous equation indicates that an antireflective coating with n = 2.2 - 2.4 would be optimum for a solar cell to be used with cover glass. Titanium oxide and tantalum oxide have been proposed and evaluated for this purpose.[1.13-1.17] Antireflecting coatings may vary in thickness from 70 to 80 nm. In theory, the coating thickness should equal 1/4 the light wavelength for minimum reflection loss.

The contacts of current commercial solar cells are formed by evaporating titanium and silver metal on the entire back surface and front contact pattern. The total thickness of this evaporated metallization is approximately 5 μm. After the metallization, the cells are usually solder dipped. The solder thickness may vary between 0.001 and 0.008 cm (0.4 - 3 mils). One of the primary considerations in the selection of the contact is the electrical behavior of the metal-semiconductor interface.

In general, such interfaces can be described as Schottky barriers. A Schottky barrier has a current voltage characteristic of the same form as that for a p-n junction. The saturation current for a Schottky barrier is as follows: [1.18]

$$I_o = A\ T^2 \exp - (\phi_B/kT) \qquad (1.4.3)$$

where A = effective Richardson constant (A cm^{-2} K^{-2})

ϕ_B = barrier height (eV)

The quantity A is approximately 100 A cm^{-2} K^{-2} and ϕ_B is approximately 0.50 (eV) for most metals in contact with p-type silicon. The saturation current (I_o) at room temperature (T = 300 K) will be between 10^{-2} and 10^{-1} A cm^{-2}. The effect that the Schottky barrier has on the solar cell will be related to the forward resistance of the barrier. Since the form of the barrier current-voltage characteristic is:

$$I = I_o(e^{qV/kT}-1) \qquad (1.4.4)$$

The dynamic impedance of the junction is as follows:

$$\frac{dV}{dI} = \frac{kT/q}{I_o}\ e^{-qV/kT} \qquad (1.4.5)$$

It can be seen that impedance of this barrier is inversely proportional to the saturation current. Since the saturation current at room temperature is very high, the impedance of a Schottky barrier is very low. If the barrier potential (ϕ_B) for a particular metal on silicon is low enough, the barrier I-V characteristic will approach low resistance ohmic behavior. This is the case for a titanium layer on p-type silicon at room temperature. At low temperatures the saturation current of such a Schottky barrier is reduced and the diode characteristics become more significant. In this case, the Schottky barrier adds a nonlinear voltage drop to the solar cell model in series with R_s. This problem has received considerable attention

in the literature. [1.19-1.24] The problem associated with nonohmic contacts can be reduced by producing a heavily doped (p+) layer on the silicon interface. In such cases, the space charge region associated with the Schottky barrier is generally reduced. Quantum mechanical tunneling of the space charge region dominates the behavior of such thin barriers, and provides a highly conductive metal semiconductor interface. Since the solar cell front contact is applied to a silicon interface which is very heavily doped due to phosphorous diffusion, the tunneling mechanism assures a low resistance ohmic contact.

REFERENCES

1.1 A. S. Grove, "Physics and Technology of Semiconductor Devices", Wiley, 1967.

1.2 L. M. Terman, "Spectral Response of Solar Cell Structures", Solid State Electronics, 2, 1, p. 1, 1961.

1.3 D. A. Kleinman, "Considerations on the Solar Cell," Bell System Technical Journal, 40, p. 81, 1961.

1.4 T. S. Moss, "The Potentialities of Silicon and Gallium Arsenide Solar Batteries," Solid-State Electronics, 1, p. 222, 1961.

1.5 B. Dale and F. P. Smith, "Spectral Response of Solar Cells," J. Appl. Phys. 32, 7, p. 1377, 1961.

1.6 J. J. Loferski and J. J. Wysocki, "Spectral Response of Photovoltaic Cells," RCA Review, 22, p. 38, 1961.

1.7 J. W. Oliver, "Minority Carrier Diffusion Analysis in Photovoltaic Devices," TRW Report 8987-0001-RU-001, 19 Feb. 1962.

1.8 H. Y. Tada, "A Survey of the Effects of Electron and Proton Radiation on Silicon Solar Cells", TM-755, Aerospace Group, Hughes Aircraft Co., NAS5-2797, June 1963.

1.9 W. C. Dash and R. Newman, "Intrinsic Optical Absorption in Single-Crystal Germanium and Silicon at 77°K and 300°, Phys. Rev. 99, 4, 1151, 1955.

1.10 M. Wolf and H. Rauschenbach, "Series Resistance Effects on Solar Cell Measurements," Advanced Energy Conversion, 3, p. 455, 1963.

1.11 W. T. Picciano, "Determination of the Solar Cell Equation Parameters Including Series Resistance from Empirical Data," Energy Conversion, 9, 1, 1969.

1.12 F. W. Sears, Optics, Addison, Cambridge, Mass., p. 173, 1949.

1.13 A. Atzei, et al., "Improved Antireflection Coatings on Silicon Solar Cells," Solar Cells, p.349, Gordon and Breach, 1971.

1.14 R. L. Crabb and A. Atzei, "Environmental Study of European Silicon Solar Cell with Improved Antireflection Coatings, Conf. Record of the Eighth Photovoltaic Specialists Conf., p. 75, 1970.

1.15 J. Roger and P. Colardelle, "Antireflecting Silicon Solar Cell with Titanium Dioxide," Conf. Record of the Eighth IEEE Photovoltaic Specialists Conf., p 84, 1970.

1.16 C. Misiano and G. Greco, "Titanium Dioxide Antireflection Coating for Silicon Solar Cells," Solar Cells, p. 363, Gordon and Breach, 1971.

1.17 J. Lindmayer and J. Allison, "The Violet Cell: An Improved Silicon Solar Cell", COMSAT Technical Review, 3, 1, 1, Spring 1973.

1.18 S. M. Sze, "Physics of Semiconductor Devices," Wiley, 1969.

1.19 C. H. Liebert, "Solar Cell Performance at Jupiter Temperature and Solar Intensity", Conf. Record of the Seventh Photovoltaic Specialists Conf., IEEE, p. 92, 1968.

1.20 R. J. Lambert, "Characteristics of Solar Cells at Low Temperatures", ibid., p. 97.

1.21 P. A. Payne and E. A. Ralph, "Low Temperature and Low Solar Intensity Characteristics of Silicon Solar Cell", Conf. Record of the Eighth IEEE Photovoltaic Specialists Conf., p. 123, 1970.

1.22 J. C. Ho, et al., "Solar Cell Low Temperature, Low Solar Intensity Operation", ibid., p. 150.

1.23 W. Luft, "Silicon Solar Cells at Low Temperature", ibid., p. 161.

1.24 H. Fisher, et al., "Some Innovations in Silicon Solar Cell Technology", Solar Cells, Gordon and Breach Science Publisher, London, 1971.

CHAPTER 2

2.0 INSTRUMENTATION TECHNIQUES FOR MEASUREMENT OF SOLAR CELL PARAMETERS

In this section, the various commonly used experimental methods for the analysis of radiation effects are discussed. The most commonly used measurement in the analysis of radiation effects in silicon solar cells is the current-voltage characteristic under illumination. Since solar cell response is a strong function of optical wavelength, the light source is a major variable in the evaluation of solar cell parameter changes.

2.1 Light Sources and Solar Simulators

The spectral irradiance of the sun at 1.5×10^{11} m (one AU) is of primary importance in solar cell analysis for earth orbits. The values of solar spectral irradiance proposed by Johnson in 1954 have been widely accepted and used for analytical purposes.[2.1] Johnson's results indicated that the solar constant was 139.5 mW/cm^2, and also that the solar spectrum closely approximates that of a 6000 K blackbody. Several high-altitude measurements made in recent years have been reviewed.[2.2] The findings indicate a solar constant of 135.3 ± 2.1 mW/cm^2. The proposed solar spectral irradiance is tabulated in Table 2.1. Silicon solar cell response is generally limited to the region between 0.3 and 1.2 μm. In this range, the solar power density is 104.4 mW/cm^2.

Among several solar simulation techniques, the most common method is the use of a xenon arc lamp with filters to remove undesired line spectra in the near infrared. Unfiltered xenon lamps are also used in the pulsed mode, which does not generate the undesired line spectra. Unfiltered carbon arcs are also used to simulate solar illumination with a reasonable spectral match. A close spectral match to the solar spectrum is obtained by the use of a xenon-filtered tungsten combination or filtered xenon source. These sources match the solar spectrum well enough that cell measurements made under these sources can be considered representative

TABLE 2.1

SOLAR SPECTRAL IRRADIANCE - PROPOSED STANDARD CURVE [2.2]

λ - Wavelength in micrometers

E(λ) - Solar spectral irradiance averaged over small bandwidth centered at λ, in $W \cdot m^{-2} \cdot \mu m^{-1}$

E(o-λ) - Area under the solar spectral irradiance curve in the wavelength range 0 to λ in $W \cdot m^{-2}$

D(o-λ) - Percentage of the solar constant associated with wavelengths shorter than λ

Solar Constant - 1353 $W \cdot m^{-2}$

	E(λ)	E(o-λ)	D(o-λ)	λ	E(λ)	E(o-λ)	D(o-λ)	λ	E(λ)	E(o-λ)	D(o-λ)
.120	.100	.005999	.00044	.525	1852	352.591	26.059	1.70	202	1221.23	90.261
.140	.030	.007299	.00053	.530	1842	361.826	26.742	1.75	180	1230.78	90.967
.150	.07	.00788	.00057	.535	1818	370.976	27.418	1.80	159	1239.25	91.593
.160	.23	.00930	.00068	.540	1783	379.979	28.084	1.85	142	1246.78	92.149
.170	.63	.01360	.00100	.545	1754	388.821	28.737	1.90	126	1253.48	92.644
.180	1.25	.02300	.00169	.550	1725	397.519	29.380	1.95	114	1259.48	93.088
.190	2.71	.04280	.00316	.555	1720	406.131	30.017	2.00	103	1264.90	93.489
.200	10.7	.10989	.00811	.560	1695	414.669	30.648	2.10	90	1274.55	94.202
.210	22.9	.27785	.02053	.565	1705	423.163	31.276	2.20	79	1283.00	94.826
.220	57.5	.67985	.05024	.570	1712	431.711	31.907	2.30	69	1290.40	95.373
.225	64.9	.98585	.0728	.575	1719	440.289	32.541	2.4	62.0	1296.95	95.8580
.230	66.7	1.31485	.0971	.580	1715	448.874	33.176	2.5	55.0	1302.80	96.2903
.235	59.3	1.62985	.1204	.585	1712	457.441	33.809	2.6	48.0	1307.95	96.6710
.240	63.0	1.93560	.1430	.590	1700	465.971	34.439	2.7	43.0	1312.50	97.0073
.245	72.3	2.27385	.1680	.595	1682	474.426	35.064	2.8	39.0	1316.60	97.3103
.250	70.4	2.63060	.1944	.600	1666	482.796	35.683	2.9	35.0	1320.30	97.5838
.255	104	3.04660	.2266	.605	1647	491.079	36.295	3.0	31.0	1323.60	97.8277
.260	130	3.65160	.2698	.610	1635	499.284	36.902	3.1	26.0	1326.45	98.0383
.265	185	4.43910	.3280	.620	1602	515.469	38.098	3.2	22.6	1328.88	98.2179
.270	232	5.48160	.4051	.630	1570	531.329	39.270	3.3	19.2	1330.97	98.3724
.275	204	6.5716	.4857	.64	1544	546.899	40.421	3.4	16.6	1332.76	98.5047
.280	222	7.6366	.5644	.65	1511	562.174	41.550	3.5	14.6	1334.32	98.6200
.285	315	8.9791	.6636	.66	1486	577.159	42.657	3.6	13.5	1335.73	98.7238
.290	482	10.9716	.8109	.67	1456	591.863	43.744	3.7	12.3	1337.02	98.8192
.295	584	13.6366	1.0078	.68	1427	606.284	44.810	3.8	11.1	1338.19	98.9056
.300	514	16.3816	1.2107	.69	1402	620.429	45.855	3.9	10.3	1339.26	98.9847
.305	603	19.1741	1.4171	.70	1369	634.284	46.879	4.0	9.5	1340.25	99.0579
.310	689	22.4041	1.6558	.71	1344	647.849	47.882	4.1	8.7	1341.16	99.1252
.315	764	26.0366	1.9243	.72	1314	661.139	48.864	4.2	7.8	1341.98	99.1861
.320	930	30.0216	2.2188	.73	1290	674.159	49.826	4.3	7.1	1342.73	99.2412
.325	975	34.5341	2.552	.74	1260	686.909	50.769	4.4	6.50	1343.4141	99.291507
.330	1059	39.6191	2.928	.75	1235	699.384	51.691	4.5	5.90	1344.0341	99.337331
.335	1081	44.9691	3.323	.76	1211	711.614	52.595	4.6	5.30	1344.5941	99.378721
.340	1074	50.3566	3.721	.77	1185	723.594	53.480	4.7	4.80	1345.0991	99.416045
.345	1069	55.7141	4.117	.78	1159	735.314	54.346	4.8	4.50	1345.5641	99.450413
.350	1093	61.1191	4.517	.79	1134	746.779	55.194	4.9	4.10	1345.9941	99.482195
.355	1083	66.5591	4.919	.80	1109	757.994	56.023	5.0	3.83	1346.3906	99.511500
.360	1068	71.9366	5.316	.81	1085	768.965	56.834	6.0	1.75	1349.1406	99.717708
.365	1132	77.4366	5.723	.82	1060	779.694	57.627	7.0	.99	1350.5506	99.818965
.370	1181	83.2191	6.150	.83	1036	790.174	58.401	8.0	.60	1351.3456	99.877723
.375	1157	89.0641	6.582	.84	1013	800.419	59.158	9.0	.380	1351.8356	99.913939
.380	1120	94.7566	7.003	.85	990	810.434	59.899	10.0	.250	1352.1506	99.937221
.385	1099	100.3016	7.413	.86	968	820.224	60.622	11.0	.170	1352.3606	99.952742
.390	1098	105.7916	7.819	.87	947	829.799	61.330	12.0	.120	1352.5056	99.963459
.395	1189	111.5091	8.241	.88	926	839.164	62.022	13.0	.087	1352.6091	99.971108
.400	1429	118.0541	8.725	.89	908	848.334	62.700	14.0	.055	1352.6801	99.976356
.405	1644	125.7366	9.293	.90	891	857.329	63.365	15.0	.049	1352.7321	99.980199
.410	1751	134.2241	9.920	.91	880	866.184	64.019	16.0	.038	1352.7756	99.983414
.415	1774	143.0366	10.571	.92	869	874.929	64.665	17.0	.031	1352.8101	99.985964
.420	1747	151.8391	11.222	.93	858	883.564	65.304	18.0	.024	1352.8376	99.987997
.425	1693	160.4391	11.858	.94	847	892.08	65.934	19.0	.02000	1352.8596	99.989623
.430	1639	168.7691	12.473	.95	837	900.50	66.556	20.0	.01600	1352.8776	99.990953
.435	1663	177.0241	13.083	.96	820	908.79	67.168	25.0	.00610	1352.9328	99.995037
.440	1810	185.7066	13.725	.97	803	916.90	67.768	30.0	.00300	1352.9556	99.996718
.445	1922	195.0366	14.415	.98	785	924.84	68.355	35.0	.00160	1352.9671	99.997568
.450	2006	204.8566	15.148	.99	767	932.60	68.928	40.0	.00094	1352.9734	99.998037
.455	2057	215.0141	15.891	1.00	748	940.18	69.488	50.0	.00038	1352.9800	99.998525
.460	2066	225.3216	16.653	1.05	668	975.58	72.105	60.0	.00019	1352.9829	99.998736
.465	2048	235.6066	17.413	1.10	593	1007.10	74.435	80.0	.00007	1352.9855	99.998928
.470	2033	245.8091	18.167	1.15	535	1035.30	76.519	100.0	.00003	1352.9865	99.999002
.475	2044	256.001	18.921	1.20	485	1060.80	78.404	1000.0	.00000	1353.0000	100.000000
.480	2074	266.296	19.681	1.25	438	1083.88	80.109				
.485	1976	276.421	20.430	1.30	397	1104.75	81.652				
.490	1950	286.236	21.155	1.35	358	1123.63	83.047				
.495	1960	296.011	21.878	1.40	337	1141.00	84.331				
.500	1942	305.766	22.599	1.45	312	1157.23	85.530				
.505	1928	315.421	23.312	1.50	288	1172.23	86.639				
.510	1882	324.926	24.015	1.55	267	1186.10	87.665				
.515	1833	334.214	24.701	1.60	245	1198.98	88.611				
.520	1833	343.379	25.379	1.65	223	1210.60	89.475				

of that in the space environment. Many other types of light sources have been used in radiation effects studies. Unfiltered and filtered incandescent tungsten sources have peak response in the red and near infrared. Since this is the wavelength region of the solar cell response which is most changed by irradiation, use of these sources will show much more severe cell radiation degradations as compared to evaluations with a suitable solar simulator. This characteristic severely limits the use of tungsten source simulation in the evaluation of radiation effects.

Filtered xenon arc solar simulators are manufactured by Spectrolab and Aerospace Controls. The spectral irradiance for the Spectrolab X-25 simulator is shown in Figure 2.1. [2.3] Similar data is shown in Figure 2.2 for a combination xenon-tungsten source simulator used by Centralab Semiconductor Products. [2.4] In Figure 2.3, the spectral irradiance is shown for a Genarco Model #ME4CWM carbon arc simulator. [2.5]

An important recent development in the field of solar simulators is the use of pulsed xenon arc lamps for solar cell and solar cell array testing.[2.6, 2.7] These developments have been prompted by the need for a suitable alternative to testing large arrays in natural sunlight on the earth's surface. In these systems, an approximately 2 msec pulse of light is produced. Solar cell output data can be accumulated during about 1 msec of the pulse length. Sophisticated electronic data handling systems are necessary to record cell or array outputs and commutate external load resistances during the light pulse. Variations in test cell current due to light intensity variations are corrected to a normalized value at the desired illumination. The high intensity peaks in the 0.8-0.9 μm region of the xenon arc spectrum are not generated by pulsed operation with high current densities. By this means, it is possible to achieve a reasonably close match to the solar spectrum. [2.7, 2.8] Array areas up to eight feet by eight feet can be illuminated with excellent temperature control, by such simulators.

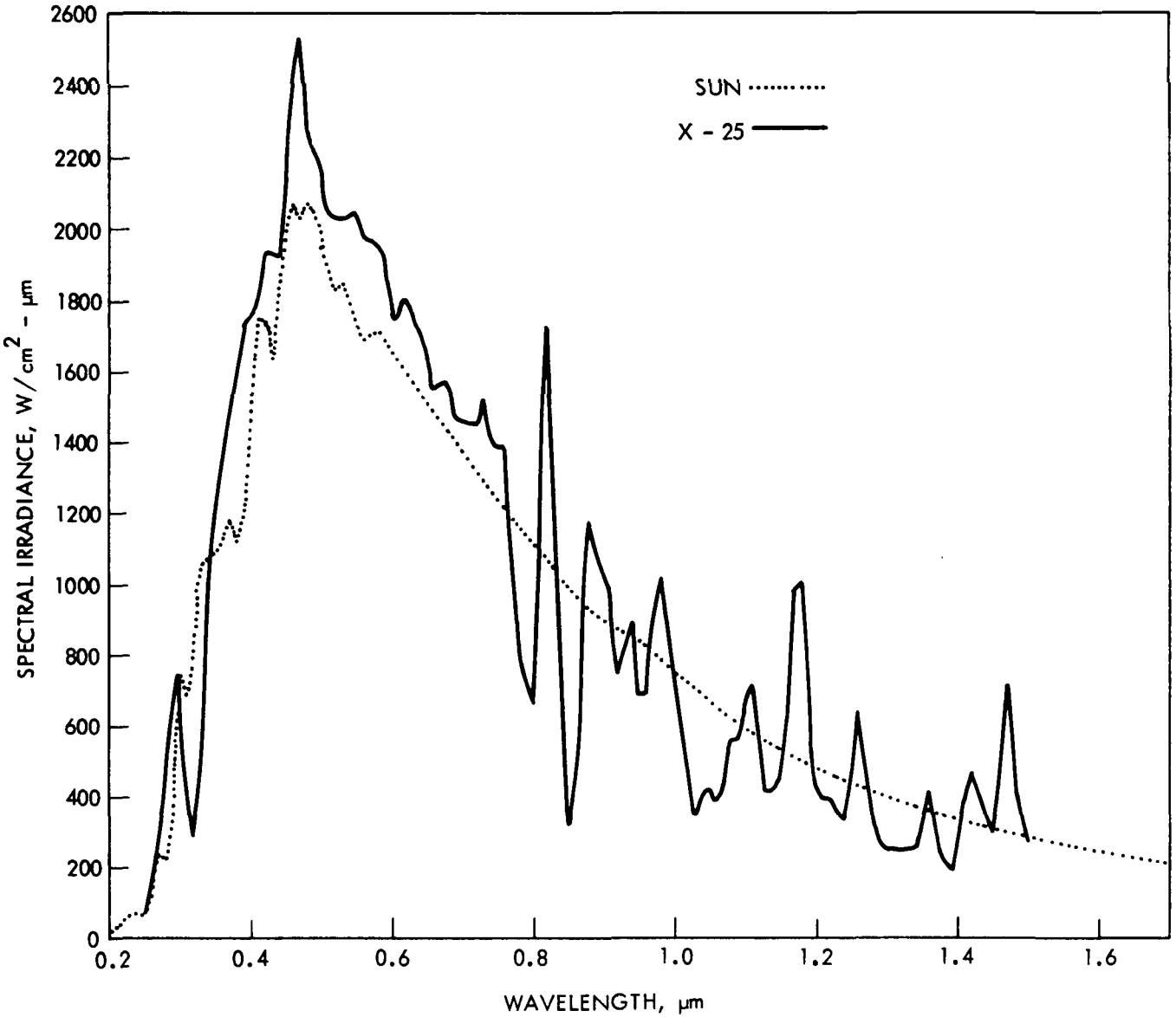

Figure 2.1 Spectral Output, Spectrolab X-25 Spectrosun[2.3]

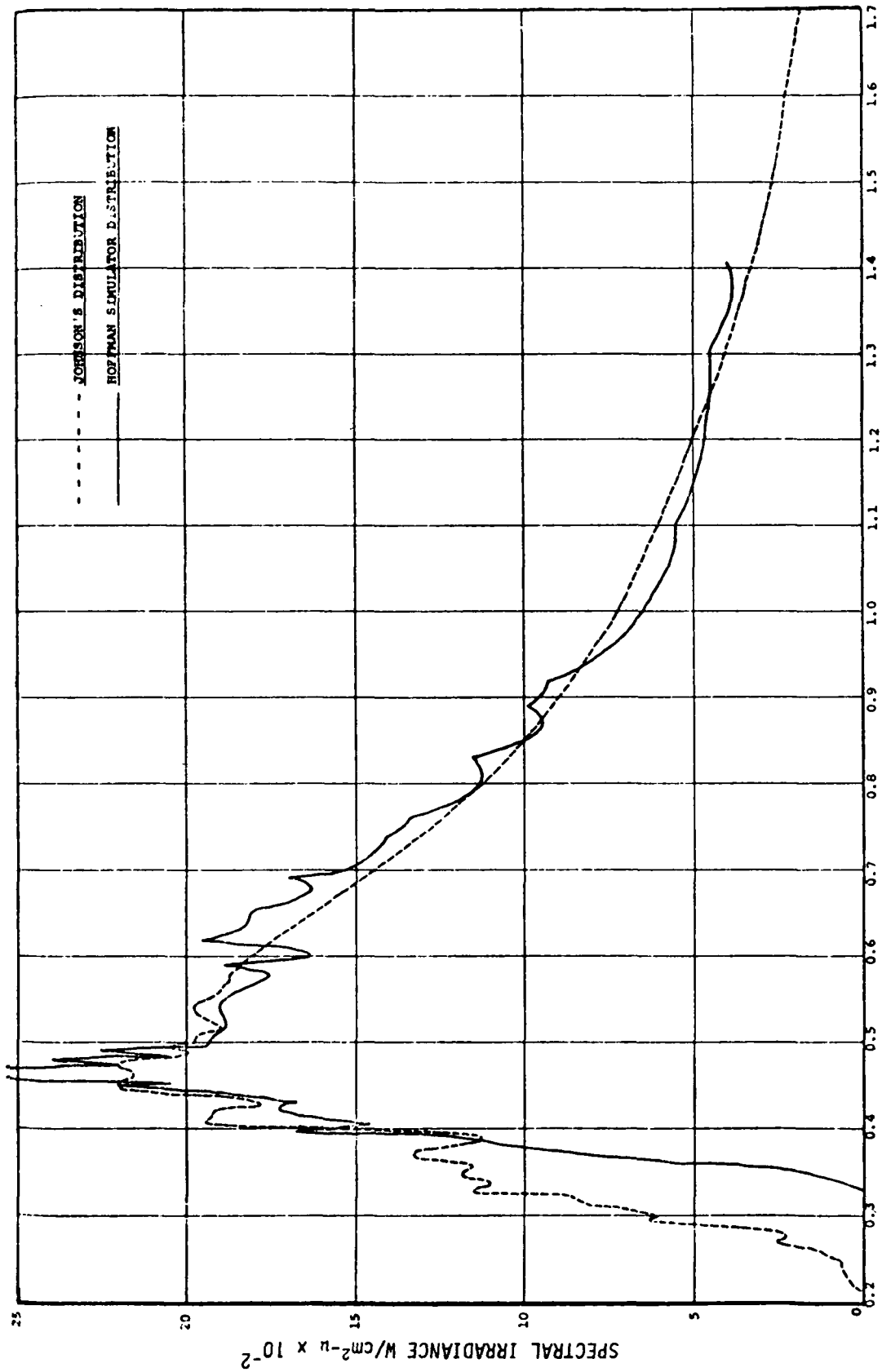

Figure 2.2 Spectral Output, Centralab Solar Simulator[2.4]

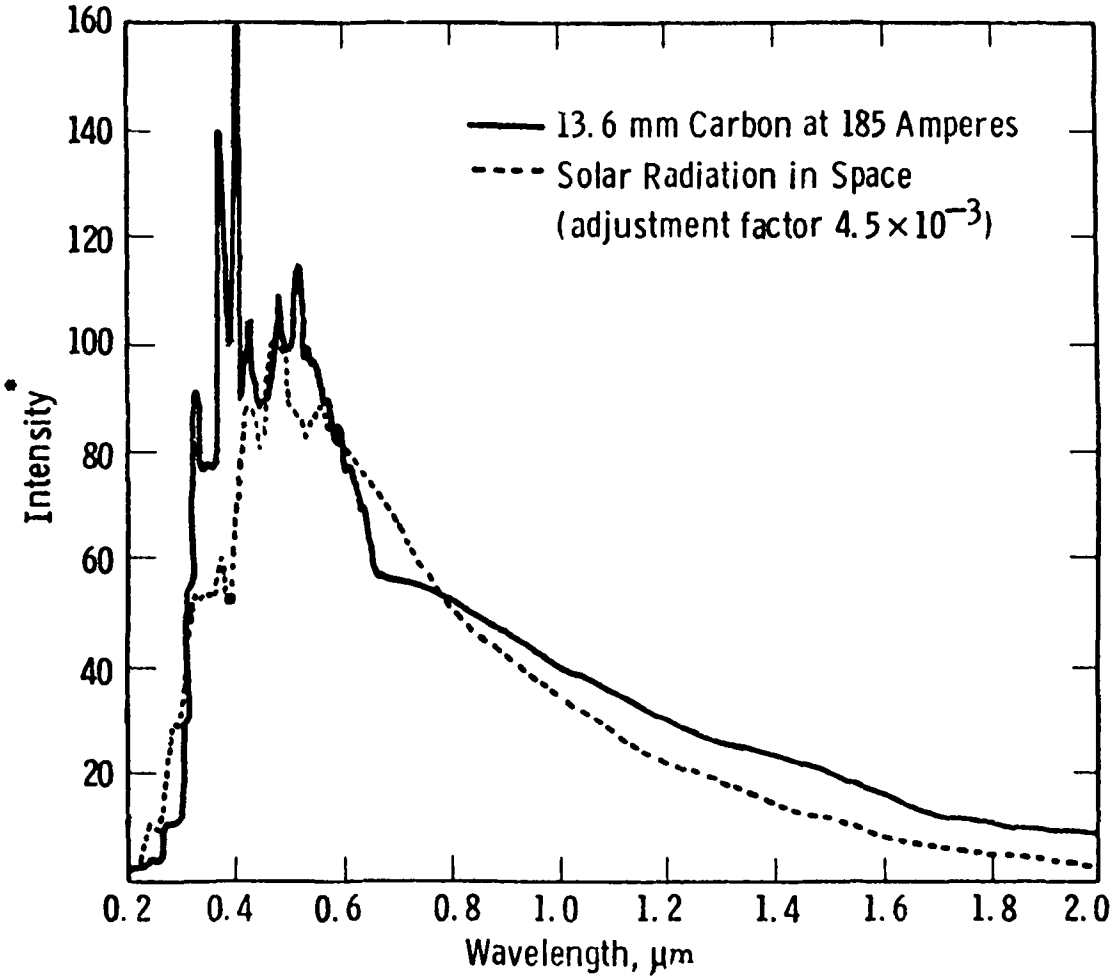

* Microwatts per cm^2 at 1 meter per 0.1 micron for 1 mm^2 of the source

Figure 2.3 Spectral Output, Carbon Arc Solar Simulator[2.5]

The extent to which a lack of solar spectral match affects a solar cell measurement can be estimated if the spectral intensity of the light source and the spectral response of the solar cell are known. The light generated current of the illuminated cell can be calculated as follows:

$$I_L\ (A/cm^2) = \int R(\lambda).E(\lambda)\ d\lambda \qquad (2.1.1)$$

where $R(\lambda)$ = solar cell response as a function of wavelength, A/W

$E(\lambda)$ = spectral irradiance, W/cm^2-μm

$d\lambda$ = an increment of wavelength, μm

The above equation can be used to determine the light-generated currents under solar and simulator illuminations. The generated current under solar illumination can be calculated from the generated current under simulator illumination if the spectral response of the cell if the spectral irradiance of the simulator is known. The relation is as follows:

$$I_L(\text{space}) = I_L(\text{simulator})\ \frac{\int R(\lambda)\cdot E(\lambda)_{\text{space}}\ d\lambda}{\int R(\lambda)\cdot E(\lambda)_{\text{sim.}}\ d\lambda} \qquad (2.1.2)$$

Solar simulator intensities are determined by the short circuit current outputs of calibrated primary or secondary standard cells. The primary standard cells, commonly in use, were generated by a NASA/JPL program of telemetered balloon flights. [2.9, 2.10] Similar programs have been conducted by aircraft and high altitude terrestial measurements.[2.11-2.14] When the effects of atmospheric absorption are properly corrected, the results are in good agreement with the balloon flight data.[2.15]

Primary standard cell availability is limited and they are considered too valuable for general usage in setting simulator intensities. For this reason, secondary standard cells are calibrated for use as working standards. Palmer has recently reviewed the methods of generating secondary standard cells and concluded that previously proposed methods of calibration may yield poor results. [2.16] Palmer has proposed the use of alternate methods which insure that secondary standard cell calibration accuracy will approach that of primary standard cells. [2.16] A solar simulator intensity which produces a standard cell response equal to that for free space at one AU is referred to as one sun, air mass zero or 135.3 mW/cm^2 (formerly 139.5 mW/cm^2). Solar simulator spectral quality should be monitored by use of narrow bandpass or cutoff filters with calibrated spectral response detectors.

2.2 Current-Voltage Characteristics

The measurement of solar cell current-voltage characteristics is the primary means of evaluating the device. The evaluation is made by measuring the cell voltage developed and the cell current into load resistances varying between zero and infinity. The measurement is simple in principle but attention to several practical details is necessary to insure accurate results. Solar cell response is a strong function of temperature. For this reason, the cell must be in thermal equilibrium at a known temperature during the measurement. With adequate heat sinking and cooling, cells measured under one sun irradiance at room temperature can be stabilized at 28°C. To insure that the voltages measured are representative of those developed on the cell contacts, separate probes are employed to measure cell voltage and current. In this way, any voltage drops which occur at the current probe-cell interfaces due to contact resistance do not cause errors in

the measured cell voltage. The load resistance may be varied manually or electronically. The current voltage data is usually plotted with an X-Y recorder. The solar cell parameters such as I_{sc} and V_{oc} can be read directly with digital meters. Multiplier circuits are available which produce a voltage proportional to the product of cell voltage and current. This output is plotted as a function of cell voltage to directly indicate the maximum power and voltage at maximum power. The cell series resistance is also determined from current-voltage characteristics at two or more different illumination levels. [2.17, 2.18]

2.3 Spectral Response Measurements

Spectral response measurements are very useful for evaluating changes in solar cells due to radiation effects. The spectral response (A/W) is a measure of the short-circuit current density generated by the cell under various monochromatic illuminations of a known power density. The spectral response is often reported in terms of relative units when absolute values of light intensities are not determined. Various schemes have been used to measure the spectral response of solar cells. High resolution monochromators are used when extreme accuracy is desired. When less accuracy is needed, narrow bandpass filters can be used as sources of monochromatic light. When a monochromator is used, there are two methods to normalize the solar cell output to the light intensity. Tungsten light sources are usually used in monochromators, and the entrance slit width can be varied to control the optical power density illuminating the cell under test. In some systems, the entrance slit width can be automatically controlled to maintain a constant optical power density on the solar cell. An alternate approach is to maintain a constant slit width and allow the optical power density on the cell to vary with wavelength, and attenuate the cell response at each wavelength measured by use of calibrated voltage dividers.

One disadvantage of these methods of measurement is that the solar cell response is determined at very low minority carrier injection levels. Solar cells irradiated with neutrons and protons have response

characteristics which are dependent upon the concentration of injected minority carriers. In such cases the cell must be illuminated with a light source similar in intensity and spectral content to the intended space environment during the spectral response evaluation. A scheme for measuring spectral response under approximate solar illumination has been suggested by Stofel.[2.19]

2.4 Irradiation Methods

The evaluation of solar cell radiation effects requires a wide range of specialized equipment and instrumentation. Charged particle accelerators are the primary sources for space radiation simulation. The range of electron energies of interest is 0.3 to 10 MeV. Electron energies of 0.3 to 3 MeV are usually obtained with Van de Graaff electrostatic or Dynamatron accelerators. Higher electron energies can be reached with linear electron accelerators. Proton energies from 0.1 to 3 MeV are obtained with Van de Graaff accelerators. Proton energies greater than 10 MeV can be obtained from cyclotrons. For lower energy protons, it is necessary to transport the proton beam and perform the irradiation in vacuum to avoid excessive energy losses. A survey of accelerator facilities has been published but is currently out of date.[2.20] The Space Radiation Effects Laboratory at Newport News, Virginia is operated for NASA specifically for space radiation simulation.[2.21] The facilities include accelerators for all electron energies of interest and a 600 MeV synchrocyclotron. Accelerators invariably produce irradiation rates which are many orders of magnitude greater than those of space environments. Real time irradiations of solar cells have been done using beta emitting sources.[2.22, 2.23] These sources generate a spectrum of electron energies and fluxes similar to that of some space environments.

A successful experiment must include accurate knowledge of the particle energy, measurement of cross sectional beam intensity at the irradiation area, as well as the intensity during the irradiation. Although there are several methods of accomplishing the above measurements, all can be done with a Faraday cup. A design of a Faraday cup

suitable for accelerators in the 1 MeV range is shown in the literature.[2.24] The desirable characteristics of a Faraday cup are as follows:

a. Shielding thickness must exceed particle energy range.

b. A high cup length-to-diameter ratio is desirable.

c. Use low Z (atomic number) materials to reduce secondary electron emission and bremsstrahlung production.

d. Cup must be in vacuum or potted.

e. Cup should be a reentrant cavity.

f. Cup should be screened to suppress secondary electron emission if necessary.

g. Cup should have remote X-Y translation to facilitate beam mapping.

A Faraday cup requires a current measuring instrument which operates in the range of 10^{-10} to 10^{-6} amperes and integrates charge. Instruments of this nature are produced by Keithley Instruments, Cleveland, Ohio and Elcor Products, Silver Spring, Maryland.

The particle energy can be determined by means of a range-energy measurement. In this measurement, increasing thickness of absorbers are introduced into a constant flux beam, while the flux of particles exiting the absorber is monitored with a Faraday cup or a radiation-degraded solar cell. If the beam is monoenergetic, a plot of cup current (or cell photocurrent) versus absorber thickness is extrapolated to zero current at an absorber thickness which is equal to the projected range of the mean particle energy of the beam. This technique is satisfactory for electrons and high energy protons. Since the beam current must remain constant as absorber thickness is increased, a second independent means of monitoring beam current must be available. Van de Graaff generators are equipped with a generating voltmeter which produces a dc voltage proportional to the potential difference on the accelerator tube. A check calibration at one operating energy is sufficient to insure accurate calibration. Corrections must be made for energy loss in the accelerator exit window and in the atmosphere between the exit port and the target.

2.5 Diffusion Length Measurement

The importance of minority carrier diffusion length (or lifetime) in the study of solar cells was discussed in Section 1.0. The changes in this parameter are of primary importance in the solar cell degradation in radiation environments. A method using gamma ray irradiation for experimental measurement of minority carrier diffusion length was suggested by Gremmelmaier.[2.25] This technique requires the uniform generation of electron-hole pairs throughout the active volume of the p-n junction device. Under these conditions the generated current density (J_L) is expressed as follows:

$$J_L = e\, q_o (L_p + W + L_n) \qquad (2.5.1)$$

where e = electronic charge

q_o = generation rate of electron-hole pairs

L_p = hole diffusion length in an n-type layer

W = width of space charge layer

L_n = electron diffusion length in a p-type layer

Since L_p and W are usually very small compared to L_n, they may be neglected, and the measured short circuit current becomes proportional to the diffusion length in the p-type base region (L_n). The generation rate, determined for this uniform radiation, thus allows accurate determination of diffusion length from the measured short circuit current.

There are several experimental methods of uniformly injecting electron-hole pairs. In addition to the use of gamma radiation, high energy electrons, high energy protons[2.26] and infrared light[2.27, 2.28] have been used to achieve uniform injection. To achieve uniform injection in a solar cell irradiated with 1 Mev electrons, it is necessary to introduce a 0.030 cm (0.012 in.) aluminum shield immediately in front of the cell during a normal incidence front irradiation. The details of this procedure and the experimental evaluation of the generation rate have been covered by Rosenzweig.[2.26]

The experimental measurement of diffusion length by the above methods has several inherent limitations. Since the diffusion length is that distance from which 1/e of injected minority carriers will diffuse to the junction during their lifetime, the diffusion length concept involves both minority carrier lifetime and diffusion. Minority carrier lifetime, in the most general case, could vary throughout the active region of a solar cell. In practice this situation arises when solar cells are irradiated with low energy protons which do not penetrate the entire active volume of the cell. Diffusion lengths of solar cells with a nonuniform minority carrier lifetime in the active base region cannot be measured by the above methods. Surface recombination at the solar cell back contact can also cause errors in measured diffusion lengths. These errors are negligible for cells in which the thickness exceeds two or three times the diffusion length.

The measurement of diffusion length by the above methods also assumes the external cell-current generated is collected entirely by diffusion of excess minority carriers to the junction. Some recent designs of solar cell structure utilize "drift fields." In such cases, excess minority carrier collection is aided by the presence of an electric field in the base region; and the short circuit current under conditions of uniform pair production cannot be related to diffusion length by the above equation.

An additional limitation arises if 1 MeV electron or other high energy radiations are used in the diffusion length measurement. The radiation flux must be kept low to minimize damage to the cell during the measurement. The 1 MeV electron beam current during such a measurement is approximately 10^{-9} A/cm^2. The generation rate of excess minority carriers produced by this electron flux is considerably lower than that produced by solar illumination at 135 mW/cm^2. In most cases the diffusion length or lifetime is not dependent upon the concentration of excess minority carriers. In such cases, the diffusion length measured with low levels of injected minority carriers is the same as that for a cell under

one sun illumination. Silicon solar cells irradiated with protons and neutrons exhibit injection level dependence of the diffusion length, and must be illuminated with simulated solar illumination to allow accurate measurement of the diffusion length. The schemes used by Denney[2.29] for proton irradiated cells and Stofel, et al.[2.19] for neutron irradiated cells have shown that the diffusion lengths of such cells measured under approximate solar illumination are roughly two times greater than that measured under low injection level conditions.

2.6 Statistical and Error Analysis

The analysis of radiation effects in solar cells involves the collection and evaluation of large amounts of experimental data. Such data are often presented in graphical or tabular form without the use of statistical analysis. The basic statistical tools, which have application in the analysis of radiation effects data, along with the nature and causes of errors in the data, will be discussed.

A common situation in the analysis of irradiated solar cells involves measurements of engineering or physical parameters on a group of solar cells exposed to a particular environment or radiation fluence. The characteristics of such a data set are a central tendency and a distribution about this central value. The most suitable measure of the central tendency is the arithmetic mean ($\bar{x}$). The arithmetic mean is defined as follows:

$$\bar{x} = \sum_{i=1}^{n} \frac{x_i}{n} \qquad (2.6.1)$$

where x_i = measured value on cell i

n = number of cells measured

The degree to which measured values are dispersed or scattered can be described in several ways. One such measure is the range or difference between the largest and smallest measured values in a group. A second measure of the dispersion in a group of measurements is the standard deviation. The standard deviation (σ) is defined as follows:

$$\sigma = \left[\sum_{i=1}^{n} \frac{(x_i - \bar{x})^2}{n - 1} \right]^{\frac{1}{2}} \qquad (2.6.2)$$

An additional measure of dispersion is the variance, which is defined as the square of the standard deviation (σ^2).

Solar cell evaluations usually involve sample sizes of less than 30 and more often from 3 to 10. When such small sample sizes are used, the mean of experimental results may not be representative of a similar experiment involving a large number of samples. The maximum difference which may occur between the mean value of a small sample and the mean value of a large sample having a normal or Gaussian distribution can be calculated for any desired probability. This difference is referred to as the confidence limits of a mean value. The confidence limits expressed relative to the mean value are as follows:

$$\bar{x} \pm t_c \frac{\sigma}{\sqrt{n}} \qquad (2.6.3)$$

where t_c is the critical percentile value for Students' t distribution. Values of t_c may be obtained from statistical manuals or handbooks. For example, if 95% confidence levels are desired for a sample size of 5, t_c is equal to 2.78.

When solar cell experimental data are collected for increasing radiation fluences, it is desirable to display the data graphically in a manner which reveals fundamental empirical relationships. As an example, it has been empirically observed that many parameters of irradiated solar cells such as I_{sc}, V_{oc}, and P_{max} can be described by equations similar to the following relation:

$$P_{max}(\Phi) = P_{maxo} - C \log (1 + \Phi/\Phi_x) \qquad (2.6.4)$$

where $P_{max}(\Phi)$ = maximum power to load at fluence Φ

P_{maxo} = maximum power to load before irradiation

Φ = radiation fluence

Φ_x = a constant dependent on radiation energy and cell type

C = a constant dependent on radiation type

Computer programs can be employed to fit equations to experimental data. In most cases, however, curves can be fitted to experimental data by manual means as well.

The coefficient of correlation is a measure of the degree to which an analytical expression can describe variations in experimental data. The coefficient of correlation is defined as follows:

$$r = \pm \left[1 - \frac{\sum_{i=1}^{n} (x_i - x_{eqn})^2}{\sum_{i=1}^{n} (x_i - \bar{x})^2} \right]^{\frac{1}{2}} \qquad (2.6.5)$$

where x_{eqn} = value of x from fitted analytical expression

$\bar{x}$ = mean value of experimental data

x_i = experimentally observed value

If the fitted analytical expression or curve has a correlation coefficient of 1, it explains all of the experimentally observed variation. If an unexplained variation exists, the correlation coefficient will be between -1 and +1. It is usually possible to describe experimental solar cell data by expressions which have correlation coefficients very close to one. A few examples of the application of statistical methods to solar cell data have appeared in the literature.[2.30, 2.31, 2.32]

In addition to the random errors that affect data, there are systematic errors which are inherent to the operation of instruments. These errors involve limitations of the accuracy with which electron fluence, electron energy, solar simulator intensity, etc., can be determined with particular instruments. When an experiment is designed, it is desirable to insure that the random and systematic instrumentation errors are negligible or minor with respect to the accidental errors. In such cases, the results can be analyzed assuming that the dispersion or distribution in a group of measurements is due only to the accidental error and characteristic deviation in the sample group due to manufacturing differences.

REFERENCES

2.1 F. S. Johnson, J. of Meteorology, Vol. 11, 6, 431, 1954.

2.2 Anon, "Solar Electromagnetic Spectrum", NASA SP 8005, Revised, May, 1971.

2.3 Courtesy of J. Castle, Spectrolab.

2.4 D. B. Bickler, "The Hoffman Solar Simulator", Proceedings of the Solar Working Group Conf., Vol. II, 6-1, Feb 1962.

2.5 J. M. Hicks, "Solar Cell Neutron Investigation", AFAPL-TR-70-24, May 1970.

2.6 R. W. Opjorden, "Pulsed Xenon Solar Simulator System", Conf. Record of the Eighth IEEE Photovoltaic Specialists Conf., 312, 1970.

2.7 Anon, "Large Area Pulsed Solar Simulator", Marketing Data, TRW Systems Group.

2.8 J. H. Goncz and P. B. Newell, "Spectra of Pulsed and Continuous Xenon Discharge", J. Opt. Soc. Am., 56, 1, 87, 1966.

2.9 J. A. Zoutendyk, "The Space Calibration of Standard Solar Cells Using High-Altitude Balloon Flights", Proceedings of the Fourth Photovoltaic Specialists Conf.,Vol II, C-4, 1964.

2.10 D. W. Ritchie, "Development of Photovoltaic Standard Cells for NASA",ibid., C-5.

2.11 F. J. McKendry, H. W. Kuzminski and C. P. Hadley, "Comparison of Flight and Terrestral Solar Measurements on Silicon Cells, ibid, C-3.

2.12 H. W. Brandhorst, Jr., "Airplane Testing of Solar Cells", ibid, C-2.

2.13 M. Audibert, "Calibration of Solar Cells for Space Applications" Solar Cells, Gordon and Breach Science Publishers, London, 1971.

2.14 M. W. Walkden, "Calibration of Solar Cells in Uncollimated Sunlight", ibid.

2.15 H. W. Brandhorst, Jr., "Calibration of Solar Cells Using High-Altitude Aircraft", ibid.

2.16 J. M Palmer, "Solar Cell Standardization: A Practical Approach to Secondary Standard Generation", ibid.

2.17 R. J. Hardy, "Theoretical Analysis of the Series Resistance of a Solar Cell", Solid-State Electronics, 10, 765, 1967.

2.18 M. S. Imanura and J. I. Portscheller, "An Evaluation of the Methods of Determining Solar Cell Series Resistance", Conf. Record of the Eighth IEEE Photovoltaic Specialists Conf., 102, 1970.

2.19 E. J. Stofel, et al., "Neutron Damage to Silicon Solar Cell",IEEE Trans. on Nuc. Science, NS-16, 5, 97,, 1969.

2.20 D. J. Hamman and W. H. Veazie, Jr., "Survey of Particle Accelerations", REIC Report No. 31, Part II, Sept. 15, 1964.

2.21 SREL Users Handbook, Space Radiation Effects Laboratory, Newport News, Virginia.

2.22 D. L. Reynard and D. G. Peterson, "Results of a Real-Time Irradiation of Lithium P/N and Conventional N/P Silicon Solar Cells", Conf. Record of the Ninth IEEE Photovoltaic Specialists Conf. , 303, May 1972.

2.23 M. C. Whiffen and E. B. Trent, "The Effects of Radiation on Lithium Doped Solar Cells", Lockheed-Georgia Co., Report # ER-11150, July 1971.

2.24 F. M. Smits, et al., "Report of Solar Cell Work at Bell Telephone Laboratories", Proceedings of Solar Working Group Conf., Vol. I, 9-1, Feb. 1962.

2.25 R. Gremmelmaier, "Irradiation of P-N Junctions with Gamma Rays: A Method for Measuring Diffusion Lengths", Proc. I.R.E., 46, 6, 1045, 1958.

2.26 W. Rosensweig, "Diffusion Length Measurement by Means of Ionizing Radiation", Bell Systems Tech. J. 41, 1573, 1962.

2.27 J. R. Bilinski, et al., "Proton-Neutron Damage Equivalence in Si and Ge Semiconductors", IEEE Trans. on Nuc. Science, NS-10, 5, 71, 1963.

2.28 B. L. Gregory, "Minority Carrier Recombination in Neutron Irradiation Silicon", IEEE Trans. on Nuc. Science, NS-16, 6, 53, 1969.

2.29 J. M. Denney and R. G. Downing, "Proton Radiation Damage in Silicon Solar Cells", TRW Systems Report No. 8653-6026-KU-000, 16 July 1963.

2.30 E. L. Brancato, "Determination of Significant Differences in Solar Cell Experiments", Transcript of the Photovoltaic Specialists Conf., Vol. I, B-5-1, April 1963.

2.31 D. L. Reynard, "Engineering Experimental Program on the Effects of Near-Space Radiation in Lithium Doped Solar Cells", Philco-Ford Report WDL-TR4725, 10 Nov. 1971.

2.32 D. J. Curtin and A. Meulenberg, "Statistical Analysis of One MeV Electron Irradiation of Silicon Solar Cells", Conf. Record of the Eighth IEEE Photovoltaic Specialists Conf., p. 193, 1970.

CHAPTER 3

3.0 RADIATION EFFECTS

The behavior of solar cells in a radiation environment can be described in terms of the changes in the engineering output parameters of the devices. This approach limits the understanding of the physical changes which occur in the device. Since other environmental factors may need consideration, an understanding of a physical model provides a basis for estimates of the behavior in a complex environment. In addition, solar arrays of the future will become more complex and may utilize materials which are affected by different aspects of radiation damage. For these reasons, the engineer should be aware of all aspects of the interaction of radiation with matter, and understand the physical models which describe the processes.

3.1 The Theory of Radiation Damage

The radiation usually of interest in the study of degradation of materials and devices consists of energetic or fast massive particles (i.e., electrons, protons, neutrons, or ions). The origin of these particles may be particle accelerators, the natural space radiation environment, nuclear reactions, or secondary mechanisms such as Compton electrons produced by gamma rays. Because they have mass, energy and possibly charge, these particles or other particles generated by them can interact in several ways with materials. The dominant interactions are:

a. Inelastic Collisions with Atomic Electrons. Inelastic collisions with bound atomic electrons are usually the predominant mechanism by which an energetic charged particle loses kinetic energy in an absorber. In such a collisions, electrons experience a transition to an execited state (excitation) or to an unbound state (ionization).

b. Elastic Collisions with Atomic Nuclei. Energetic charged particles may have coulombic interactions with the positive charge of the atomic nucleus through Rutherford scattering. In some cases the amount of energy transferred to the atom will displace it from its position in a crystalline lattice.

This energetic displaced atom may in turn undergo similar collisions with other atoms of the material. Energetic particles may also interact directly by a hard sphere collision with the nucleus. The probability of this type of event is usually less than that for Rutherford scattering, except at higher energies. If sufficient energy is transferred to displace an atom from its lattice site, that atom will probably be energetic enough to displace many other atoms.

c. Inelastic Collisions with Atomic Nuclei. This general category of interaction includes several processes which are important in radiation damage studies. Highly energetic protons undergo inelastic collisions with the atomic nucleus. In this process the energetic proton interacts with the nucleus and leaves the nucleus in an excited or activated state. The excited nucleus emits energetic nucleons and the recoiling nucleus is displaced from its lattice site. This recoiling nucleus in turn causes more displacements. This process is also referred to as spallation. Collisions between neutrons of thermal energy and nuclei can also be included in this group. However, these interactions are of little importance in solar array degradation.

The major types of radiation damage phenomena in solids which are of interest to the solar array designer are ionization and atomic displacement. It is important to classify an effect into one of these two categories, if possible, because the general behavior of each phenomenon has been characterized to a large extent.

Ionization

Ionization is the process of removing orbital electrons from an atom. It may occur in atoms or molecules in gases, liquids or solids. The measure of the intensity of an ionizing radiation is the Roentgen. This unit is defined by a charge generation of 2.58×10^{-4} coulomb/kilogram of air. The measure of the absorbed dose in any material of interest is usually defined in terms of the absorbed energy per unit mass. The accepted unit of absorbed dose is the rad (100 ergs/gm or 0.01 joules/kg).

Through the use of the concept of absorbed dose, various radiation exposures can be reduced to absorbed dose units which will reflect the degree of ionization damage in the material of interest. This concept can be applied to electron, gamma and X-ray radiations of all energies. For electrons, the particle fluence is multiplied by the electronic stopping power of the electron energy of interest to determine the absorbed dose. In this manner, the effects of an exposure to fluxes of trapped electrons of various energies in space can be reduced to an absorbed dose. In general, this practice is also applicable to proton irradiations; however, some caution must be exercised. In some types of materials, the effects of the ionization caused by heavy particles is confined to the vicinity of the particle track. If homogeneous ionization is produced by protons in the absorber material of interest, one can convert proton fluences to absorbed doses and sum them with doses from other radiations.

The variations of stopping power and range for electrons and protons of various energies can be seen in Figures 3.1 and 3.2. The data presented are for silicon and have been normalized for density in the usual manner. The stopping power and range of a fast particle are not strong functions of the atomic number of the absorber material. For this reason, the data in Figures 3.1 and 3.2 can be used for materials with a similar atomic number with a negligible error.

Radiation may affect solar cell array materials by several ionization-related effects. The reduction of transmittance in solar cell cover slides is an important effect of ionizing radiation. The darkening is caused by the formation of color centers in glass or oxide materials. The color centers form when ionizing radiation excites an orbital electron to the conduction band. These electrons become trapped by impurity atoms in the oxide to form charged defect complexes which can be relatively stable at room temperature. Radiation produces similar darkening effects which may be observed in cover slide coatings and adhesives.

Radiation produces many ionization-related effects in organic materials. These changes all result from the production of ions, free electrons, and free radicals. As a result of these actions, transparent polymers are

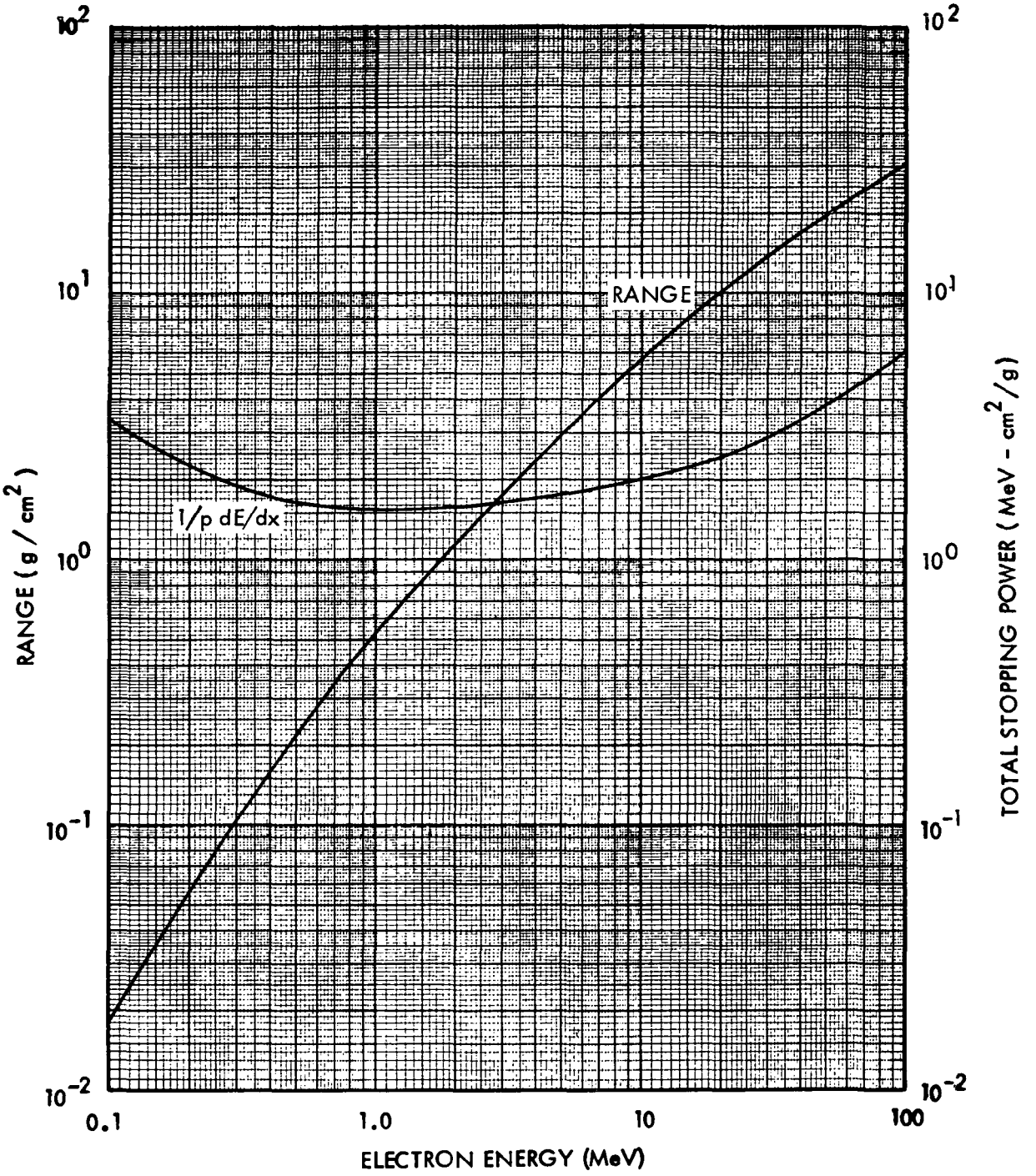

Figure 3.1 Stopping Power and Range Curves for Electrons in Silicon, Reference, Berger and Seltzer, NASA SP-3036, 1966.

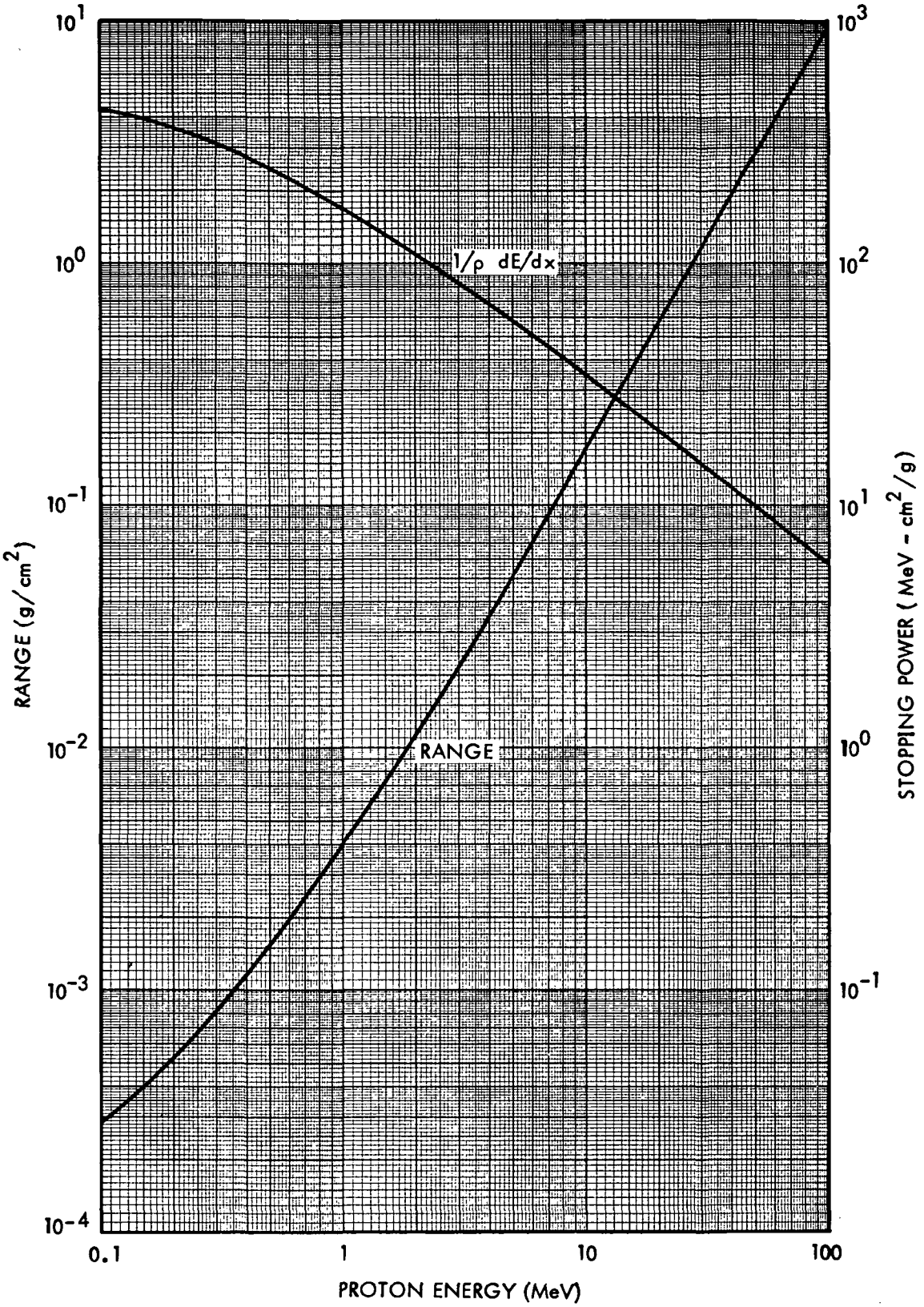

Figure 3.2 Stopping Power and Range Curves for Protons in Silicon. Reference, Janni, AFWL-TR-65-150, 1966.

darkened and crosslinking between main-chain members may drastically alter the mechanical properties. The contemplated use of polymeric materials in flexible extended solar arrays will require the array designer to have knowledge of the ionization-related radiation effects in those materials.

The use of silicon dioxide as a surface passivation coating and dielectric material in silicon devices is the reason for a wide range of ionization-related radiation effects in electronic hardware. The development of trapped charges in these oxides may cause increased leakage currents, decreased gain, and surface channel development in bipolar transistors and increased threshold voltages in MOS field effect transistors. The presence of ionizing radiation in silicon excites the electrons of the valence band to the conduction band, creating electron-hole pairs in much the same way that carrier pairs are generated by visible light. Although an optical photon of energy equal or greater than 1.1 eV will create an electron-hole pair, roughly three times this amount of energy must be absorbed from a high energy particle to produce the same carriers. In silicon devices, the electron-hole pairs which are generated by ionizing radiation cause photocurrents in the same manner as solar illumination.

Atomic Displacement

The loss of energy by fast electrons and protons caused by collision processes with the electrons of an absorber or target material account for a large fraction of the dissipated energy. For electrons and protons in the range of 0.1 to 10 MeV, these electron collisions determine the particle range in an absorber. Despite this fact, a different type of collision process is the basis for the damage which permanently degrades silicon solar cells in the space environment. The basis for this damage is the displacement of silicon atoms from their lattice sites by fast particles in the crystalline absorber. These displaced atoms undergo other reactions and finally form stable defects which produce significant changes in the equilibrium carrier concentrations and the minority carrier lifetime.

The displacement of an atom from a lattice site requires a certain miminum energy similar to that of other atomic movements. The energy of sublimation for a silicon atom is 4.9 eV. The energy for the formation of a vacancy in the silicon lattice is 2.3 eV. The displacement of an atom involves the formation of a vacancy, the formation of an interstitial atom and other electronic and phonon losses. It is reasonable to expect that the energy of displacement is several times larger than the energy of formation for a vacancy. Seitz has estimated that the displacement energy is roughly four times the sublimation energy.[3.1] Electron threshold energies of 145 keV and 125 keV have been reported by various investigators.[3.2, 3.3, 3.4] The following equation relates the electron threshold energy to the displacement energy.[3.1]

$$E_d = 2 \frac{m_e}{M} \frac{E_t}{m_e c^2} (E_t + 2 m_e c^2) \qquad (3.1.1)$$

where E_d = displacement energy (MeV)

E_t = threshold energy (MeV)

m_e = electron mass (1/1836)

M = atomic weight, Si (28)

$m_e c^2$ = electronic mass-energy equivalence, 0.511 MeV

The reported threshold energies indicate displacement energies of 12.9 eV or 11.0 eV, respectively.

Although proton threshold energies have not been determined, they can be calculated from the classical form of the above equation:

$$E_d = \frac{4 \cdot M_p \cdot M}{(M_p + M)^2} E_t \qquad (3.1.2)$$

where M_p = proton mass, 1. The above values of displacement energies indicate proton or neutron thresholds of 97.5 or 82.5 eV in silicon. Since particles below the threshold energies cannot produce displacement damage, the space environment energy spectrums are effectively cut off below these values.

For particles above the threshold energy, the probability of an atomic displacement can be described in terms of a displacement cross section. Using this concept, the number of displacements can be estimated from:

$$N_d = n_a \sigma \bar{\nu} \Phi \qquad (3.1.3)$$

where N_d = number of displacements per unit volume

n_a = number of atoms per unit volume of absorber (5×10^{22} silicon atoms/cm^3)

σ = displacement cross section (cm^2)

$\bar{\nu}$ = average displacements per primary displacement

Φ = radiation fluence (particles/cm^2)

The displacement cross sections for fast electrons of various energies can be calculated from the relativistic generalization of the Rutherford scattering cross section equation.[3.1] For silicon, the calculated displacement cross section for 1 MeV electrons is about 68×10^{-24} cm^{-2} and increases only 10% for electron energies of 5 MeV and greater. The electron displaced silicon atom may receive enough energy to in turn displace other silicon atoms. The mechanism for these secondary displacements is Rutherford interactions for silicon atoms of energies greater than 10^3 eV and hard sphere collisions for lower energy atoms. Although different theories of the production of secondary displacements have been presented, their results are very similar. Using the model of Kinchin and Pease,[3.5] the average number of displacements in silicon is 1.53 for a 1 MeV electron. The electron energy variation of the various parameters is shown below.

TABLE 3.1

SILICON DISPLACEMENT PARAMETERS, VARIOUS ELECTRON ENERGIES

Electron Energy (Mev)	σ (10^{-24} cm^2)	$\bar{\nu}$	$\sigma\nu$ (10^{-24} cm^2)	$n_a\sigma\bar{\nu}$ (cm^{-1})	$\frac{\Delta N_d/\Delta\Phi}{5.2}$
1	68	1.53	104	5.2	1.0
2	73	2.00	146	7.3	1.4
5	77	2.76	212	10.6	2.0
10	77	3.39	261	13.0	2.5
20	77	4.09	314	15.7	3.0
40	77	4.74	363	18.2	3.5

The direct result of the radiation is the production of vacant lattice sites (vacancies) and silicon atoms which come to rest in the interstices of the crystal lattice (interstitials). The distribution of vacancies will not be uniform, because the vacancies from secondary displacements will lie relatively close to the associated primary vacancy.

The experimental studies must be reviewed to gain a more complete model of displacement damage in silicon. Vacancies and interstitials are reactive chemical species and are particularly mobile and unstable at room temperature. In n-type silicon, it has been shown that vacancies react with oxygen impurities to form close coupled vacancy-oxygen pairs (V-O)[3.6-3.9] (see Figure 3.3), and with impurity donor atoms, such as phosphorus and arsenic, to form close coupled vacancy-donor pairs (V-P, V-As)[3.6, 3.10] (see Figure 3.3). Both defects are electrically active and can become negatively charged by accepting an electron from the conduction band. The acceptor energy levels of the V-O and V-P pairs are 0.17 eV and 0.4 eV below the bottom of the conduction band.[3.11, 3.12] These defects are recombination centers and their formation during electron irradiation of n-type silicon reduces the minority carrier lifetime.[3.13] Since these defects are formed from single vacancies, considerations of

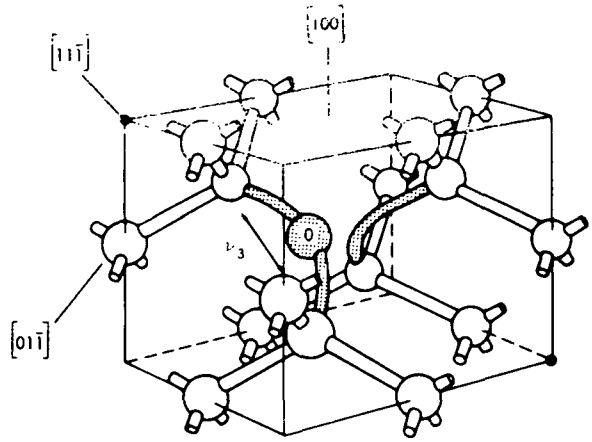

A model of the oxygen-vacancy complex or the Si-A center.

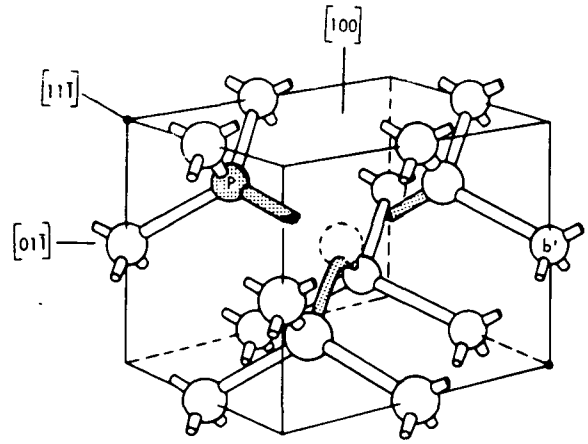

A model of the phosphorus-vacancy complex or the Si-E center.

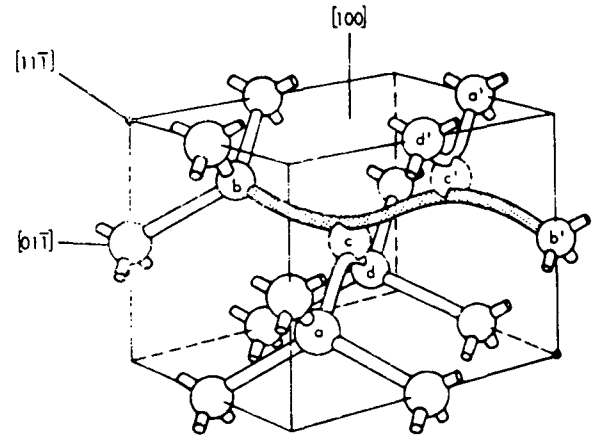

Model of the divacancy.

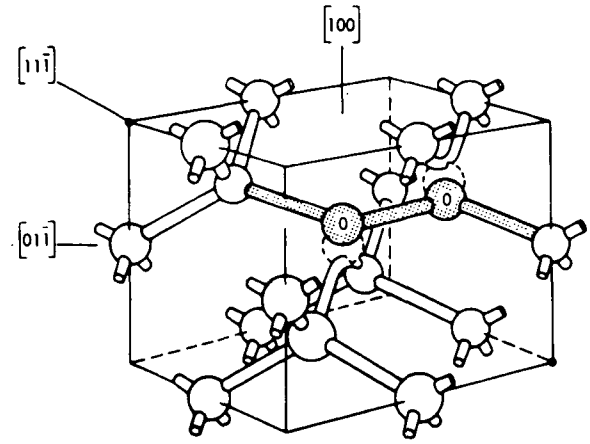

RCA tentative model for the K-center.

Figure 3.3 Atomistic Models of Radiation Defects in Silicon
Reference, M. M. Sokoloski, "Structure and Kinetics of Defects in Silicon" NASA TN D-4154, 1967

mass action indicate that the formation of these defects might have the same variation with incident electron energy as that for the formation of single vacancies ($\sigma\bar{v}$). This relationship has been verified experimentally.[3.14] The V-P pair anneals rapidly near 150 C[3.15] and the V-O pair anneals rapidly near 350°C.[3.9] The introduction rates (change in defect concentration per unit fluence) for these defects are in the range of 0.1 to 0.3 cm^{-1} for 1 MeV electrons. Since the calculated displacement rate is 5.2 cm^{-1}, it appears that many of the vacancies are involved in other reactions at room temperature, such as recombination with interstitial atoms.

The electron irradiation of p-type silicon at room temperature results in a defect structure with net donor characteristics.[3.11, 3.12] This defect can donate an electron to (i.e., accept a hole from) the valence band. The energy level of this donor defect is located 0.27 to 0.30 eV above the top of the valence band. The room temperature introduction rate of this defect in silicon by 1 MeV electrons is roughly 0.03 cm^{-1}. This value is considerably lower than those of defects found in n-type silicon. In addition, the introduction rate of this defect by 10 MeV electrons is about 16.5 times greater than that for 1 MeV electrons.[3.14] Since the single displacement rate increases by only a factor of 2.5 with that electron energy increase, this defect appears to involve a more complex structure. It has been shown that defects involving the coupling of more than one vacancy will result in defects with introduction rates which increase more rapidly with electron energy than does the displacement rate.[3.16, 3.17] Two defect structures (divacancy[3.18, 3.19] and "K" center[3.20]), which have been studied by electron spin resonance techniques, may explain this behavior. These defects, shown in Figure 3.3, involve the coupling of two vacancies in each defect. Several attempts to determine the dominant recombination center in electron irradiated p-type silicon have yielded conflicting results.[3.11, 3.12, 3.21, 3.22] Recent experiments have indicated that a defect with an energy level in the range of 0.27 ± 0.02 eV above the top of the valence band controls recombination in electron irradiated p-type silicon.[3.22] This conclusion is consistent with the known energy dependence of p-type silicon in that the diffusion

length damage coefficient has been shown to vary with electron energy[3.23] in the same manner as the introduction rate of the E_v + 0.3 eV level defect.[3.12]

The production of displacement damage in silicon by energetic protons is considerably different because the displacement cross sections are several orders of magnitude larger than those for fast electrons and vary rapidly with proton energy. The calculated silicon displacement cross section for 1 MeV protons is 3.5×10^{-20} cm^2.[3.1] The average number of atomic displacements ($\bar{\nu}$) resulting from such a primary displacement is 4.8.[3.5] Using equation 3.1.3, the displacement rate is found to be 8500 cm^{-1} for 1 MeV protons in silicon. The range of a 1 MeV proton in silicon is only 17.5 μm; therefore its energy and displacement rate will change rapidly after it enters a silicon crystal. The variation of the displacement rate with proton energy has been calculated by several authors. These results are shown in Figure 3.4. Although there are some differences in results, the displacement rate is proportional to (lnE)/E for protons of energies between 1 MeV and 10MeV. Above 10 MeV, the various models differ as to the relative influence of Rutherford scattering, nuclear scattering, and inelastic processes of spallation. Experimentally measured defect introduction rates for proton irradiation of silicon are less than one tenth of the calculated displacement rates. The defect energy levels in proton irradiated silicon are those previously discussed for electron irradiated silicon.[3.29-3.31] The proton damage, however, will be highly inhomogeneous because the secondary displacements occur near the site of the primary displacement.

Neutron displacement damage in silicon is characterized by two important differences. The silicon displacement cross section for a 1 MeV neutron is 2.4×10^{-24} cm^2. This value is well below those for 1 MeV protons and 1 MeV electrons. For this reason, the number of primary displaced silicon atoms will be relatively small. The second difference involves the amount of energy transferred to the displaced silicon atom by the neutron. Since the 1 MeV neutron-silicon interaction is a hard sphere rather than coulombic collision, an average of about 70 keV is transferred to the recoiling silicon atoms. The subsequent secondary collisions between silicon atoms will displace about 1500

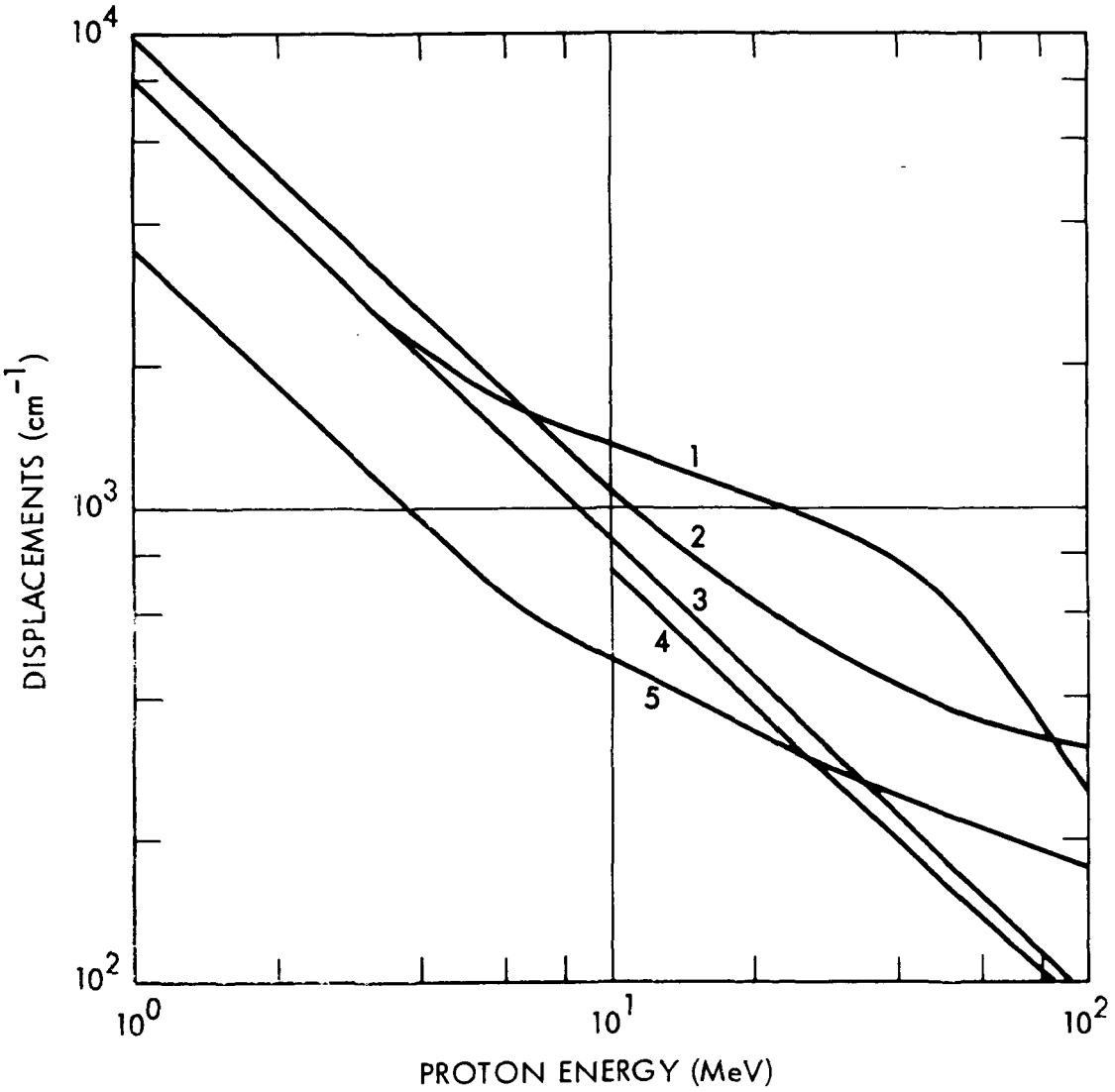

Figure 3.4 Displacement Rate in Silicon for Protons; Curve 1 (ref. 3.24), Curve 2 (ref. 3.25), Curve 3 (ref. 3.26), Curve 4 (ref. 3.27), Curve 5 (ref. 3.28)

silicon atoms. This displacement damage will be clustered near the site of the primary displacement. The defects identified in neutron irradiated silicon include those previously discussed for electron damage. Theoretical models of the neutron damage indicate that the high concentration of electrically active defects in the cluster causes the center of the cluster to behave as intrinsic silicon.[3.32] This intrinsic silicon core is separated from the bulk silicon by a layer of space charge. Extensions of this model have been used to explain the majority carrier removal and minority carrier recombination behavior of neutron irradiated silicon.[3.33-3.35]

The main importance of the displacement defects produced by the irradiation of silicon solar cells is in their effect on the minority carrier lifetime of the silicon. In particular, the lifetime in the bulk p-type silicon of an n-p solar cell is the major radiation sensitive parameter. Since minority carrier lifetimes are inversely proportional to the recombination rates, the reciprocal lifetime contributions caused by various sets of recombination centers can be added to determine the inverse of the lifetime as follows:

$$\frac{1}{\tau} = \frac{1}{\tau_o} + \frac{1}{\tau_e} + \frac{1}{\tau_p} + \cdots \tag{3.1.4}$$

where τ = minority carrier lifetime

τ_o = minority carrier lifetime before irradiation

τ_e = minority carrier lifetime due to electron irradiation

τ_p = minority carrier lifetime due to proton irradiation

One of the most commonly used analytical tools for the determination of the particle type and energy dependence of degradation in silicon solar cells has been developed from the basic relationship for lifetime degradation:

$$\frac{1}{\tau} = \frac{1}{\tau_o} + K_\tau \Phi \tag{3.1.5}$$

where τ = final minority carrier lifetime

τ_0 = initial minority carrier lifetime

Φ = irradiation fluence

K_τ = damage coefficient (lifetime)

Minority carrier diffusion length is a more applicable and more easily determined parameter for solar cell analysis than minority carrier lifetime. Using $L^2 = D\tau$, the above expression becomes:

$$\frac{1}{L^2} = \frac{1}{L_0^2} + K_L \Phi \tag{3.1.6}$$

where L = final minority carrier diffusion length

L_0 = initial minority carrier diffusion length

Φ = particle fluence

K_L = damage coefficient (diffusion length)

$= K_\tau / D$

When the fluence is sufficiently high so that $L << L_0$ we have:

$$K_L = 1/L^2\Phi \tag{3.1.7}$$

If the L vs Φ relationship exhibits the proper -1/2 slope, the damage coefficient, K_L, can be used to uniquely define the particle type and energy dependence of silicon solar cell degradation.

The minority carrier lifetime or diffusion length in an irradiated solar cell may be a function of the concentration of excess or nonequilibrium minority carriers present in the semiconductor. In solar cells, this behavior is referred to as injection level dependence. This behavior is usually associated with solar cells damaged with high energy protons or neutrons. Gregory[3.33] has shown that the injection level dependence of lifetime in neutron irradiated solar cells does not follow classical predictions and has proposed a model based on the behavior of clustered

damage. The methods of measuring minority carrier lifetime or diffusion length often involve the injection of excess minority carrier concentrations which are many orders of magnitude smaller than those found in solar cells operating in space. Such methods are inadequate for the generation of data for the prediction of proton and neutron irradiated solar cell performance in space.

3.2 Theory of Silicon Solar Cell Damage

The basic solar cell equations can be used to describe the changes which occur during irradiation. This method would require data regarding the changes in the light generated current (i.e., I_{sc}), and data regarding changes in the series resistance, shunt resistance, and the basic diode parameters of saturation current and diode quality factor. Although such a method would be a logical analysis, most investigations have not reported enough data to determine the variations in the above parameters. The usual practice in the study of solar cell damage has been to reduce the experimental data in terms of changes in the cell short circuit current, open circuit voltage, and maximum power.

It is also possible to characterize solar cell damage in terms of the changes in the minority diffusion length. Since the diffusion length can be measured experimentally and is a measure of the amount of displacement damage in the base of the solar cell, this method has been suggested. There are several practical and fundamental limitations to this scheme. The most serious limitations involve the evaluation of low energy proton damage in terms of diffusion length. Very low energy protons do considerable displacement damage within the junction space charge region of a solar cell. This nonuniform damage increases the diode saturation current (I_0) and quality factor (n) by mechanisms which are not related to minority carrier diffusion. This damage can cause serious reduction in solar cell V_{oc} without changing the cell diffusion length. In addition, the relation between diffusion length and the solar cell output parameters is not well defined, diffusion length is more difficult to measure than cell output parameters (particularly in the case of proton irradiated cells), and accurate measurement of diffusion length in thin or drift

field cells is extremely difficult. Because of these problems, methods have been evolved to evaluate solar cell radiation effects in terms of common engineering output parameters. Experience has shown that the variation of common solar cell output parameters during irradiation can be descirbed as shown for I_{sc} in the following case:

$$I_{sc} = I_{sco} - C \log \left(1 + \frac{\Phi}{\Phi_x}\right) \tag{3.2.1}$$

The constant Φ_x represents the radiation fluence at which the I_{sc} behavior changes from constant to a direct function of the logarithum of the fluence. The constant C has dimensions of mA/decade fluence and represents the decrease in I_{sc} per decade increase in radiation fluence in the logarithmic region. Although the above relationship is only empirical, there is some theoretical justification for the expression. Several observers have reported that the relation between the solar cell short circuit current and the diffusion length is as follows:[3.36,3.37]

$$I_{sc} = A \ln L + B \tag{3.2.2}$$

The constants A and B are dependent upon the spectral content and intensity of the light source used to measure I_{sc}. Tada has shown that the above expression is theoretically valid over a wide range of diffusion lengths for tungsten illuminations and to a lesser range under solar illumination.[3.38] A previously discussed relation, equation (3.1.6) can be transformed as follows:

$$L = \left(K_L \Phi + \frac{1}{L_o^2}\right)^{-1/2} \tag{3.2.3}$$

and substituted in equation (3.2.2). The resulting expression

$$I_{sc} = B - \frac{A}{2} \ln \left(K_L \Phi + \frac{1}{L_o^2}\right) \tag{3.2.4}$$

has the same form as equation (3.2.1).

The variation of solar cell V_{oc} during irradiation also may be empirically characterized by an expression similar to equation (3.2.1).

$$V_{oc} = V_{oco} - C' \log \left(1 + \frac{\Phi}{\Phi_x}\right) \tag{3.2.5}$$

In general the open circuit voltage of a silicon solar cell can be represented by the following equation which was discussed in Chapter 1:

$$V_{oc} = \frac{kT}{q} \ln \frac{I_{sc}}{I_o} \tag{3.2.6}$$

In using this expression, it is assumed that the saturation current (I_o) is dominated by the diffusion component. In such cases the saturation current density is given by equation (1.2.5). If this expression is combined with equation (3.2.3), the following expression for the saturation current as a function of radiation fluence is obtained:

$$I_o = q\, D_n\, n_p\, S \left(K_L \Phi + \frac{1}{L_o^2}\right)^{1/2} \tag{3.2.7}$$

where S is the cell area. Equations (3.2.4) and (3.2.7) can be substituted into equation (3.2.6) to obtain the following expression:

$$V_{oc} = \frac{kT}{q} \ln \left[\frac{B - \frac{A}{2} \ln \left(K_L \Phi + \frac{1}{L_o^2}\right)}{q\, D_n\, n_p \left(K_L \Phi + \frac{1}{L_o^2}\right)^{1/2}} \right] \tag{3.2.8}$$

The radiation fluence term (Φ) appears twice in the above expression. The fluence term in the numerator will have a much lesser effect on V_{oc} than that in the denominator because it appears as the natural logarithm of the fluence rather than as the square root of the fluence. It appears therefore that the V_{oc} variation with radiation fluence is dominated by the denominator of equation (3.2.8) and can be approximated by equation (3.2.5).

The maximum power (P_{max}) of a solar cell can be represented as the product of I_{sc}, V_{oc}, and a constant as follows:

$$P_{max} = F \cdot I_{sc} \cdot V_{oc} \tag{3.2.9}$$

where F is the form or fill factor. The fill factor (F) is relatively insensitive to radiation which penetrates uniformly through a solar cell. For this reason, the variation of P_{max} with irradiation is the same as

that for the product of I_{sc} and V_{oc}. Equations (3.2.1) and (3.2.5) can be substituted into (3.2.9) and the resulting expression approaches the form of:

$$P_{max} = P_{maxo} - C'' \log \left(1 + \frac{\Phi}{\Phi_x}\right) \qquad (3.2.10)$$

Expressions of this form are found to closely describe the variation of P_{max} during irradiation.

3.3 The Concept of Damage Equivalence

The wide range of electron and proton energies present in the space environment necessitates some method of describing the effects of various types of radiation in terms of a radiation environment which can be produced under laboratory conditions. Since the changes in most solar cell parameters due to irradiation are in some way related to the minority carrier diffusion length, it is possible to determine an equivalent damage based upon this parameter. In Figure 3.5, the diffusion length changes are shown for 10Ω-cm, n-p silicon solar cells which have been subjected to several different types of irradiation. The results are described by equation (3.2.3) where the constant K_L is dependent upon the radiation type.

The concept of damage equivalence can alternatively be based on common solar cell parameters. The variation of short circuit current density for 10 ohm-cm n-p solar cells irradiated in various environments is shown in Figure 3.6. The J_{sc} variation in each environment is described by equation (3.2.1). In this case two constants, C and Φ_x, are required to describe the changes in J_{sc}. Experience has shown that the constant C, under solar simulator illumination, does not vary greatly for different radiation environments. For electron irradiations in the 1 MeV and greater range, C is approximately 4.5 mA/cm^2 decade. For proton and neutron irradiations, C approaches 6 mA/cm^2 decade. For solar cells with the same starting J_{sc}, the constant Φ_x is a measure of the damage effectiveness of different radiation environments. The constant Φ_x for a particular radiation can be determined graphically at the intersection of the starting J_{sc} and the extrapolation of the linear degradation region.

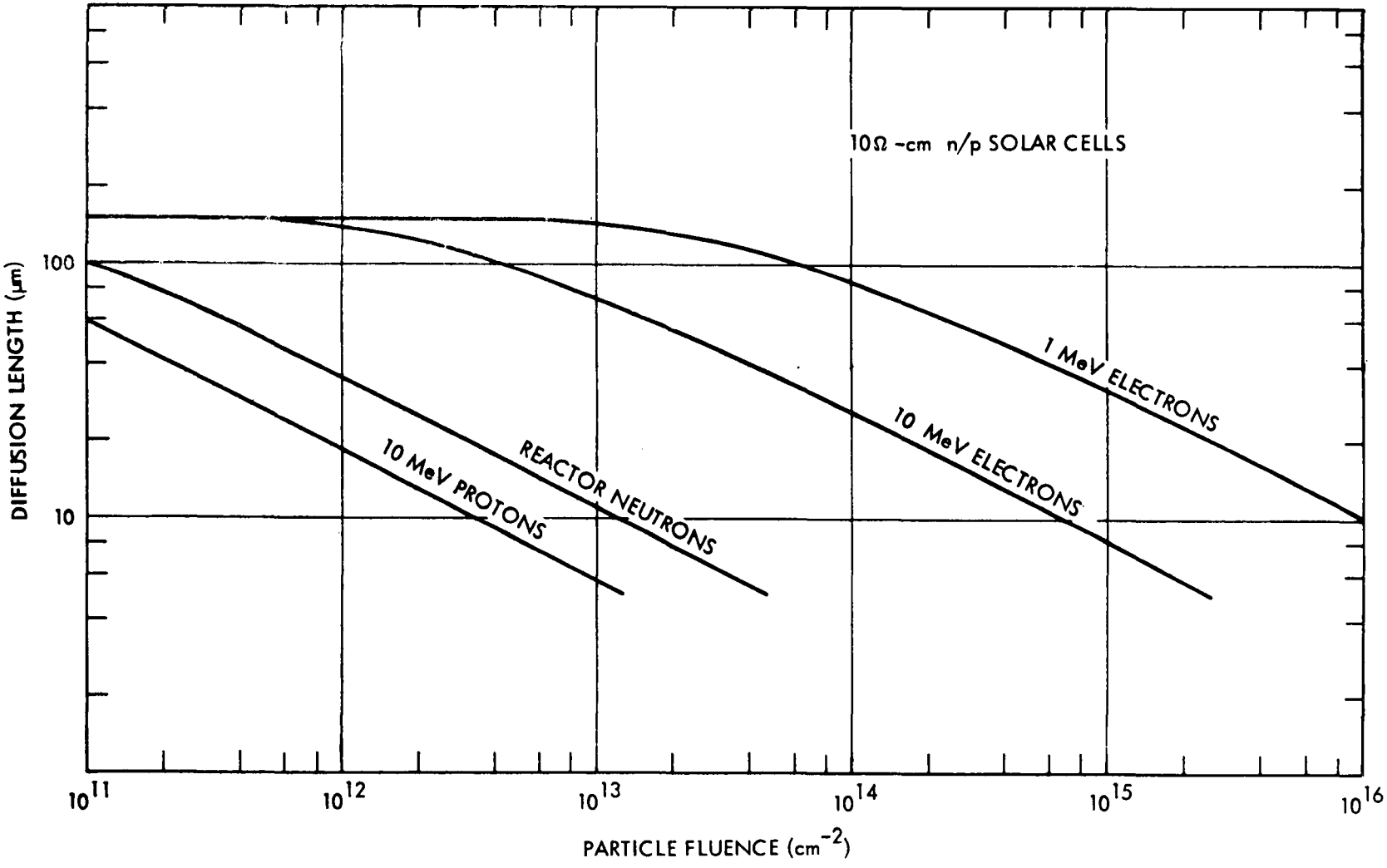

Figure 3.5 Variation of Solar Cell Diffusion Length with Fluence for Various Radiations

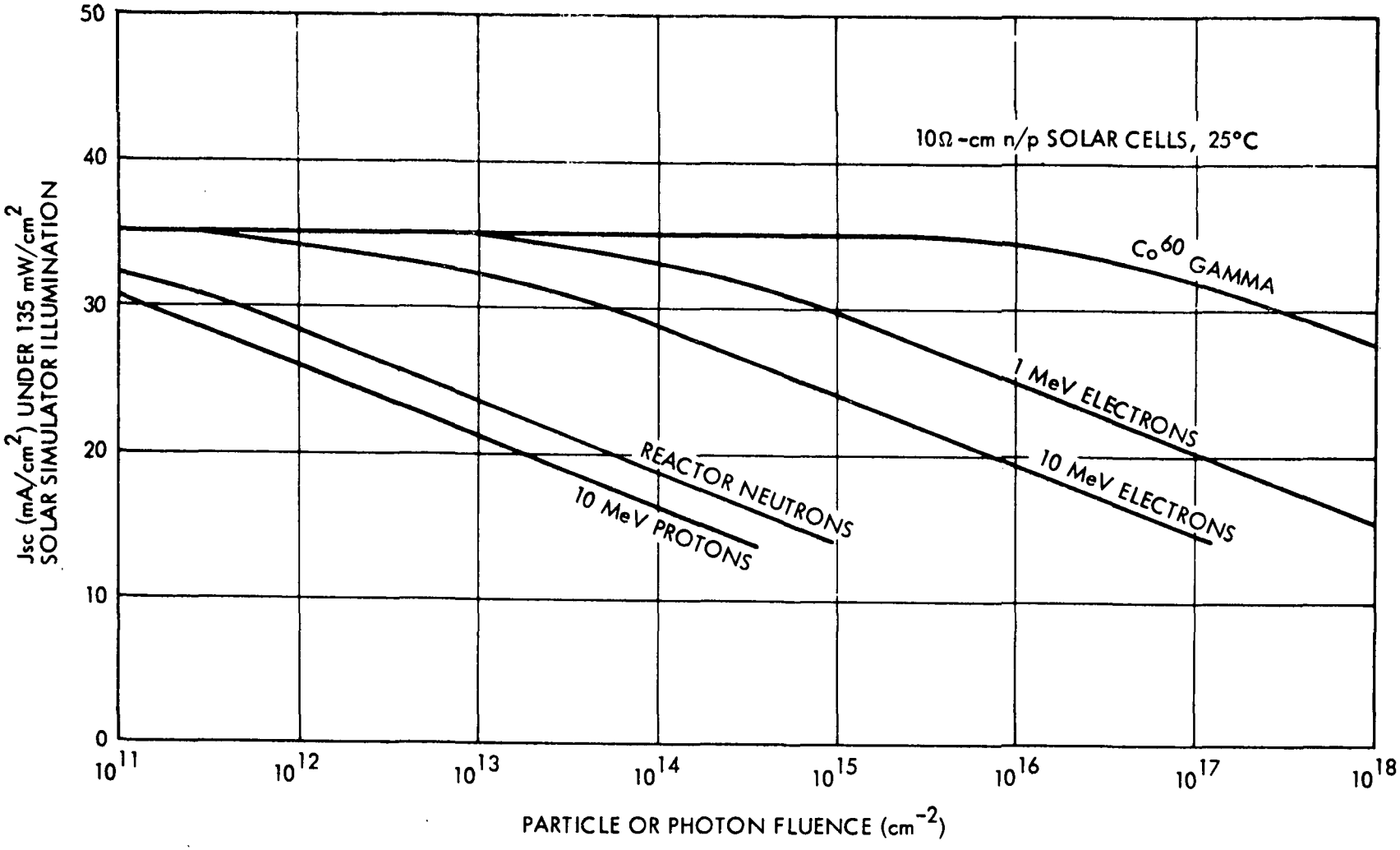

Figure 3.6 Variation of Solar Cell Short Circuit Current Density with Fluence for Various Radiations

Since the value of Φ_x is dependent upon the starting J_{sc} value, it is not a good practical measure for relative damage effectiveness. It has been the practice to define an arbitrary constant referred to as the critical fluence (Φ_c). One method of defining this value is that fluence which degrades a solar cell parameter 25% below its unirradiated state. Such a parameter is valid only when comparing cells with similar unirradiated parameters. To eliminate this problem, critical fluence may be defined alternatively as that fluence which will degrade a cell parameter to a certain value.

By use of the critical fluence (Φ_c) or the diffusion length damage coefficient (K_L), it is possible to construct a model in which the various components of a combined radiation environment can be described in terms of a damage equivalent fluence of a selected monoenergetic particle. One MeV electrons are a common and significant component of space radiation and can be produced conveniently in a test environment. For this reason, one MeV electron fluence has been used as a basis of the damage equivalent fluences which describe silicon solar cell degradation.

The use of the damage equivalent fluence scheme involves two separate problems. The first problem is to adequately describe the degradation of an unshielded silicon solar cell under one MeV electron irradiation under laboratory conditions (i.e., normal incidence). The second problem is to reduce the effect of the space radiation environment (i.e., continuous energy spectrums of electrons and protons, isotropic incidence) on a shielded silicon solar cell to a damage equivalent fluence of one MeV electrons under laboratory conditions.

3.4 One MeV Electron Irradiation of Silicon Solar Cells

In this section the effects of one MeV electron laboratory irradiation of solar cells will be reviewed and discussed. Data will be presented which will form the basis for estimating solar cell performance, after the space radiation environment is reduced to a damage equivalent one MeV fluence. A very large volume of work has been reported concerning the effects of 1 MeV electron irradiation on silicon solar cells. This section

will limit the data to evaluations done with solar simulators. The data will also be limited to types of solar cells which are currently in common use on spacecraft.

Currently n-p solar cells are in use as a primary power source on nearly all earth orbiting satellites. Variations in base resistivity and cell thickness cause significant differences in the response to 1 MeV electron irradiation.[3.23, 3.39] Other variables such as the irradiation temperature in the range of 200 to 370 K,[3.40] and p-type base dopant (boron vs. aluminum) have been shown to have little or no effect on the solar cell response to radiation.[3.41-3.44]

The variation of n-p solar cell response with base resistivity has been studied and reported for the range of 1 to 20 ohm-cm.[3.23, 3.45] Current n-p solar cell usage is confined to the ranges of 1 to 3 ohm-cm and 7-13 ohm-cm. Cells in the base resistivity range of 1-3 ohm-cm have greater initial maximum power output than cells in the 7 to 13 ohm-cm range. The radiation hardness of n-p cells in the 7 to 13 ohm-cm range is greater than that of the 1 to 3 ohm-cm range, when the hardness is determined by parameters such as the critical fluence (Φ_c) or diffusion length damage coefficient (K_L). As a result, 10 ohm-cm cells have greater maximum power output after a certain electron fluence is reached; however, the 2 ohm-cm cells produce greater maximum power at lower fluences. This crossover fluence depends upon cell thickness but is approximately 1 x 10^{14} one MeV electrons per cm^2.

Solar cell thickness has been shown to have a strong effect on the output parameters of irradiated cells.[3.39] Cell thickness does not affect measures of inherent hardness such as the critical fluence (if properly determined) or the diffusion length damage coefficient. The thickness does, however, significantly affect the cell output parameters during the initial or low fluence stage of an irradiation. A set of graphs presenting J_{sc}, V_{oc}, P_{max}, and V_{Pmax} as a function of 1 MeV electron fluence are shown in Figures 3.7 through 3.14. Separate graphs are included for n-p cells in the 1-3 ohm-cm and 7-13 ohm-cm ranges. The changes in each cell parameter are shown for several solar cell thicknesses

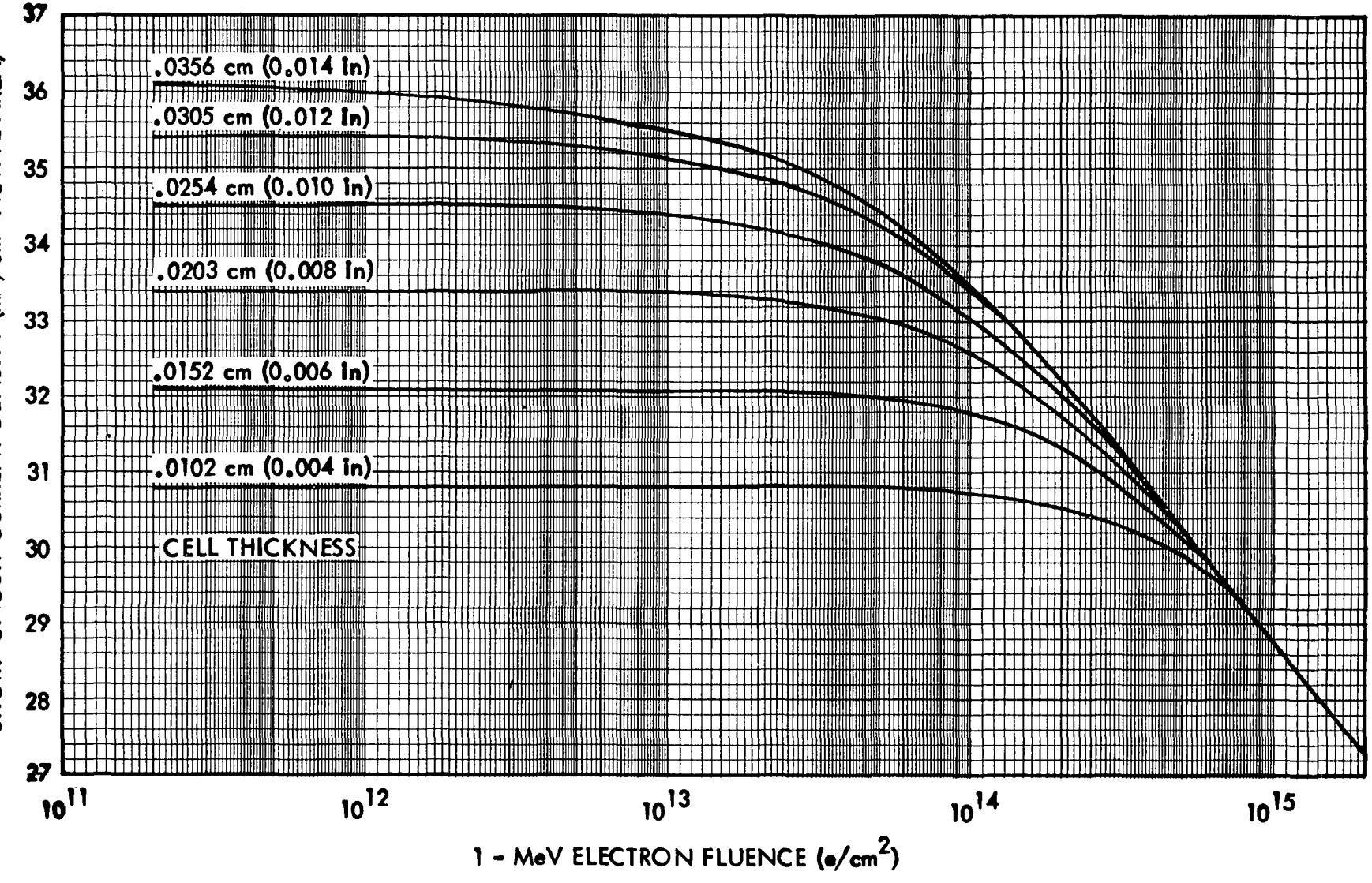

Figure 3.7 Short Circuit Current Density per Active Area vs. 1-MeV Electron Fluence for 1-3 ohm-cm N/P Silicon Cells. At 135 mW/cm^2 AMO Illumination Intensity, 28°C.

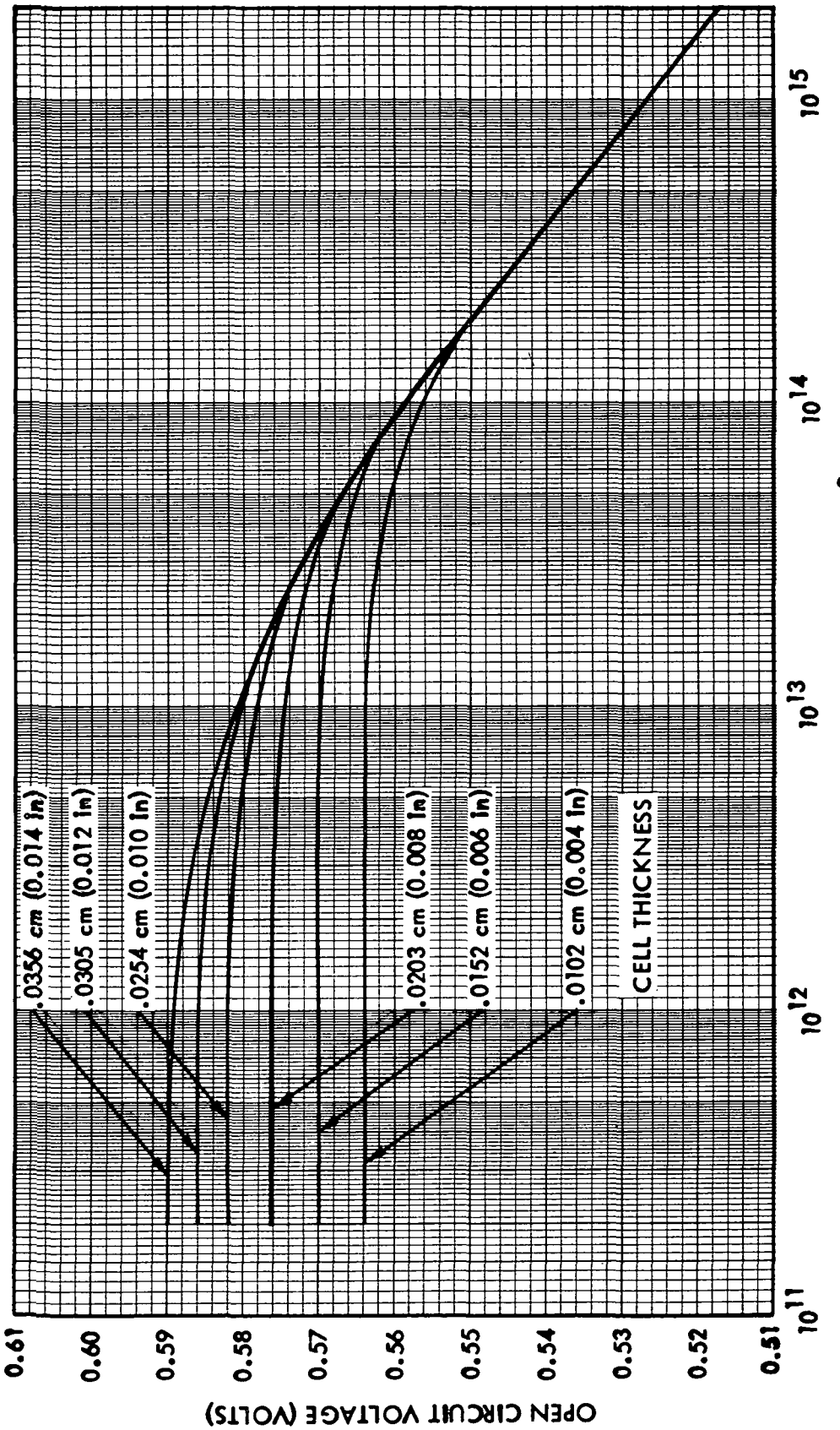

Figure 3.8 Open-circuit Voltage vs. 1-MeV Electron Fluence for 1-3 ohm-cm N/P Silicon Cells. At 135 mW/cm^2 AMO illumination, 28°C

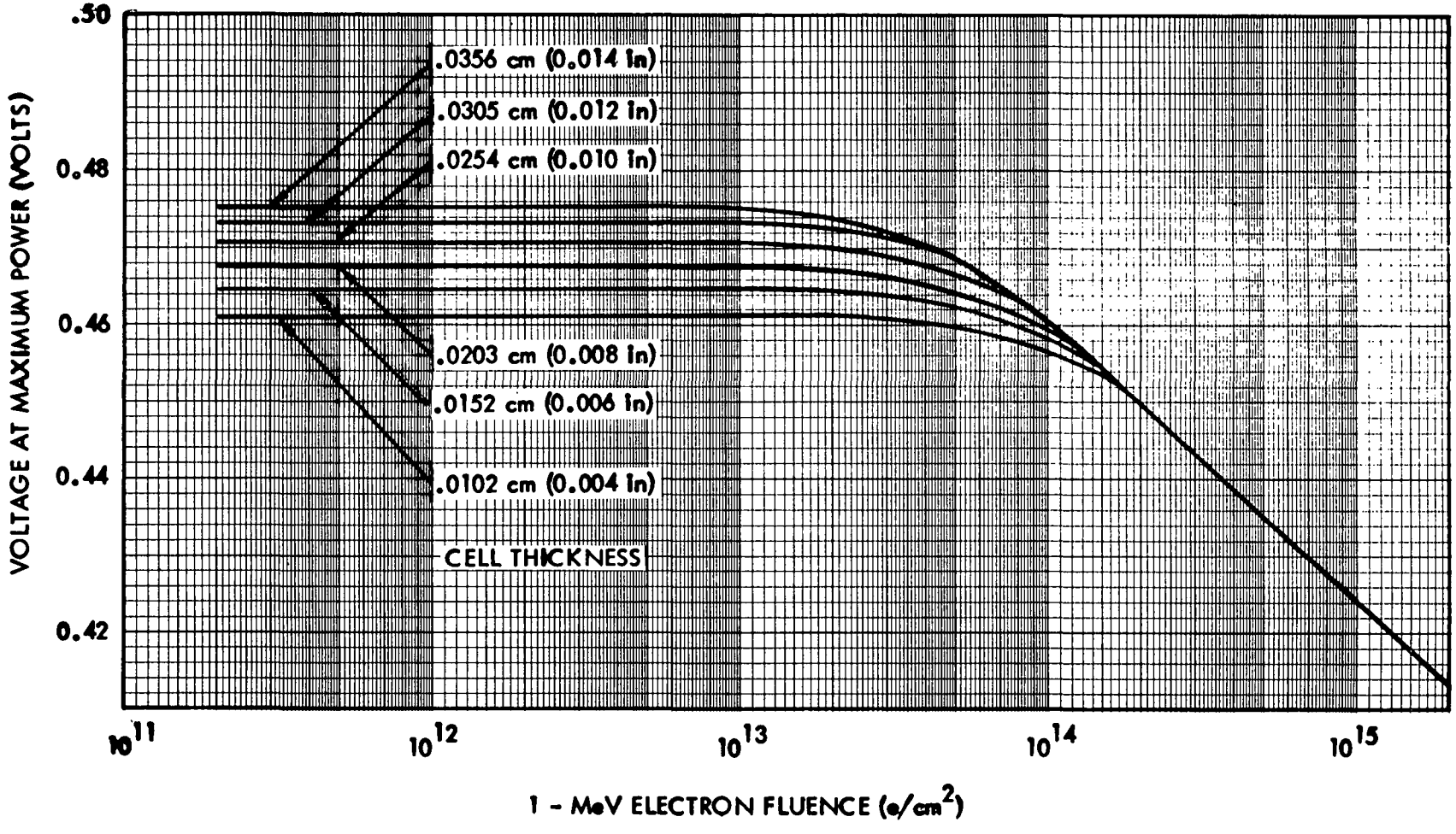

Figure 3.9 Voltage at Maximum Power Versus 1-MeV Electron Fluence for 1-3 ohm-cm N/P Silicon Cells. At 135 mW/cm^2 AMO Illumination Intensity, 28°C.

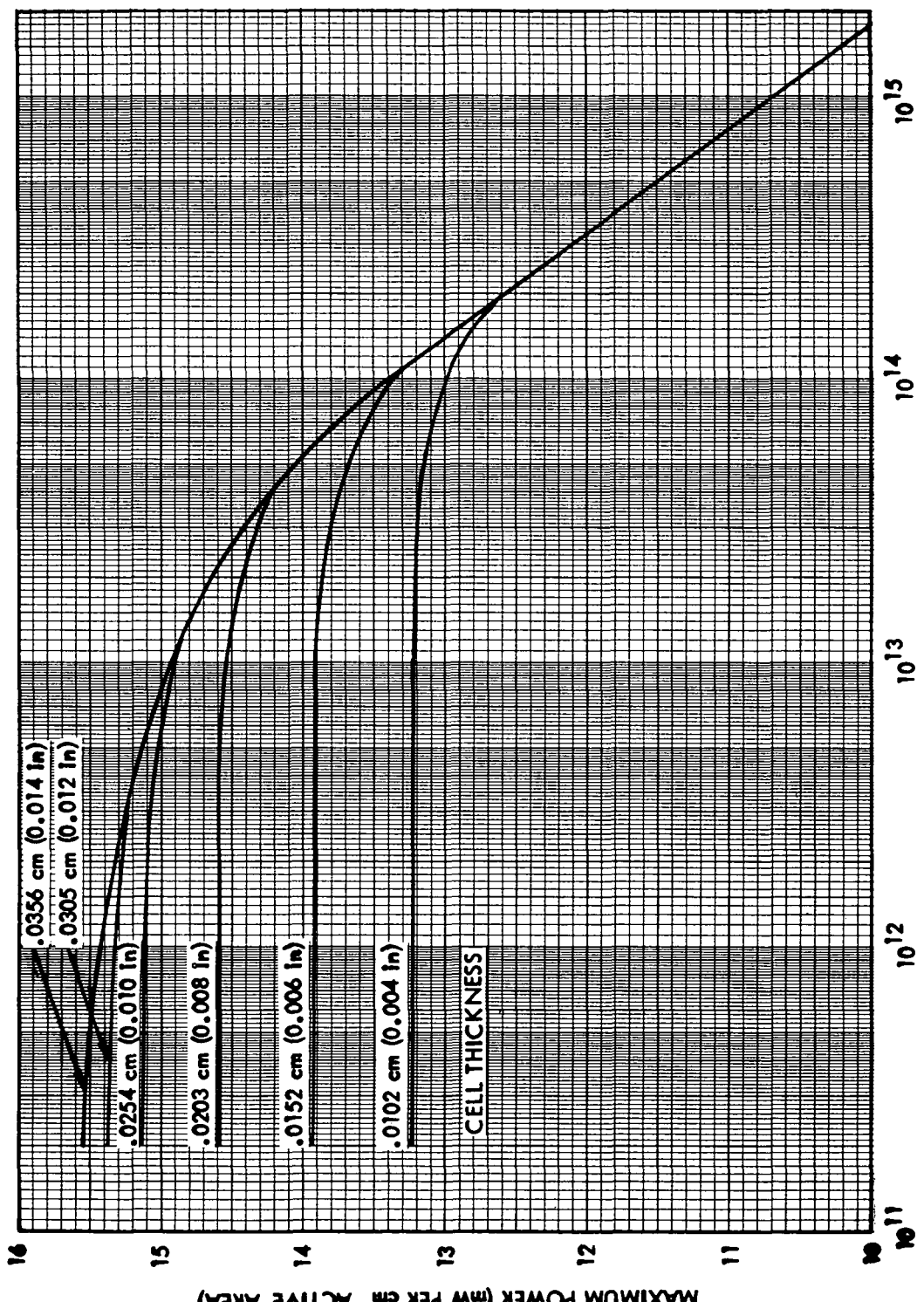

Figure 3.10 Maximum Power Density per Unit Active Area Versus 1-MeV Electron Fluence for 1-3 ohm-cm N/P Silicon Cells. At 135 mW/cm² AMO Illumination Intensity, 28°C.

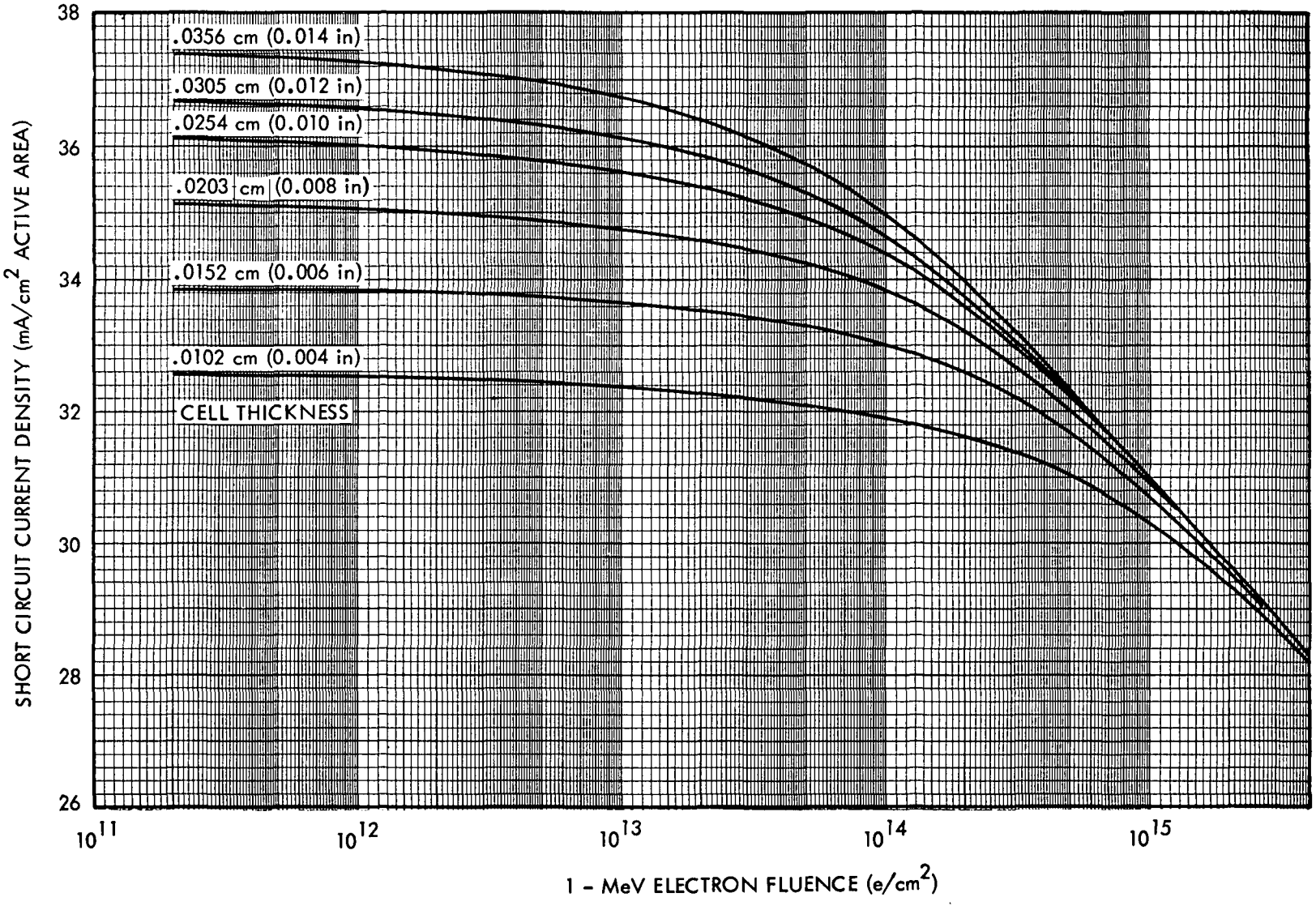

Figure 3.11 Short-circuit current density per unit active area versus 1-MeV electron fluence for 7-13 ohm-cm N/P silicon cells. At 135 mW/cm^2 illumination intensity, 28°C.

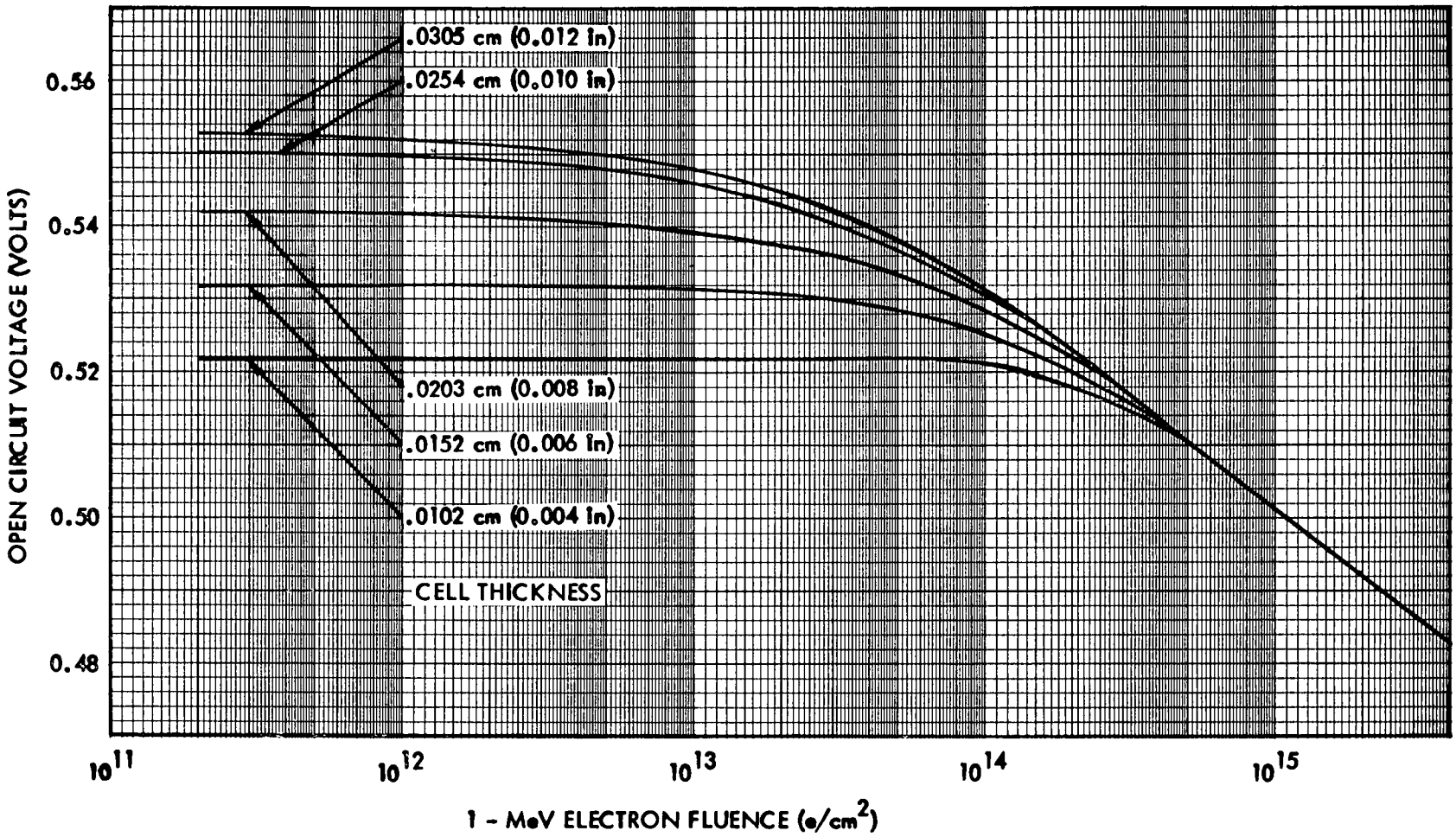

Figure 3.12 Open-Circuit Voltage Versus 1-MeV Electron Fluence for 7-13 ohm-cm N/P Silicon Cells. At 135 mW/cm^2 AMO Illumination Intensity, 28°C.

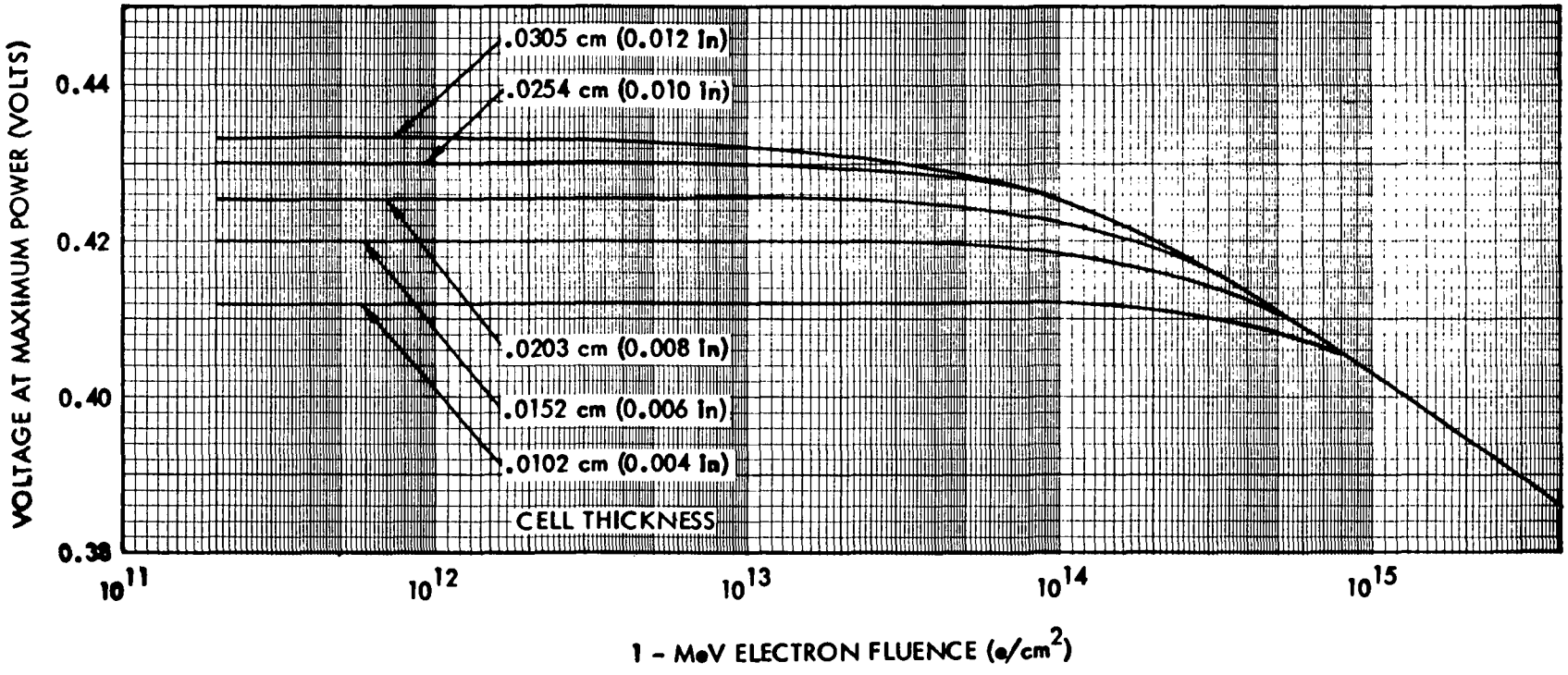

Figure 3.13 Voltage at Maximum Power Versus 1-MeV Electron Fluence for 7-13 ohm-cm N/P Silicon Cells. At 135 mW/cm^2 Illumination Intensity, 28°C.

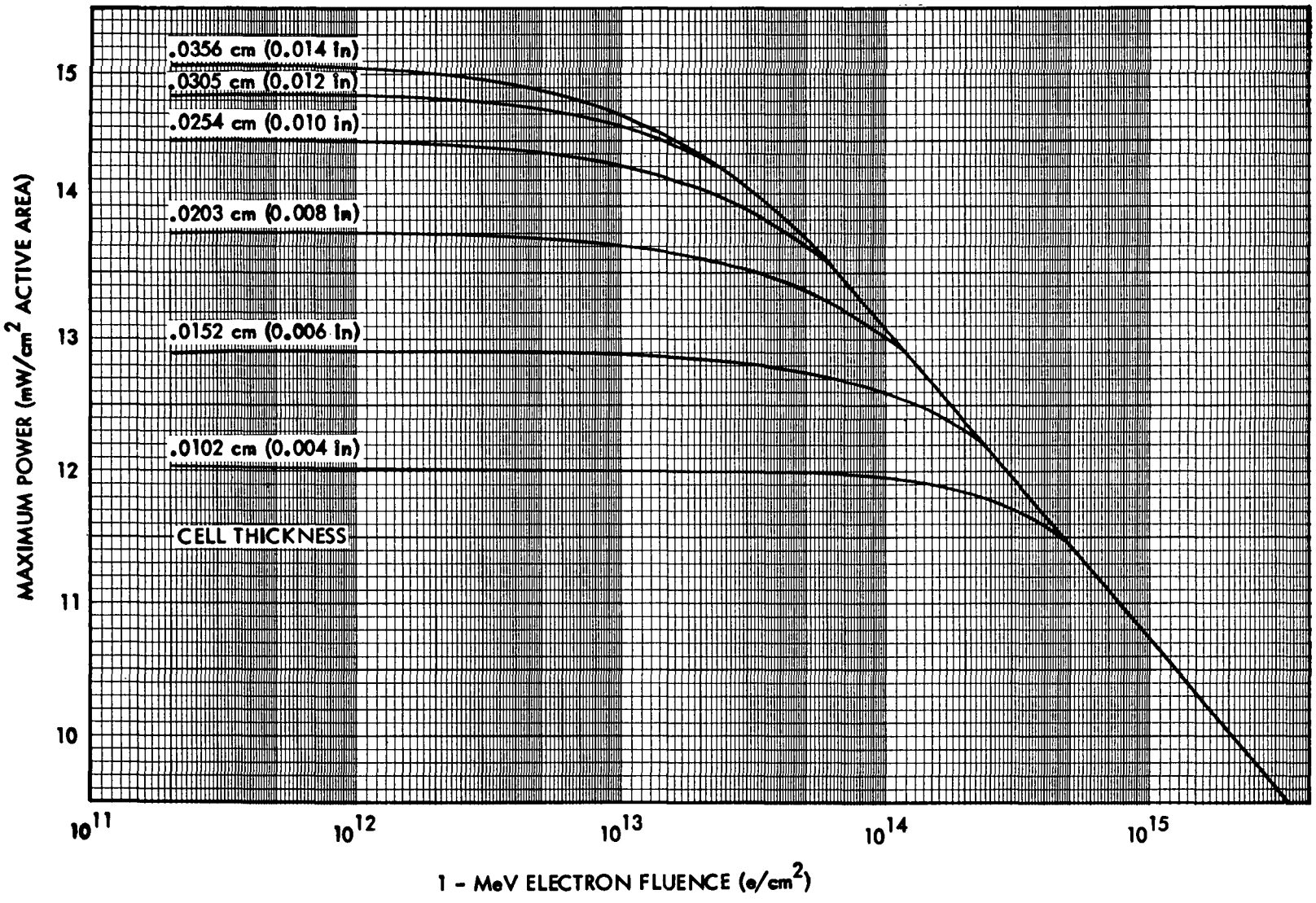

Figure 3.14 Maximum Power Density per Unit Active Area Versus 1-MeV Electron Fluence for 7-13 ohm-cm N/P Silicon Cells. At 135 mW/cm^2 AMO Illumination Intensity, 28°C.

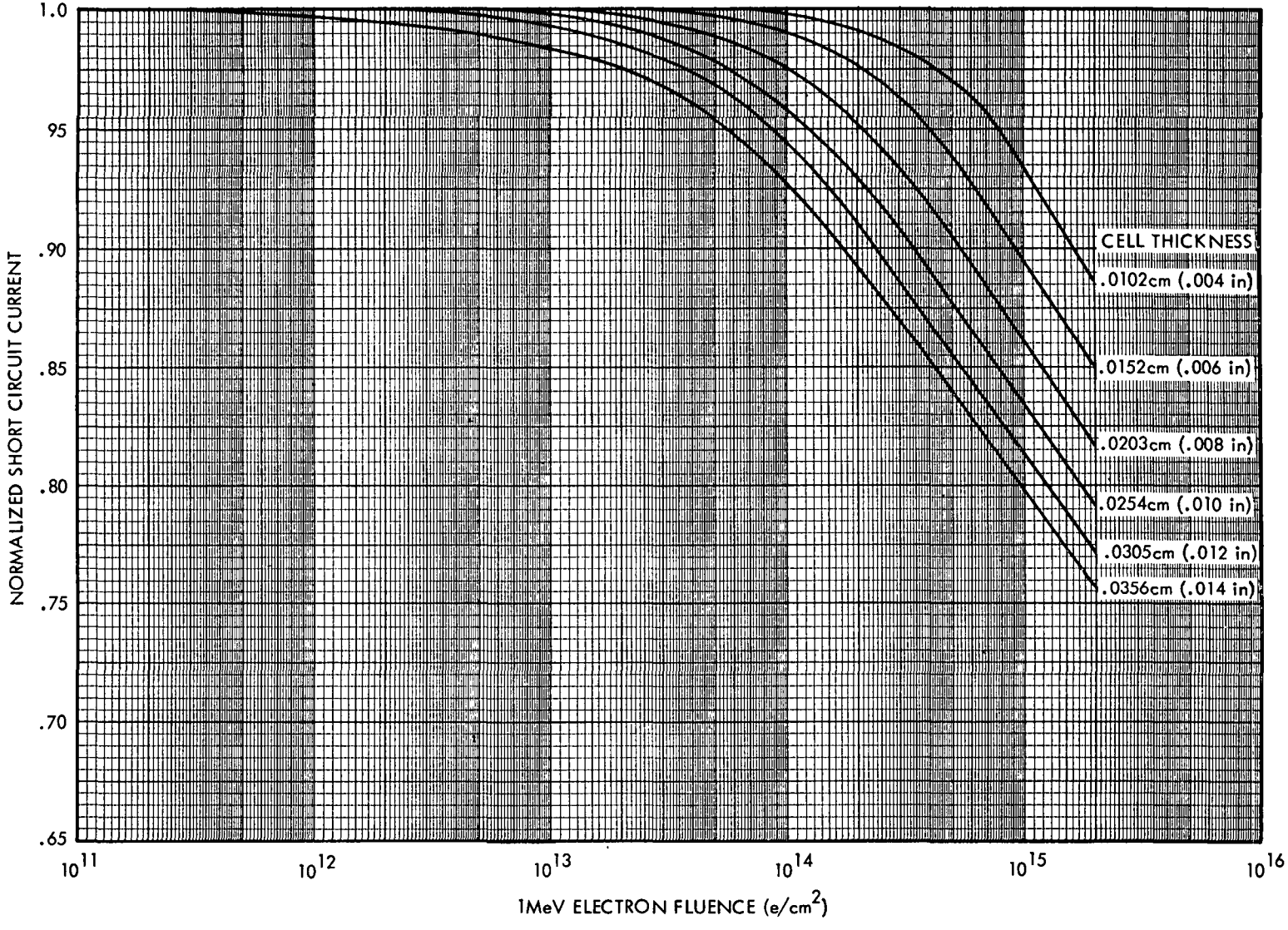

Figure 3.7a Normalized Short Circuit Current Density vs. 1-MeV Electron Fluence for 1-3 ohm-cm N/P Silicon Cells. At 135 mW/cm^2 AMO Illumination Intensity, 28° C.

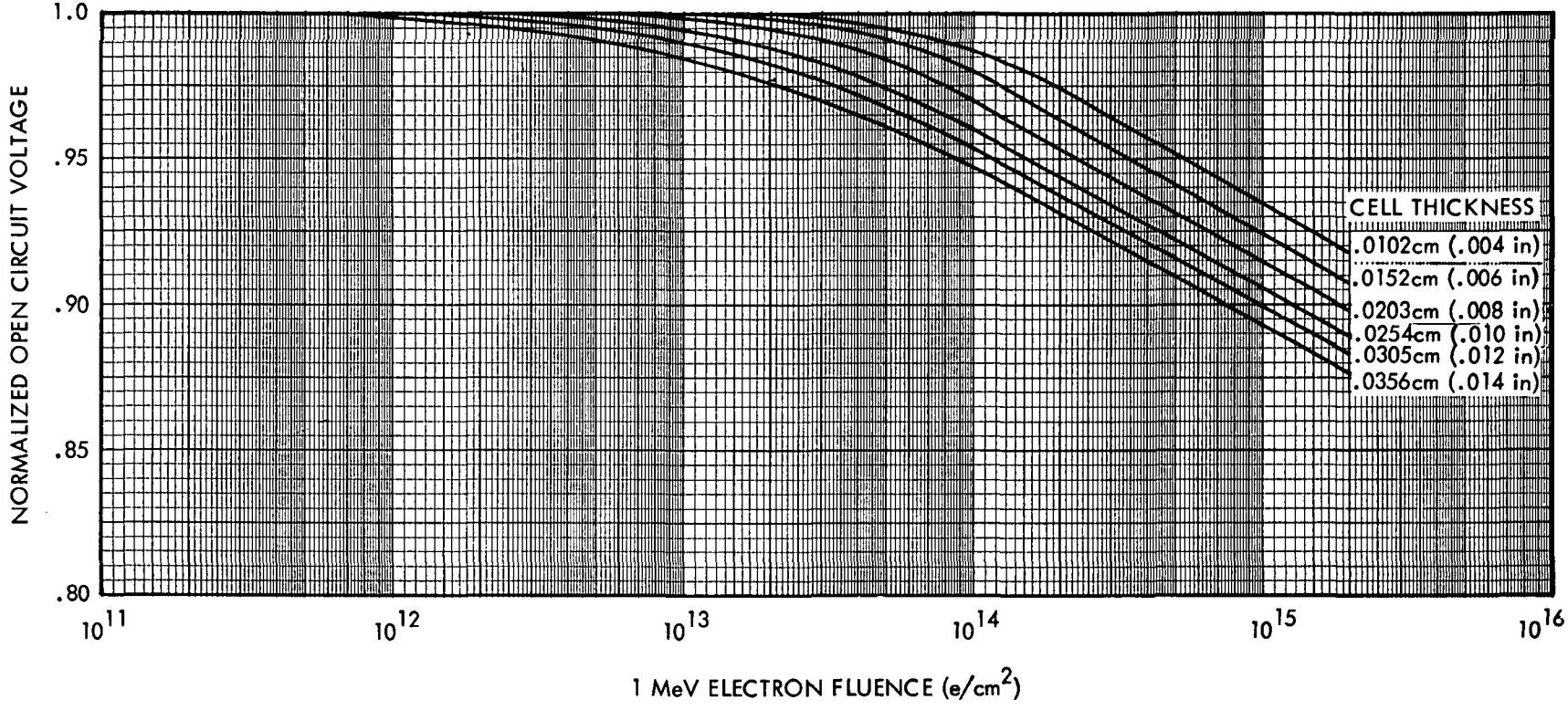

Figure 3.8a Normalized Open-Circuit Voltage vs. 1-MeV Electron Fluence for 1-3 ohm-cm N/P Silicon Cells. At 135 mW/cm^2 AMO Illumination, 28°C.

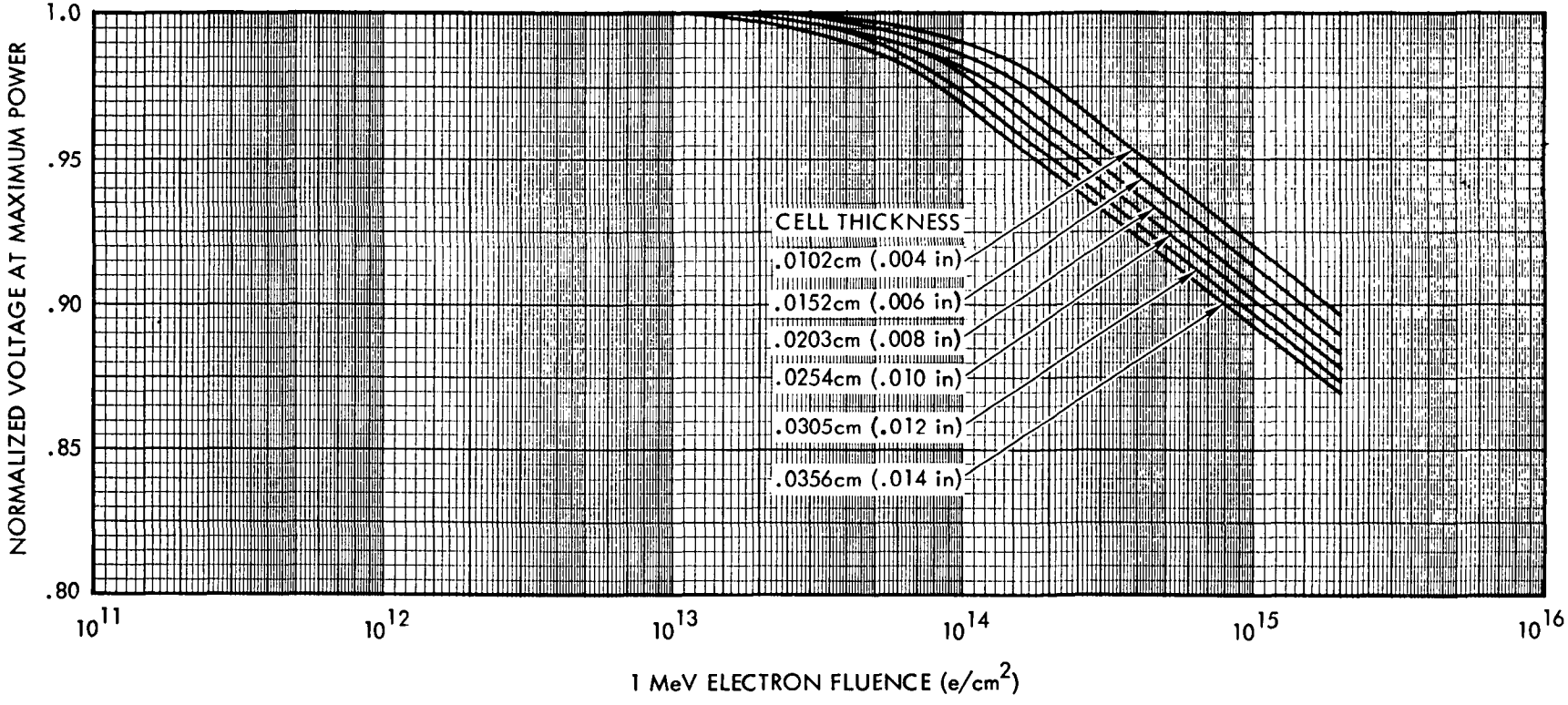

Figure 3.9a Normalized Voltage at Maximum Power vs. 1-MeV Electron Fluence for 1-3 ohm-cm N/P Silicon Cells. At 135 mW/cm^2 AMO Illumination Intensity, 28°C.

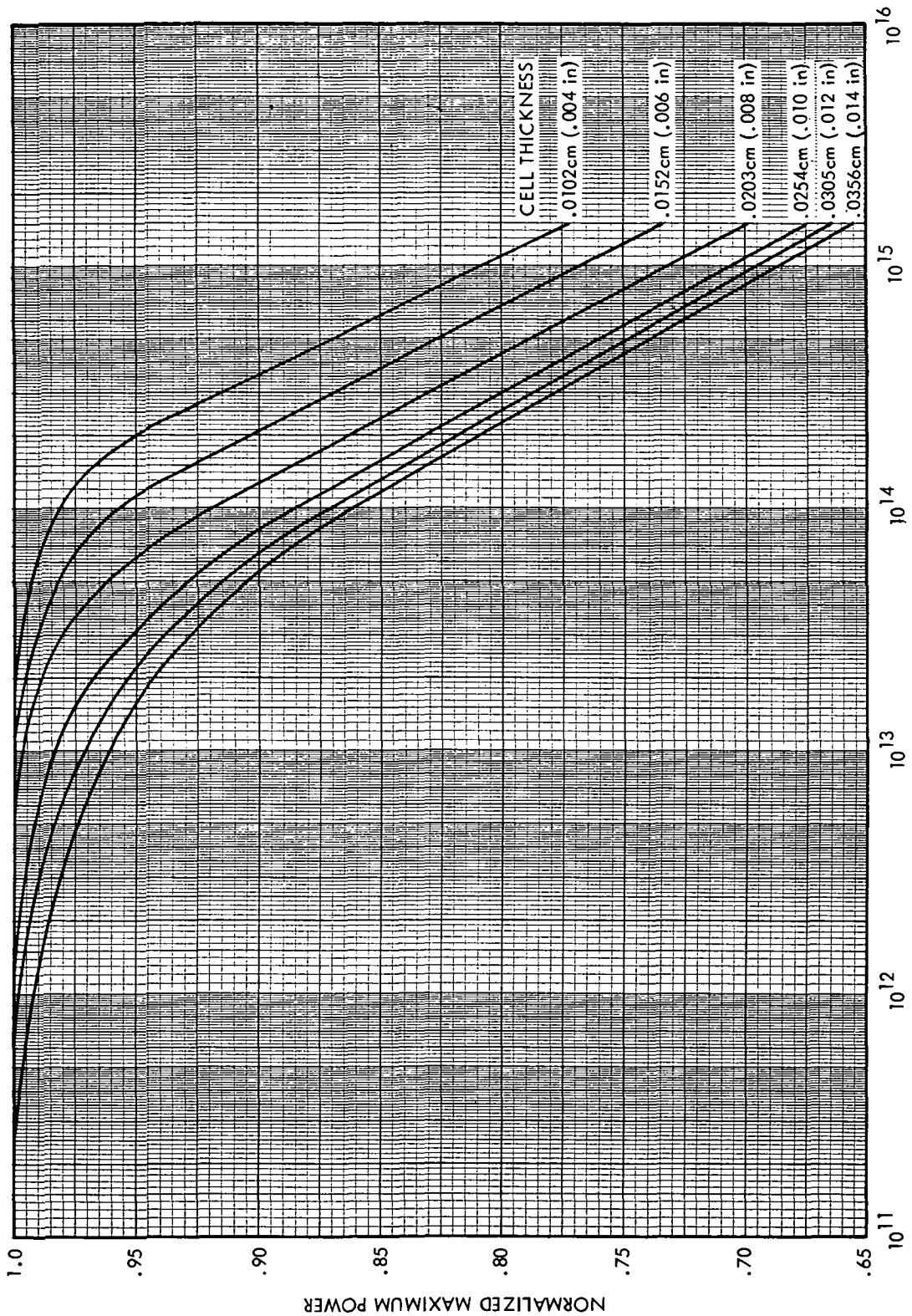

Figure 3.10a Normalized Maximum Power vs. 1-MeV Electron Fluence for 1-3 ohm-cm N/P Silicon Cells. At 135 mW/cm^2 AMO Illumination Intensity, 28°C.

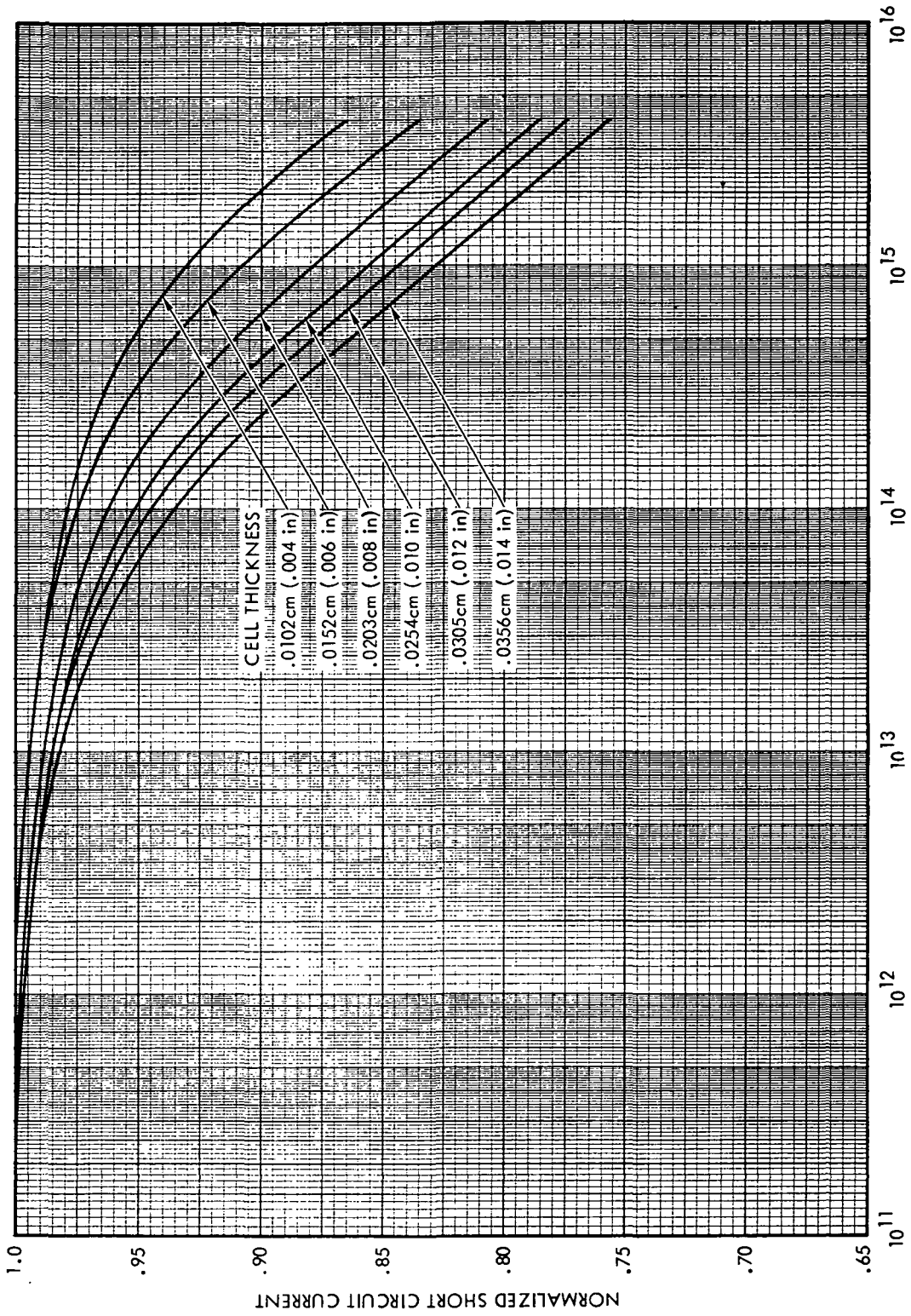

Figure 3.11a Normalized Short-Circuit Current vs. 1-MeV Electron Fluence for 7-13 ohm N/P Silicon Cells. At 135 mW/cm^2 Illumination Intensity, 28°C.

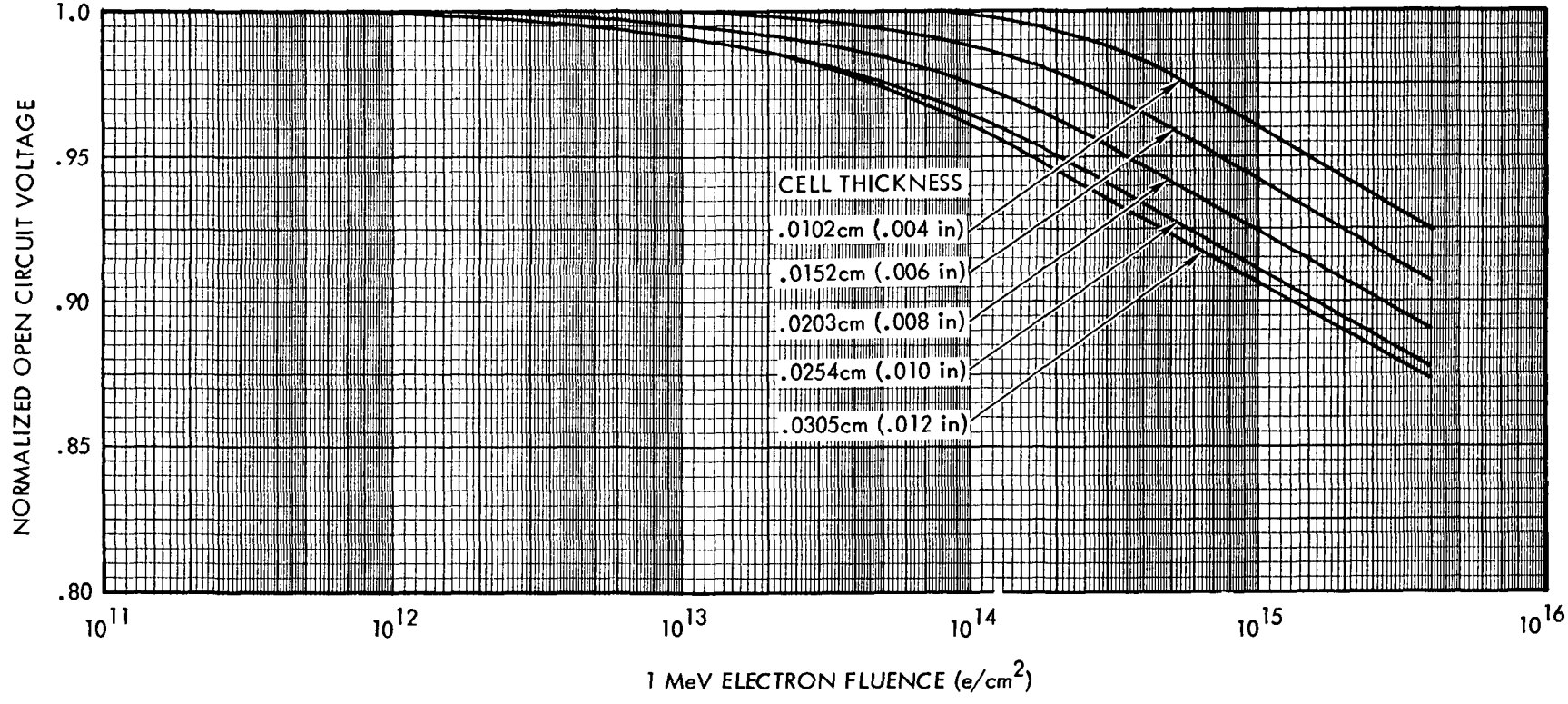

3.12a Normalized Open-Circuit Voltage vs. 1-MeV Electron Fluence for 7-13 ohm-cm N/P Silicon Cells. At 135 mW/cm^2 AMO Illumination Intensity, 28°C.

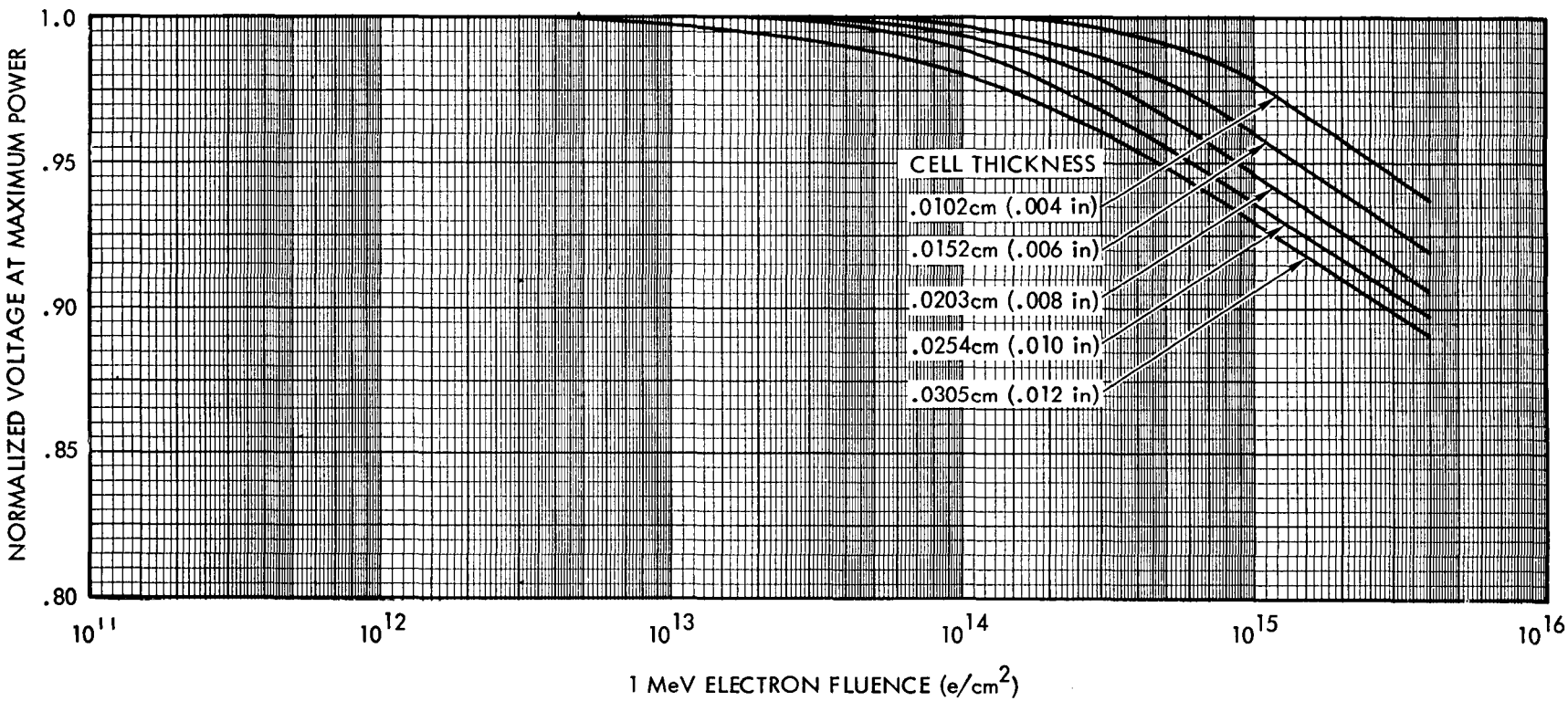

Figure 3.13a Normalized Voltage at Maximum Power vs. 1-MeV Electron Fluence for 7-13 ohm-cm N/P Silicon Cells. At 135 mW/cm^2 Illumination Intensity, 28°C.

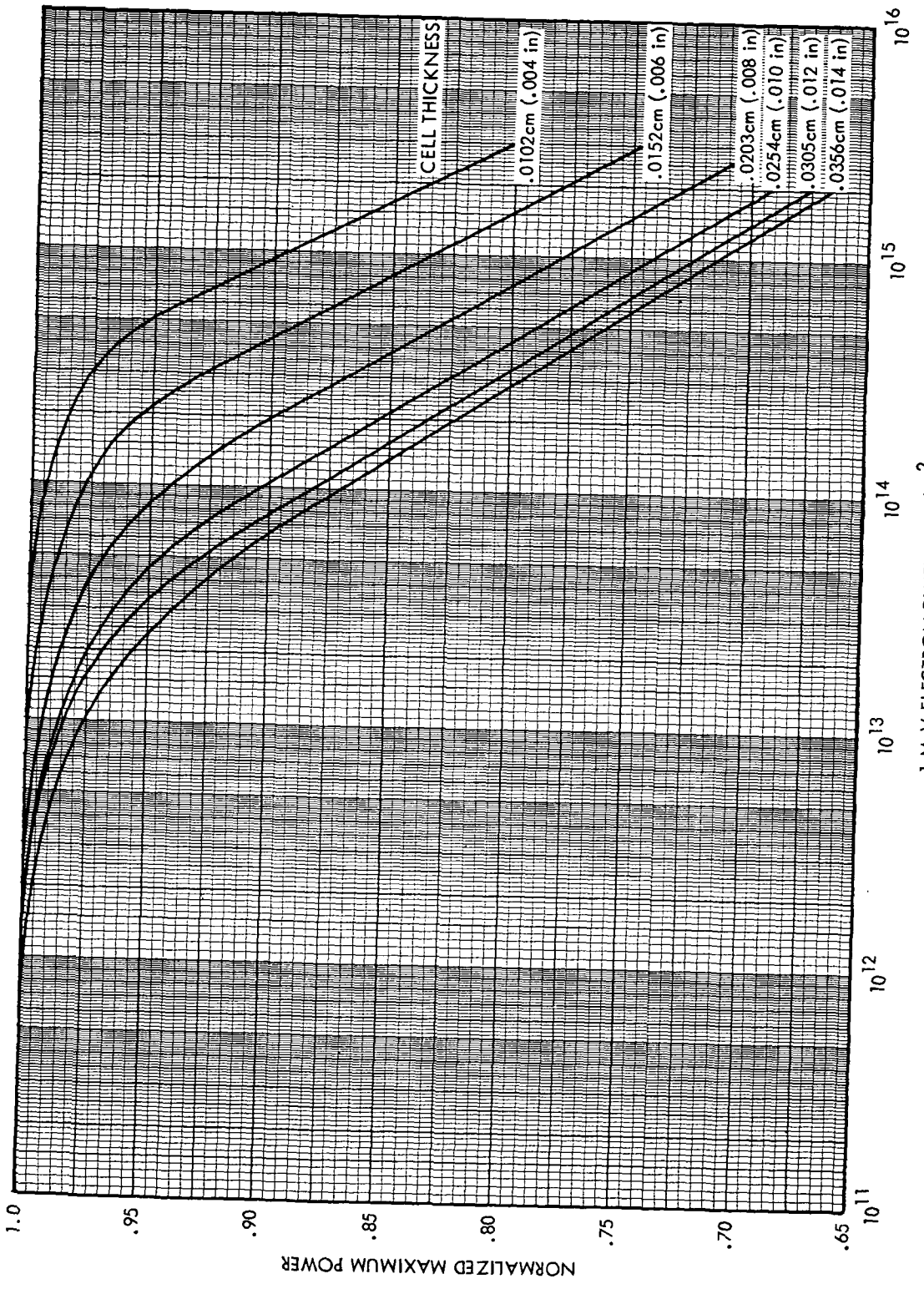

Figure 3.14a Normalized Maximum Power vs. 1-MeV Electron Fluence for 7-13 ohm-cm N/P Silicon Cells. At 135 mW/cm^2 AMO Illumination Intensity, 28°C.

on each graph. These data are a composite of data from several sources, and unpublished TRW data.[3.39, 3.44-3.47] It is emphasized that these data are intended to represent the mean behavior of current n-p solar cell production in the United States. These production practices involve use of quartz-crucible grown silicon, junction depths of approximately 0.4 μm and absence of drift field collection. Solar cells produced with significant changes in the state of the art may require revision or addition to this typical radiation environment performance data.

3.5 Effect of Electron Energy on Solar Cell Degradation

The concept of damage equivalent 1 MeV electron fluence requires some method of evaluating the damage effectiveness of electrons of various energies. This effectiveness can be measured by the diffusion length damage constant (K_L) or solar cell critical fluence (Φ_c) for various elec tron energies. Experimental data have been reported for the electron energy range of 1 to 3 MeV[3.48] and from 0.6 to 40 MeV.[3.23] The results of these studies are in essential agreement and the results of reference 3.23 are shown in Figure 3.15 (K_L) and Figure 3.16 (Φ_c). In this case Φ_c is defined as that fluence which degrades I_{sc} to 19mA/cm^2 under 100mW/cm^2 of tungsten illimination. In both figures, data are shown for cells of various resistivities. Some important observations can be made from these data. The relative variations of the K_L and Φ_c^{-1} with electron energy are identical. The relative variations of both parameters with cell base resistivity are also identical. On the basis of the experimental data, one can therefore define a relative damage effectiveness for each electron energy which will be a measure of the ratio of that electron fluence at a given energy to the 1 MeV electron fluence necessary to degrade an n-p solar cell to the same output parameter value. For instance, if a given 10 MeV electron fluence degrades a solar cell to a certain state of damage, then a 1 MeV electron fluence 16.5 times that of the 10 MeV electron fluence would be required to degrade the same cell to the same output conditions. This relationship will hold regardless of whether 2 or 10 ohm-cm resistivity cells are under consideration.

Wysocki reported data at 0.8 and 5.8 MeV which indicated that the relative electron damage constant increased more rapidly with energy.[3.49]

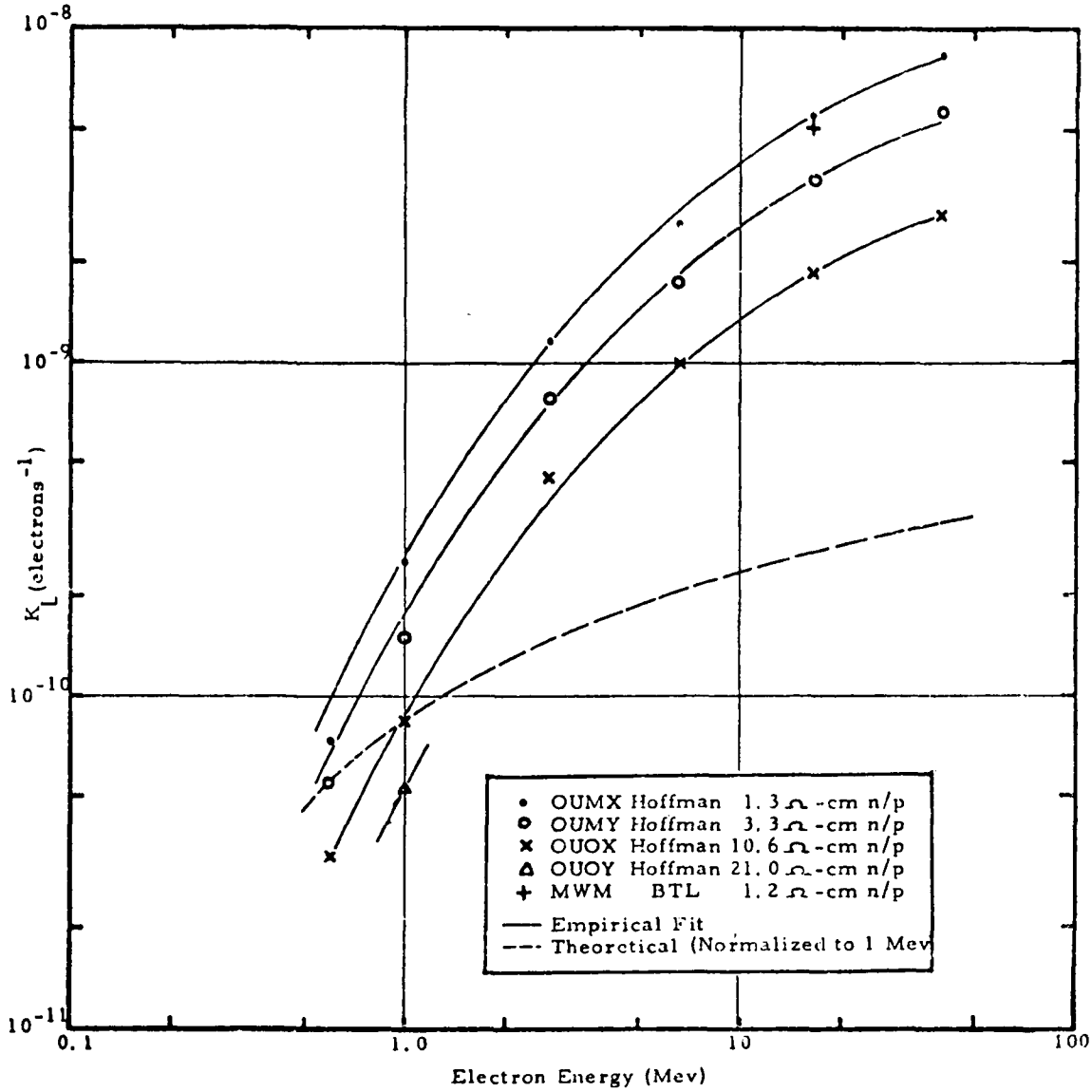

Figure 3.15 Electron Energy Dependence of K_L Values for N on P Silicon Solar Cells [3.23]

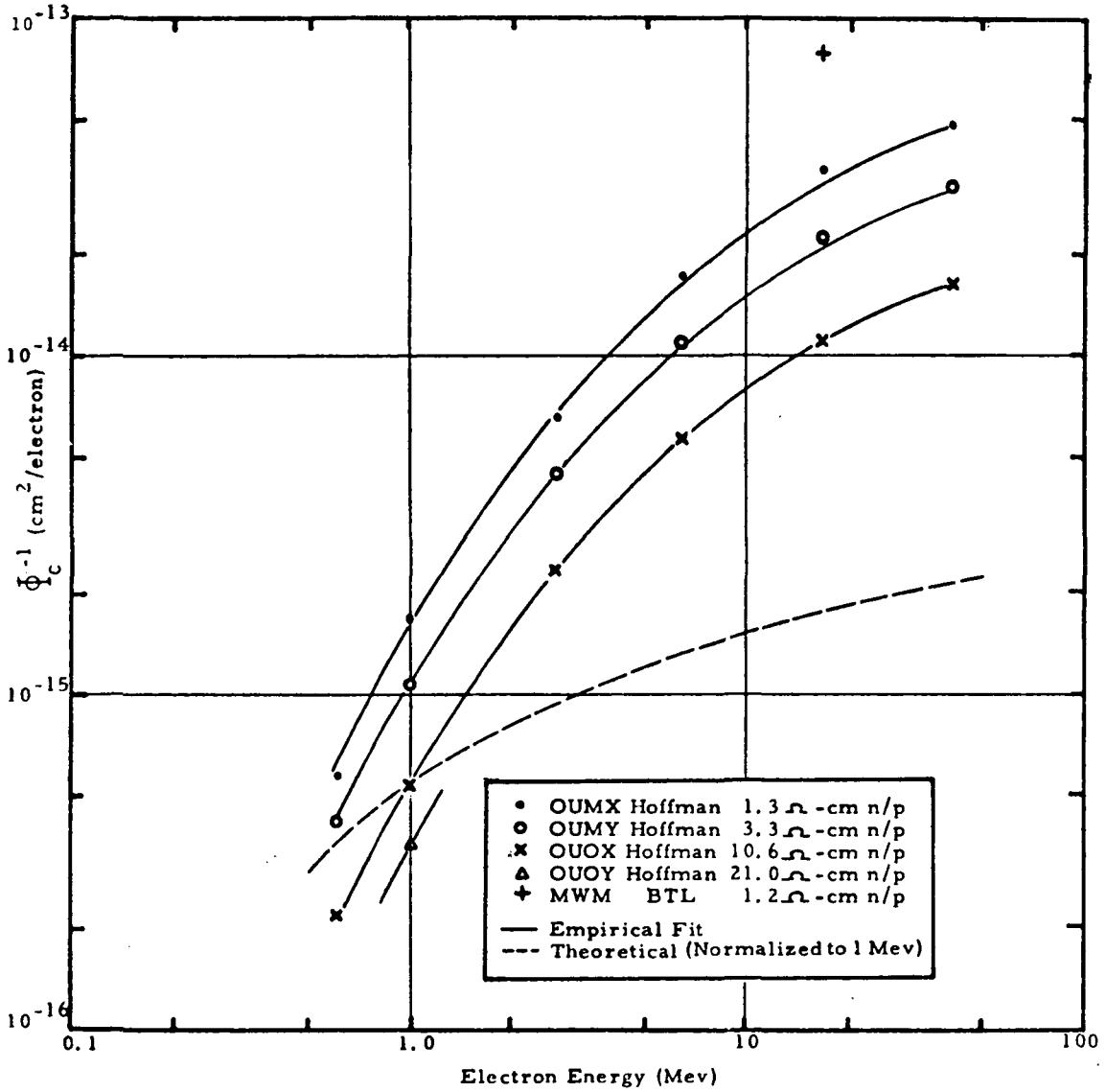

Figure 3.16 Electron Energy Dependence of Φ_c^{-1} Values for N on P Silicon Solar Cells [3.23]

Gorodetskii, et al., [3.50] reported data in rough agreement with references 3.23 and 3.48 below 2 MeV, but indicate a much slower rise above that energy. More recent studies by Bernard, et al.,[3.37] and Lesbre[3.43] indicate good agreement with the results in references 3.23 and 3.48 up to 3 MeV and 4.5 MeV, respectively.

3.6 Effect of Proton Energy on Solar Cell Degradation

The concept of damage equivalent 1 MeV electron fluence can be extended to the effects of proton irradiation. The problem is more complex, in the proton case, because the range of protons below 5 MeV is less than the thickness of a solar cell. For this reason, low energy protons produce nonuniform damage. This situation is further complicated by the fact that the damage produced per unit path length increases as the proton energy decreases. As a result, when a low energy proton is stopped in a solar cell, a large amount of damage is concentrated at the end of the proton track.

When radiation damage is uniform throughout a solar cell, the relative effectiveness of various energy particles is the same when measured by the diffusion length damage coefficients, or critical fluences determined by cell parameters such as I_{sc}, V_{oc} or P_{max}. This fact was graphically demonstrated by comparison of Figures 3.15 and 3.16. In the case of protons with energies greater than 5 MeV, the damage to solar cells is relatively uniform. In this high energy range, the general concept of equivalency is directly applicable. At lower proton energies, the general concept of equivalency is not applicable; however, it can be used in a restricted manner as discussed below.

Early experimental studies of the variation of damage in n-p silicon solar cells with higher proton energies indicated conflicting results. The results reported by workers at BTL[3.51] and TRW[3.52] are shown in Figure 3.17 in normalized form. The major difference involves the behavior of the damage constant at proton energies greater than 10 MeV. Recent experimental investigations have confirmed that the variation of damage in this proton energy range is very small.[3.53, 3.54] The results of these recent investigations are also shown in Figure 3.17.

The degradation of n-p solar cells irradiated with protons of ener-

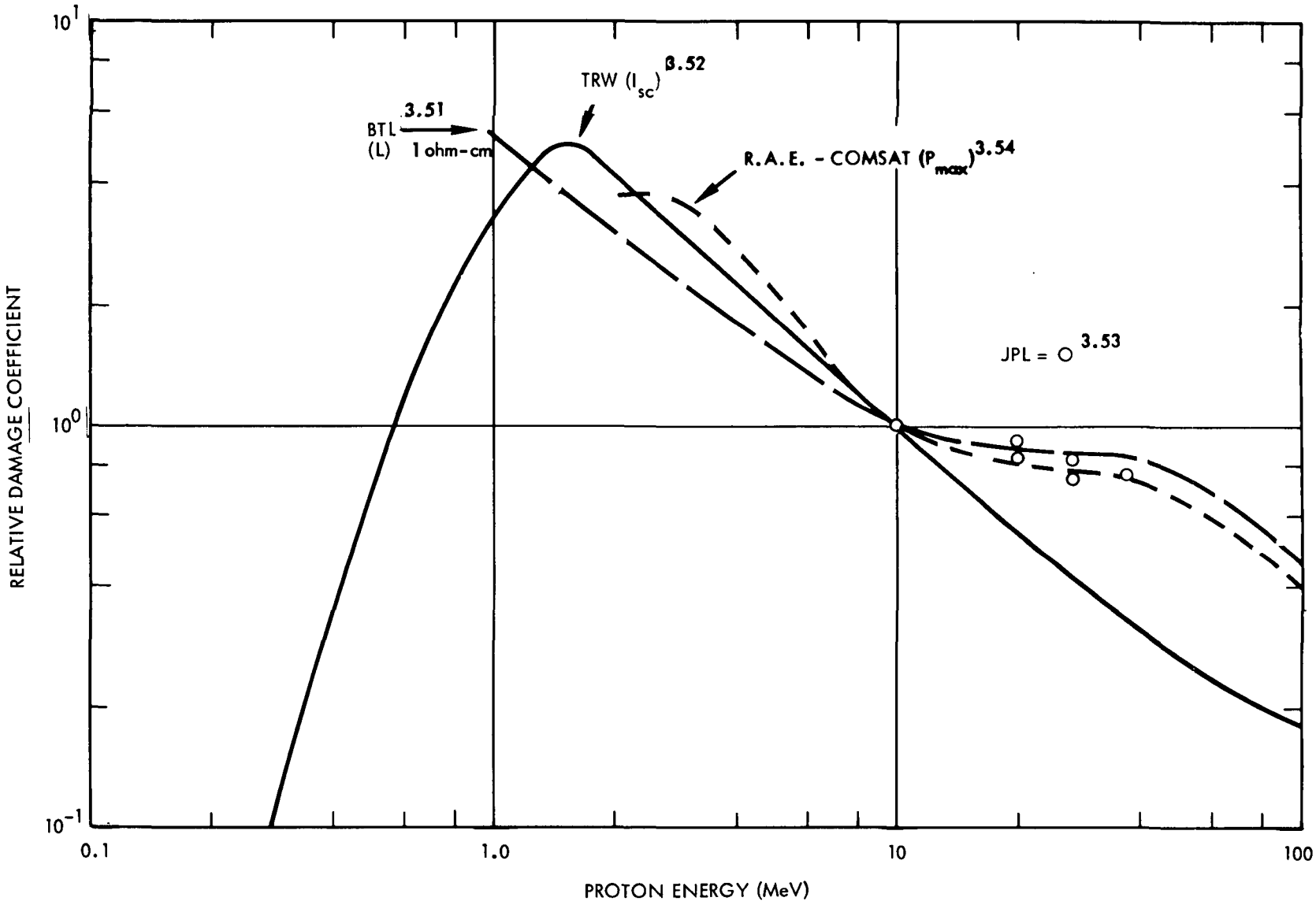

Figure 3.17 Relative Damage Coefficient for Proton Irradiation of N-P Silicon Solar Cells

gies below 3 MeV is more complex because of the nonuniform nature of the damage. Several experimental studies of low energy proton effects on unshielded solar cells have been reported in the literature.[3.41, 3.55-3.61] Although there are some differences in the reported results, a few general observations can be made. Protons in the energy range from 1.5 to 3 MeV produce a maximum in relative radiation damage in silicon solar cells. The relative damage to silicon solar cell V_{oc} and P_{max} due to low energy protons is more severe than that exhibited by the I_{sc}. Proton damage in silicon solar cells can be normalized to the damage produced by protons of one energy. The proton energy employed for normalization of relative damage should be close to that producing maximum damage in space environments, produce relatively uniform damage, and be available for laboratory evaluations. The use of 10 MeV proton damage is based on a compromise of the above requirements. The results of several studies of proton damage have been summarized in terms of relative silicon solar cell damage as a function of proton energy.[3.41, 3.53, 3.54, 3.55] These relative damage results, normalized to 10 MeV proton damage, are shown in Figure 3.18. The Results in Figure 3.18 have been shown to hold for both 10 ohm-cm and 2 ohm-cm solar cells at proton energies greater than 10 MeV.[5.33]

It is emphasized that the results in Figure 3.18 are obtained by normal incidence laboratory irradiation of solar cells from the front side. If similar data were prepared for normal incidence rear irradiations, the result would be similar for proton energies above 10 MeV.[3.53] The effects due to rear incidence protons with energies below 10 MeV would be much lower than shown in Figure 3.18[3.62] The lower effectiveness occurs because rear incident low energy protons have insufficient range in silicon to cause atomic displacements in the space charge region of the solar cell.

The variation of solar cell output parameters with 10 MeV proton fluence is described by equations (3.2.1), (3.2.5) and (3.2.10) in much the same way as is done for 1 MeV electrons. The values of the constants C, C', and C" tend to be somewhat greater than those found for 1 MeV electron irradiation. This value determines the decrease in solar cell output parameter per decade of radiation fluence. The fact that these

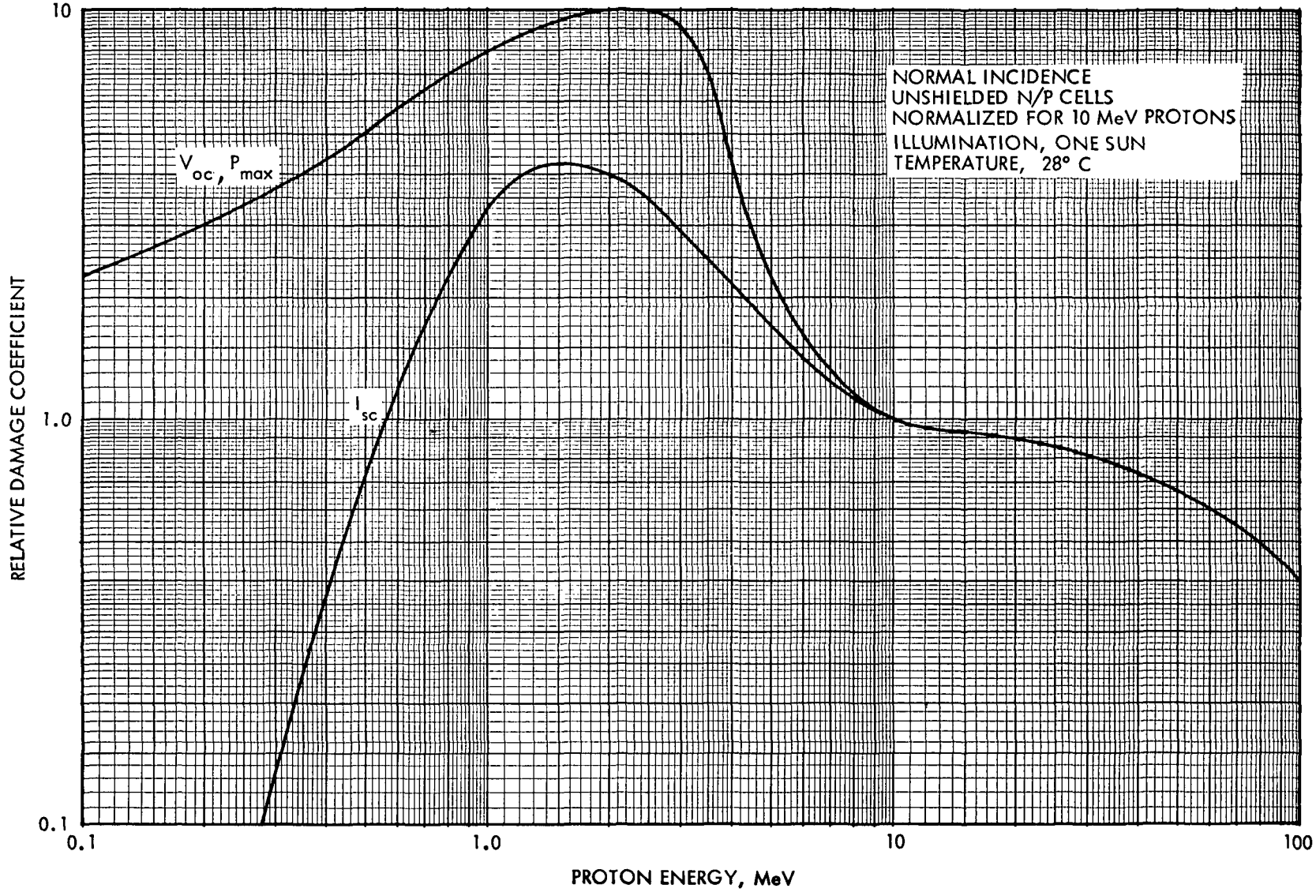

Figure 3.18 Relative Damage Coefficient for Proton Irradiation of N-P Silicon Solar Cells

constants are somewhat different for electron and proton irradiation indicates that the concept of equivalency between the different types of radiation has limitations and is basically an approximation. This equivalence is further discussed in Chapter 6.

3.7 Additional Effects of Low Energy Protons

In addition to the low energy proton effects on unshielded cells discussed in the previous section, there are two aspects of low energy proton damage to be considered. These involve the effects of low energy protons on small unshielded gap areas on the front of solar cells and on unshielded backs of solar cells.

When the ATS-1 and Intelsat II-F4 satellites suddenly exhibited degradations in power output of the order of 20% in weeks to a month after launch, the importance of low energy proton damage was dramatically demonstrated. Subsequent efforts related this anomalous degradation to the bombardment of narrow exposed surface areas of the solar cells by the intense low-energy proton fluence existing at synchronous altitude. The exposed areas resulted from slightly undersized or improperly applied cover slides which bared up to a 0.038 cm (15 mils) strip of solar cell surface. The high-intensity low-energy proton fluence, though incapable of penetrating the solar cell to a depth of more than a few microns, was able to produce junction damage which would shunt the power producing capability of the whole device. Exposed strips as narrow as 0.005 cm (2 mils) were sufficient to drastically alter the device's power producing capability. The absence of this effect in earlier solar array systems was attributed to shingling and overlapping adhesive.

The results discussed in the previous section clearly indicated that low energy proton irradiation has an inordinately greater effect upon solar cell V_{oc} and P_{max} as compared to similar irradiations with electrons or higher energy protons. The anomalous degradation of the ATS-1 and Intelsat II-F4 prompted many investigations into the effects

of low energy proton irradiation on partially shielded solar cells.[3.63-3.67] Curiously, Brucker and coworkers observed and reported this degradation effect in laboratory studies several months before the launch of ATS-1.[3.63] The results of these studies indicated that unshielded areas amounting to less than 1% of the total cell area can cause significant effects on cell power output. As a result of these studies, array manufacturers have taken measures to cover all areas of the silicon cell front surface with a cover slide and fill any gaps between the metallized base and cover slide with adhesive.

The changes caused by the irradiation of small unshielded areas of solar cells with low energy protons can be explained in terms of solar cell theory. It was previously mentioned that the range of low energy protons in silicon is limited to less than the cell thickness. Particles which do not penetrate the cell produce defects only to their depth of penetration. This limited penetration results in unusual effects in the case of protons because lower energy protons produce more displacements per unit path length. The results of this behavior are shown graphically in Figure 3.19. In this figure, the calculated number of displaced silicon atoms per unit proton path is plotted as a function of depth in silicon for a 3 MeV proton (range 92.7 μm). It can be seen that the damage rises rapidly to a maximum near the end of the proton track. Every proton which is stopped in the silicon produces such a damage peak at the end of its track. Protons which enter the silicon with energies of 0.5 MeV or less produce damage which is concentrated within a few microns of the cell surface. The space charge region of a modern cell extends from 0.4 to 1 micron below the cell surface. For this reason, low energy proton displacement damage is concentrated in the junction region.

The entire solar cell junction can be considered to be an array of small parallel diodes, each having a characteristic described by the parallel combination of equations (1.2.3) and (1.2.6). Damage to only a small portion of this parallel diode array results in an increased effective leakage or saturation current for the entire array.[3.61, 3.63] In Section 1.2, the nature of the generation-recombination current was discussed.

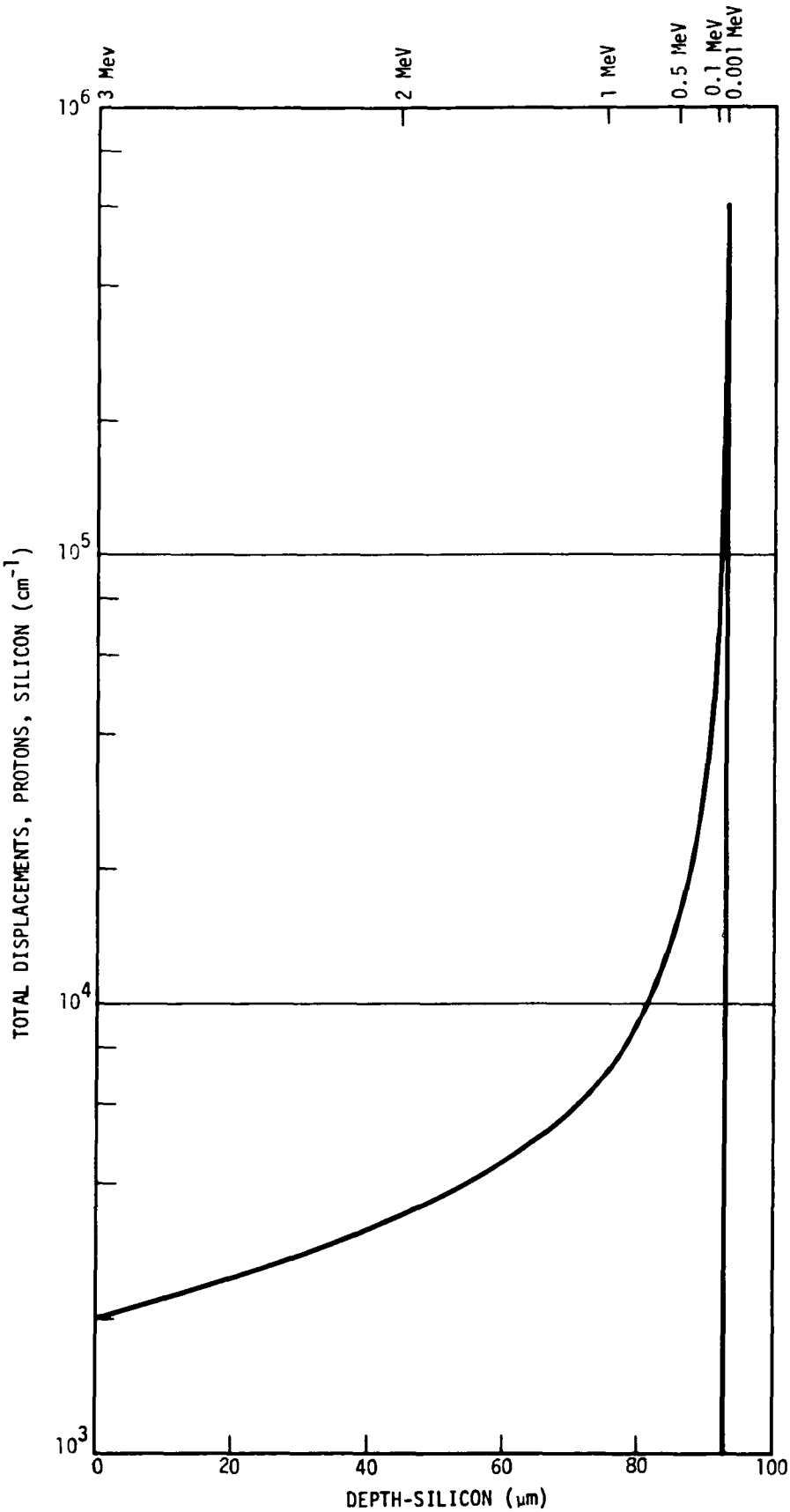

Figure 3.19 Atomic Displacements as a Function of Depth for a 3 MeV Proton in Silicon [3.26]

The saturation current due to generation-recombination in the space charge region (equation 1,2.7) increases linearly as the carrier lifetime decreases (i.e., displacement damage increases) in the space charge region. The increased leakage current of a solar cell reduces the cell V_{oc} because of the relationship of V_{oc} and I_o (junction leakage current) shown in equation (1.3.9). Since cell diode forward current (I_{D2}) is increased at all voltages, the cell P_{max} will also decrease because of low energy proton damage to small areas of the junction.

This effect is illustrated in Figure 3.20. A partially shielded solar cell was irradiated with 3×10^{13} p/cm^2 of 0.250 MeV protons. The current-voltage characteristics of this cell are shown before and after irradiation. The data indicate that the protons entered the silicon through a 0.0076 cm gap between the cover slide and the metallized bus strip. Although the I_{sc} of the cell was unaffected by the irradiation, significant degradations occurred in V_{oc} and P_{max}. Since solar cells are usually operated near the maximum power point, such changes have grave implications on in-flight performance.

It has been observed in laboratory studies that the effects of low energy protons on small unshielded areas of cells produce a maximum in the degradation at a fluence of about 3×10^{13} p/cm^2. It has been suggested that the reversal of degradation is due to carrier removal effects.[3.61,3.68] Considerable data exist regarding the effect of proton energy spectrum and busbar-cover slide gap width on the degradation.[3.65] Most reported laboratory studies have been confined to normal incidence proton irradiations.

In the past, solar cell usage has been confined to body-mounted solar cells on spinning satellites. Such applications provide a large measure of back shielding to a solar array. The requirements for increased spacecraft power and reduced weight have established trends toward the usage of oriented solar panels with minimal back shielding. Stofel has shown that low energy proton back side irradiation degrades silicon solar

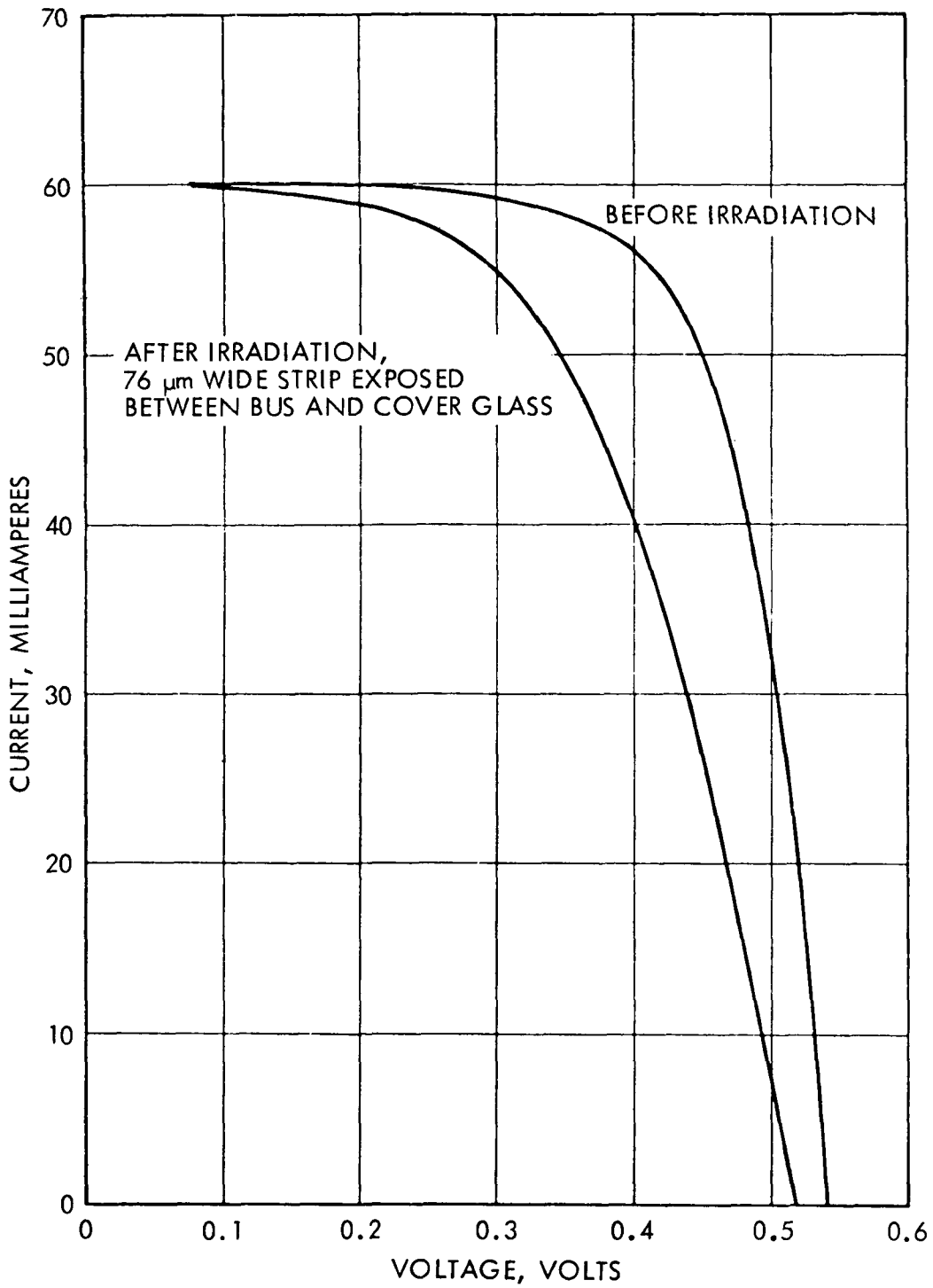

Figure 3.20 Low Energy Proton Junction Damage, 0.250 MeV Protons, $3 \times 10^{13} p/cm^2$, Partially Shielded N-P Solar Cell

cells through carrier removal effects.[3.61, 3.65] The use of thin soldered back contacts or other minimal back shielding should greatly reduce these effects.

3.8 Effect of Temperature and Illumination Intensity on Radiation Damage

The commonly used solar cell output parameters (I_{sc}, V_{oc}, and P_{max}) vary with temperature in a near linear manner in the temperature range of -50° to +100°C. The expression for V_{oc} (equation 1.3.9) varies directly with temperature and contains three other terms which vary with temperature (n, J_L, and J_o). The saturation current J_o increases rapidly as a function of temperature, and causes dV_{oc}/dT to have a relatively large negative value. The actual value of dV_{oc}/dT for unirradiated 2 to 10 ohm-cm cells varies from -2.4 to -2.1 mV/°C respectively or about -0.4%/°C regardless of resistivity. The temperature variation of I_{sc} is influenced by temperature variation of the absorption coefficient (α), and the minority carrier diffusion length (L) as indicated by equation (1.3.4). This causes a relatively small positive value of dI_{sc}/dT. The normalized value of dI_{sc}/dT found in unirradiated solar cells is approximately +0.05%/°C. The variation of current and voltage at P_{max} behaves similarly to that of the I_{sc} and V_{oc}, and because the temperature coefficient of V_{oc} is large and negative, this behavior is reflected in the temperature coefficient of P_{max} which is also large and negative. The normalized values of dP_{max}/dT are approximately 0.6%/°C for unirradiated solar cells. If dI_{sc} is normalized to the I_{sc}, this parameter is invarient with illumination intensity. The normalized or fractional dV_{oc}/dT decreases with illumination.

There are very limited data concerning the variation of the above temperature coefficients with irradiation. Luft has reported that the dV_{oc}/dT of silicon solar cells bombarded with 1 MeV electrons does not change significantly during irradiation.[3.69] Hayes and Ellis reported similar results for cells irradiated with 22 MeV protons or 2.4 MeV electrons.[3.42] The dI_{sc}/dT, however, is increased significantly by electron and proton irradiation. Luft's data indicate a roughly two-fold increase in dI_{sc}/dT between unirradiated cells and those irradiated

with 10^{14} one MeV electrons/cm^2, and a four-fold increase with 10^{16} one MeV electrons/cm^2. The data presented by Haynes and Ellis indicate that 22 MeV proton irradiations produce similar increases in dI_{sc}/dT. The increase in dI_{sc}/dT is due to the change in d_T/dT (i.e., dL/dT) caused by irradiation. The absolute dP_{max}/dT of cells irradiated with electrons or protons is decreased with fluence, however, when normalized to the unirradiated P_{max}, it exhibits a small negative increase with fluence.

Luft has also reported that the normalized or fractional temperature coefficient of I_{sc} for both unirradiated and 1 MeV electron irradiated solar cells is independent of illumination intensity. The normalized or fractional temperature coefficient of V_{oc} for both unirradiated and 1 MeV electron irradiated solar cells decreases linearly with increasing illumination.[3.69]

It should be emphasized that the above observations are based on "after the fact" measurements on solar cells which were irradiated at approximately 28°C. For this reason, they are not an indication of the effect of irradiation temperature on the production of radiation damage. A study at TRW indicated that the diffusion length damage constant (K_L) of n-p solar cells is independent of 1 MeV electron irradiation temperatures between -80°C and +130°C, but increases significantly at lower temperatures.[3.40] Workers at NRL have reported data which confirmed an increase in K_L at low temperatures.[3.70, 3.71, 3.72]

A study of 1 MeV electron radiation effects on silicon solar cells under extremely low temperature and low illumination (Jupiter environment) has been reported.[3.72] Debs and Hanes reported a study of 3 MeV proton damage to solar cells under Jupiter environment conditions. Their results indicate that n-p cells have higher starting efficiencies; however, after higher proton fluences, p-n 20 ohm-cm cells are more efficient.[3.73]

Although illumination has been shown to effect the evaluation of radiation damage in silicon solar cells through injection level effects, it has been assumed that the production of displacement type radiation damage in silicon solar cells is independent of illumination intensity

during irradiation. Reynard has reported that during real time beta ray irradiations, silicon solar cells, illuminated and electrically loaded, degraded more severely than similar cells irradiated dark without load.[3.74] The results of a similar study did not confirm the above result.[3.75]

Crabb recently reported that float zone silicon solar cells degraded with 1 MeV electrons exhibit a secondary degradation when illuminated with a 10 sun illumination intensity.[3.76]

3.9 Effects of Neutron and Gamma Radiation on Solar Cells

The radiation associated with nuclear weapons degrades solar arrays in the same manner as the radiation of the space environment. Solar array designers must allow for these effects when weapon events are included in the environment. The radiation from a weapon event is delivered at a much higher rate than space radiation. Because of these high radiation rates, other aspects of radiation effects become more apparent immediately following a nuclear radiation pulse.

The most important aspect of neutron radiation on silicon solar cells is displacement damage which reduces the minority carrier lifetime in the same manner as protons and electrons. When silicon devices receive neutron irradiation at room temperature, a large fraction of the displacement damage anneals within 100 seconds after the irradiation. The ratio of the damage produced to that which does not anneal is referred to in the literature as the annealing factor.[3.77, 3.34]

Annealing factors larger than 10 have been reported. Such behavior is not suprising, because calculated displacement rates for various radiations are usually much greater than those found experimentally. The transient annealing of neutron damage is not an important consideration in the design of solar arrays; however, the nonannealing component of neutron damage will contribute to the permanent damage produced by space radiation. This aspect of neutron damage has been studied by Brucker,[3.78] Downing,[3.79] Morris,[3.80] Stofel,[3.81] and Hicks.[3.82] Most of these studies utilized fission neutrons from nuclear reactors. If the fission spectrum of such reactors is averaged by weighting each

energy component by its theoretical displacement damage factor,[3.83] the mean neutron energy is very close to 1 MeV. The degradation of n-p silicon solar cell parameters with neutron irradiation is shown in Figure 3.21.[3.81] Neutron fluences may be converted to damage equivalent 1 MeV electron fluences by following expression:

$$\Phi_{1\ \text{MeV}\ e} = 2000 \times \Phi_{1\ \text{MeV}\ n} \qquad (3.9.1)$$

When neutron damage is evaluated with a solar simulator and described by equation (3.2.1), the constant C is approximately equal to 6 mA/cm^2 per decade fluence. This value is significantly larger than that found for electron irradiation. Similar slope values are found in cells irradiated with high energy protons. Work by Gregory[3.33] and Stofel[3.81] has shown that diffusion lengths measured in neutron-irradiated solar cells increase with the excess minority carrier concentration. This behavior is similar to that reported for proton-irradiated solar cells.

Gamma ray radiation interacts with silicon mainly by the production of Compton electrons. These secondary particles have energies high enough to cause displacement damage in silicon solar cells. The effect of gamma radiation on silicon solar cells has been reported by Fang[3.84] and Hicks.[3.82] The results of Cobalt 60 gamma irradiation of n-p silicon solar cells are shown in Figure 3.6. The permanent damage aspects of prompt gamma radiation from nuclear weapons can usually be neglected.

The most important aspect of gamma radiation from weapons is the transient photocurrent generated in the array during a nuclear event. The primary photocurrent can be estimated from the following expression:

$$I_{pp} = 6.4(\mu A\ cm^{-3}\ rad^{-1}\ sec) \cdot \dot{\gamma} \cdot A \cdot L \qquad (3.9.2)$$

where $\dot{\gamma}$ = dose rate (rad/sec)

L = diffusion length (cm)

A = cell junction area (cm^2)

The transient rise and fall of the photocurrent has been treated by Wirth and Rogers.[3.85] The peak current values developed by solar cells under these conditions can be very large and may cause problems in circuits interfacing with the solar array. Current limiting by the external load

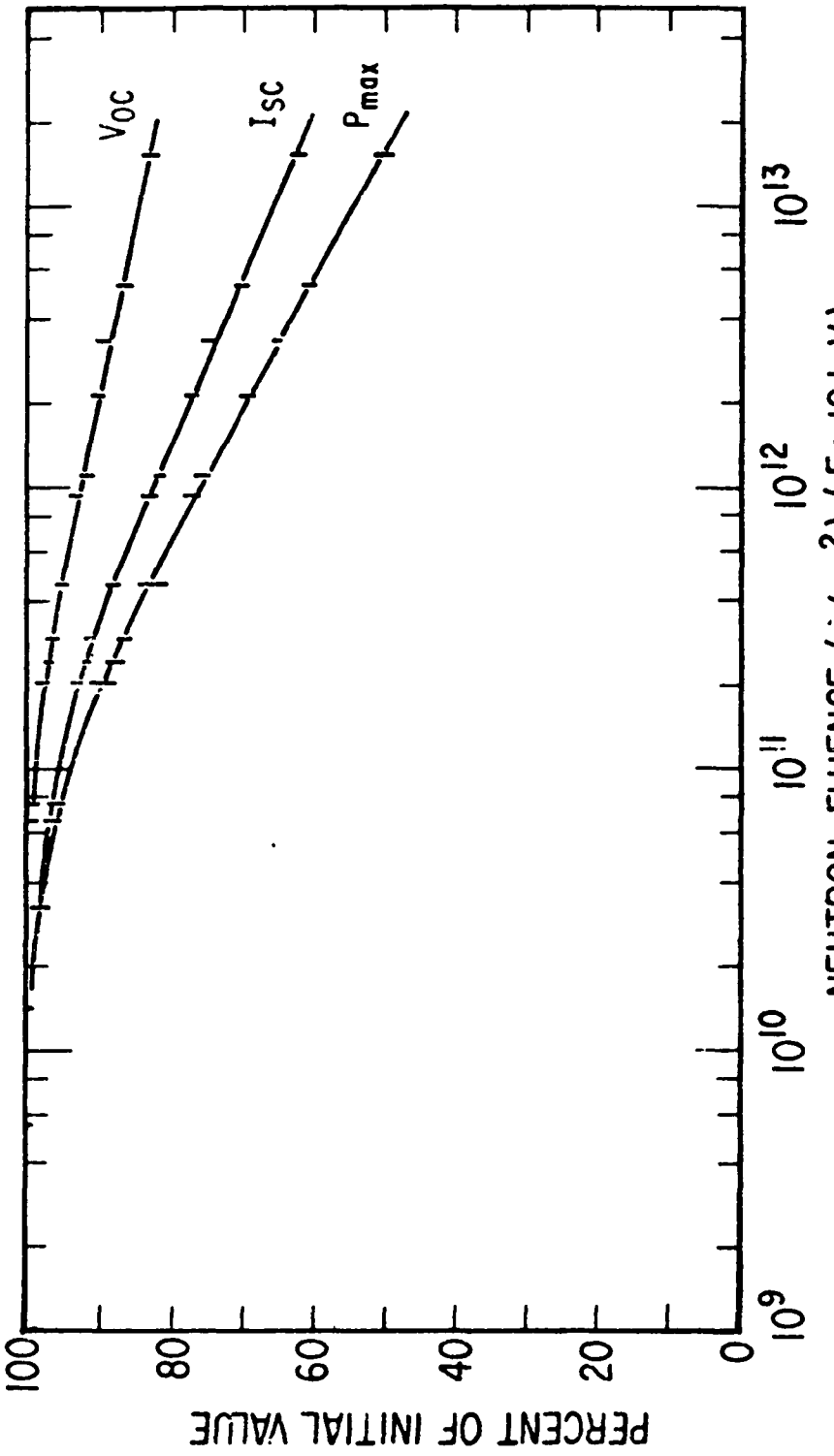

Figure 3.21 Neutron irradiation-induced change in n/p silicon solar cells (space sunlight illumination).[3.81]

and the internal cell series resistance may limit the observed photocurrents to values well below the generated current. Under very intense pulses of such ionizing radiation at room temperature the cell V_{oc} saturates at approximately 0.7 V.[3.86-3.88] This value appears to be related to the barrier potential (V_b) of the junction as determined by capacitance-voltage measurements.

3.10 Lithium Doped Solar Cells

Interest in this field began with Vavilov's report of a radiation resistant diode made with lithium-doped, crucible grown silicon.[3.89] Wysocki later reported lithium-doped solar cells which degraded under electron irradiation, but rapidly recovered at room temperature.[3.90] Float zone silicon, with a characteristic lower oxygen concentration, was used to achieve this result. Subsequent work indicated that recovery also occurred in lithium-doped, quartz-crucible silicon solar cells. Since this initial work, the general subject was studied in two ways. Empirical changes in the manufacturing techniques for lithium-doped solar cells were evaluated with the aim of optimizing the recovery effect.[3.91, 3.92] Other studies were directed at the development of a physical model of the degradation and recovery processes in lithium-doped silicon.

Some of the more pertinent facts gained during these studies are as follows. The lithium concentration in a solar cell is not uniform, but increases in a linear or near linear manner with distance from the solar cell junction. This characteristic can be used to advantage to produce cells with exceptionally high open-circuit voltages. Solar cells *with low or insufficient lithium concentrations do not recover in a satis*factory manner. Float zone silicon solar cells with exceptionally high lithium concentrations lose efficiency during storage in the unirradiated condition. These same cells, when irradiated and recovered, also exhibit a time-dependent loss of efficiency. This loss has been related to the room temperature diffusion of lithium into the active area of the cell. It has also been observed that higher lithium concentrations cause faster recovery rates. Because of the recovery rate dependence of the radiation damage in lithium-doped solar cells, it was difficult to evaluate cell performance by accelerator irradiations. Real time irradiations of

lithium-doped solar cells have been done with beta particle sources. The results of these beta irradiations indicated that some types of lithium-doped solar cells are slightly superior to n-p cells under some temperature conditions. The major potential advantages of lithium-doped solar cells over conventional n-p solar cells are in regard to proton[3.53, 3.90] and neutron damage.[3.79, 3.93] Figure 3.22 shows that lithium doped solar cells are clearly superior to conventional cells. The long recovery period following a neutron exposure would probably be a severe limitation in military spacecraft. The most advantageous uses of lithium-doped solar cells would be for spacecraft in proton dominated orbits with high proton fluxes. At present, such orbits are not commonly used. A summary of the current state of the art in lithium-doped solar cells was recently published by Berman,[3.94]

3.11 Radiation Effects on Shielding Materials

The degradation due to radiation effects on solar cell cover slide material in space is difficult to assess. The different radiation components of the environment act individually and synergistically on the elements of the shielding material and also cause changes in the interaction of shielding elements. The complexity is illustrated in Table 3.2, where the various effects reported for commonly used cover materials are summarized and referenced. In addition to the data in Table 3.2, a large volume of data have been presented in the literature regarding materials currently not in use for shielding solar cells. In this section, the emphasis will be on solar cell shielding material currently used in array construction.

The cover glass shielding currently in use in most spacecraft construction is usually fabricated from Corning #0211 Microsheet or Corning #7940 fused silica. Where thin covers are desired, the usage tends toward Microsheet, because it is relatively inexpensive in thin sections. Where thicker covers are desired, Corning #7940 fused silica is used to avoid the darkening due to radiation. Cover glasses are always used with a MgF_2 antireflecting front coating and an ultraviolet rejecting filter on the rear surface. Cover glasses are usually attached to solar cells with silicone elastomers.

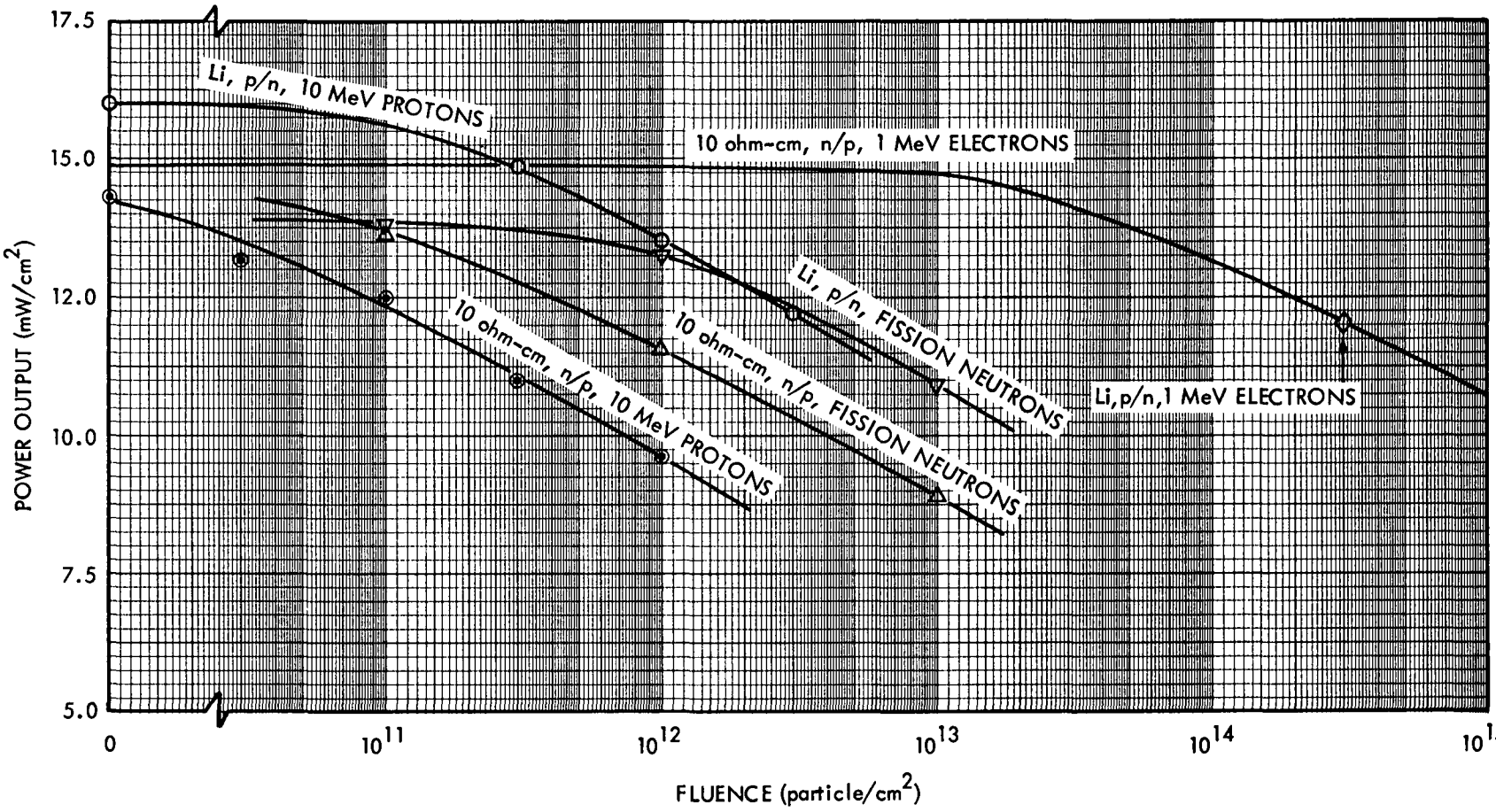

Figure 3.22 Recovered Power Output of Irradiated Conventional and Lithium Doped Solar Cells [3.53, 3.93]

TABLE 3.2

RADIATION EFFECTS ON SHIELDING MATERIALS

	Anti-Reflective Coating On Cover Glass	Cover Glass		Blue Filter On Cover Glass	Silicone Adhesives
		Corning #0211 Microsheet	Corning #7940 Fused Quartz		
keV Protons	Degrades Transmission 3.95, 3.96 3.97				
MeV Protons		Degrades Transmission 3.95, 3.98, 3.104	No Transmission Loss 3.95, 3.98	Degrades Transmission 3.95, 3.98	No Transmission Loss 3.109
MeV Electrons		Degrades Transmission 3.98, 3.99, 3.100, 3.102, 3.103, 3.105	No Transmission Loss 3.98, 3.100, 3.101, 3.102, 3.103, 3.105	Degrades Transmission 3.100, 3.105	No Transmission Loss 3.109
Ultraviolet Light		Bleaches Transmission Loss Due to Radiation 3.107	Degrades Transmission 3.106 No Absorptance Change 3.108	Degrades Transmission, Reduced μV Rejection 3.110	Degrades Transmission 3.100, 3.109

Most experimental assessments of radiation effects are based on accelerated testing in which a complete space environment is not simulated. This may account for some of the differences between darkening of cover glass material observed in laboratory radiation studies and space flight data for covered solar cells which indicated that radiation effects in cover materials were insignificant.[3.111]

The radiation effects observed in cover materials can be characterized as ionization damage rather than displacement damage. In general, ionization effects are usually dependent upon the absorbed dose and to that degree are independent of particle type or energy. Some exceptions to this rule occur in the case of highly charged massive particles. In such cases, the ionization effects may be concentrated along the particle track rather than uniformly distributed.[3.112] It is reasonable to assume that the ionization damage produced in cover materials by space electrons and protons is related to the total absorbed dose. This assumption allows the various radiation components of the space environment to be reduced to a total dose, without a laborious determination of degradation constants for each energy and particle. It also allows the use of experimental data from a single ionizing environment such as 1 MeV electrons.

The most significant radiation effects in cover materials involve changes in the transmission of light in the visible and near infrared region. These data are commonly reported as spectral transmission data. The use of cover-glass spectral-transmission data in determining changes in solar cell output is rather cumbersome. This procedure was outlined by Campbell.[3.98] An alternate approach to the reporting of the data is the use of so-called "wide band" transmission loss. In this method, solar cell short-circuit currents are measured under sun simulated conditions, with cover slides attached. The cover slides are attached with a thin liquid film with an index of refraction (n = 1.4) similar to that of silicone adhesive. Cyclohexane and n-amyl alcohol have been used for this purpose. The "wide band" transmittance is defined as the solar cell I_{sc} with an irradiated cover slide in place divided by the solar cell I_{sc} with the unirradiated cover slide in place. Such measurements are influenced by solar cell spectral response. Results

determined with unirradiated solar cells will not be representative of those for irradiated solar cells. This error is probably negligible compared to the uncertainty of the available experimental data.

Since the "wide band" transmission loss is a measure of the loss in light transmitted, it directly affects the light generated current (I_L) and likewise the short circuit current (I_{sc}). It is desirable to use the "wide band" transmission data to estimate the change in solar cell P_{max}. Equation (3.2.9) indicates that cell P_{max} is proportional to the product of I_{sc} and V_{oc}. Because V_{oc} is proportional to ln I_{sc}, the following relation can be developed to estimate the change in P_{max} due to cover slide darkening from transmission data:

$$\frac{P_{max}}{P_{maxo}} = T\left[\frac{\ln (T \cdot I_{sc})}{\ln (I_{sc})}\right] \qquad (3.11.1)$$

where P_{max}/P_{maxo} = the fractional change in P_{max}

T = the "wide band" transmission of irradiated cover glass

I_{sc} = the short circuit current of cell with unirradiated cover glass

To aid in the estimation of solar array losses due to reduced transmission from radiation effects in cover slide materials, data relating transmittance to absorbed dose is required. In Figure 3.23, "wide band" transmittance is shown for various absorbed doses. The absorbed doses were produced by 1 MeV electron irradiations in a room temperature, air environment which included no ultraviolet illumination. This electron radiation is sufficiently penetrating to produce a relatively uniform dose through the entire cover slide, coating, and filter. The P_{max}/P_{maxo} data shown in Figure 3.23 was calculated from the "wide band" transmittance value by use of equation (3.11.1). The data in Figure 3.23 include 0.0152 cm (0.006 in.) 7940 fused silica and 0211 Microsheet cover slides with antireflecting coating and blue filter. It is an established fact that Corning #7940 fused silica exhibits little or no darkening due to radiation in the visible region. Since the transmission loss for 7940

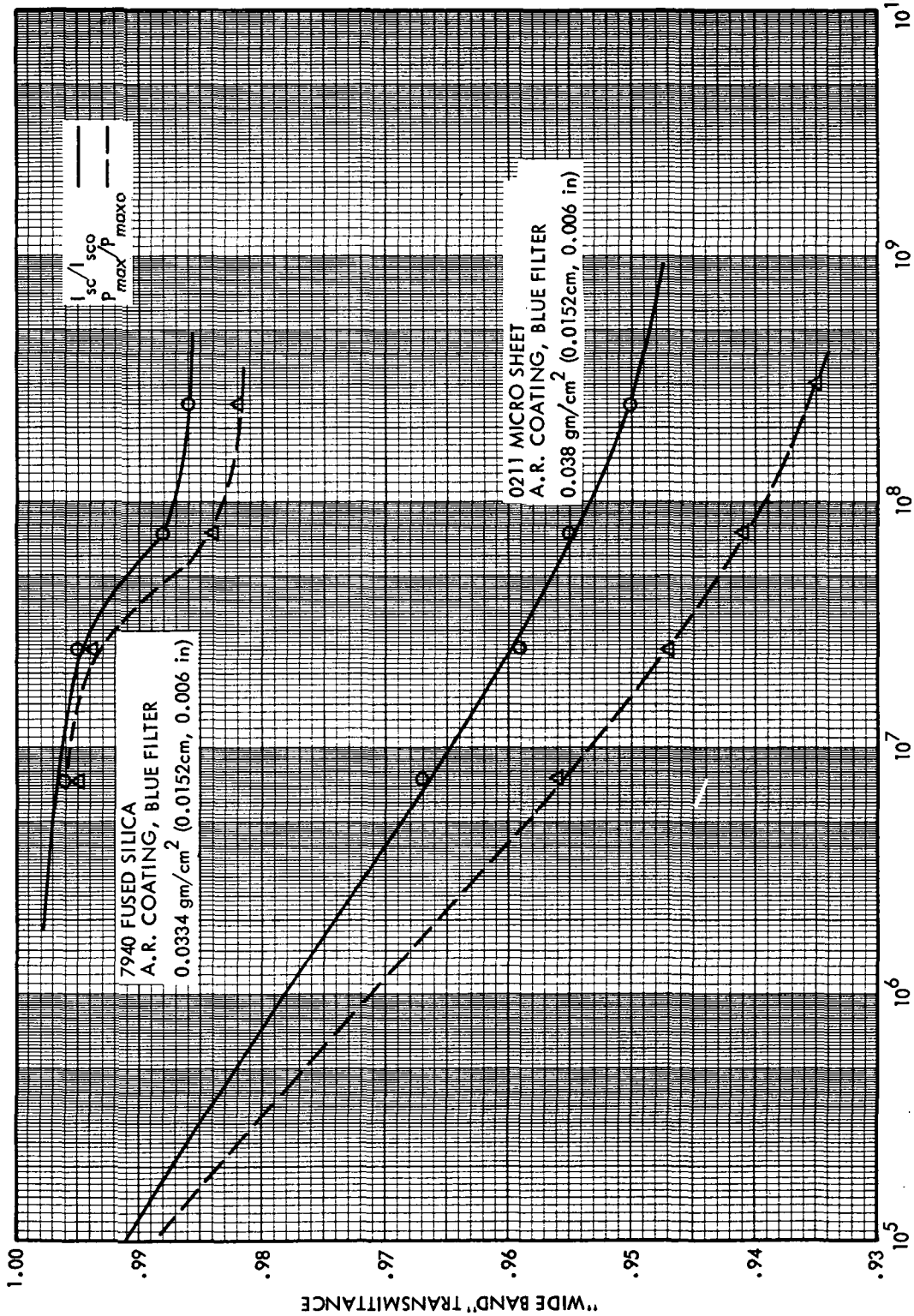

Figure 3.23 Variation of Cover Glass Transmittance with Absorbed Dose

cover glasses must be assumed to be due to changes in the filter, the data can also be used for thicker cover slices. For thicker 0211 Microsheet cover glass, the data in Figure 3.23 cannot be used.

The dose-depth profiles experienced by cover glass shielding in space are highly non-uniform due to the low energy protons stopped in the front surface. To accurately estimate the transmission through a cover glass with such a dose-depth profile, would require the integration of absorption coefficients (as a function of dose) through the cover glass and its thin film layer. The lack of absorption coefficient data for these materials for various doses in a total space environment does not allow such evaluations at this time.

The diversity of technical opinions on transmission loss in cover glass due to space radiation also includes those who do not include this factor in array power estimates and those who simply allow for a 2% to 4% initial loss due to cover glasses and adhesive darkening due to radiation and ultraviolet effects. Recent studies by Luedke at TRW indicated that nearly all darkening produced in 0211 Microsheet by a dose of 10^7 rad(SiO_2) was bleached by a relatively short ultraviolet light exposure.[3.107] Such results indicate that the use of data such as that in Figure 3.23 is probably an overly conservative practice and emphasizes the importance of performing cover glass darkening studies in a realistic environment. Some investigations have reported results which indicate that cerium doping of glass reduces or eliminates darkening due to irradiation.[3.104, 3.113] Other studies indicated that hydrogen impregnation of glasses reduces transmission losses due to irradiation effects.[3.114]

REFERENCES

3.1 F. Seitz and J. S. Koehler, "Displacement of Atoms During Irradiation", Solid State Physics, Vol. 2, p.305, Academic Paris, 1956.

3.2 J. J. Loferski and P. Rappaport, "Radiation Damage in Ge and Si Detected by Carrier Lifetime Changes - Damage Thresholds", Phys. Rev., 111, 2, 432, 1958.

3.3 H. Flicker, J. J. Loferski and J. Scott-Monck, "Radiation Defect Introduction Rates in n- and p- Type Silicon in the Vicinity of the Radiation Damage Threshold", Phys. Rev. 128, 6, 2557, 1962.

3.4 N. N. Gersimenko, et al., "Threshold Energy for the Formation of Radiation Defects in Semiconductors", Soviet Physics - Semiconductors, 5, 8, 1439, 1972.

3.5 G. W. Kinchen and R. S. Pease, "The Displacement of Atoms in Solids by Radiation", Report Prog. Phys. 18, 1, 1955.

3.6 G. Benski, "Paramagnetic Resonance in Electron Irradiated Silicon", J. Appl. Phys. 30, 8, 1195, 1959.

3.7 G. D. Watkins, J. W. Corbett and R. M. Walker, "Spin Resonance in Electron Irradiated Silicon", J. Appl. Phys., 30, 8, 1198, 1959.

3.8 G. D. Watkins and J. W. Corbett, "Defects in Irradiated Silicon. I. Electron Spin Resonance of the Si-A Center", Phys. Rev. 121, 4, 1001, 1961.

3.9 J. W. Corbett, et al., "Defects in Irradiated Silicon. II Infrared Absorption of the Si-A Center", Phys. Rev. 121, 4, 1015, 1961.

3.10 G. D. Watkins and J. W. Corbett, "Defects in Irradiated Silicon: Electron Paramagnetic Resonance and Electron-Nuclear Double Resonance of the Si-E Center", Phys. Rev., 134, 5A, A1359, 1964.

3.11 G. K. Wertheim, "Energy Levels in Electron-Bombarded Silicon", Phys. Rev. 105, 1730, 1957.

3.12 G. K. Wertheim, "Electron-Bombardment Damage in Silicon", Phys. Rev. 110, 1272, 1958.

3.13 H. Saito and M. Hirata, "Nature of Radiation Defects in Silicon Single Crystals", Japanese J. of Appl. Phys., 2, 11, 678, 1963.

3.14 J. R. Carter, Jr., "Effect of Electron Energy on Defect Introduction in Silicon", J. Phys. Chem. Solids, 27, 913, 1966.

3.15 M. Hirata, et al., "Effects of Impurities on the Annealing Behavior of Irradiated Silicon", J. Appl. Phys., 30, 6, 2433, 1967.

3.16 H. Flicker and W. R. Patterson, III, "Theoretical Calculation of the Direct Production of Divacancies in Silicon", J. Appl. Phys. 37, 13, 4998, 1966.

3.17 S. M. Gorodetskii and L. B. Kreinin, "A Possible Mechanism for the Formation of Complex Radiation Defects in Silicon Caused by Electron Bombardment", Soviet Physics-Doklady, 13, 7, 660, 1969.

3.18 G. Benski, "A New Paramagnetic Center in Electron Irradiated Silicon", J. Phys. Chem. Solids, 24, 1, 1963.

3.19 G. D. Watkins and J. W. Corbett, "Defects in Irradiated Silicon: Electron Paramagnetic Resonance of the Divacancy", Phys. Rev. 138, 2A, A543, 1965.

3.20 N. Almeleh and B. Goldstein, "Electron Paramagnetic Resonance and Electrical Properties in Electron-Irradiated p-Type Silicon", Phys. Rev. 149, 687, 1966.

3.21 J. A. Baicker, "Recombination and Trapping in Normal and Electron-Irradiated Silicon", Phys. Rev. 129, 1174, 1963.

3.22 S. M. Gorodetskii, et al., "Recombination in p-Type Silicon Irradiated with Fast Electrons", Soviet Physics-Semiconductors, Vol. 5, 7, 1280, 1972.

3.23 R. G. Downing, J. R. Carter, Jr. and J. M. Denney, "The Energy Dependence of Electron Damage in Silicon", Proceedings of the Fourth Photovoltaic Specialists Conference, Vol. I, A-5-1, 1964

3.24 J. A. Baicker, H. Flicker, J. Vilms, "Proton Induced Lattice Displacement in Silicon", Appl. Phys. Letters, 2, 5, 104, 1963.

3.25 G. W. Simon, J. M. Denney, and R. G. Downing, "Energy Dependence of Proton Damage in Silicon", Phys. Rev. 129, 6, 2454, 1963.

3.26 Yu. V. Bulgakov and M. A. Kumakhov, "Spatial Distribution of Radiation Defects in Materials Irradiated with Beams of Monoenergetic Particles", Soviet Physics-Semiconductors, Vol. 5, 11, 1334, 1969.

3.27 J. R. Bilinski, et al., "Proton-Neutron Damage Equivalence in Si and Ge Semiconductors", IEEE Trans. on Nuc. Sci. NS-10, 5, 71, 1963.

3.28 Y. Gervais de Lafond, "Interactions Proton-Silicum Et Proton-Germanium Entre 1 Et 3000 MeV", Thesis, University of Toulouse, 12 May 1969.

3.29 J. R. Carter, Jr., "Study of Energy Levels in High Energy Proton Damaged Silicon", IEEE Trans. on Nuc. Sci. NS-11, 1, 290, 1964.

3.30 R. Breckenridge, "Proton-Produced Defects in n-Type Silicon", NASA TN D-4830, 1968.

3.31 D. Bielle-Daspet, "Effects De Protons De Grande Energie Sur Les Proprietes Electriques Du Silicium Et Du Germanium", Thesis, University of Toulouse, 2 March 1970.

3.32 B. R. Gossick, "Disordered Regions in Semiconductors Bombarded by Fast Neutrons", J. Appl. Phys., 30, 8, 1214, 1959.

3.33 B. L. Gregory, "Minority Carrier Recommendations in Neutron Irradiated Silicon", IEEE Trans. on Nuc. Sci., NS-16, 6, 53, 1969.

3.34 R. E. Leadon, "Model for Short-Term Annealing of Neutron Annealing of Neutron Damage in p-Type Silicon", IEEE Trans. on Nuc. Sci., NS-17, 6, 110, 1970.

3.35 R. R. Holmes, "Carrier Removal in Neutron Irradiated Silicon", IEEE Trans. on Nuc. Sci., NS-17, 6, 137, 1970.

3.36 J. M. Denney, et al., "Effect of 1 MeV Electrons Bombardment on Solar Cells", TRW Systems Report 8653-6018-KU-000, 11 Feb. 1963.

3.37 J. Bernard, et al., "Effects of Proton and Electron Radiation on French Silicon Solar Cells", Solar Cells, Gordon and Breach, London, p. 623, 1971.

3.38 H. Y. Tada, "A Theoretical Model for Low-Energy Proton Irradiation Silicon Solar Cells", Proceedings of the Fifth Photovoltaic Specialists Conf., Vol. II, D-8-1, 1966.

3.39 J. H. Martin, R. L. Statler and E. L. Ralph, "Radiation Damage to Thin Silicon Solar Cells", Advances in Energy Conversion Engineering, ASME 1967.

3.40 J. R. Carter, Jr., R. G. Downing and H. Flicker, "Effects of High Energy Electrons in Silicon and Silicon Solar Cells", TRW Report 4161-6023-R000, 25 May 1966.

3.41 J. R. Carter, Jr. and R. G. Downing, "Effects of Low Energy Protons and High Energy Electrons on Silicon", NASA CR-404, March 1966.

3.42 G. H. Haynes and W. E. Ellis, "Effects of 22 MeV Proton and 2.4 MeV Electron Radiation on Boron and Aluminum-Doped Silicon Solar Cells", NASA TND-4407, April 1968.

3.43 D. Lesbre, "Amelioration De La Resistance Des Cellules Solaires Aux Rayonnements", Thesis, University of Toulouse, 12 May 1969.

3.44 W. R. Cherry and R. L. Statler, "Photovoltaic Properties of U. S. and European Silicon Cells Under 1-MeV Electron Irradiation", Goddard Space Flight Center, X-716-68-204, April 1968.

3.45 W. Luft and H. S. Rauschenbach, "Effects of Base Resistivity in the Characteristics of N-or-P Silicon Solar Cells", Conf. Record of the Sixth Photovoltaic Specialists, Vol. III, 75, 1967.

3.46 E. L. Ralph, "Performance of Very Thin Silicon Solar Cells", Conf. Record of the Sixth Photocoltaic Specialists Conf., IEEE, Vol. I, 98, 1967.

3.47 R. L. Crabb, "Status Report on Thin Silicon Solar Cells For Large Flexible Arrays", Solar Cells, Gordon and Breach, p. 35, 1971.

3.48 W. Brown, I. Gabbe and W. Rosenzweig, "Results of the Telstar Radiation Experiments", Bell System Tech. J. XLII, 4, Part 2, 1505, July 1963.

3.49 J. J. Wysocki, "Radiation Studies on GaAs and Si Devices", IEEE Trans. on Nuc. Sci., NS-10, 5, 60, 1963.

3.50 S. M. Gorodetskii, et al., "Influence of Electron Bombardment on Some Parameters of Silicon Photocells", Soviet Physics-Semiconductors, Vol. 2, 1, 90, 1968.

3.51 W. Rosenzweig, F. M. Smits and W. L. Brown, "Energy Dependance of Proton Irradiation Damage in Silicon", J. Appl. Phys. 35, 9, 2707, 1964.

3.52 J. M. Denney and R. G. Downing, "Proton Radiation Damage in Silicon Solar Cells", TRW Systems Report 8653-6026-KV-000, 16 July 1963.

3.53 B. E. Anspaugh, to be published.

3.54 A. Meulenberg, Jr., and F. C. Treble, to be published, Tenth PVSC.

3.55 D. Reynard, "Proton and Electron Irradiation of N/P Silicon Solar Cells", Lockheed Missile and Space Co. Report 3-56-65-4, 12 April 1965.

3.56 J. J. Wysocki, et al., "Low-Energy Proton Bombardment of GaAs and Si Solar Cells", IEEE Trans. on Electronic Devices, ED-13, 4, 420, 1966.

3.57 E. A. Lodi, et al., "Low Energy Proton Degradation in Silicon Solar Cells", Proceedings of the Fourth Photovoltaic Specialists Conf., Vol. 1, A-4-1, 1964.

3.58 A. G. Stanley, "Comparison of Low-Energy Proton Damage in Ion-Implanted and Diffused Silicon Solar Cells", Proc. of IEEE, p 321, Feb 1971.

3.59 I. Nashiyama, et al., "Proton and Deuteron Irradiation Damage in Silicon Solar Cells", Japanese J. of Appl. Phys. 10, 11, 1564, 1971.

3.60 R. R. Brown, "Surface Effects in Silicon Solar Cells", IEEE Trans. on Nuc. Sci., NS-14, 6, 260, 1967.

3.61 E. Stofel and D. Joslin, "Low-Energy Proton Damage to Silicon Solar Cells", IEEE Trans. on Nuc. Sci., NS-17, 6, 250, 1970.

3.62 E. Stofel and D. Joslin, "Low-Energy Proton Irradiation of Solar Cell Back Contacts", Conf. Record of the Eighth Photovoltaic Specialists Conf., 209, 1970.

3.63 G. J. Brucker, et al., "Low Energy Proton Damage in Partially Shielded Solar Cells", Proc. IEEE 54, 798, 1966.

3.64 W. D. Brown, "ATS Power Subsystem Radiation Effects Study", Hughes Aircraft Company, NAS 5-3823, SSD-80089R, 1968.

3.65 L. J. Goldhammer, "Solar Cell Radiation Flight Report", Hughes Aircraft Co. Report SSD-90329R, 30 May 1969.

3.66 R. L. Statler and D. J. Curtin, "Low Energy Proton Damage in Silicon Solar Cells", Conf. Record of the Seventh Photovoltaic Specialists Conference, IEEE, 177, 1968.

3.67 R. L. Statler and D. J. Curtin, "Radiation Damage in Silicon Solar Cells from Low Energy Protons", IEEE Trans. Electron Devices ED-18, 7, 412, 1971.

3.68 D. J. Curtin, "Testing of Solar Cells for Communication Satellites", Solar Cells, Gordon and Breach, London, p 605, 1971.

3.69 W. Luft, "Effects of Electron Irradiation on N on P Silicon Solar Cells", Advanced Energy Conversion, 5, 21, 1965.

3.70 R. L. Statler, et al., "Annual Report for Solar Cell Research", Naval Research Laboratory, Under Work Order 8056, 15 Oct 1969.

3.71 N. D. Wilsey, "The Effect of Boron Concentration on Radiation Damage in Silicon Solar Cells", Conf. Record of the Ninth Photovoltaic Specialists Conf., IEEE, 338, 1972.

3.72 N. D. Wilsey and R. J. Lambert, "Low Temperature Irradiations of Silicon Solar Cells with 1 MeV Electrons", Conf. Record of the Eighth Photovoltaic Specialists Conf., IEEE, 169, 1970.

3.73 R. J. Debs and N. R. Hanes, "Preliminary Results of Radiation and Jupiter Environment Tests on Solar Cells", ibid., 155.

3.74 D. L. Reynard and D. G. Peterson, "Results of Real-Time Irradiation of Lithium P/N and Conventional N/P Silicon Solar Cells", Conf. Record of the Ninth IEEE Photovoltaic Specialists Conf., p 303, 1972.

3.75 M. C. Whiffen and E. B. Trent, "The Effects of Radiation on Lithium Doped Solar Cells", Lockheed-Georgia Co. Report ER-11150, July 1971.

3.76 R. L. Crabb, "Photon Induced Degradation of Electron Irradiated Silicon Solar Cells", Conf. Record Ninth IEEE Photovoltaic Specialists Conf., p 329, 1971.

3.77 H. H. Sander and B. L. Gregory, "Transient Annealing in Semiconductor Devices Following Pulsed Neutron Irradiation", IEEE Trans on Nuc. Sci. NS-13, 6, 63, 1966.

3.78 G. J. Brucker and B. Markow, "Neutron Damage in Silicon Solar Cells", Conf. Record of the Sixth Photovoltaics Specialists Conf. Vol. III, p 53, 1967.

3.79 E. L. Ralph, et al., "Lithium Doped Hardened Solar Cell Optimization", AFAPL-TR-70-35, May 1970.

3.80 W. M. Morris, "Effect of 14 MeV Neutrons on Silicon Solar Cells", Thesis, University of Utah, June 1970.

3.81 E. J. Stofel, T. B. Stewart and J. R. Ornelas, "Neutron Damage to Silicon Solar Cells", IEEE Trans. on Nuc. Sci., NS-16, 5, 97, 1969.

3.82 J. M. Hicks, "Solar Cell Neutron Damage Investigations", AFAPL-TR-70-24, May 1970.

3.83 E. C. Smith, "Theoretical and Experimental Determination of Neutrons Energy Deposition in Silicon", IEEE Trans. on Nuc. Sci., NS-13, 6, 11, 1966.

3.84 P. H. Fang, "Gamma Irradiation of Lithium Silicon Solar Cells", Conf. Record of the Seventh Photovoltaic Specialists Conf., p 113, 1968.

3.85 J. L. Wirth and S. C. Rogers, "The Transient Response of Transistors and Diodes to Ionizing Radiation", IEEE Trans on Nuc. Sci., NS-11, 5, 24, 1964.

3.86 J. M. Blinov, et al., "Photo-EMF of PN Junctions in a Strongly Excited Semiconductor", Soviet Physics-JETP Letters, 3, 234, 1966.

3.87 N. Holonyak, et al., "An Experimental Investigation of the Maximum Photo-EMF of a P Junction", J. Appl. Phys., 38, 5422, 1967.

3.88 D. Girton, "P-N Diode Saturation Using Laser", Proc. IEEE, 51, 938, 1963.

3.89 V. S. Vavilov, "Radiation Damage in Semiconductors", p 115, Academic Press, N. Y., 1964.

3.90 J. J. Wysocki, "Lithium-Doped Radiation- Resistant Silicon Solar Cells", IEEE Trans on Nuc. Sci. NS-13, 6, 168, 1966.

3.91 T. J. Faith, "Damage and Recovery Characteristics of Lithium-Containing Solar Cell", IEEE T-NS-18, 6, 371, 1971.

3.92 T. J. Faith, "Radiation Characteristics and Mission Consideration in Lithium-Containing Solar Cells", IEEE T-NS-19, 6, 371, 1972.

3.93 J. R. Carter, Jr. and R. G. Downing, "Behavior of Lithium in Irradiated Solar Cells", Conf. Record of the Eighth IEEE Photovoltaic Specialists Conf., p 240, 1970.

3.94 P. A. Berman, "Summary of Results of JPL Lithium-Doped Solar Cell Development Program", Conf. Record of the Ninth IEEE Photovoltaic Specialists Conf., p 281, 1972.

3.95 A. C. Wilbur and D. L. Anderson, "An Exploratory Study of the Interplanetary Environmental Effects on Solar-Cell Cover Glasses", Conf. Record of the Seventh Photovoltaic Specialists Conf., IEEE, p 184, 1968.

3.96 E. E. Luedke, "Low Energy Proton Effects on MgF_2", TRW Systems IOC 68-3346.11-43, 26 Sept 1968.

3.97 E. E. Luedke, "Degradation of Antireflective Coating (MgF_2)", TRW Systems IOC 68-3346.11-47, 8 Oct. 1968.

3.98 F. J. Campbell, "Effects of Space Radiation on Solar Cell Cover Materials", Transcript of the Photovoltaic Specialists Conf., Vol. II, D-2, 1963.

3.99 F. J. Campbell and R. J. Lambert, "Effects of Shielding on Electron Damage to Solar Cells", Proceedings of the Photovoltaic Specialists Conf., Vol. I, A-9, 1964.

3.100 F. J. Campbell, "Status of Solar Cell Cover Material Radiation Damage", Proceedings of the Fifth Photovoltaic Specialists Conf., Vol. II, D-2.1, 1966.

3.101 J. L. Patterson and G. A. Haynes, "Effects of High-Energy Electron Radiation on Solar Cell Shields", Transcript of the Photovoltaic Specialists Conference, Vol. II, D-2, 1963.

3.102 G. A. Haynes, "High-Energy Radiation and Solar Cell Shields", Fourth Photovoltaic Specialists Conference, Vol. I, A-10, 1964.

3.103 G. A. Haynes and W. E. Miller, "Effects of 1.2 and 0.3 MeV Electrons on the Optical Transmission Properties of Several Transparent Materials", NASA TN D-2620, 1965.

3.104 G. A. Haynes, "Effect of Radiation on Cerium-Doped Solar-Cell Cover Glass", NASA TN D-6024, 1970.

3.105 D. L. Reynard, "Irradiation of Solar Cell Cover Slides and Adhesives with 1.5 MeV Electrons", Lockheed Aircraft Company Report LMSC 3-56-64-5, August 1964.

3.106 L. B. Fogdall and S. S. Cannaday, "Space Radiation Effect of a Simulator Venus-Mercury Flyby or Solar Absorbance and Transmittance Properties of Solar Cells, Cover Glasses, Adhesives and Kapton Film", AIAA Paper No. 71-452, April 1971.

3.107 E. E. Luedke, "Charged Particle Exposure of Microsheet Second Surface Mirrors", TRW Systems IOC 8526.16-73-37, 8 March 1973.

3.108 J. P. Millard, "Results from the Thermal Control Coating Experiment on OSO-III", Thermal Design Principle of Spacecraft and Entry Bodies, Academic Press, p 769, 1969.

3.109 J. G. Haynos, "Investigation of Resinous Materials for Use as Solar Cell Adhesive", NASA TMX 55333, 1965.

3.110 E. E. Luedke, private communication

3.111 J. M. Denney, et al., "Final Flight Report Tetrahedral Research Satellites 1963-14B, 1963-14C, 1963-30B, Vol. II, Experiments and Results", TRW Systems Report 8685-6006-RU-000, 15 Feb 1964.

3.112 R. L. Fleishcer, P. B. Price and R. M. Walker, "Nuclear Tracks in Solids", Scientific American, 220, 6, 30, 1969.

3.113 R. L. Crabb, "Evaluation of Cerium Stabilized Microsheet Coverslips for Higher Solar Cell Outputs", Conf. Record of the Ninth IEEE Photovoltaic Specialists Conf., p 185, 1972.

3.114 S. P. Faile, W. R. Harding and A. E. Wallis, "Hydrogen Impregnated Glass Covers for Hardened Solar Cells", Conf. Record of the Eighth IEEE Photovoltaic Specialists Conference, p 88, 1970.

CHAPTER 4

4.0 RELATIVE DAMAGE COEFFICIENTS FOR SPACE RADIATION

A large volume of experimental data is available for normal incidence irradiation of unshielded solar cells. These data are not directly applicable in the prediction of space radiation effects because of the omnidirectional nature of the space radiation and because of the energy degrading effects of cover glass (shielding). In this section, the analytical methods of calculating the damage effectiveness of each component of the space radiation will be detailed. The damage effectiveness of space radiation is calculated relative to normal incidence 1 MeV electrons and 10 MeV protons on unshielded solar cells. This concept of the damage effectiveness or relative damage constant (D) is an extension of the previously discussed concept of equivalent fluence. It will allow the reduction of all components of the space radiation to an equivalent laboratory (normal incidence, monoenergetic) irradiation. In this way, laboratory data can be used to predict the behavior of shielded solar arrays in space. In addition, the similar problem of calculating energy deposition at various depths in shielding will be discussed.

4.1 Geometrical Aspects of Radiation Fluences

An omnidirectional flux is defined as the number of radiation particles of a particular type and energy which isotropically traverse a test sphere of unit cross-sectional area per unit time. The commonly used sources of space radiation literature tabulate the environment in terms of omnidirectional fluxes with units of particles cm^{-2} day^{-1}. A commonly repeated derivation in the literature regarding the conversion of omnidirectional fluxes to unidirectional fluxes is as follows.[4.1] Assume a unit of plane area in space with an incident omnidirectional flux of particles.

Φ_n = the component of the omnidirectional flux which is normal to a surface

Φ_o = the omnidirectional flux

4π = solid angle of test sphere (steradians)

θ = angle of radiation incidence (from normal)

$d\Omega$ = an increment of solid angle

$= 2\pi \sin\theta \, d\theta$ (for rotational symmetry)

$\cos\theta$ = projected area of unit plane area

$$\Phi_n = \frac{\Phi_o}{4\pi}\int_0^{\pi/2} \cos\theta \, d\Omega + \frac{\Phi_o}{4\pi}\int_{\pi/2}^{\pi} \cos\theta \, d\Omega \qquad (4.1.1)$$

$$= \frac{\Phi_o}{4\pi}\int_0^{\pi/2} 2\pi \sin\theta \cos\theta \, d\theta + \frac{\Phi_o}{4\pi}\int_{\pi/2}^{\pi} 2\pi \sin\theta \cos\theta \, d\theta$$

$$\Phi_n = \frac{\Phi_o}{2}$$

The above derivation implies that the unidirectional fluence is equal in intensity or "equivalent" to the omnidirectional flux divided by 2. Likewise, if the unit plane area has infinite back shielding (i.e., integrate θ from o to $\pi/2$ only), one-fourth of the omnidirectional fluence is equal to the intensity of the unidirectional normally incident fluence. The above expression determines the normal component of an omnidirectional flux. The conversion of an omnidirectional flux to an equivalent unidirectional flux must properly weight the damage effectiveness of all angular components.

The expression for the effectiveness or relative damage constant, weighted for all angular components of an omnidirectional monoenergetic flux and assuming infinite back shielding, is as follows:

$$D(E,t) = \frac{1}{2}\int_0^{\pi/2} D(E_0, \theta) \cdot 2\pi \sin\theta \, d\theta \qquad (4.1.2)$$

where $D(E,t)$ = relative damage coefficient of omnidirectional radiation particles with energy E, relative to unidirectional 1 MeV electrons or 10 MeV protons

$D(E_o, \theta)$ = damage coefficient of unidirectional radiation particles with angle of incidence (θ) and energy (E_o) relative to unidirectional 1 MeV electrons or 10 MeV protons

t = shielding thickness; for the case of $t=0$, $E=E_o$

The quantity $2\pi \sin \theta \, d\theta$ is an increment of solid angle as in equation (4.1.1). Equation (4.1.2) must be further modified to reflect the energy degradation in the cover glass shields used on silicon solar cells ($t \neq 0$).

4.2 Effect of Shielding on Radiation

A common solar cell configuration involves infinite back shielding and an optically transparent finite shield covering the front surface of the cell. The assumption of infinite back shielding is not always valid, and the differences in both shield thickness and material require separate treatments for front and back radiation. If an omnidirectional flux of radiation particles with energy E is incident on a solar cell shield of thickness t, the particles not stopped in the shielding will exit the shielding (i.e., enter the silicon) with an energy of E_0. The energy E_0 will be a strong function of the angle of incidence because of varying path length in the shield. The particle track length in the shield is equal to $t/\cos \theta$. By subtracting the particle track length in the shield ($t/\cos \theta$) from the range of the particle, R(E), in the shield material, one can determine the residual range, $R(E_0)$, of a particle with energy E_0. Thus:

$$E_0(E,\theta,t) = R^{-1}\left[R(E) - \frac{t}{\cos \theta}\right] \qquad (4.2.1)$$

where R^{-1} is a convenient form used to represent an inverse function of the range-energy relation R. Proton and electron range-energy data suitable for this calculation have been conveniently tabulated by Janni[4.2] and Berger and Seltzer.[4.3, 4.4]

4.3 Electron Space Radiation Effects

The evaluation of $D(E,\theta)$ is necessary to complete the integration of equation (4.1.2). The data regarding the experimental evaluation of the relative damage coefficient for n-p silicon solar cells, D(E) for various electron energies at normal incidence is presented in Figure 4.1 (dashed line). Electrons in the MeV energy range penetrate silicon solar cells thoroughly enough that the damage produced by an electron can be considered uniform along its track. For this reason, the amount of displacement

damage produced by a high energy electron is proportional to the total track length produced in a solar cell, and hence:

$$D(E_o,\theta) \propto \quad \text{(particle track length)} \cdot \text{(projected cell area)} \qquad (4.3.1)$$

The length of an individual electron track in a solar cell is proportional to sec θ or $1/\cos\theta$. The number of electrons intercepted by the cell is proportional to its projected area normal to the direction of the radiation or cos θ. The net result of these two factors on equation (4.3.1) is cancellation of the terms involving the angle of incidence (θ), and $D(E,\theta)$ is shown to be independent of θ or equal to $D(E)$. The fact that fast electron damage of unshielded silicon solar cells is independent of the angle of incidence was experimentally confirmed by Barrett.[4.5]

Equation (4.1.2) for the case of electron space radiation can be modified to the following expression:

$$D(E,t) = \frac{1}{2} \int_0^{\pi/2} D(E_o,0)\, 2\pi \sin\theta \, d\theta \qquad (4.3.2)$$

Equation (4.3.2) can be evaluated with the aid of equation (4.2.1) to evaluate E_o and the data in Figure 4.1 to evaluate $D(E_o,0)$. The integration of equation (4.3.2) has been performed by machine and the results are also shown in Figure 4.1. The results are also tabulated in Table 4.1. Because of electron straggling, there might be some question regarding the suitability of equation (4.2.1) to determine E_o, however use of alternate Monte Carlo methods yielded results identical to those in Figure 4.1. Rosenzweig published similar space electron damage factor curves.[4.6] Barrett also published a similar analysis based on the diffusion length damage coefficient and empirically fitted analytical expressions to the data.[4.5]

The evaluation of ionization dose in solar array materials due to omnidirectional space electron fluences is analogous to that just completed for silicon solar cell degradation. In the case of absorbed dose, the energy deposited by the radiation in the shielding is determined in terms of rads or joules per kilogram. To evaluate this energy deposition

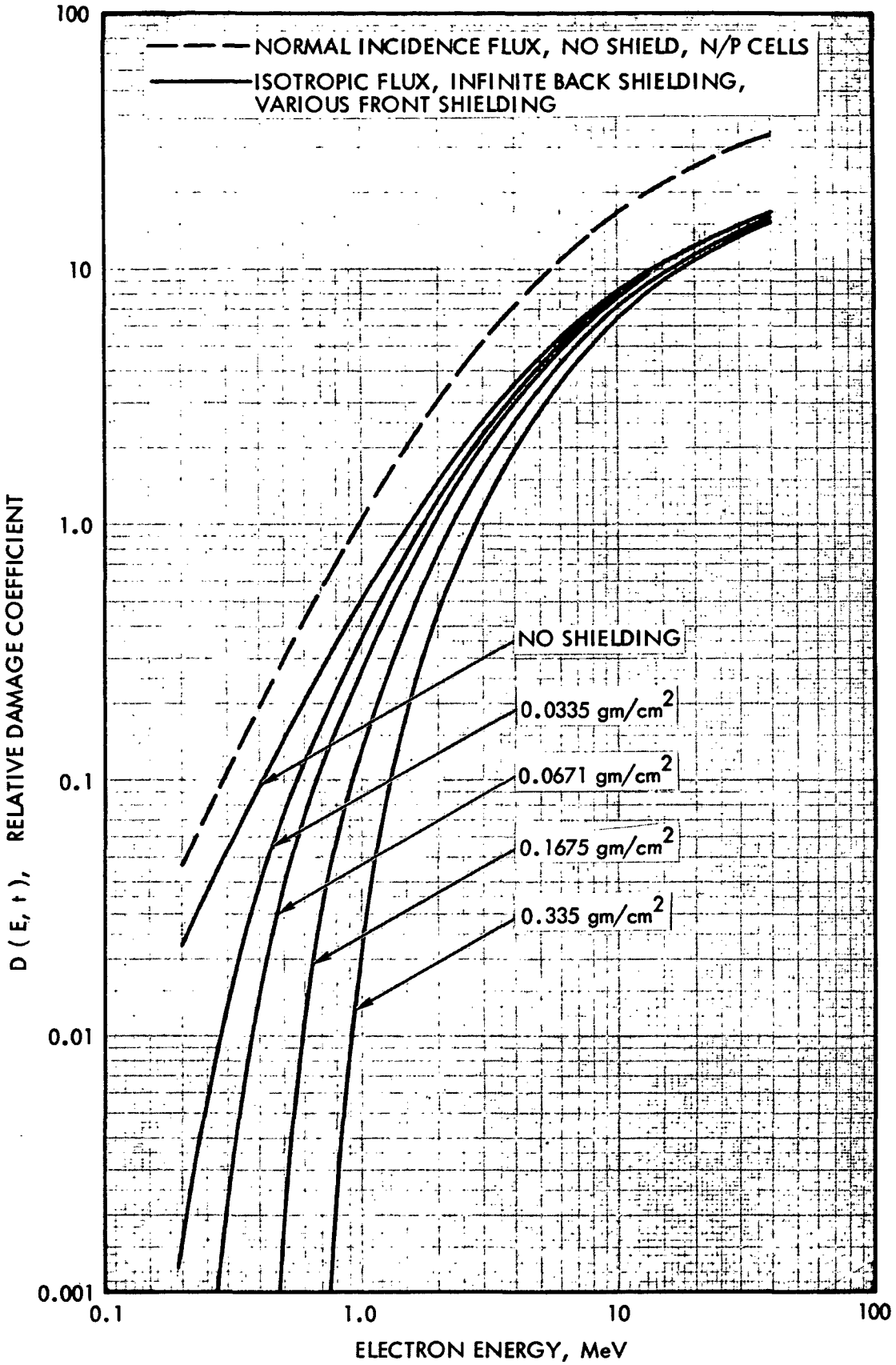

Figure 4.1. Relative Damage Coefficients for Space Electron Irradiation of Shielded N/P Silicon Solar Cells

ELECTRON DAMAGE COEFFICIENT FOR JSC
OMNIDIRECTIONAL TO EQUIV 1 MEV ELECTRON

ENERGY		SHIELD THICKNESS, GM/CM2						
(MEV)	(J)	0.	1.68E-02	3.35E-02	6.71E-02	1.12E-01	1.68E-01	3.35E-01
.01	1.60E-15	4.17E-05	0.	0.	0.	0.	0.	0.
.02	2.40E-15	9.79E-05	0.	0.	0.	0.	0.	0.
.02	3.20E-15	1.79E-04	0.	0.	0.	0.	0.	0.
.03	4.80E-15	4.21E-04	0.	0.	0.	0.	0.	0.
.04	6.40E-15	7.71E-04	0.	0.	0.	0.	0.	0.
.06	9.61E-15	1.81E-03	0.	0.	0.	0.	0.	0.
.08	1.28E-14	3.32E-03	0.	0.	0.	0.	0.	0.
.10	1.60E-14	5.30E-03	8.47E-06	0.	0.	0.	0.	0.
.12	1.92E-14	7.78E-03	3.05E-04	0.	0.	0.	0.	0.
.15	2.40E-14	1.24E-02	1.67E-03	8.96E-06	0.	0.	0.	0.
.17	2.72E-14	1.62E-02	3.20E-03	2.78E-04	0.	0.	0.	0.
.20	3.20E-14	2.28E-02	6.47E-03	1.52E-03	0.	0.	0.	0.
.22	3.60E-14	2.92E-02	9.98E-03	3.31E-03	9.23E-08	0.	0.	0.
.25	4.00E-14	3.65E-02	1.43E-02	5.85E-03	2.36E-04	0.	0.	0.
.28	4.40E-14	4.45E-02	1.96E-02	9.18E-03	1.05E-03	0.	0.	0.
.30	4.80E-14	5.35E-02	2.57E-02	1.34E-02	2.51E-03	0.	0.	0.
.33	5.28E-14	6.54E-02	3.38E-02	1.92E-02	5.07E-03	7.14E-05	0.	0.
.36	5.76E-14	7.85E-02	4.32E-02	2.62E-02	8.63E-03	7.00E-04	0.	0.
.40	6.40E-14	9.80E-02	5.79E-02	3.75E-02	1.51E-02	2.75E-03	0.	0.
.45	7.20E-14	1.22E-01	7.80E-02	5.38E-02	2.52E-02	7.22E-03	3.00E-04	0.
.50	8.00E-14	1.47E-01	9.99E-02	7.27E-02	3.82E-02	1.41E-02	2.11E-03	0.
.55	8.81E-14	1.75E-01	1.24E-01	9.38E-02	5.41E-02	2.36E-02	5.89E-03	0.
.60	9.61E-14	2.05E-01	1.50E-01	1.17E-01	7.23E-02	3.60E-02	1.19E-02	0.
.65	1.04E-13	2.36E-01	1.77E-01	1.41E-01	9.14E-02	4.98E-02	1.98E-02	0.
.70	1.12E-13	2.69E-01	2.05E-01	1.66E-01	1.12E-01	6.56E-02	3.00E-02	7.89E-06
.80	1.28E-13	3.40E-01	2.69E-01	2.24E-01	1.60E-01	1.03E-01	5.61E-02	2.41E-03
.90	1.44E-13	4.17E-01	3.38E-01	2.87E-01	2.13E-01	1.45E-01	8.79E-02	1.01E-02
1.00	1.60E-13	5.00E-01	4.14E-01	3.57E-01	2.74E-01	1.95E-01	1.27E-01	2.42E-02
1.10	1.76E-13	5.83E-01	4.91E-01	4.30E-01	3.37E-01	2.48E-01	1.69E-01	4.31E-02
1.20	1.92E-13	6.70E-01	5.73E-01	5.07E-01	4.06E-01	3.08E-01	2.18E-01	6.71E-02
1.40	2.24E-13	8.59E-01	7.50E-01	6.75E-01	5.59E-01	4.42E-01	3.32E-01	1.31E-01
1.60	2.56E-13	1.06E+00	9.39E-01	8.56E-01	7.25E-01	5.91E-01	4.62E-01	2.13E-01
1.80	2.88E-13	1.26E+00	1.13E+00	1.04E+00	9.00E-01	7.51E-01	6.04E-01	3.11E-01
2.00	3.20E-13	1.47E+00	1.34E+00	1.24E+00	1.09E+00	9.23E-01	7.60E-01	4.24E-01
2.25	3.60E-13	1.73E+00	1.59E+00	1.49E+00	1.32E+00	1.14E+00	9.61E-01	5.76E-01
2.50	4.00E-13	2.00E+00	1.85E+00	1.74E+00	1.57E+00	1.37E+00	1.17E+00	7.46E-01
2.75	4.40E-13	2.27E+00	2.12E+00	2.01E+00	1.82E+00	1.61E+00	1.40E+00	9.30E-01
3.00	4.80E-13	2.51E+00	2.37E+00	2.26E+00	2.07E+00	1.86E+00	1.64E+00	1.13E+00
3.25	5.20E-13	2.76E+00	2.61E+00	2.49E+00	2.30E+00	2.08E+00	1.86E+00	1.33E+00
3.50	5.60E-13	3.00E+00	2.85E+00	2.73E+00	2.53E+00	2.31E+00	2.07E+00	1.53E+00
3.75	6.00E-13	3.25E+00	3.09E+00	2.97E+00	2.77E+00	2.54E+00	2.30E+00	1.73E+00
4.00	6.40E-13	3.50E+00	3.34E+00	3.22E+00	3.01E+00	2.77E+00	2.52E+00	1.93E+00
4.25	6.80E-13	3.72E+00	3.57E+00	3.45E+00	3.24E+00	3.00E+00	2.74E+00	2.13E+00
4.50	7.20E-13	3.95E+00	3.79E+00	3.67E+00	3.46E+00	3.22E+00	2.96E+00	2.33E+00
4.75	7.60E-13	4.17E+00	4.02E+00	3.89E+00	3.68E+00	3.44E+00	3.17E+00	2.53E+00
5.00	8.00E-13	4.40E+00	4.24E+00	4.12E+00	3.90E+00	3.65E+00	3.39E+00	2.74E+00
5.25	8.41E-13	4.62E+00	4.46E+00	4.34E+00	4.12E+00	3.87E+00	3.60E+00	2.94E+00
5.50	8.81E-13	4.84E+00	4.68E+00	4.55E+00	4.34E+00	4.08E+00	3.81E+00	3.14E+00
5.75	9.21E-13	5.06E+00	4.90E+00	4.77E+00	4.55E+00	4.30E+00	4.02E+00	3.34E+00
6.00	9.61E-13	5.28E+00	5.12E+00	4.99E+00	4.77E+00	4.51E+00	4.23E+00	3.54E+00
6.25	1.00E-12	5.49E+00	5.33E+00	5.20E+00	4.97E+00	4.71E+00	4.43E+00	3.73E+00
6.50	1.04E-12	5.71E+00	5.55E+00	5.41E+00	5.19E+00	4.92E+00	4.63E+00	3.92E+00
6.75	1.08E-12	5.93E+00	5.77E+00	5.63E+00	5.40E+00	5.13E+00	4.84E+00	4.11E+00
7.00	1.12E-12	6.15E+00	5.98E+00	5.85E+00	5.61E+00	5.34E+00	5.04E+00	4.31E+00
8.00	1.28E-12	6.88E+00	6.73E+00	6.60E+00	6.38E+00	6.12E+00	5.83E+00	5.08E+00
9.00	1.44E-12	7.60E+00	7.44E+00	7.32E+00	7.09E+00	6.83E+00	6.53E+00	5.78E+00
10.00	1.60E-12	8.30E+00	8.15E+00	8.02E+00	7.79E+00	7.52E+00	7.22E+00	6.46E+00
15.00	2.40E-12	1.06E+01	1.05E+01	1.04E+01	1.02E+01	1.00E+01	9.75E+00	9.06E+00
20.00	3.20E-12	1.23E+01	1.23E+01	1.22E+01	1.20E+01	1.18E+01	1.16E+01	1.10E+01
25.00	4.00E-12	1.36E+01	1.35E+01	1.35E+01	1.33E+01	1.31E+01	1.29E+01	1.24E+01
30.00	4.80E-12	1.47E+01	1.47E+01	1.46E+01	1.45E+01	1.43E+01	1.41E+01	1.36E+01
40.00	6.40E-12	1.65E+01	1.64E+01	1.64E+01	1.62E+01	1.61E+01	1.59E+01	1.54E+01

Table 4.1. Electron Damage Coefficients

at various depths in the shielding, an expression similar to equation (4.3.2) can be used. Equation (4.3.2) is modified to the extent that the electron stopping power

$$\left(-\frac{1}{\rho}\frac{dE}{dx}\right)_{collision}$$

replaces $D(E_0)$, and $D(E,t)$ becomes the absorbed dose per unit fluence. The results of this integration are shown in Figure 4.2 and in Table 4.2. Rosenzweig has published similar curves.[4.6]

4.4 Proton Space Radiation Effects

For proton space radiation, the evaluation of equation (4.1.2) is more complex than that previously discussed for electrons. Two problems arise in the treatment of space protons with energies less than about 10 MeV, because of their limited penetration and increased damage production. One problem exists because the relative damage constants based on silicon solar cell I_{sc}, V_{oc}, and P_{max} are different and diverge at low proton energies. The second problem is that low energy proton damage has been experimentally characterized only for normal incidence irradiation, and basic considerations indicate that the damage is a strong function of the angle of incidence. The normal incidence proton coefficients for energies of 10 MeV and greater can be assumed to be independent of the angle of radiation incidence for the same reasons discussed for electron irradiation in the previous section.

The physical distribution of low energy proton damage was discussed in section 3.6. The most significant aspect of the low energy proton damage is the fact that a majority of the displacements are produced at the end of the proton track, as illustrated in Figure 3.19. The high damage concentration near the end of the proton track allows the construction of a simple damage model for the prediction of the effect of angle of incidence on low energy proton damage in silicon solar cells. It is assumed that the effect of a low energy proton, of arbitrary angle of incidence and energy, is roughly equal to that of a normally incident proton with a range equal to the perpendicular penetration of the non-normal incident

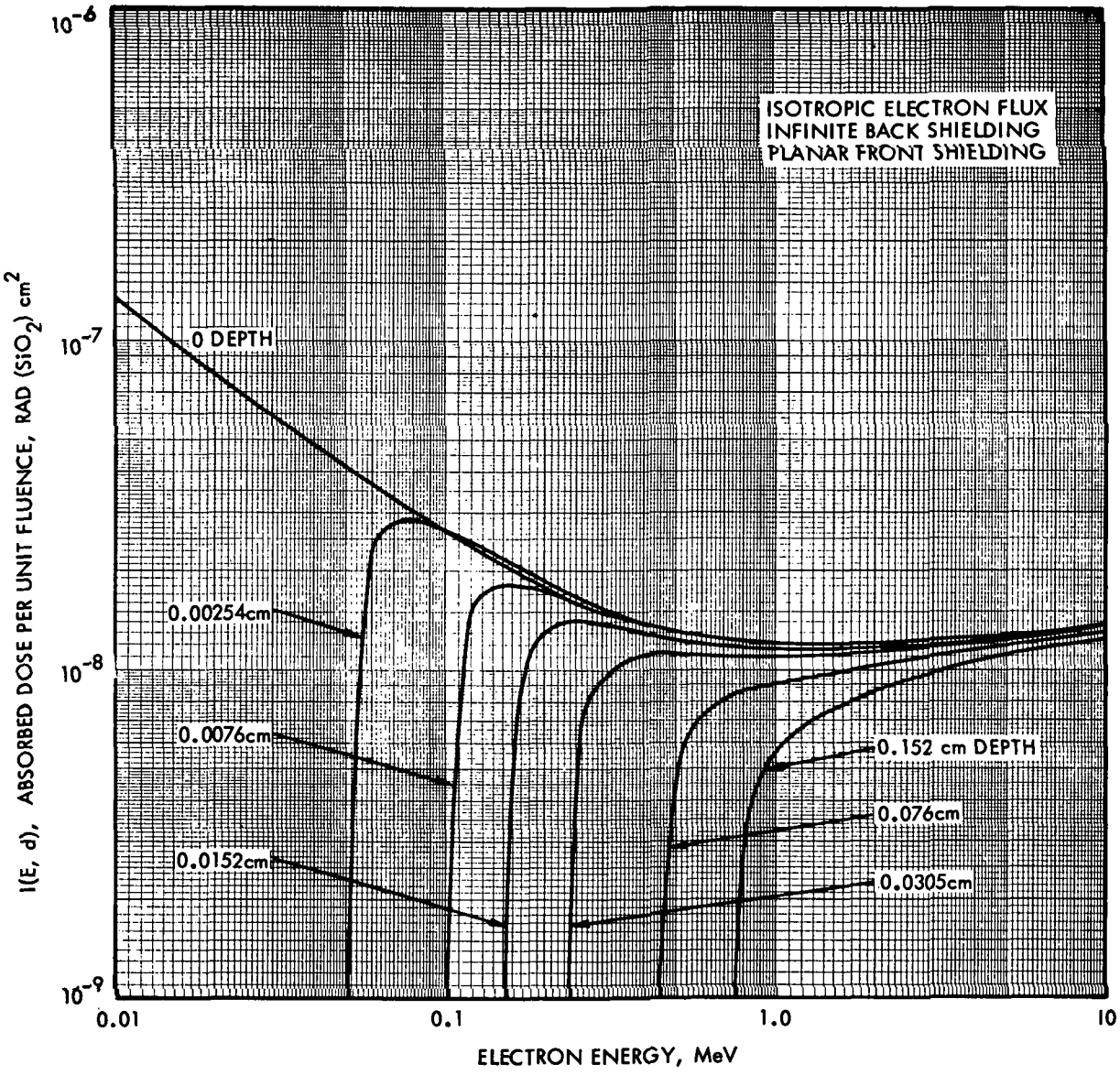

Figure 4.2. Absorbed Dose Per Unit Fluence of Space Electrons for Various Depths in Planar Fused Silica Shielding

ELECTRON STOPPING POWER
RAD(SILICON)/UNIT OMNIDIRECTIONAL FLUX

ENERGY		SHIELD THICKNESS, GM/CM2						
(MEV)	(J)	6.15E-03	1.84E-02	3.69E-02	7.38E-02	1.23E-01	1.84E-01	3.69E-01
.01	1.60E-15	0.	0.	0.	0.	0.	0.	0.
.02	2.40E-15	0.	0.	0.	0.	0.	0.	0.
.02	3.20E-15	0.	0.	0.	0.	0.	0.	0.
.03	4.80E-15	0.	0.	0.	0.	0.	0.	0.
.04	6.40E-15	0.	0.	0.	0.	0.	0.	0.
.06	9.61E-15	2.29E-08	0.	0.	0.	0.	0.	0.
.08	1.28E-14	2.86E-08	0.	0.	0.	0.	0.	0.
.10	1.60E-14	2.67E-08	0.	0.	0.	0.	0.	0.
.12	1.92E-14	2.44E-08	1.57E-08	0.	0.	0.	0.	0.
.15	2.40E-14	2.15E-08	1.83E-08	0.	0.	0.	0.	0.
.17	2.72E-14	2.01E-08	1.81E-08	9.48E-09	0.	0.	0.	0.
.20	3.20E-14	1.85E-08	1.74E-08	1.31E-08	0.	0.	0.	0.
.22	3.60E-14	1.74E-08	1.67E-08	1.39E-08	0.	0.	0.	0.
.25	4.00E-14	1.66E-08	1.61E-08	1.41E-08	4.81E-09	0.	0.	0.
.28	4.40E-14	1.60E-08	1.55E-08	1.40E-08	8.04E-09	0.	0.	0.
.30	4.80E-14	1.54E-08	1.51E-08	1.39E-08	9.51E-09	0.	0.	0.
.33	5.28E-14	1.49E-08	1.46E-08	1.36E-08	1.04E-08	0.	0.	0.
.36	5.76E-14	1.44E-08	1.42E-08	1.34E-08	1.08E-08	4.75E-09	0.	0.
.40	6.40E-14	1.40E-08	1.37E-08	1.31E-08	1.11E-08	7.07E-09	0.	0.
.45	7.20E-14	1.35E-08	1.33E-08	1.28E-08	1.12E-08	8.34E-09	1.54E-09	0.
.50	8.00E-14	1.32E-08	1.30E-08	1.25E-08	1.13E-08	9.02E-09	4.95E-09	0.
.55	8.81E-14	1.30E-08	1.27E-08	1.23E-08	1.12E-08	9.40E-09	6.38E-09	0.
.60	9.61E-14	1.27E-08	1.25E-08	1.22E-08	1.12E-08	9.64E-09	7.24E-09	0.
.65	1.04E-13	1.26E-08	1.24E-08	1.20E-08	1.12E-08	9.78E-09	7.76E-09	0.
.70	1.12E-13	1.25E-08	1.23E-08	1.19E-08	1.11E-08	9.90E-09	8.14E-09	0.
.80	1.28E-13	1.23E-08	1.21E-08	1.18E-08	1.11E-08	1.01E-08	8.64E-09	2.86E-09
.90	1.44E-13	1.22E-08	1.20E-08	1.17E-08	1.11E-08	1.02E-08	8.96E-09	4.60E-09
1.00	1.60E-13	1.21E-08	1.19E-08	1.16E-08	1.11E-08	1.02E-08	9.19E-09	5.60E-09
1.10	1.76E-13	1.21E-08	1.19E-08	1.16E-08	1.11E-08	1.03E-08	9.37E-09	6.26E-09
1.20	1.92E-13	1.21E-08	1.19E-08	1.16E-08	1.11E-08	1.04E-08	9.53E-09	6.74E-09
1.40	2.24E-13	1.20E-08	1.19E-08	1.17E-08	1.12E-08	1.06E-08	9.80E-09	7.46E-09
1.60	2.56E-13	1.21E-08	1.19E-08	1.17E-08	1.13E-08	1.07E-08	1.00E-08	7.97E-09
1.80	2.88E-13	1.21E-08	1.20E-08	1.18E-08	1.14E-08	1.09E-08	1.02E-08	8.37E-09
2.00	3.20E-13	1.22E-08	1.20E-08	1.18E-08	1.15E-08	1.10E-08	1.04E-08	8.71E-09
2.25	3.60E-13	1.22E-08	1.21E-08	1.19E-08	1.16E-08	1.11E-08	1.06E-08	9.05E-09
2.50	4.00E-13	1.23E-08	1.22E-08	1.20E-08	1.17E-08	1.13E-08	1.08E-08	9.35E-09
2.75	4.40E-13	1.24E-08	1.23E-08	1.21E-08	1.18E-08	1.14E-08	1.10E-08	9.61E-09
3.00	4.80E-13	1.24E-08	1.23E-08	1.22E-08	1.19E-08	1.16E-08	1.11E-08	9.85E-09
3.25	5.20E-13	1.25E-08	1.24E-08	1.23E-08	1.20E-08	1.17E-08	1.13E-08	1.01E-08
3.50	5.60E-13	1.26E-08	1.25E-08	1.24E-08	1.21E-08	1.18E-08	1.14E-08	1.02E-08
3.75	6.00E-13	1.26E-08	1.26E-08	1.24E-08	1.22E-08	1.19E-08	1.15E-08	1.04E-08
4.00	6.40E-13	1.27E-08	1.26E-08	1.25E-08	1.23E-08	1.20E-08	1.16E-08	1.06E-08
4.25	6.80E-13	1.28E-08	1.27E-08	1.26E-08	1.23E-08	1.21E-08	1.17E-08	1.07E-08
4.50	7.20E-13	1.28E-08	1.27E-08	1.26E-08	1.24E-08	1.21E-08	1.18E-08	1.09E-08
4.75	7.60E-13	1.29E-08	1.28E-08	1.27E-08	1.25E-08	1.22E-08	1.19E-08	1.10E-08
5.00	8.00E-13	1.29E-08	1.28E-08	1.27E-08	1.25E-08	1.23E-08	1.20E-08	1.11E-08
5.25	8.41E-13	1.30E-08	1.29E-08	1.28E-08	1.26E-08	1.24E-08	1.21E-08	1.12E-08
5.50	8.81E-13	1.30E-08	1.29E-08	1.28E-08	1.27E-08	1.24E-08	1.21E-08	1.13E-08
5.75	9.21E-13	1.30E-08	1.30E-08	1.29E-08	1.27E-08	1.25E-08	1.22E-08	1.14E-08
6.00	9.61E-13	1.31E-08	1.30E-08	1.29E-08	1.28E-08	1.25E-08	1.23E-08	1.15E-08
6.25	1.00E-12	1.31E-08	1.31E-08	1.30E-08	1.28E-08	1.26E-08	1.23E-08	1.16E-08
6.50	1.04E-12	1.32E-08	1.31E-08	1.30E-08	1.29E-08	1.26E-08	1.24E-08	1.17E-08
6.75	1.08E-12	1.32E-08	1.31E-08	1.31E-08	1.29E-08	1.27E-08	1.24E-08	1.17E-08
7.00	1.12E-12	1.32E-08	1.32E-08	1.31E-08	1.29E-08	1.27E-08	1.25E-08	1.18E-08
8.00	1.28E-12	1.34E-08	1.33E-08	1.32E-08	1.31E-08	1.29E-08	1.27E-08	1.21E-08
9.00	1.44E-12	1.35E-08	1.34E-08	1.34E-08	1.32E-08	1.31E-08	1.29E-08	1.23E-08
10.00	1.60E-12	1.36E-08	1.35E-08	1.35E-08	1.33E-08	1.32E-08	1.30E-08	1.25E-08
15.00	2.40E-12	1.39E-08	1.39E-08	1.38E-08	1.38E-08	1.36E-08	1.35E-08	1.31E-08
20.00	3.20E-12	1.42E-08	1.42E-08	1.41E-08	1.40E-08	1.40E-08	1.38E-08	1.35E-08
25.00	4.00E-12	1.44E-08	1.43E-08	1.43E-08	1.42E-08	1.42E-08	1.41E-08	1.38E-08
30.00	4.80E-12	1.45E-08	1.45E-08	1.45E-08	1.44E-08	1.43E-08	1.42E-08	1.40E-08
40.00	6.40E-12	1.47E-08	1.47E-08	1.47E-08	1.46E-08	1.46E-08	1.45E-08	1.43E-08

Table 4.2. Electron Stopping Power, Rad/Unit Omnidirectional Flux

proton. To partially correct the inaccuracies of this proposed model, a factor is employed which relates the ratio of the total displacements produced by the non-normally incident proton to those of a normally incident proton with the same perpendicular penetration in the silicon solar cell. The low energy proton relative damage coefficient given by the above model can be expressed as follows:

$$D(E_o,\theta) = D(E_n,0) \cdot \frac{N_{td}(E_o) \cos \theta}{N_{td}(E_n)} \qquad (4.4.1)$$

where $D(E_o,\theta)$ = relative damage coefficient for a proton entering silicon solar cell with energy E_o at an angle θ

$D(E_n,0)$ = relative damage coefficient for a proton of normal incidence ($\theta = 0$) with range equal to $R(E_o) \cos \theta$ or energy E_n

$N_{td}(E_o)$ = the total number of silicon displacements created by a proton entering the silicon with energy E_o

$\cos \theta$ = the projected area of a unit cell area

$E_n = R^{-1}[R(E_o) \cos \theta]$

When the range of a proton incident at angle θ exceeds the product of the thickness of the cell and the secant of θ, $D(E_o,\theta)$ is calculated as follows:

$$D(E_o,\theta) = D(E_o,0) \qquad (4.4.2)$$

Equations (4.4.1) and (4.4.2) allow the evaluation of equation (4.1.2). This integration has been done by machine using the $D(E_o,0)$ values shown in Figure 3.18. Separate integrations were done for $D(E_o,0)$ values based on I_{sc}, V_{oc} and P_{max}.

Evaluation of equation 4.1.2 for cell thicknesses of 0.0254 cm (0.010 in.) and 0.0457 cm (0.018 in) has shown that, for practical purposes, the results can be considered independent of cell thickness. The results of these integrations for several coverslide thicknesses are shown in Figures 4.3 and 4.4. The same data are printed in tabular form in Tables 4.3 and 4.4.

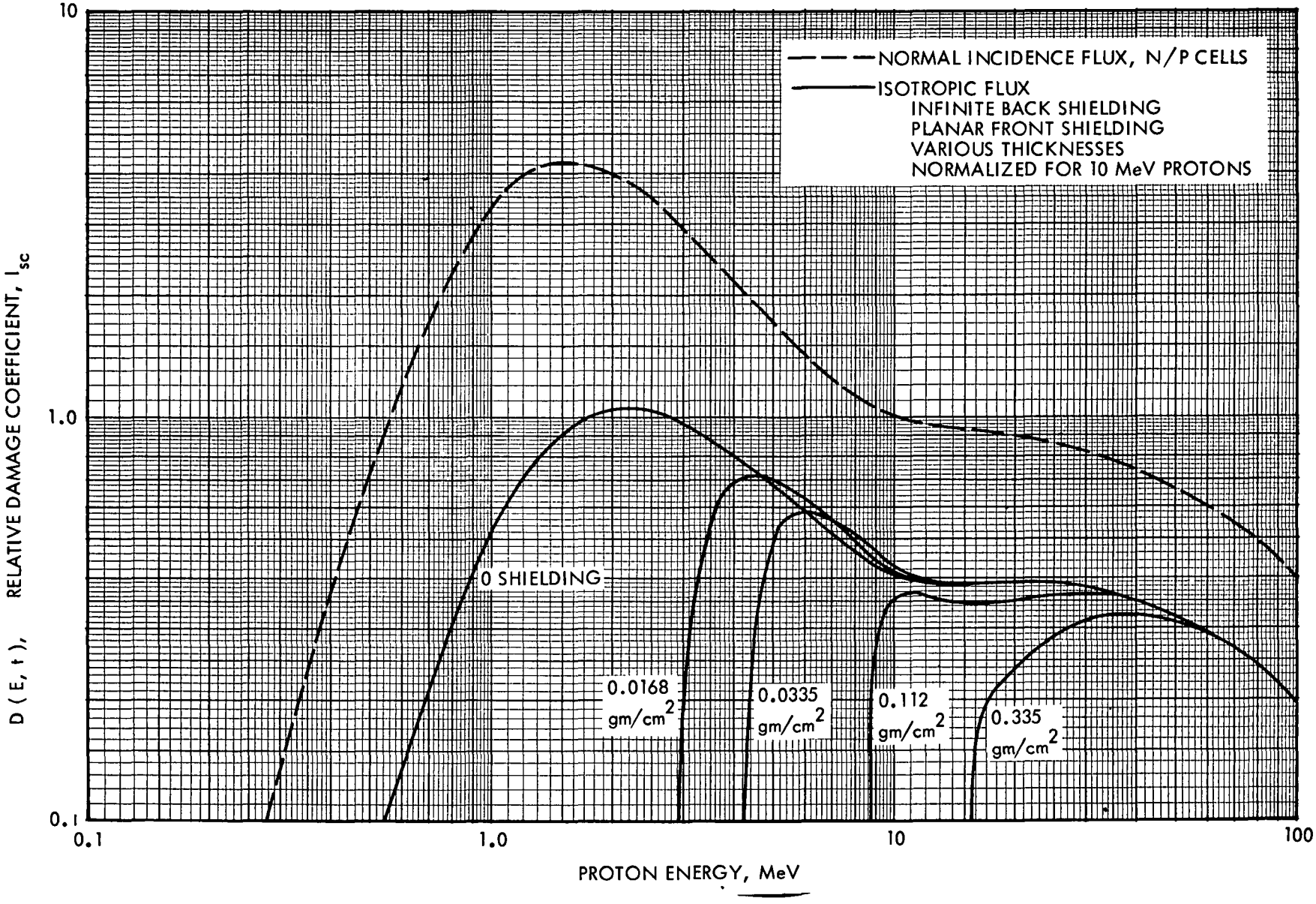

Figure 4.3 Relative Damage Coefficients for Space Proton Irradiation of Shielded N/P Silicon Solar Cells (Based on I_{sc})

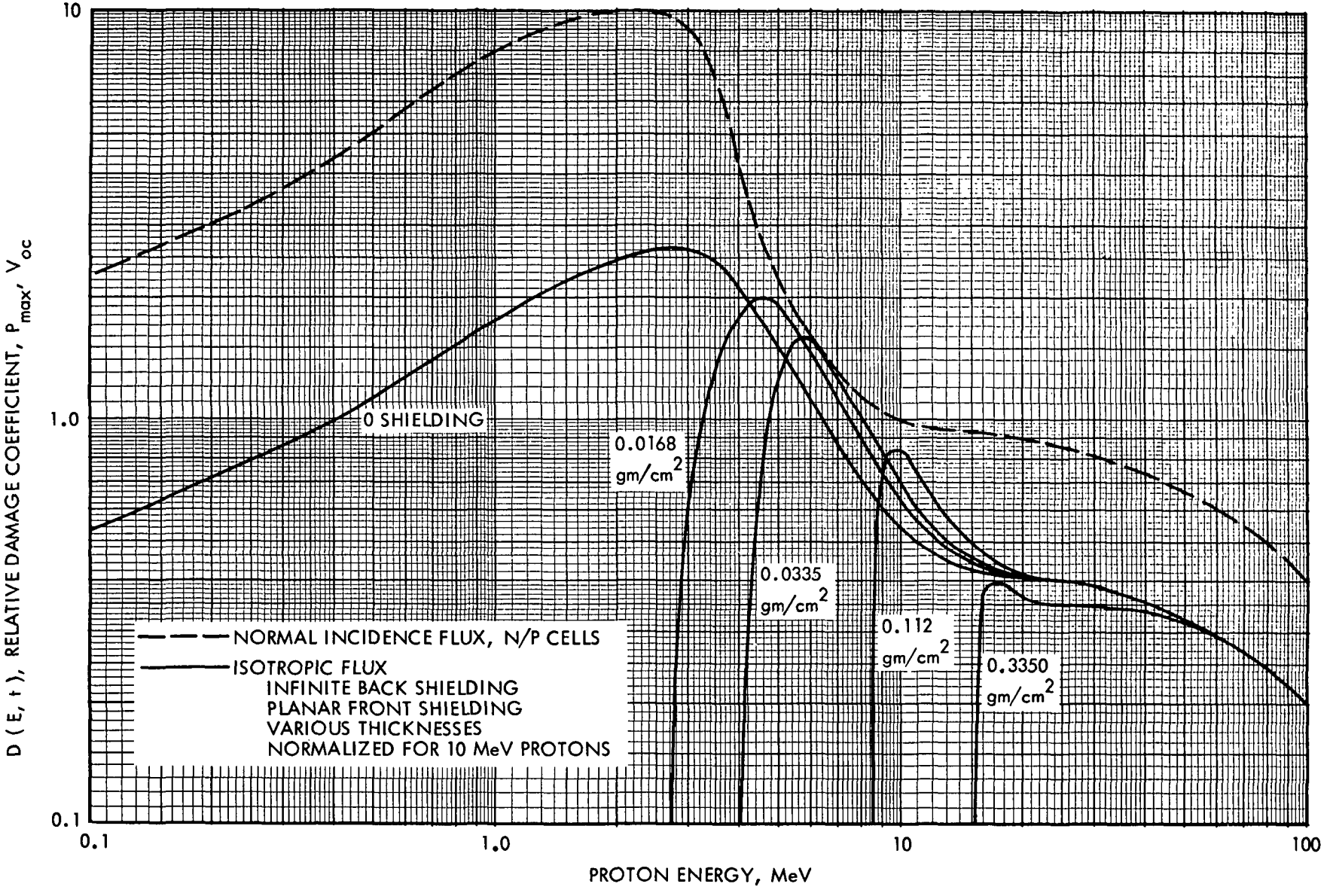

Figure 4.4 Relative Damage Coefficients for Space Proton Irradiation of Shielded N/P Silicon Solar Cells (Based on P_{max} or V_{oc})

TRW SYSTEMS

PROTON DAMAGE COEFFICIENT FOR JSC
OMNIDIRECTIONAL TO EQUIV 10 MEV PROTON

ENERGY		SHIELD THICKNESS, GM/CM2						
(MEV)	(J)	0.	1.68E-02	3.35E-02	6.71E-02	1.12E-01	1.68E-01	3.35E-01
.10	1.60E-14	2.42E-04	0.	0.	0.	0.	0.	0.
.15	2.40E-14	1.03E-03	0.	0.	0.	0.	0.	0.
.20	3.20E-14	3.03E-03	0.	0.	0.	0.	0.	0.
.30	4.80E-14	1.39E-02	0.	0.	0.	0.	0.	0.
.40	6.40E-14	3.89E-02	0.	0.	0.	0.	0.	0.
.60	9.61E-14	1.49E-01	0.	0.	0.	0.	0.	0.
.80	1.28E-13	3.23E-01	0.	0.	0.	0.	0.	0.
1.00	1.60E-13	5.20E-01	0.	0.	0.	0.	0.	0.
1.20	1.92E-13	7.08E-01	0.	0.	0.	0.	0.	0.
1.40	2.24E-13	8.52E-01	0.	0.	0.	0.	0.	0.
1.60	2.56E-13	9.51E-01	0.	0.	0.	0.	0.	0.
1.80	2.88E-13	1.01E+00	0.	0.	0.	0.	0.	0.
2.00	3.20E-13	1.04E+00	0.	0.	0.	0.	0.	0.
2.20	3.52E-13	1.04E+00	0.	0.	0.	0.	0.	0.
2.40	3.84E-13	1.04E+00	0.	0.	0.	0.	0.	0.
2.60	4.16E-13	1.02E+00	3.25E-05	0.	0.	0.	0.	0.
2.80	4.48E-13	9.95E-01	4.01E-02	0.	0.	0.	0.	0.
3.00	4.80E-13	9.63E-01	1.79E-01	0.	0.	0.	0.	0.
3.20	5.12E-13	9.28E-01	3.46E-01	0.	0.	0.	0.	0.
3.40	5.44E-13	8.93E-01	4.80E-01	0.	0.	0.	0.	0.
3.60	5.76E-13	8.59E-01	5.78E-01	0.	0.	0.	0.	0.
3.80	6.08E-13	8.26E-01	6.45E-01	0.	0.	0.	0.	0.
4.00	6.40E-13	7.95E-01	6.87E-01	1.25E-03	0.	0.	0.	0.
4.20	6.72E-13	7.71E-01	7.10E-01	7.20E-02	0.	0.	0.	0.
4.40	7.04E-13	7.48E-01	7.18E-01	2.07E-01	0.	0.	0.	0.
4.60	7.36E-13	7.24E-01	7.18E-01	3.27E-01	0.	0.	0.	0.
4.80	7.68E-13	7.02E-01	7.11E-01	4.18E-01	0.	0.	0.	0.
5.20	8.33E-13	6.60E-01	6.88E-01	5.28E-01	0.	0.	0.	0.
5.60	8.97E-13	6.21E-01	6.61E-01	5.72E-01	0.	0.	0.	0.
6.00	9.61E-13	5.85E-01	6.31E-01	5.83E-01	2.12E-03	0.	0.	0.
6.40	1.02E-12	5.55E-01	6.01E-01	5.79E-01	1.74E-01	0.	0.	0.
6.80	1.09E-12	5.28E-01	5.72E-01	5.66E-01	3.19E-01	0.	0.	0.
7.20	1.15E-12	5.03E-01	5.45E-01	5.49E-01	3.94E-01	0.	0.	0.
7.60	1.22E-12	4.81E-01	5.21E-01	5.29E-01	4.31E-01	0.	0.	0.
8.00	1.28E-12	4.62E-01	4.99E-01	5.10E-01	4.48E-01	6.18E-06	0.	0.
9.00	1.44E-12	4.24E-01	4.52E-01	4.65E-01	4.47E-01	2.73E-01	0.	0.
10.00	1.60E-12	4.02E-01	4.19E-01	4.29E-01	4.25E-01	3.53E-01	0.	0.
11.00	1.76E-12	3.91E-01	4.00E-01	4.05E-01	4.01E-01	3.66E-01	2.06E-01	0.
12.00	1.92E-12	3.88E-01	3.89E-01	3.89E-01	3.84E-01	3.61E-01	2.84E-01	0.
13.00	2.08E-12	3.86E-01	3.85E-01	3.81E-01	3.72E-01	3.51E-01	3.05E-01	0.
14.00	2.24E-12	3.86E-01	3.84E-01	3.79E-01	3.66E-01	3.45E-01	3.09E-01	0.
15.00	2.40E-12	3.89E-01	3.84E-01	3.78E-01	3.66E-01	3.42E-01	3.10E-01	0.
16.00	2.56E-12	3.92E-01	3.86E-01	3.79E-01	3.64E-01	3.42E-01	3.11E-01	1.44E-01
18.00	2.88E-12	3.93E-01	3.89E-01	3.83E-01	3.69E-01	3.46E-01	3.17E-01	2.16E-01
20.00	3.20E-12	3.94E-01	3.90E-01	3.85E-01	3.73E-01	3.54E-01	3.27E-01	2.41E-01
22.00	3.52E-12	3.93E-01	3.90E-01	3.86E-01	3.75E-01	3.59E-01	3.36E-01	2.60E-01
24.00	3.84E-12	3.92E-01	3.89E-01	3.84E-01	3.76E-01	3.63E-01	3.44E-01	2.77E-01
26.00	4.16E-12	3.90E-01	3.87E-01	3.83E-01	3.75E-01	3.64E-01	3.48E-01	2.92E-01
28.00	4.48E-12	3.87E-01	3.84E-01	3.81E-01	3.75E-01	3.65E-01	3.51E-01	3.03E-01
30.00	4.80E-12	3.82E-01	3.80E-01	3.78E-01	3.72E-01	3.64E-01	3.53E-01	3.12E-01
34.00	5.44E-12	3.69E-01	3.68E-01	3.67E-01	3.64E-01	3.59E-01	3.51E-01	3.22E-01
38.00	6.08E-12	3.59E-01	3.58E-01	3.57E-01	3.54E-01	3.51E-01	3.45E-01	3.25E-01
42.00	6.72E-12	3.47E-01	3.47E-01	3.46E-01	3.45E-01	3.43E-01	3.38E-01	3.23E-01
46.00	7.36E-12	3.35E-01	3.34E-01	3.34E-01	3.34E-01	3.32E-01	3.30E-01	3.19E-01
50.00	8.00E-12	3.24E-01	3.23E-01	3.23E-01	3.23E-01	3.22E-01	3.20E-01	3.13E-01
55.00	8.81E-12	3.09E-01	3.09E-01	3.09E-01	3.09E-01	3.09E-01	3.09E-01	3.04E-01
60.00	9.61E-12	2.97E-01	2.97E-01	2.97E-01	2.97E-01	2.97E-01	2.97E-01	2.94E-01
65.00	1.04E-11	2.82E-01	2.83E-01	2.83E-01	2.84E-01	2.84E-01	2.84E-01	2.84E-01
70.00	1.12E-11	2.70E-01	2.70E-01	2.70E-01	2.71E-01	2.72E-01	2.72E-01	2.72E-01
80.00	1.28E-11	2.46E-01	2.47E-01	2.47E-01	2.48E-01	2.48E-01	2.49E-01	2.50E-01
90.00	1.44E-11	2.24E-01	2.24E-01	2.25E-01	2.26E-01	2.27E-01	2.28E-01	2.30E-01
100.00	1.60E-11	1.99E-01	2.00E-01	2.01E-01	2.02E-01	2.03E-01	2.04E-01	2.08E-01
130.00	2.08E-11	1.49E-01	1.49E-01	1.50E-01	1.50E-01	1.51E-01	1.52E-01	1.55E-01
160.00	2.56E-11	1.18E-01	1.19E-01	1.19E-01	1.19E-01	1.20E-01	1.20E-01	1.22E-01
200.00	3.20E-11	9.23E-02	9.24E-02	9.25E-02	9.28E-02	9.31E-02	9.35E-02	9.46E-02

Table 4.3. Proton Damage Coefficients for J_{sc}

PROTON DAMAGE COEFFICIENT FOR VOC AND PMAX
OMNIDIRECTIONAL TO EQUIV 10 MEV PROTON

ENERGY		SHIELD THICKNESS, GM/CM2						
(MEV)	(J)	0.	1.68E-02	3.35E-02	6.71E-02	1.12E-01	1.68E-01	3.35E-01
.10	1.60E-14	5.29E-01	0.	0.	0.	0.	0.	0.
.15	2.40E-14	6.30E-01	0.	0.	0.	0.	0.	0.
.20	3.20E-14	7.13E-01	0.	0.	0.	0.	0.	0.
.30	4.80E-14	8.61E-01	0.	0.	0.	0.	0.	0.
.40	6.40E-14	9.94E-01	0.	0.	0.	0.	0.	0.
.60	9.61E-14	1.27E+00	0.	0.	0.	0.	0.	0.
.80	1.28E-13	1.54E+00	0.	0.	0.	0.	0.	0.
1.00	1.60E-13	1.79E+00	0.	0.	0.	0.	0.	0.
1.20	1.92E-13	1.99E+00	0.	0.	0.	0.	0.	0.
1.40	2.24E-13	2.15E+00	0.	0.	0.	0.	0.	0.
1.60	2.56E-13	2.29E+00	0.	0.	0.	0.	0.	0.
1.80	2.88E-13	2.41E+00	0.	0.	0.	0.	0.	0.
2.00	3.20E-13	2.50E+00	0.	0.	0.	0.	0.	0.
2.20	3.52E-13	2.56E+00	0.	0.	0.	0.	0.	0.
2.40	3.84E-13	2.61E+00	0.	0.	0.	0.	0.	0.
2.60	4.16E-13	2.64E+00	2.25E-02	0.	0.	0.	0.	0.
2.80	4.48E-13	2.65E+00	2.76E-01	0.	0.	0.	0.	0.
3.00	4.80E-13	2.64E+00	6.08E-01	0.	0.	0.	0.	0.
3.20	5.12E-13	2.59E+00	9.36E-01	0.	0.	0.	0.	0.
3.40	5.44E-13	2.52E+00	1.22E+00	0.	0.	0.	0.	0.
3.60	5.76E-13	2.42E+00	1.47E+00	0.	0.	0.	0.	0.
3.80	6.08E-13	2.30E+00	1.66E+00	0.	0.	0.	0.	0.
4.00	6.40E-13	2.16E+00	1.81E+00	4.67E-02	0.	0.	0.	0.
4.20	6.72E-13	2.02E+00	1.93E+00	2.86E-01	0.	0.	0.	0.
4.40	7.04E-13	1.89E+00	2.00E+00	5.69E-01	0.	0.	0.	0.
4.60	7.36E-13	1.76E+00	2.01E+00	8.36E-01	0.	0.	0.	0.
4.80	7.68E-13	1.65E+00	1.99E+00	1.07E+00	0.	0.	0.	0.
5.20	8.33E-13	1.45E+00	1.83E+00	1.43E+00	0.	0.	0.	0.
5.60	8.97E-13	1.28E+00	1.64E+00	1.60E+00	0.	0.	0.	0.
6.00	9.61E-13	1.14E+00	1.47E+00	1.58E+00	3.73E-02	0.	0.	0.
6.40	1.02E-12	1.02E+00	1.31E+00	1.47E+00	4.50E-01	0.	0.	0.
6.80	1.09E-12	9.27E-01	1.18E+00	1.34E+00	8.45E-01	0.	0.	0.
7.20	1.15E-12	8.46E-01	1.07E+00	1.22E+00	1.10E+00	0.	0.	0.
7.60	1.22E-12	7.78E-01	9.70E-01	1.11E+00	1.17E+00	0.	0.	0.
8.00	1.28E-12	7.20E-01	8.89E-01	1.01E+00	1.12E+00	3.69E-03	0.	0.
9.00	1.44E-12	6.06E-01	7.31E-01	8.27E-01	9.53E-01	7.61E-01	0.	0.
10.00	1.60E-12	5.37E-01	6.24E-01	6.95E-01	8.02E-01	8.42E-01	0.	0.
11.00	1.76E-12	4.95E-01	5.54E-01	6.05E-01	6.85E-01	7.48E-01	5.74E-01	0.
12.00	1.92E-12	4.69E-01	5.09E-01	5.44E-01	6.01E-01	6.56E-01	6.55E-01	0.
13.00	2.08E-12	4.52E-01	4.80E-01	5.03E-01	5.43E-01	5.83E-01	6.06E-01	0.
14.00	2.24E-12	4.40E-01	4.60E-01	4.77E-01	5.03E-01	5.30E-01	5.50E-01	0.
15.00	2.40E-12	4.33E-01	4.47E-01	4.58E-01	4.75E-01	4.92E-01	5.05E-01	0.
16.00	2.56E-12	4.29E-01	4.39E-01	4.46E-01	4.56E-01	4.65E-01	4.71E-01	3.77E-01
18.00	2.88E-12	4.19E-01	4.26E-01	4.30E-01	4.33E-01	4.32E-01	4.28E-01	3.96E-01
20.00	3.20E-12	4.14E-01	4.18E-01	4.20E-01	4.20E-01	4.16E-01	4.08E-01	3.70E-01
22.00	3.52E-12	4.09E-01	4.11E-01	4.12E-01	4.11E-01	4.06E-01	3.96E-01	3.56E-01
24.00	3.84E-12	4.05E-01	4.05E-01	4.05E-01	4.04E-01	3.99E-01	3.90E-01	3.50E-01
26.00	4.16E-12	4.01E-01	4.00E-01	4.00E-01	3.97E-01	3.93E-01	3.85E-01	3.49E-01
28.00	4.48E-12	3.96E-01	3.95E-01	3.94E-01	3.92E-01	3.88E-01	3.80E-01	3.49E-01
30.00	4.80E-12	3.90E-01	3.89E-01	3.89E-01	3.87E-01	3.83E-01	3.76E-01	3.49E-01
34.00	5.44E-12	3.75E-01	3.75E-01	3.75E-01	3.74E-01	3.72E-01	3.67E-01	3.47E-01
38.00	6.08E-12	3.63E-01	3.63E-01	3.63E-01	3.62E-01	3.60E-01	3.57E-01	3.43E-01
42.00	6.72E-12	3.50E-01	3.51E-01	3.51E-01	3.50E-01	3.50E-01	3.47E-01	3.36E-01
46.00	7.36E-12	3.38E-01	3.38E-01	3.38E-01	3.38E-01	3.38E-01	3.36E-01	3.29E-01
50.00	8.00E-12	3.26E-01	3.26E-01	3.26E-01	3.27E-01	3.26E-01	3.26E-01	3.21E-01
55.00	8.81E-12	3.12E-01	3.12E-01	3.12E-01	3.12E-01	3.13E-01	3.13E-01	3.10E-01
60.00	9.61E-12	2.99E-01	2.99E-01	2.99E-01	2.99E-01	3.00E-01	3.00E-01	2.98E-01
65.00	1.04E-11	2.84E-01	2.84E-01	2.85E-01	2.86E-01	2.86E-01	2.87E-01	2.87E-01
70.00	1.12E-11	2.71E-01	2.71E-01	2.72E-01	2.73E-01	2.73E-01	2.74E-01	2.75E-01
80.00	1.28E-11	2.47E-01	2.48E-01	2.48E-01	2.49E-01	2.50E-01	2.51E-01	2.52E-01
90.00	1.44E-11	2.25E-01	2.25E-01	2.26E-01	2.26E-01	2.27E-01	2.29E-01	2.31E-01
100.00	1.60E-11	2.00E-01	2.01E-01	2.01E-01	2.02E-01	2.04E-01	2.05E-01	2.09E-01
130.00	2.08E-11	1.49E-01	1.50E-01	1.50E-01	1.51E-01	1.52E-01	1.53E-01	1.56E-01
160.00	2.56E-11	1.19E-01	1.19E-01	1.19E-01	1.19E-01	1.20E-01	1.20E-01	1.22E-01
200.00	3.20E-11	9.23E-02	9.24E-02	9.26E-02	9.28E-02	9.31E-02	9.35E-02	9.46E-02

Table 4.4. Proton Damage Coefficients for V_{oc} and P_{max}

The values of relative damage constants for omnidirectional fluences of protons on shielded solar cells allow a space proton environment to be reduced to an equivalent fluence of normally incident 10 MeV protons on unshielded silicon solar cells. Experimental studies of silicon solar cells have indicated that a fluence of normally incident 10 MeV protons produces damage which can be approximated by a fluence of 1 MeV electrons which is 3000 times that of the 10 MeV proton fluence.

The evaluation of the absorbed dose in shielding materials due to space protons requires an analysis similar to that done for space electrons. For this evaluation an expression similar to equation (4.3.2) is used. The quantity $D(E_o)$ is replaced by the stopping power $(-\frac{1}{\rho}\frac{dE}{dx})$ for protons of energy (E_o) and the quantity $D(E,t)$ becomes the absorbed dose per unit incident omnidirectional-flux protons of energy E and at shielding depth t. The result of this integration for several shielding thicknesses of fused quartz are shown in Figure 4.5 and Table 4.5. Rosenzweig has published similar data.[4.6]

4.5 Alpha Particle Space Radiation Effects

Solar flares have been shown to have a component of energetic alpha particles (helium nuclei). The evaluation of the effects of solar flare events on solar arrays requires alpha particle data similar to that for electrons and protons. Smith and Blue compared effects of 10.5 MeV protons and 42 MeV alpha particles on silicon solar cell degradation.[4.7] The results showed that the 42 MeV alpha particle flux degraded the silicon cells 3.8 times as fast as a similar flux of 10.5 MeV protons. These results were in good agreement with a theoretical damage ratio of 4.

Based on the experimental results of Smith and Blue, the proton damage constant curve shown in Figure 4.4 can be translated a factor of four higher in energy and a factor of four higher in relative damage constant to represent a similar family of relative damage constants for alpha particles in space. Although the relationship found by Smith and

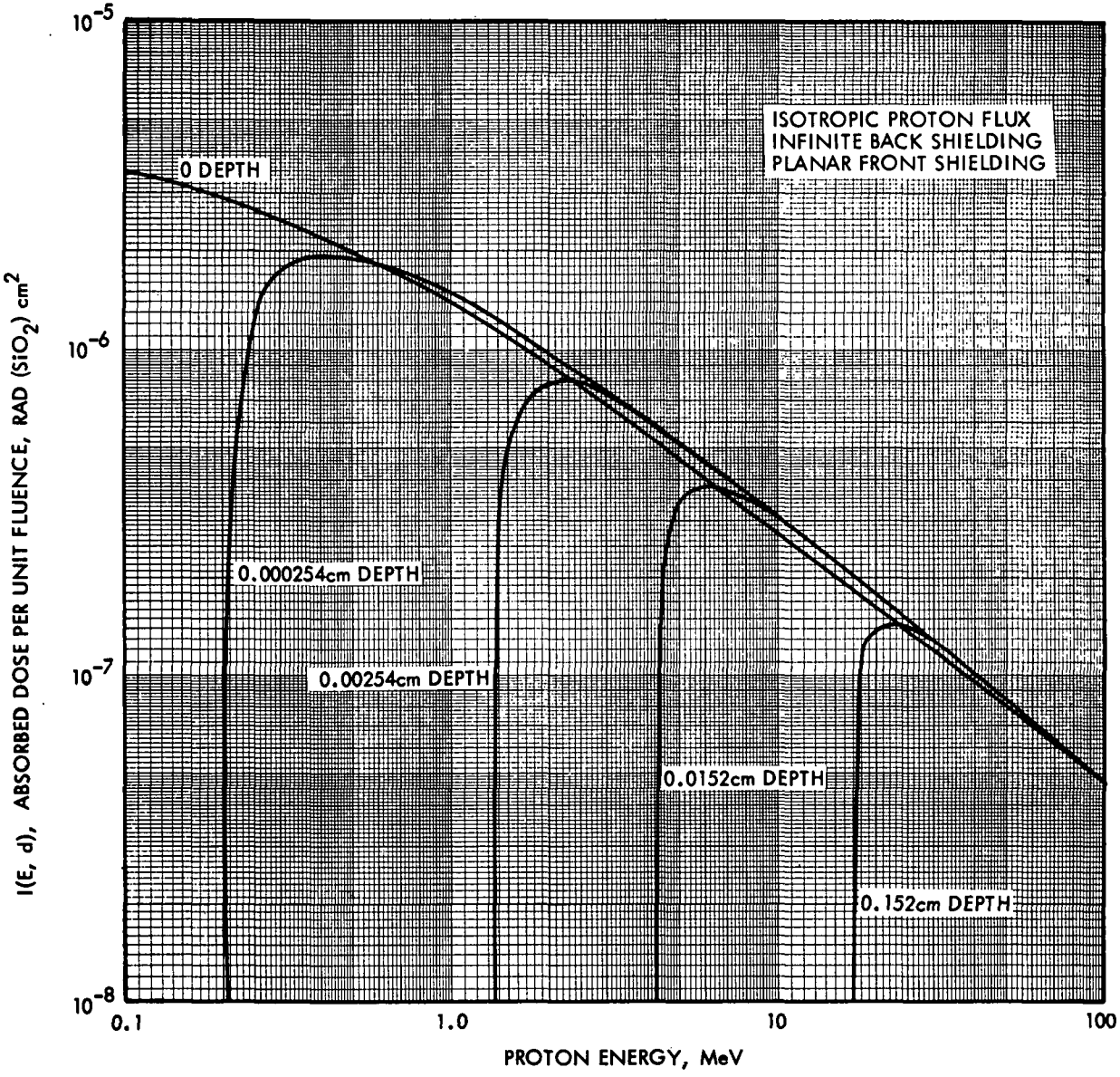

Figure 4.5 Absorbed Dose Per Unit Fluence of Space Proton for Various Depths in Planar Fused Silica Shielding

PROTON STOPPING POWER
RAD(SILICON)/UNIT OMNIDIRECTIONAL FLUX

ENERGY		SHIELD THICKNESS, GM/CM2						
(MEV)	(J)	6.15E-03	1.84E-02	3.69E-02	7.38E-02	1.23E-01	1.84E-01	3.69E-01
.10	1.60E-14	0.	0.	0.	0.	0.	0.	0.
.15	2.40E-14	0.	0.	0.	0.	0.	0.	0.
.20	3.20E-14	0.	0.	0.	0.	0.	0.	0.
.30	4.80E-14	0.	0.	0.	0.	0.	0.	0.
.40	6.40E-14	0.	0.	0.	0.	0.	0.	0.
.60	9.61E-14	0.	0.	0.	0.	0.	0.	0.
.80	1.28E-13	0.	0.	0.	0.	0.	0.	0.
1.00	1.60E-13	0.	0.	0.	0.	0.	0.	0.
1.20	1.92E-13	0.	0.	0.	0.	0.	0.	0.
1.40	2.24E-13	2.87E-07	0.	0.	0.	0.	0.	0.
1.60	2.56E-13	6.15E-07	0.	0.	0.	0.	0.	0.
1.80	2.88E-13	7.37E-07	0.	0.	0.	0.	0.	0.
2.00	3.20E-13	7.90E-07	0.	0.	0.	0.	0.	0.
2.20	3.52E-13	8.02E-07	0.	0.	0.	0.	0.	0.
2.40	3.84E-13	7.92E-07	0.	0.	0.	0.	0.	0.
2.60	4.16E-13	7.73E-07	0.	0.	0.	0.	0.	0.
2.80	4.48E-13	7.49E-07	1.62E-07	0.	0.	0.	0.	0.
3.00	4.80E-13	7.23E-07	3.25E-07	0.	0.	0.	0.	0.
3.20	5.12E-13	6.97E-07	4.15E-07	0.	0.	0.	0.	0.
3.40	5.44E-13	6.71E-07	4.66E-07	0.	0.	0.	0.	0.
3.60	5.76E-13	6.46E-07	4.95E-07	0.	0.	0.	0.	0.
3.80	6.08E-13	6.22E-07	5.10E-07	0.	0.	0.	0.	0.
4.00	6.40E-13	6.00E-07	5.16E-07	0.	0.	0.	0.	0.
4.20	6.72E-13	5.79E-07	5.16E-07	7.39E-08	0.	0.	0.	0.
4.40	7.04E-13	5.59E-07	5.13E-07	1.98E-07	0.	0.	0.	0.
4.60	7.36E-13	5.41E-07	5.07E-07	2.67E-07	0.	0.	0.	0.
4.80	7.68E-13	5.23E-07	5.00E-07	3.11E-07	0.	0.	0.	0.
5.20	8.33E-13	4.92E-07	4.82E-07	3.59E-07	0.	0.	0.	0.
5.60	8.97E-13	4.64E-07	4.63E-07	3.80E-07	0.	0.	0.	0.
6.00	9.61E-13	4.39E-07	4.44E-07	3.87E-07	0.	0.	0.	0.
6.40	1.02E-12	4.17E-07	4.25E-07	3.86E-07	8.78E-08	0.	0.	0.
6.80	1.09E-12	3.97E-07	4.07E-07	3.80E-07	1.86E-07	0.	0.	0.
7.20	1.15E-12	3.79E-07	3.90E-07	3.72E-07	2.34E-07	0.	0.	0.
7.60	1.22E-12	3.63E-07	3.75E-07	3.63E-07	2.61E-07	0.	0.	0.
8.00	1.28E-12	3.48E-07	3.60E-07	3.53E-07	2.76E-07	0.	0.	0.
9.00	1.44E-12	3.16E-07	3.28E-07	3.28E-07	2.88E-07	1.36E-07	0.	0.
10.00	1.60E-12	2.90E-07	3.01E-07	3.05E-07	2.84E-07	2.03E-07	0.	0.
11.00	1.76E-12	2.68E-07	2.78E-07	2.83E-07	2.73E-07	2.26E-07	7.98E-08	0.
12.00	1.92E-12	2.50E-07	2.59E-07	2.64E-07	2.61E-07	2.31E-07	1.52E-07	0.
13.00	2.08E-12	2.34E-07	2.42E-07	2.48E-07	2.48E-07	2.29E-07	1.79E-07	0.
14.00	2.24E-12	2.20E-07	2.27E-07	2.33E-07	2.35E-07	2.24E-07	1.91E-07	0.
15.00	2.40E-12	2.09E-07	2.15E-07	2.20E-07	2.23E-07	2.17E-07	1.94E-07	0.
16.00	2.56E-12	1.98E-07	2.03E-07	2.09E-07	2.12E-07	2.09E-07	1.93E-07	3.12E-08
18.00	2.88E-12	1.80E-07	1.84E-07	1.89E-07	1.93E-07	1.93E-07	1.86E-07	1.17E-07
20.00	3.20E-12	1.65E-07	1.69E-07	1.73E-07	1.77E-07	1.78E-07	1.75E-07	1.38E-07
22.00	3.52E-12	1.53E-07	1.56E-07	1.59E-07	1.63E-07	1.65E-07	1.65E-07	1.43E-07
24.00	3.84E-12	1.42E-07	1.45E-07	1.48E-07	1.52E-07	1.54E-07	1.55E-07	1.42E-07
26.00	4.16E-12	1.34E-07	1.36E-07	1.38E-07	1.42E-07	1.44E-07	1.45E-07	1.38E-07
28.00	4.48E-12	1.26E-07	1.28E-07	1.30E-07	1.33E-07	1.35E-07	1.37E-07	1.33E-07
30.00	4.80E-12	1.19E-07	1.21E-07	1.23E-07	1.25E-07	1.28E-07	1.29E-07	1.28E-07
34.00	5.44E-12	1.08E-07	1.09E-07	1.10E-07	1.13E-07	1.15E-07	1.16E-07	1.17E-07
38.00	6.08E-12	9.87E-08	9.96E-08	1.01E-07	1.03E-07	1.04E-07	1.06E-07	1.08E-07
42.00	6.72E-12	9.12E-08	9.19E-08	9.29E-08	9.44E-08	9.59E-08	9.73E-08	9.94E-08
46.00	7.36E-12	8.49E-08	8.55E-08	8.63E-08	8.76E-08	8.89E-08	9.01E-08	9.22E-08
50.00	8.00E-12	7.95E-08	8.00E-08	8.07E-08	8.18E-08	8.29E-08	8.40E-08	8.61E-08
55.00	8.81E-12	7.38E-08	7.42E-08	7.48E-08	7.56E-08	7.66E-08	7.76E-08	7.95E-08
60.00	9.61E-12	6.90E-08	6.93E-08	6.97E-08	7.05E-08	7.13E-08	7.21E-08	7.39E-08
65.00	1.04E-11	6.49E-08	6.52E-08	6.55E-08	6.61E-08	6.68E-08	6.75E-08	6.91E-08
70.00	1.12E-11	6.13E-08	6.15E-08	6.18E-08	6.24E-08	6.30E-08	6.36E-08	6.50E-08
80.00	1.28E-11	5.54E-08	5.55E-08	5.58E-08	5.62E-08	5.66E-08	5.71E-08	5.82E-08
90.00	1.44E-11	5.07E-08	5.09E-08	5.10E-08	5.13E-08	5.17E-08	5.21E-08	5.30E-08
100.00	1.60E-11	4.69E-08	4.70E-08	4.72E-08	4.74E-08	4.77E-08	4.80E-08	4.87E-08
130.00	2.08E-11	3.90E-08	3.90E-08	3.91E-08	3.92E-08	3.94E-08	3.95E-08	4.00E-08
160.00	2.56E-11	3.38E-08	3.38E-08	3.38E-08	3.39E-08	3.40E-08	3.41E-08	3.44E-08
200.00	3.20E-11	2.92E-08	2.92E-08	2.92E-08	2.92E-08	2.93E-08	2.94E-08	2.95E-08

Table 4.5. Proton Stopping Power, Rad/Unit Omnidirectional Flux

Blue may not extend to lower particle energies, a set of effective damage constants for alpha particles, obtained by the above two translations, is shown in Figure 4.6. Data are shown based on P_{max} and V_{oc}. Data based on I_{sc} may be obtained similarly for alpha particle effects.

4.6 Alternative Approaches

The previously discussed methods of analyzing the effects of space radiation on shielded silicon solar cells can be summarized as follows. An effective damage constant was developed which represents the relative effect of an omnidirectional (isotropic) fluence of monoenergetic particles on a shielded solar cell in terms of an equivalent unidirectional irradiation by 1 MeV electrons or 10 MeV protons. The concept involves energy degradation of particles by the shielding and the effects of the energy and angle of incidence of particles entering the silicon solar cell.

An alternate approach to the problem has been used by Carosella[4.9] and Piccianno and Reitman.[4.10] This method involves the calculation of the spectrum of particle energies exiting the cover slide (i.e., entering the silicon) of a solar cell with infinite back shielding. The calculation is extremely laborious and must be repeated for every environment considered. The calculation of this "modified" energy spectrum destroys all angular information in the data and yields a spectrum which is neither monodirectional, omnidirectional or isotropic. The problems relating to the angular content of the "modified" spectrum emerging from the shielding are of no consequence in the calculation of absorbed dose, electron damage, or high energy proton damage. It has been shown that these quantities are independent of the angle of incidence. It is therefore justified to weight the "modified" spectrum with relative damage coefficients to evaluate electron damage in terms of a damage equivalent monoenergetic normal incidence fluence. In the case of low energy protons, the use of the referenced methods incorrectly assumes that proton damage is independent of the angle of incidence. This shortcoming is particularly serious in the case of many common space environments in which the lower energy proton damage dominates the solar cell degradation. The procedures used in this chapter are based on techniques previously described by Tada.[4.10, 4.11]

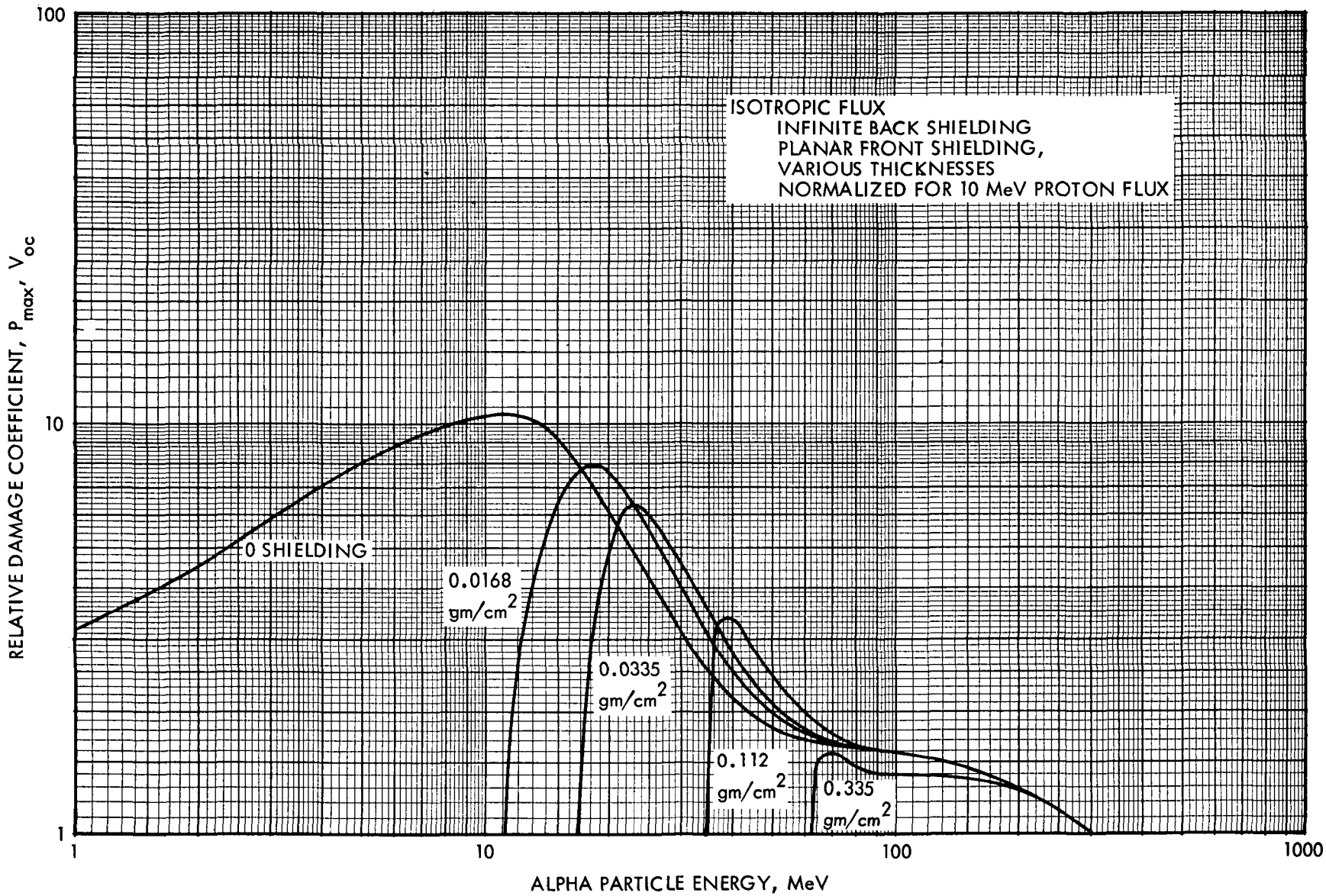

Figure 4.6 Relative Damage Coefficients for Space Alpha Particle Irradiation of Shielded N/P Silicon Solar Cells (Based on P_{max} or V_{oc})

REFERENCES

4.1 D. P. LeGalley and A. Rosen (Eds.), "Space Physics, John Wiley and Sons, New York,p. 693, 1964.

4.2 J. E. Janni,"Calculations of Energy Loss, Range, Pathlength, Straggling, Mutiple Scattering, and the Probability of Inelastic Nuclear Collisions for 0.1 to 1000 MeV Protons", AFWL-TR-65-150, Sept. 1966.

4.3 M. J. Berger and S. M. Seltzer, "Tables of Energy Losses and Ranges of Electrons and Positrons, Paper 10, NAS-NRC Publication 1133, 1964, also NASA SP-3012 1964.

4.4 M. J. Berger and S. M. Seltzer, "Additional Stopping Power and Range Tables for Protons, Mesons, and Electrons, NASA SP-3036, 1966.

4.5 M. J. Barrett, "Electron Damage Coefficients in P-Type Silicon", IEEE Trans on Nuc. Sci., NS-14,6,82, 1967.

4.6 W. Rosenzweig, "Space Radiation Effects in Silicon Devices", IEEE Trans on Nuc. Sci., NS-12,5,18,1965.

4.7 A. B. Smith and J. W. Blue, "A Comparison of Solar Cell Damage by Alpha Particles and Protons",NASA TN D-3427, May 1966.

4.8 C. A. Carosella, "Shielding of Solar Cells against Van Allen Belt Protons", J. Spacecraft, 5, 7, 878, 1968.

4.9 W. T. Picciano and R. A. Reitman, Flight Data Analysis of Power Subsystems Degradation at Near Synchronous Altitude, Philco-Ford Report WDL-TR4223, 15 July 1970.

4.10 H. Y. Tada, "A Pertinent Method of Converting an Omnidirectional Flux to an Equivalent 10-MeV Flux in the Presence of Protective Shield", TRW, STL IOC 9270.1-3, January, 1965.

4.11 H. Y. Tada "Estimating Solar Cell Degradation in the Space Radiation Environment", TRW, E.R., 71-8715.6-6-022, July, 1971.

CHAPTER 5

5.0 THE SPACE RADIATION ENVIRONMENT

The radiation environment near the earth, detrimental to solar cell performance, consists of electrons and protons trapped in the geomagnetic field, corpuscular radiation associated with large solar flare activity, and to a lesser extent, galactic cosmic-ray radiation, Near Jupiter, an environment similar to the earth's trapped particle radiation is expected, but the intensity could be far greater than that near earth, due primarily to the anticipated large magnetic field. In the following sections, each environemt is qualitatively described to assist the reader in determining the proper environment for use on making solar cell degradation estimates. Quantitative, or detailed, descriptions of each environment are beyond the scope of this manuscript.

5.1 Geomagnetically Trapped Radiation

The geomagnetic dipole field is responsible for the existence of a radiation belt near the earth, holding the trapped charged particles for long periods of time. It is a plasma confined in an inhomogeneous magnetic field, and the understanding of transport, loss and capture mechanisms has improved considerably over recent years. The dynamics of this radiation environment are greatly influenced by solar activity.

Geomagnetically trapped radiation may be either of natural origin or of artificial origin, such as high-altitude nuclear explosions. A particle has to possess a charge to be trapped in a geomagnetic field, and the constituents are electrons and protons. Regardless of the origin, the particle with just the right momentum and pitch angle will be trapped in the field. The particles will then spiral about a field line with varying pitch angle and curvature in the inhomogeneous field. They continue the motion until they reach the mirror (or reflection) point where the pitch angle becomes zero, and then bounce back into the other hemisphere. They continue to bounce back and forth between the mirror points (latitudinal motion), and at the same time drift in the longitudinal

direction as the result of forces due to the gradient of field strength and the curvature of field lines. During a quiescent state (periods of normal solar activity), therefore, the trapped particles can be characterized by three periodic motions: (a) cyclotron oscillation about the field line with Larmor frequency, (b) latitudinal motion between mirror points, and (c) longitudinal drift. The direction of motion for electrons is obviously opposite to that of protons because of an opposite charge. Near the mirror points, the particles collide with upper atmospheric gases, gradually losing their energy and changing trajectory until they are lost in the lower atmosphere.

At some distance from the earth, the field is distorted by the "solar wind" as shown in Figure 5.1. It is a plasma from the sun, consisting mostly of protons with average energy of a few keV and of density on the order of $10/cm^3$. The solar wind interacts with the geomagnetic field resulting in the formation of a shock wave. As the solar plasma passes the shock wave, the random speeds of the particles increase, and the magnetic field becomes turbulent. There is a region of hot plasma near the earth-sun line on the day side. The solar wind deforms the geomagnetic field and squeezes it into a cavity called the magnetosphere. The magnetosheath ranges from 10 to 14 earth radii.

The geomagnetic field lines just behind the magnetosheath are qualitatively similar to those associated with the simple dipole model and trap corpuscular radiation as described above. During quiescence, a relatively steady flow of solar wind blows the field away from the sun, contributing to an asymmetric shape of the radiation belt, compressed on the sun's side and forming the tail of the magnetosphere and the thin neutral layer on the dark side of the earth.

McIlwain[5.1] has proposed a coordinate system consisting of the magnetic field B and the integral invariant I which can adequately relate measurements made at different geographic locations. He introduced a parameter $L = f(B,I)$, analogous to a physical distance in a dipole field (the equatorial radius of a magnetic shell), thus reducing the number of variables needed to describe the physical situation of trapped charged

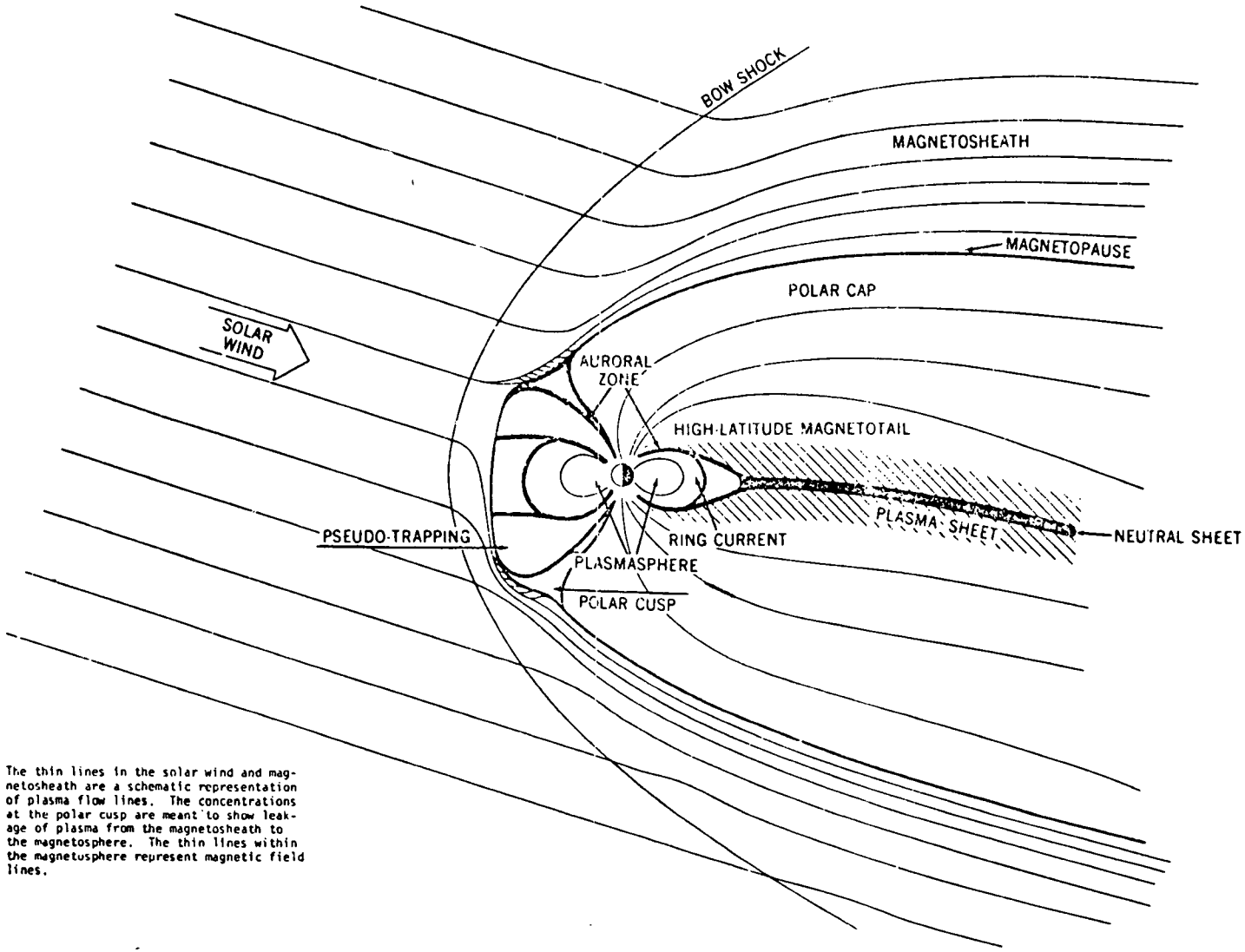

Figure 5-1. Regions of the Magnetosphere Shown in the Noon-Midnight Meridian Plane

particles and presenting field data in a manner which facilitates its physical interpretation. For a radial distance of R and a dipole moment of M, the transformation using the dipole relation is expressed as follows:

$$B = \frac{M}{R^3}\left(4 - \frac{3R}{L}\right)^{1/2} \qquad (5.1.1)$$

where R is L $\cos^2 \lambda$, M is the geomagnetic dipole moment, and λ is the magnetic latitude, McIlwain expanded the parameter L into a polynomial function of a variable which is a function of I, B, and M and elegantly represented the physical phenomena of trapped particles.

Since its introduction, numerous particle field data were presented in this (B,L) coordinate system. Vette and coworkers have concentrated efforts on the compilation of particle field data reported by numerous investigators and have constructed models of the radiation environment. These data are regarded as the best consolidated source of information available on trapped radiation environments, and are used as the single source of data on this subject throughout this manuscript. The reader may consult the referenced publications[5.2-5.8] for detailed and quantitative discussions of the trapped electron and proton environment models.

5.1.1 Trapped Protons

The most recent description of the trapped proton environment is presented in references 5.2 through 5.4. The largest proton concentration of intermediate energies is near the earth within an L-value of four (geocentric) earth radii, peaked at about two earth radii. The high energy protons concentrate even closer to the earth, peaked at 1.5 earth radii whereas the distribution of the lower energy protons extends nearly to synchronous altitude (L = 6.6 R_e). Generally speaking, the energy spectrum becomes softer as the L-value increases. At synchronous altitude, the spectrum is so soft that practically no protons with energy greater than two MeV exist.

5.1.2 Trapped Electrons

Trapped electrons with energies of a few hundred keV extend to the outer boundary of the magnetosphere, which fluctuates at 8 to 10 earth radii. There are two intense regions: an inner one covers the L-values in the range of $1.2 < L < 2.8$ and peaks about 1.4 earth radii, whereas the outer zone ranges $3 < L < 11$ and peaks at around 4 to 5 earth radii with the flux about 10^7 electrons/cm^2-sec for both zones.

The outer zone is a very dynamic region of space, and the particles are considered to be pseudo-trapped because the lifetimes are shorter than the drift time around the earth. However, powerful sources supply electrons to this region of space, and thus substantial fluxes are always present. In this zone, the flux has large short-term temporal variations related to the local time as well as a long-term change in the average flux associated with a solar cycle.

In the inner zone, the effect of storms on the average flux is significant at high L-values and higher energies. A long-term increase in the inner zone flux is correlated with the increased solar activity. Another source of temporal variation is due to a decay of residual electrons from the Starfish nuclear explosion. These temporal variations are accommodated in the recent compilation of data and publications on AE3, AE4 and AE5 by Vette.[5.5-5.8]

5.2 Orbital Integration

5.2.1 Circular Orbits

Vette and coworkers have time integrated both the trapped proton and electron environments for convenient energy ranges and tabulated the average daily fluence for various altitudes and inclinations. There are two forms of spectra in his data: one is of the form of integral flux and another difference flux, the latter of which should not be confused with the differential flux.

If $\phi(E)$ is a differential flux at energy E in MeV, normally expressed in terms of particles/cm^2-sec-MeV, and $\Phi(>E)$ is an integral flux with an

energy greater than E, expressed in particles/cm^2-sec, the relationship of these two quantities is

$$\Phi(>E) = \int_{\infty}^{E} \phi(E)\, dE \qquad (5.2.1)$$

$$= \sum_{j} \phi(E_j)\, \Delta E_j$$

On the other hand, the difference fluence $\Delta\Phi$ is simply

$$\Delta\Phi_j = \Phi(>E_j) - \Phi(>E_j + \Delta E) \qquad (5.2.2)$$

5.2.2 Trajectories Other Than Circular Orbits

For the spacecraft trajectories other than circular orbits tabulated in references 5.2 through 5.7, the radiation environment encountered by the spacecraft may be determined by some other method.

One approximation for hand calculations is to divide the trajectory into small segments with suitable time intervals $\Delta t(r,i)$, so that during this flight time interval the environment can be regarded the same as that of a circular orbit at altitude r and inclination i. The environment weighted by flight time then becomes

$$\Phi(>E,I) = \sum_{R} \Phi'(>E,r,i) \cdot \Delta t(r,i) \qquad (5.2.3)$$

The difficulty of this approximation is that (a) the Φ' is averaged over a circular orbit so that the Φ' is not equal to an instantaneous flux at (r,i), and (b) the i is constantly changing if $i \neq 0$. Thus an error can be very large; in fact, it will be appropriate only for an order of magnitude calculation if $i \neq 0$.

A more accurate and simpler way of determining the environment is to determine a trajectory on an isoflux contour map of energy E_n plotted on geographic coordinates. By knowing instantaneous flux at (r,i) and the time interval $\Delta t(r,i)$, the integral flux can be time integrated by

$$\Phi(>E_n) = \sum_R \Phi(>E_n, r, i) \cdot \Delta t(r, i) \qquad (5.2.4)$$

This calculation will determine the flux of an integral spectrum at E_n. If isoflux contour maps for different energies are available, a series of such calculations leads to several points on an integral spectrum.

The most sophisticated way to determine the environment is to make use of the physically significant coordinate system (B,L) so that uncertainties and inaccuracies attributable to the geographic coordinate system are eliminated. A set of state vectors or classical orbital elements can be used to solve Kepler's equation and generate a trajectory with suitable time intervals. These geographic coordinates are then transformed into geomagnetic shell coordinates (B,L) on which isoflux contour maps are plotted. This approach is computationally involved and hence is practical only with the aid of a computer.

The instantaneous flux $\phi(>E_n, t_j)$ is thus determined and is time integrated on each flux map of energy E_n in the following manner:

$$\Phi(>E_n) = \sum_j \phi(>E_n, t_j) \cdot \Delta t_j \qquad (5.2.5)$$

Upon time integration of instantaneous flux throughout a given trajectory, performed on one isoflux contour map of specified energy E_n and particle type, one point is finally determined in an integral flux-energy spectrum $\Phi(>E)$. If similar calculations are performed on a number of maps of different energies, exactly the same number of points can be determined in the final spectrum.

An energy spectrum at an arbitrary point in space, in general, is a function of both B and L coordinates and can be expressed in either exponential or power form. If such a distribution function in either form is applicable to an entire energy region for all points in space, only one isoflux contour map is required to determine the time integrated flux-energy spectrum.

If $FN(>E_n,>E_k,L_j')$ is an energy distribution function for a partitioned energy greater than E_k

$$\phi(>E_k,t_j) = \phi(>E_n,t_j) \cdot FN(>E_n,>E_k,L_j') \qquad (5.2.6)$$

The L_j' in FN is the L value in the input table and is the nearest to the computed value L_j. The E_n is an energy specified in an isoflux contour map. The flux $\phi(>E_k,t_j)$ is integrated in each energy shell E_k as the time integration proceeds throughout a trajectory.

The distribution function for an exponential spectrum with a parameter $E_o(>E_n,B,L)$ is defined as

$$FN(>E_n,>E_k,t_j) = \exp\left[(E_n - E_k)/E_o(>E_n,B_j,L_j)\right] \qquad (5.2.7)$$

$$= \exp\left[(E_n - E_k)/E_o(>E_n,t_j)\right]$$

The FN is thus normalized at E_n, and hence the E_n should agree with the energy specifying an isoflux contour map. For a power form, the distribution function is defined as

$$FN(>E_n,>E_k,t_j) = (E_k/E_n)^{-P(>E_n,B_j,L_j)}$$

$$= (E_k/E_n)^{-P(>E_n,t_j)}$$

where $P(>En, B_jL_j)$ = Exponent of power form which depends on the energy specifying the isoflux contour map, as well as special location of trajectory in B-L coordinate (B_j,L_j)

and again the FN is normalized at E_n. As an example of the above method, the geomagnetically-trapped proton environment is machine calculated for a highly elliptical orbit with an inclination of 63.5 degrees and is shown in Figure 5.2.

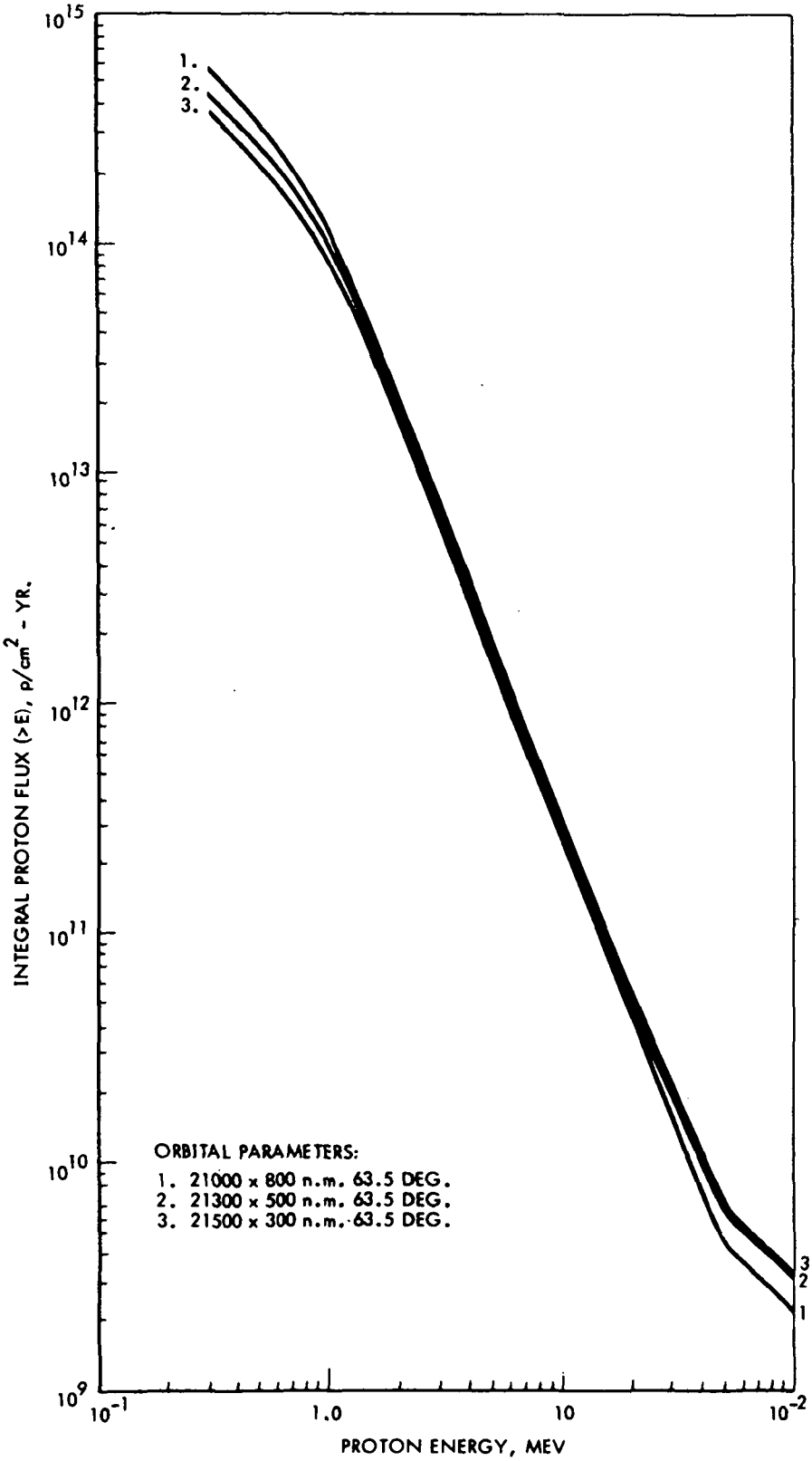

Figure 5.2 Geomagnetically Trapped Proton Environment in a Highly Elliptical Orbit

5.3 Cosmic-Ray (Galactic Cosmic-Ray) Radiation

Galactic cosmic rays are a highly penetrating radiation originating beyond the solar system. They possess energies greater than 1 BeV (some may exceed 10^8 BeV) and are capable of extraordinary interactions with matter in the upper atmosphere such as spallation, fission, fragmentation, and the subsequent secondary processes. The local cosmic-ray radiation in the atmosphere contains protons, neutrons, pi-mesons, mu-mesons, electrons, photons, and strange particles.

Near the upper limits of the atmosphere, the primary radiation, consisting of 79 percent protons and 20 percent alpha particles, predominates over the products of nuclear reactions and the decay products, thus the components change with altitude.

The ability of charged particles to penetrate a magnetic field is limited by the Lorentz force and is measured by a quantity called the magnetic rigidity, defined by the ratio of the momentum to the charge. The radius of curvature of charged particles in the field is then related to the magnetic rigidity, and hence the ability of particle penetration. The magnetic cutoff momentum, and hence the cutoff energy, for a given vertically incident particle at a given altitude is closely related to the latitude of the geomagnetic field. Only protons with energies greater than about 15 BeV can penetrate the earth's magnetic field at the equator.

One remarkable characteristic of cosmic rays is their isotropy. The average diurnal effect is very small; however, there is a definite relationship between the fluctuation and solar activity in general; 27-day effects, an 11-year fluctuation cycle, and the Forbush decrease associated with the magnetic storms are examples. Although the energy is very high, the flux is negligibly small compared with other environments considered, and this environment is ignored in solar cell array degradation cases at present.

5.4 Solar Flare (Solar Cosmic-Ray) Radiation

Solar flares occur in the neighborhood of sunspots, very seldom emit white light, and cause a sudden increase in intensity of the hydrogen

alpha line (6,563 Å). After its inception, the flare rapidly expands over an area of a few million to a billion square miles of the solar disk, reaching a peak intensity and gradually decaying and completely disappearing within several minutes to several hours, depending on the size of the flare.

Within half an hour or more following the appearance of large solar flares, energetic particles, consisting mostly of protons, are detected at the earth, particularly in the polar regions inside the auroral zones. The radiation dies away with a time constant of one to three days. The constituent particles are electrons, protons, alpha particles, and very small numbers of medium nuclei (C, N, and O). The ratios of protons to alpha particles, and of protons to medium nuclei vary considerably between solar events, whereas the ratio of alpha particles to medium nuclei remains relatively constant.

Although the fluctuation in flux intensity is much more severe and random than those of galactic cosmic rays, the following phenomena were observed in the past: (a) there may be an 11-month cycle in the peak number of events, (b) there is a semiannual variation which has maxima in March and September, probably near the equinoxes, (c) the maximum number of events occurs on the average near the September equinox and the minimum during December or January, (d) the number of flares varies with the 11-year solar cycle, and (e) there is a definite tendency for flare events producing a large proton fluence to occur during the increase or decrease of sunspot activity rather than during the maximum.[5.9] Predicted and observed sunspot numbers for the previous solar cycle are shown in Figure 5.3.[5.10]

Solar flare particle fluxes arriving at the earth are highly time dependent in intensity, spectrum and isotropy. The rise time naturally varies with individual event and is strongly energy-dependent, reaching the maximum intensity first at higher energies and thus showing a harder spectrum at the beginning. After the peak of radiation, the integral flux decays with time at a rate approximately proportional to t^{-n}, where t is time and n is a number, roughly equal to 3. The particle flux arriving in the upper atmosphere is for the most part isotropic; however, significant anisotropics frequently exist for shorter durations, arriving from a highly preferred and fairly narrow direction in space from 30° to

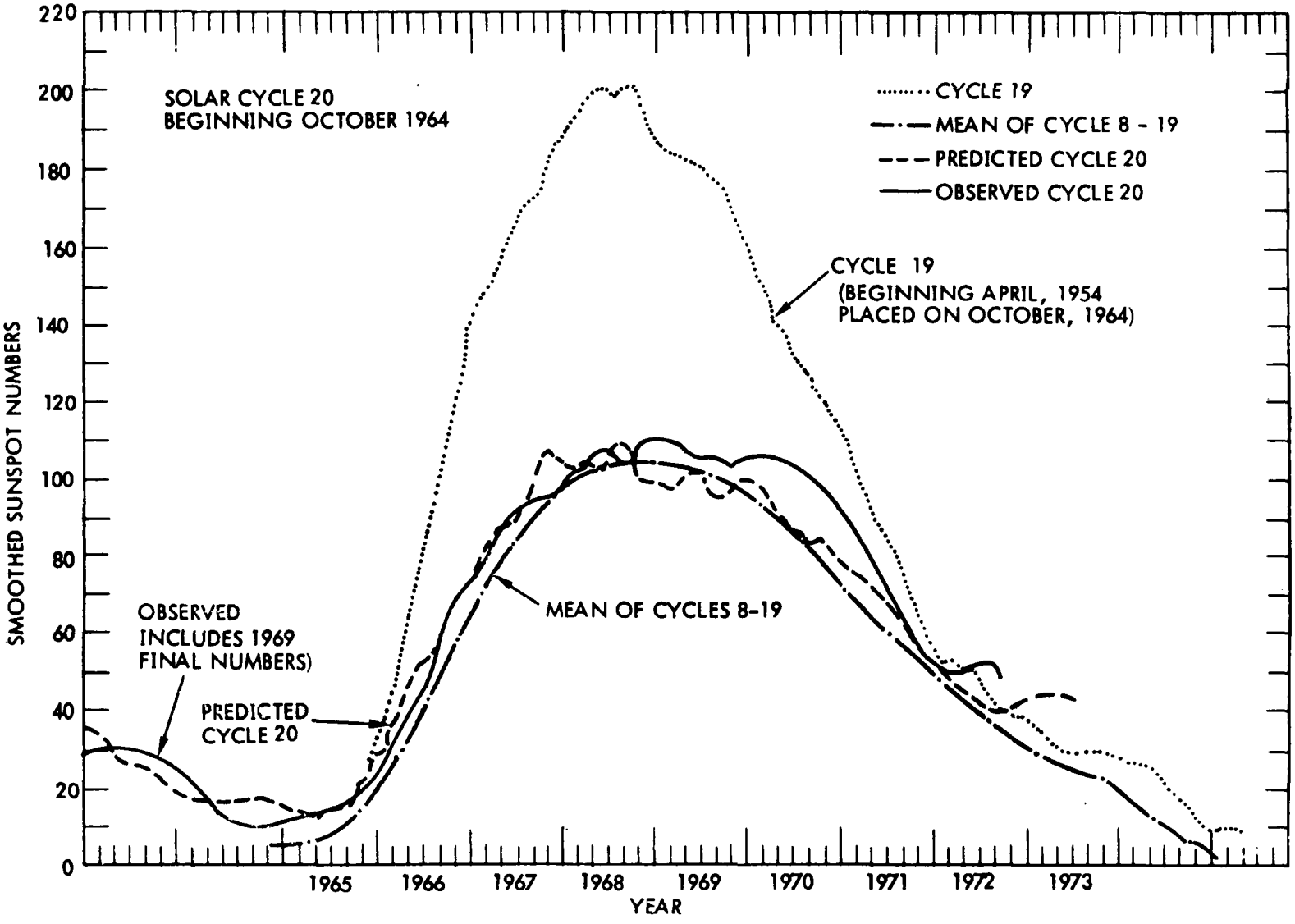

Figure 5.3 Predicted and Observed Sunspot Numbers[5.10]

60° west of the earth-sun line for a period of a few minutes.

A model described by McCracken[5.11] is largely based on experimental observation. The following is an excerpt from his article:

> "Figure 5.4* shows the model for the magnetic regime created by the plasma disturbance originating in a large solar flare (not necessarily a flare that results in a large proton event). The plasma ejected by the flare carries the lines of force of the sunspot with it, the lines of force being stretched outward from the sunspot in a quasi-radial fashion. The sun's rotation causes the lines to curve westward. The configuration of the lines of force near the leading edge of the plasma disturbance is not yet known; however, it is known to exclude cosmic rays from outside, and to inhibit the escape of cosmic rays injected at points inside the magnetic regime.
>
> In the Forbush decrease, the arrival of the leading edge of the plasma disturbance at the earth initiates the magnetic storm, and once the earth is inside the magnetic regime, some galactic cosmic rays are screened away from the earth. This phenomenon now provides a direct magnetic connection from the earth to the sunspot group. Consequently, if another flare were now to produce cosmic rays, they would travel rapidly along the magnetic lines of force to the earth. They would, therefore, arrive at the earth soon after the occurrence of the flare (about 20 minutes), and the maximum intensity would rapidly be reached. The divergent nature of the magnetic lines of force implies that the cosmic rays would tend to become collimated, eventually travelling roughly parallel to the lines of force. Also, the particles would be partially trapped within the magnetic configuration; and so after a period of anisotropy, a period of isotropy may be observed.
>
> At a point outside the magnetic regime, Figure 5.4a*, there is no direct connection to the sunspot, and hence cosmic rays cannot arrive rapidly at the earth. They can only arrive by diffusion across the lines of force-a process that tends to delay and isotropize them. Therefore, an appreciable time delay exists between particle production and arrival at the earth (30-120 minutes), and the intensity rises slowly to a maximum some hours after the flare. The maximum omnidirectional intensity of radiation is less than that which would be observed if the earth has a direct magnetic connection to the sunspot. The radiation may be mildly anisotropic, with the maximum intensity oriented along the lines of force leading to the sun, but not to the sunspot group in which the flare occurred."

*Figure numbers altered from original text.

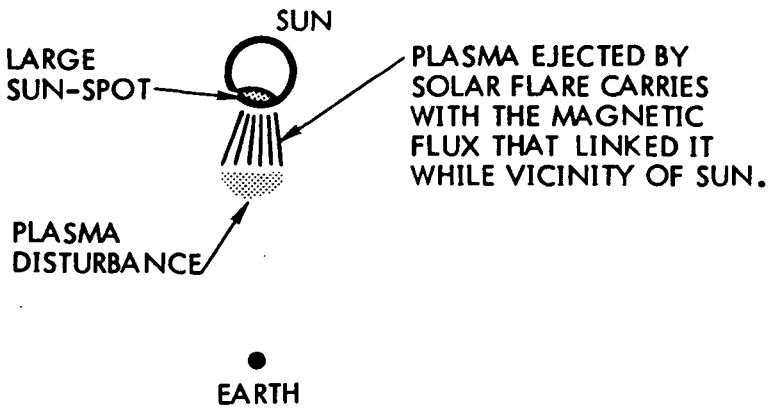

(a) 6 HOURS AFTER FLARE

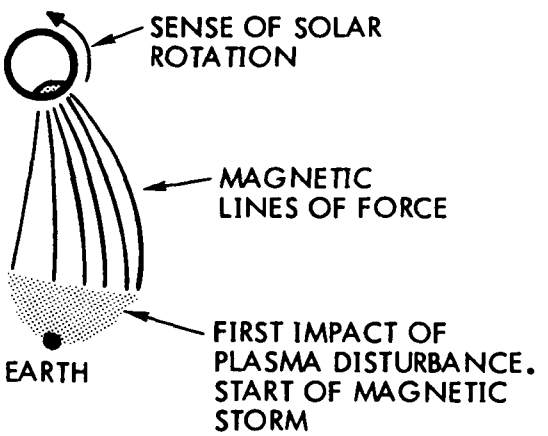

(b) ABOUT 24 HOURS AFTER FLARE

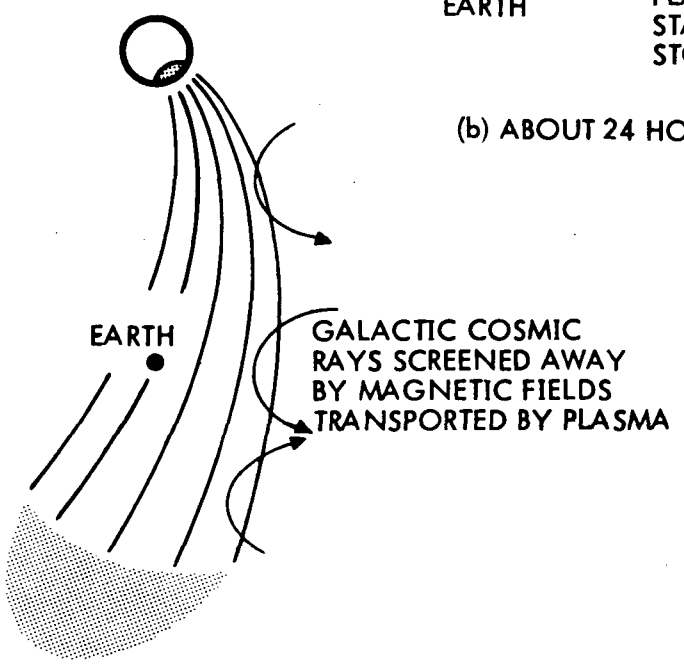

(c) ABOUT 48 HOURS AFTER FLARE

Figure 5.4 Changes of the Interplanetary Magnetic Field Regime Model with Time[5.11]

Until recently, observations of solar flare particles were made only for those with relatively high energies (10, 30 and 100 MeV), and much higher than the energy range of normal interest in connection with solar cell degradation. The time integrated spectrum normally exhibits an exponential form with respect to rigidity and is customarily expressed in terms of the characteristic rigidity R_o as follows:

$$\Phi(>R) = \Phi(>R_o) \cdot e^{(1-R/R_o)} \qquad (5.4.1)$$

where

R = rigidity $\left(\frac{\text{joule}}{\text{coulomb}}\right)$, $\left(\frac{\text{volt}\cdot\text{amp}\cdot\text{sec}}{\text{coulomb}}\right)$, or (volt)

$= pc/zq = \sqrt{E^2 - (m_o c^2)^2}/zq$

$= \sqrt{T(T + 2m_o c^2)}/zq$

E = total energy

T = kinetic energy

p = momentum (MeV/c),(joule sec/m), or (newton·sec)

$m_o c^2$ = rest mass energy, 938 MeV per proton

zq = atomic charge

$\Phi(>R)$ = integral flux having rigidity greater than R

The R_o varies not only with each event but within the spectrum of an event. Integral solar proton flux is tabulated in Table 5.1 for selected flare events from the year of 1956 through 1962 together with the characteristic rigidity. The characteristic rigidity $R_o(10\text{-}30)$ is computed from the flux at 10 and 30 MeV and $R_o(30\text{-}100)$ at 30 and 100 MeV respectively. The annual integral flux is shown in Table 5.2. The R_o computed for the annual flux is smaller during the years near sunspot maximum (50 $\sim$ 70 MV) but the total annual fluence is higher during these years.

Since solar flare particle fluxes are rich in low rigidities, a strong cutoff phenomenon is expected. During the quiescent state, the cutoff rigidity at low latitude is a strong function of direction as

TABLE 5.1 INTEGRAL PROTON FLUX AT 10, 30, AND 100 MeV AND CORRESPONDING CHARACTERISTIC RIGIDITY R_o (5.12)

DATE	(> 10 MeV)	ϕ(> 30 MeV)	ϕ(> 100 MeV)	R_o(30-100)	R_o(10-30)
		(protons/cm^2)		(MV)	
2/23/56	1.8×10^9	1.0×10^9	3.5×10^8	195	173
3/11/56	-	-	-	-	-
8/ 3/56	-	2.5×10^7	6×10^6	144	-
11/13/56	-	-	-	-	-
1/20/57	-	2×10^8	7×10^6	61	-
4/ 3/57	-	-	-	-	-
6/22/57	-	-	-	-	-
7/ 3/57	-	2×10^7	-	-	-
8/ 9/57	-	1.5×10^6	-	-	-
8/29/57	-	1.2×10^8	3×10^6	56	-
9/21/57	-	1.5×10^6	-	-	-
10/20/57	-	5×10^7	1×10^7	127	-
11/ 4/57	-	9×10^6	-	-	-
2/ 9/58	-	1×10^7	-	-	-
3/23/58	2×10^9	2.5×10^8	1×10^7	64	49
4/10/58	-	5×10^6	-	-	-
7/ 7/58	1.8×10^9	2.5×10^8	9×10^6	62	52
8/16/58	4×10^8	4×10^7	1.6×10^6	64	44
8/22/58	8×10^8	7×10^7	1.8×10^6	56	42
8/26/58	1.5×10^9	1.1×10^8	2.0×10^6	51	39
9/22/58	9×10^7	6×10^6	1×10^5	50	38
5/10/59	5.5×10^9	9.6×10^8	8.5×10^7	84	58
6/13/59	-	8.5×10^7	-	-	-
7/10/59	4.5×10^9	1.0×10^9	1.4×10^8	104	68
7/14/59	7.5×10^9	1.3×10^9	1.0×10^8	80	58
7/16/59	3.3×10^9	9.1×10^8	1.3×10^8	105	79
8/18/59	-	1.8×10^6	-	-	-

TABLE 5.1 (Continued)

DATE	(> 10 MeV)	ϕ(> 30 MeV)	ϕ(> 100 MeV)	R_0(30-100)	R_0(10-30)
		(protons/cm^2)		(MV)	
1/11/60		4×10^5	-	-	-
4/ 1/60	1.5×10^7	5.0×10^6	8.5×10^5	116	93
4/ 5/60	-	1.1×10^6	-	-	-
4/28/60	1.3×10^7	5.0×10^6	7×10^5	104	102
4/29/60	-	7×10^6	-	-	-
5/ 4/60	1.2×10^7	6×10^6	1.2×10^6	127	147
5/ 6/60	-	4×10^6	-	-	-
5/13/60	1.5×10^7	4×10^6	4.5×10^5	94	77
6/ 1/60	-	4×10^5	-	-	-
8/12/60	-	6×10^5	-	-	-
9/ 3/60	9×10^7	3.5×10^7	7×10^6	127	108
9/26/60	2×10^7	2.0×10^6	1.2×10^5	73	44
11/12/60	4×10^9	1.3×10^9	2.5×10^8	124	91
11/15/60	2.5×10^9	7.2×10^8	1.2×10^8	114	82
11/20/60	1.4×10^8	4.5×10^7	8×10^6	118	90
7/11/61	1.7×10^7	3×10^6	2.4×10^5	81	59
7/12/61	5×10^8	4×10^7	1×10^6	56	40
7/18/61	1×10^9	3×10^8	4×10^7	102	85
7/20/61	1.5×10^7	5×10^6	9×10^5	120	93
9/28/61	5×10^7	6×10^6	1.1×10^6	121	48
11/10/61	-	-	-	-	-
2/ 4/62	-	-	-	-	-
10/23/62	6×10^5	1.2×10^5	1×10^4	83	63

TABLE 5.2. OBSERVED ANNUAL INTEGRAL SOLAR PROTON FLUX [5.12]

Year	Number of Events	Integral Flux (protons/cm^2)			R_o
		Φ(>10 MeV)	Φ(>30 MeV)	Φ(>100 MeV)	(MV)
1956	4	2.0×10^9	1.0×10^9	3.5×10^8	250
1957	9	---	4.0×10^8	2.0×10^7	60
1958	8	7.0×10^9	7.8×10^8	2.4×10^7	50
1959	6	$2,2 \times 10^{10}$	4.2×10^9	4.6×10^8	70
1960	15	6.8×10^9	2.2×10^9	3.8×10^8	130
1961	6	1.6×10^9	3.5×10^8	4.2×10^7	90
1962	2				
1963	1				
	52				
	Solar-cycle total	3.9×10^{10}	9.0×10^9	1.3×10^9	100 (av.)

well as of latitude (approximately proportional to $\cos^4 \lambda$ for large geomagnetic latitudes), and hence of L. Galactic cosmic rays follow this normal Störmer cutoff as do the flare particles just before the plasma cloud hits the geomagnetic field. After the impact of the plasma front, the field is disturbed (magnetic storm) in such a manner that the field due to a time-dependent ring current appears to superimpose on the normal geomagnetic dipole field, causing the disturbed line of force to stretch further out of the earth at a given latitude. As a result, the particle rigidity necessary to penetrate at a given latitude is greatly reduced, and the cutoff energy becomes time dependent. A recent satellite observation indicated that the cutoff energy at synchronous altitude seems to be much less than that many expected, and that flare protons with energy as low as a few hundred keV were observed during the storm. If this is the case, the cutoff energy due to the geomagnetic field becomes insignificant at this altitude, because the cutoff due to a solar cell cover shield is normally far greater than the magnetic cutoff during a storm. If both altitude and latitude are low, the field perturbation due to the storm may be insignificantly small compared with that of the quiescent state, and the Störmer cutoff approximation may prevail. The geomagnetic shielding phenomena are shown in Figure 5.5[5.13] for protons in a class three flare on July 18, 1961.

For the purpose of predicting the size and spectrum of solar flare proton events, many statistical analyses have been made on proton events observed near or on the earth. Unfortunately, the correlation between the prediction and observations has been rather poor. A Poisson distribution may be appropriate for sunspot numbers and solar flares on the sun, but not for solar flare proton events. The flares which are large enough to emit a large number of energetic particles and further satisfy the requirements of protons to reach the earth obviously belong to a special class of solar flare events. Phenomena observed during solar cycle 19 are enumerated below for review, placing particular emphasis on those which appear to be dependent on solar activity.

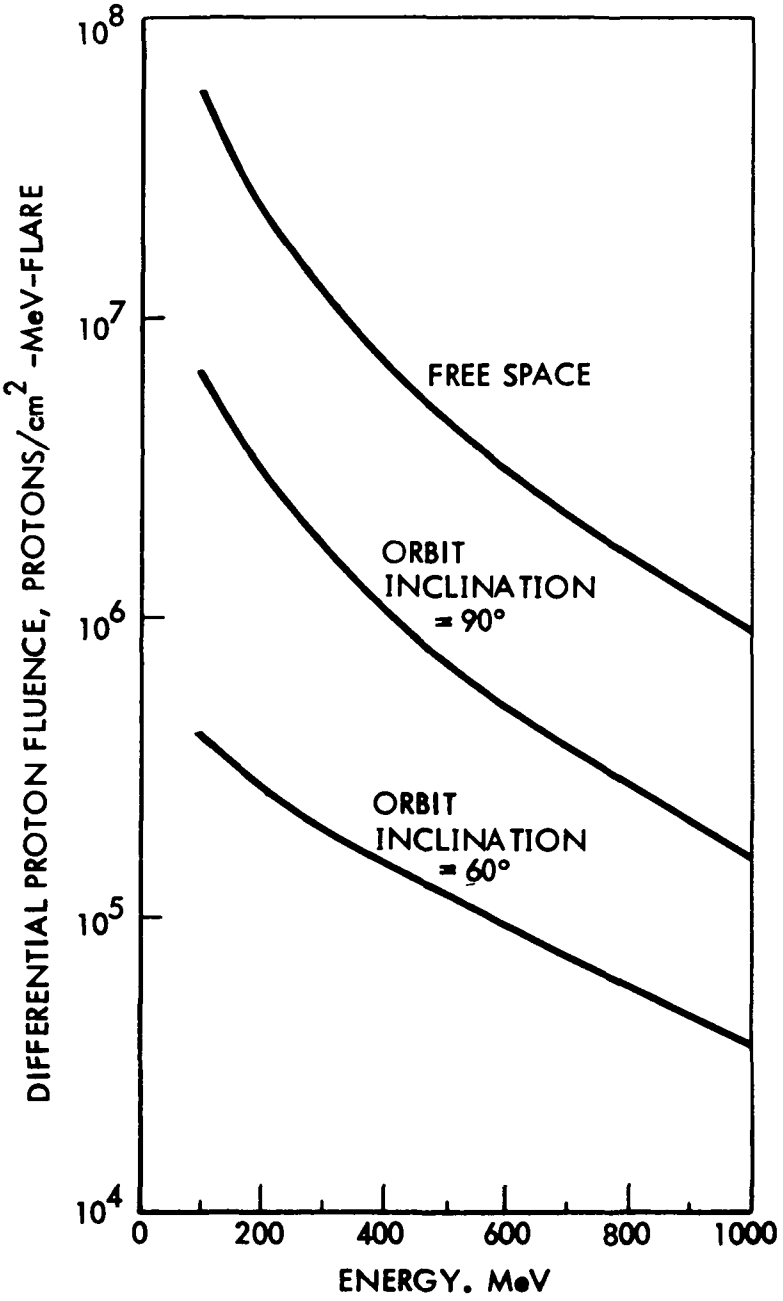

Figure 5.5 Solar Flare Proton Environment at 200 n. mi. Circular Orbit Due to Flare Event on July 18, 1961, Class Three Flare[5.13]

a. The flares capable of producing large proton events tend to occur when the rate of change in annual sunspot number becomes greater.

b. The characteristic rigidity of solar flare protons is randomly distributed throughout an 11-year cycle, but both the annual expectation value and variance are not. During a period of increasing or decreasing sunspot activity, the R_0 becomes larger on the average than that during the maximum, and the variance becomes smaller during the solar maximum. That is to say, the solar flare proton events are relatively steady and confined in a smaller rigidity range during the solar maximum, whereas the size and spectrum become erratic when the rate of change in sunspot activity becomes severe.

c. The size of each event, as measured by an integral proton flux of energy greater than 30 MeV, is almost randomly distributed over an 11-year cycle, but a line connecting the successive annual fluence plotted against sunspot number is not a single-valued function.

A model was developed to implement the above observations. With the aid of the model, annual free space solar flare proton fluxes of energy greater than 10 and 30 MeV are determined for each year of cycles 20 and 21, and are tabulated in Tables 5.3 and 5.4, respectively. These predictions are compared with those described in reference 5.13 as well as with some experimental observations compiled by King.[5.15] These predicted flux values agree with the experimental values very well for most of the years of cycle 20 except for the years of 1966 and 1970. The discrepancy between the predicted and the observed $\Phi(>10$ MeV) can be as large as a factor of 7, as in the case of 1966 and 1970, when the annual flux variation is considered. However, the overall discrepancy between observed and predicted Φ is within a factor of 2 when the flux is integrated over the 11-year solar cycle. The August 1972 event is a severe fluctuation in magnitude and time of occurrence with respect to the 11-year cycle; yet the predicted annual value is within a factor of 4 of the observed value. Despite the crudeness of this technique and a disappointing prediction for some years of cycle 20, this technique will provide a much better estimate than those cited in reference 5.13, 2n

TABLE 5.3 BOTH PREDICTED AND OBSERVED ANNUALLY INTEGRATED SOLAR FLARE PROTON FLUXES FOR CYCLE 20

	PREDICTED IN REFERENCE 5.13				PREDICTED BY TADA MODEL					OBSERVED[5.15]	
YEAR	Φ(>10)	CF(>10)	Φ(>30)	R_0(10-30)	SSN[+]	Φ(>10)	CF(>10)	Φ(>30)	R_0(10-30)	Φ(>10)	Φ(>30)
1964	4.5E9	---	1.0E9	67		$\lesssim$1.0E8	---	---	---	---	---
1965	4.5E9	1/350	1.0E9	67		$\lesssim$1.0E8	---	---	---	1.3E7	---
1966	2.3E10	1/26	5.0E9	67	46**	1.3E8	6.7	4.7E7	100	8.7E8	---
1967	2.3E10	1/56	5.0E9	67	90**	4.8E8	1/1.2	1.3E8	90	4.1E8	2.2E7
1968	4.5E10	1/41	1.0E10	67	107**	8.0E8	1.4	1.0E8	50	1.1E9	1.5E8
1969	4.5E10	1/38	1.0E10	67	108**	1.7E9	1/1.4	2.2E8	50	1.2E9	2.5E8
1970	4.5E10	1/145	1.0E10	67	103**	2.1E9	1/6.8	6.8E8	90	3.1E8	1.7E7
1971	2.3E10	1/24	5.0E9	67	70**	1.8E9	1/1.9	5.1E8	80	9.5E8	2.5E8
1972	2.3E10	1/33	5.0E9	67	70*	1.8E9	3.8	2.4E8	50	6.9E9	3.9E9
1973	4.5E9	---	1.0E9	67	26*	$\lesssim$1.0E8	---	---	---		
1974	4.5E9	---	1.0E9	67	17*	$\lesssim$1.0E8	---	---	---		
Total	2.5E11		5.4E10			7.5E9		1.9E9		1.2E10	

SSN Smoothed sunspot number averaged over one year

** Observed, reference 5.10

* Predicted as nominal in reference 5.13 and shown in Figure 5.6

Φ(>10) Integral proton flux of energy greater than 10 MeV, protons/cm^2-yr

R_0(10-30) Characteristic magnetic rigidity calculated at energies of 10 and 30 MeV, MV

CF(>10) Correlation factor (CF) defined as:

$$CF\ (>10) = \Phi(>10)\ (\text{Observed})/\Phi(>10)(\text{Predicted})$$

TABLE 5.4. PREDICTED ANNUALLY INTEGRATED SOLAR FLARE PROTON FLUXES FOR CYCLE 21

Year	Predicted In Reference 5.13		Predicted By Tada Model			
	$\Phi(>10)$	$\Phi(>30)$	$SNN^{5.13}$	$\Phi(>10)$	$\Phi(>30)$	$R_o(10\text{-}30)$
1975	4.5E9	1.0E9	19	$\gtrsim$1.0E8	---	----
76	4.5E9	1.0E9	38	1.2E8	---	50
77	4.5E9	1.0E9	65	2.3E8	1.1E8	145
78	2.3E10	5.0E9	86	5.5E8	7.2E7	50
79	2.3E10	5.0E9	90	8.0E8	8.3E7	45
80	4.5E10	1.0E10	79	1.3E9	2.7E7	65
81	4.5E10	1.0E10	66	1.2E9	4.1E7	95
82	4.5E10	1.0E10	51	7.0E8	1.5E8	65
83	2.3E10	5.0E9	?			
84	2.3E10	5.0E9	?			
85	4.5E9	1.0E9	?			
86	4.5E9	1.0E9	?			
TOTAL	2.6E11	5.5E10		4.9E9	8.5E8	

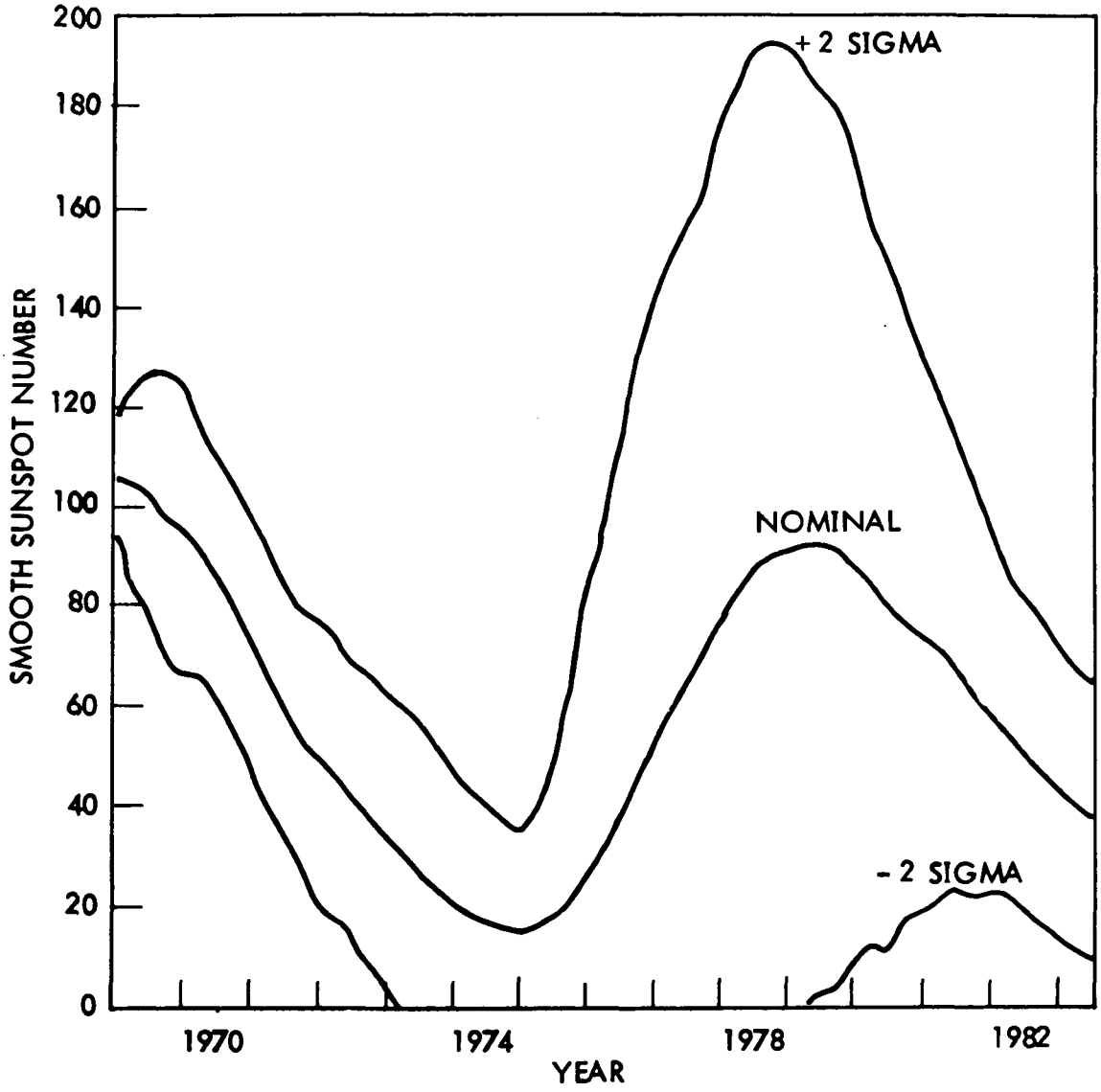

Figure 5.6 Predicted Smoothed Sunspot Number for Solar Cycle 21[5.13]

improvement of better than a factor of 10. The environment specified in reference 5.13 is shown in Figure 5.7, together with data taken from references 5.11 and 5.12 for comparison.

5.5 Jupiter Trapped Radiation Environment

Earth observations of decimetric RF noise emanating from the vicinity of Jupiter suggest the following as a Jovian environment:

a. Radio emission generated near Jupiter is synchrotron radiation.

b. Charged particles are responsible for the RF noise and are trapped by a magnetic field as in the case of near earth environment.

c. The magnetic field is probably due to a dipole in large part and is very strong as compared with that of earth (probably $\sim 10^{-5}$ of telsa at the Jovian equator).

d. Consequently, the intensity of the Jovian radiation belt is far greater than that of the earth's radiation belt which can be scaled upward accordingly to satisfy the observed synchrotron radiation.

Prospective models for the Jovian radiation belt were postulated and discussed at the Conference on Jupiter Radiation Belt Workshop held at JPL, Pasadena, California, July 1971. A few well-known experts on the earth's radiation belt raised questions about some postulates and assumptions made in the proposed model. These questionable aspects will become clarified in the not too distant future as space probes fly over Jupiter. The first in situ data will probably be available from the Pioneer 10 mission in December 1973. The post-workshop radiation models are shown in Figure 5.8.

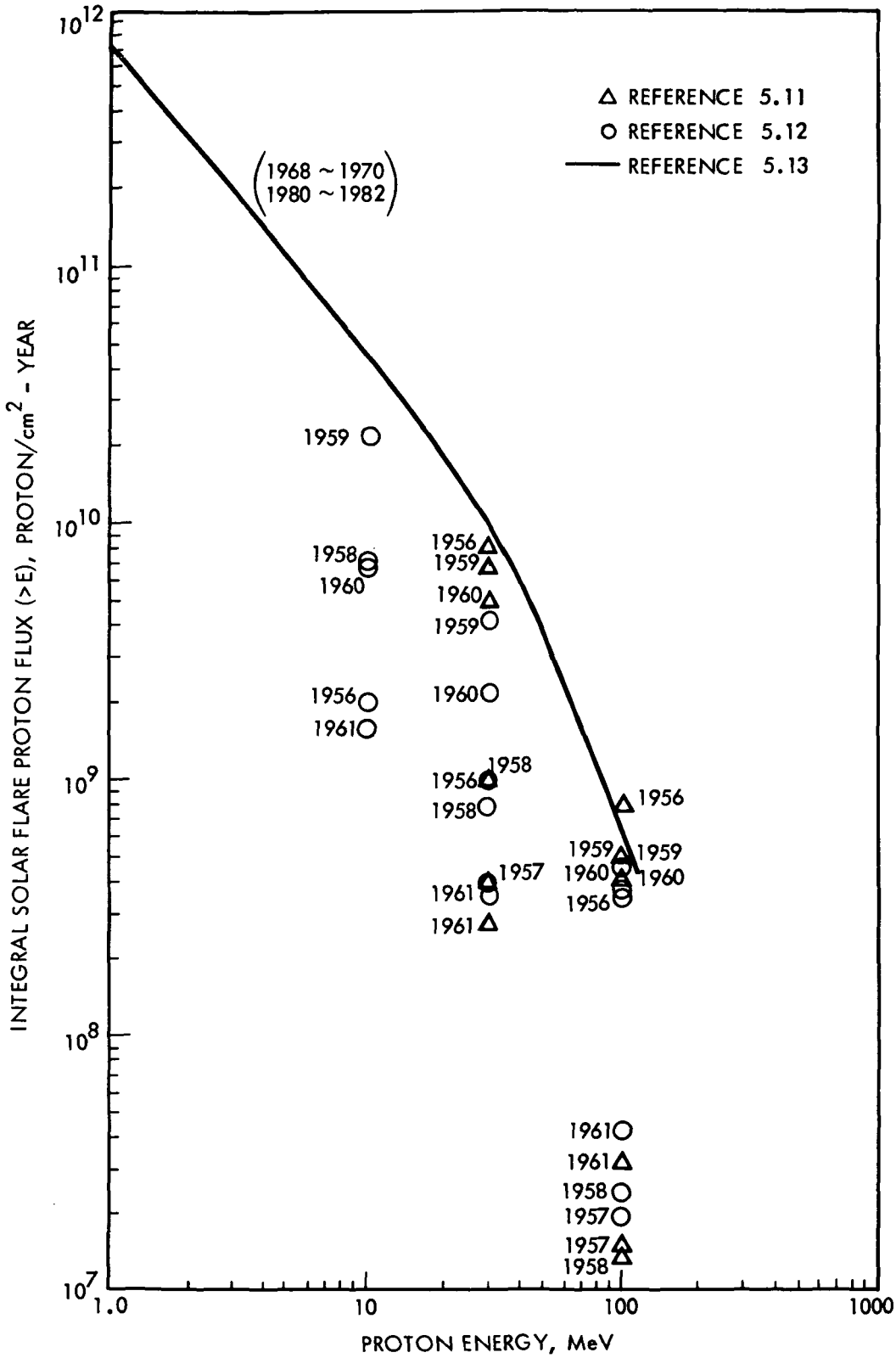

Figure 5.7 Solar Flare Proton Environment of the Last Solar Cycle, 19

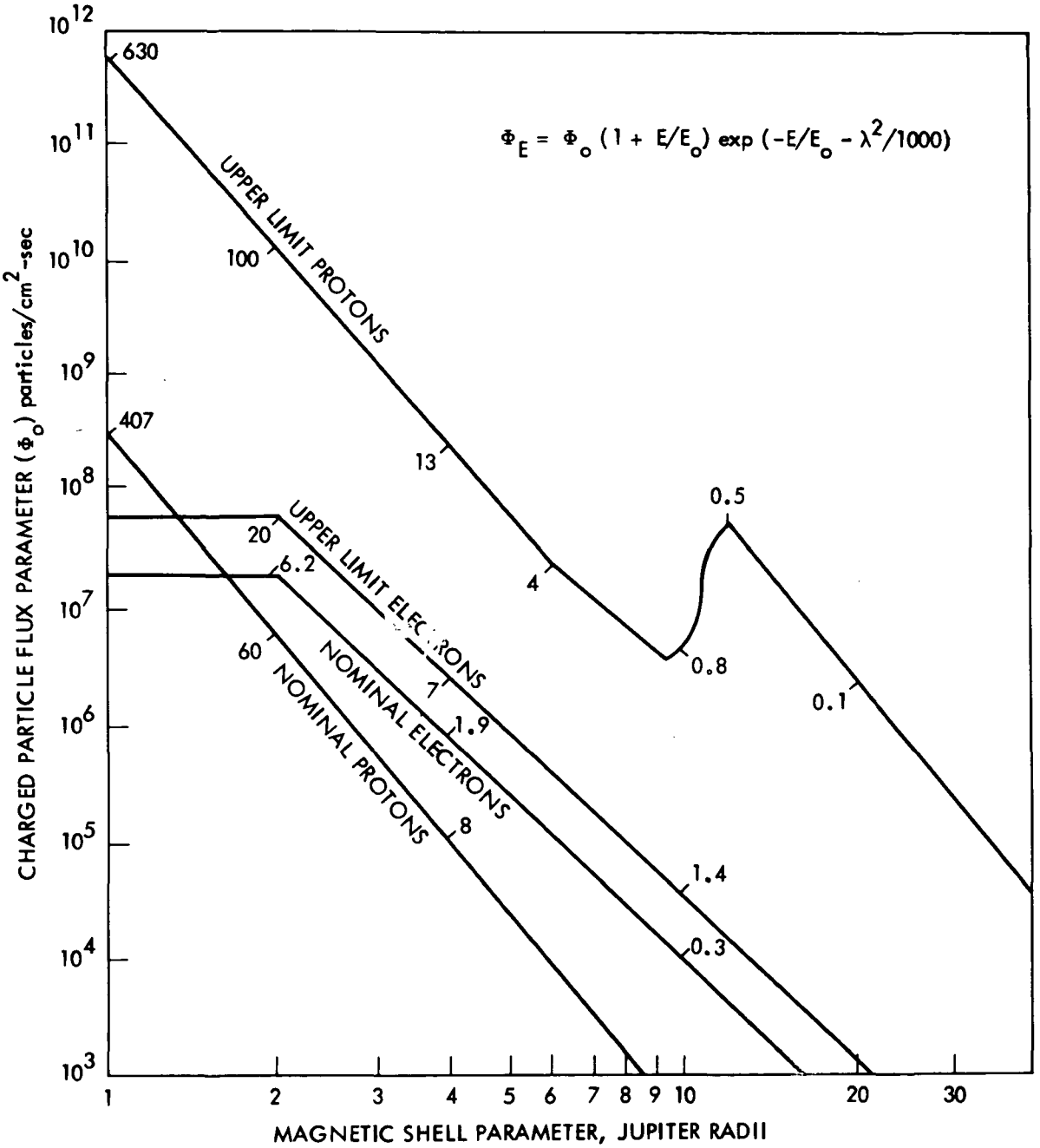

Figure 5.8 Fluxes of charged particles in Jupiter's trapped radiation belts, as functions of distance from the magnetic dipole in the magnetic equatorial plane. Local values of the characteristic energy E_o are shown in MeV.[5.16]

REFERENCES

5.1 C. W. McIlwain, "Coordinates for Mapping the Distribution of Magnetically Trapped Particles," J. Geophys. Res. 66, 3681, 1961.

5.2 J. H. King, "Models of Trapped Radiation Environment, Vol. IV, Low Energy Protons," NASA SP-3024, 1967.

5.3 J. P. Lavine and J. I. Vette, "Models of the Trapped Radiation Environment, Vol. V, Inner Belt Protons," NASA SP-3024, 1969.

5.4 J. P. Lavine and J. I. Vette, "Model of the Trapped Radition Environment, Vol. VI, High Energy Protons," NASA SP-3024, 1970.

5.5 J. I. Vette and A. B. Lucero, "Models of Trapped Radiation Environment, Vol. III, Electrons at Synchronous Altitudes," NASA SP-3024 1967.

5.6 G. W. Singley and J. I. Vette, "The AE-4 Model of the Outer Radiation Zone Electron Environment," NASA, NSSDC 72-06, 1972.

5.7 M. J. Teague and J. I. Vette, "The Inner Zone Electron Model AE-5," NASA, NSSDC 72-10, 1972.

5.8 G. W. Singley and J. I. Vette, "A Model Environment for Outer Zone Electrons," NASA, NSSDC 72-13, 1972.

5.9 P. M. Blair, Jr. and H. Y. Tada, "Environments of SYNCOM, Mark II", TM-732, Aerospace Group, Hughes Aircraft Co., 1972.

5.10 Solar Geophysical Data, Prompt report, No. 342-part 1, USDC, NOAA, Feb 1973.

5.11 F. B. McDonald, (Ed.), Solar Proton Manual, NSAS TR R-169, Dec.1963.

5.12 W. R. Webber, "An Evaluation of Radiation Hazard Due to Solar Particle Events," The Boeing Co., Report D2-90469, Dec. 1963

5.13 D. K. Weidner, "Natural Space Environment Criteria for 1975-1985 NASA Space Stations," NASA TM X-53865, Aug. 1969, Second Edition, 10 Aug. 1970.

5.14 D. K. Weidner, "Space Environment Criteria Guidelines for Use in Space Vehicle Development", 1969, rev., NASA TM X-53815, Aug. 1970.

5.15 J. H. King, Letter dated Sept. 29,1972, NASA, GSFC, NSSDC.

5.16 A. J. Beck, Jr., (Ed.) "Proceedings of the Jupiter Radiation Belt Workshop," JPL TM 33-543, JPL, July 1972.

CHAPTER 6

6.0 SOLAR ARRAY DEGRADATION CALCULATIONS

In the previous sections, the three basic input elements necessary to perform degradation calculations were developed. The first of these elements is degradation data for solar cells under normal incidence 1 MeV electron irradiation. The second input element is the effective relative damage coefficients for omnidirectional space electrons and protons of various energies for solar cells with various thickness of cover glasses. The third input element is space radiation environment data which has been integrated for the orbit of interest. The section will cover the use of the above inputs to complete a solar array degradation estimate.

6.1 General Procedure, Equivalent Fluence

The effective relative damage coefficients allow the conversion of various energy space electrons and protons into equivalent fluences. The equivalent fluences are based on normal-incidence monoenergetic irradiations for which the degradations of the solar cells of interest are characterized. The process of weighting an integral energy spectrum of electrons for a given orbit can be described as follows:

$$\Phi_{1\ \text{MeV}\ e} = \sum_{E=0}^{\infty} [\Phi(>E) - \Phi(>E + \Delta E)] \cdot D(E,t) \qquad (6.1.1)$$

where

$\Phi_{1\ \text{MeV}\ e}$ = the damage equivalent 1 MeV electron fluence (e/cm^2-year)

$\Phi(>E) - \Phi(>E + \Delta E)$ = the isotropic particle fluence having energies in a small energy increment greater than energy E (e/cm^2-year)

$D(E,t)$ = the relative damage coefficient for isotropic fluences of space particles of energy E on solar cells shielded by cover glass of thickness t (dimensionless)

The quantities $\Phi(>E) - \Phi(>E + \Delta E)$ for a range of energies are also known as the difference spectrum. This spectrum can be generated from an integral energy spectrum for any energy increments desired. For the case of space protons, equation (6.1.1) can also be used with the exception that D(E,t) values for protons are based on 10 MeV proton fluences rather than 1 MeV electrons. The calculated equivalent fluence will therefore be a damage equivalent 10 MeV proton fluence. The equivalent 10 MeV proton fluence can be converted to equivalent 1 MeV electron fluence as follows:

$$\Phi_{1\ \text{MeV}\ e} = \Phi_{10\ \text{MeV}\ p} \times 3000 \qquad (6.1.2)$$

The above relationship is an approximation which must be made for the purpose of combining electron and proton damage. In Section 3.3, the differences between electron and proton degradation were discussed. Since the slope of the degradation curve (the constant C in equation 3.2.1) is different for 1 MeV electron and 10 MeV proton irradiations, the constant in equation (6.1.2) will differ depending on the level of degraded cell output at which this constant is determined. At present, the best information available indicates a value equal to 3000 when cell output parameters are degraded by 25%. In cases when the cell degradation is entirely dominated by proton damage, such as circular earth orbits below 1000 km (550 n mi), the cell degradation could be estimated more accurately by calculating the equivalent 10 MeV proton fluence, and referring to 10 MeV proton cell damage curves which are not currently available.

An additional problem arises in calculating equivalent fluences for proton environments. The results shown in Figures 4.3 and 4.4 have shown that different values of D(E,t) for proton irradiation are found when this damage constant is based on cell I_{sc} or P_{max} and V_{oc}. This differs with the results of electron irradiation where one value of D(E,t) describes the behavior of all cell output parameters. Because of the two sets of D(E,t) values for proton irradiation, two different equivalent 10 MeV proton fluences must be considered. One of these will

describe the variation of solar cell P_{max} and V_{oc}. The other will describe the variation of solar cell I_{sc}.

The values of D(E,t) have been calculated by assuming infinite back shielding. Although this condition is often approached in the body-mounted solar arrays of spinning spacecraft, it is not generally true. The designer must also evaluate the contribution of equivalent fluence resulting from radiation incident on the back side of the solar cells. The result is a front and a back component of equivalent fluence. A question arises as to the values of D(E,t) to be used for back irradiations. In the case of trapped space electron irradiation, it is reasonable to use the same values of D(E,t) for both front and back irradiations. The only problem in this case is to reduce the backshielding offered by the panels, satellite, etc., to an equivalent in gm/cm^2 of planar shielding.

The case for space protons is considerably more complex because of the nonpenetrating nature of low energy protons. There is a need for D(E,t) values calculated from rear irradiation experimental results. If such data were available, it is expected that the values of D(E,t) below 10 MeV would be considerably smaller than those found for front irradiation with protons. This difference would be expected because rear incident low-energy protons are shielded from the space charge region of the solar cell by the bulk region of the cell. Since the desired proton back irradiation D(E,t) is not available, the only alternative is to use the front irradiation data. To allow for the self-shielding effect for cells irradiated with protons from the rear, the thickness of the cell, minus 0.011 gm/cm^2 (0.002 in) should be included in the total backshielding.

The various contributions and variations of equivalent fluence which can be encountered in a natural space environment are summarized in Table 6.1. Columns in the right side of the table indicate the contributions from the various radiation components to the two different types of equivalent fluence. Although the most general case can involve all the contributions shown in Table 6.1, in a typical earth orbit only a few of these contributions may be significant.

TABLE 6.1

SUMMARY OF EQUIVALENT FLUENCE CONTRIBUTIONS

		Contributions	
		I_{sc}	P_{max}, V_{oc}
1.	Trapped electrons, front, (I_{sc}, P_{max}, V_{oc})	X	X
2.	Trapped electrons, back, (I_{sc}, P_{max}, V_{oc})	X	X
3.	Trapped protons, front, (I_{sc})	X	
4.	Trapped protons, back, (I_{sc})	X	
5.	Trapped protons, front, (P_{max}, V_{oc})		X
6.	Trapped protons, back (P_{max}, V_{oc})		X
7.	Flare protons, front, (I_{sc})	X	
8.	Flare protons, back, (I_{sc})	X	
9.	Flare protons, front, (P_{max}, V_{oc})		X
10.	Flare protons, back, (P_{max}, V_{oc})		X

Thus, 1, 2, 3, 4, 7, and 8 contribute to the I_{sc} total equivalent fluence and 1, 2, 5, 6, 9, and 10 to the P_{max}, V_{oc} total equivalent fluence.

The calculation of equivalent fluence and subsequent estimation of degraded solar cell output from the data in Figures 3.7 through 3.14 yields data which are valid for temperatures of 28°C and solar illumination power densities of 135 mW/cm^2. When degraded solar cell outputs are desired for temperatures other than 28°C, corrections can be made by use

of the temperature coefficients discussed in Section 3.8. The evaluation of changes in solar cell response due to reduced light transmission in the cover slide materials will be covered in the next section.

6.2 General Procedure, Absorbed Dose

To use the cover glass darkening data previously presented, a procedure is necessary to evaluate the absorbed dose produced by the various radiation components of the space environment. This can be done by use of the data developed in Section 4.0. The procedure is similar to that used for equivalent fluence, with the exception that the absorbed dose is a point function and therefore varies with depth in the cover material. To calculate the absorbed dose at a particular depth in the cover materials, the following expression is used:

$$\text{Dose}(d) = \sum_{E=0}^{\infty} [\Phi(>E) - \Phi(>E + \Delta E)] \cdot I(E,d) \qquad (6.2.1)$$

where Dose(d) = the absorbed dose in the cover material at a depth d

I(E,d) = the absorbed dose per unit fluence for isotropic space radiation particles of energy E at depth d in the shielding material. Figs 4.2 and 4.5, Table 4.2 and 4.5

The absorbed dose must be calculated at several depths in the cover material and the electron and proton portions of the environment must be summed to determine the dose-depth profile. The necessity of including contributions from back radiations must also be considered. In practice, the dose deposited will decrease greatly with increasing depth into the cover materials. The greater dose near the surface is due largely to low-energy trapped protons, and contributes little to the average dose deposited in the cover materials. Because of the current uncertainties in evaluating cover material transmission loss in space, there is little object in an extremely accurate evaluation of the surface dose. When the average dose deposited in the cover material is known, the degradation in transmission can be estimated from the data in Section 3.11. These loss factors may then be applied to the estimated solar cell output parameter values.

6.3 Rough Degradation Calculations

A rough determination of the equivalent fluence can be made by manual calculation. The calculation follows the procedure described by equations (6.1.1) and (6.1.2). The examples to be shown are designed for simplicity rather than accuracy. The energy increments (E_1, E_2) used in these rough calculations are those commonly tabulated in circular orbit integrations[6.1-6.7] The D(E,t) values used are taken from Tables 4.1, 4.3 and 4.4 for the mean energy value of the energy increment. Calculations are shown for cover glass thickness of 0.0335 gm/cm^2 (0.006 in fused silica), 0.0671 gm/cm^2 (0.012 in fused silica), and 0.1675 gm/cm^2 (0.030 in fused silica). The details of such an equivalent fluence calculation are shown in Table 6.2 for trapped proton radiation in a circular orbit at 835 km (450 n mi) altitude and 90° inclination. The D(E,t) values used in Table 6.2 are those based on P_{max} and V_{oc}.

Several observations can be made regarding the calculations in Table 6.2. The largest contribution to the equivalent fluence for 0.0335 gm/cm^2 (0.006 inch fused silica) shielding occurs in the flux increment between 4 and 6 MeV. The equivalent fluence contributions from protons with energies greater than 30 MeV appear to be negligible. The use of the D(E,t) value for 5 MeV (1.25) leads to serious equivalent fluence errors in the energy increment of 4 to 6 MeV because D(E,t) changes very rapidly with energy in this region. The equivalent 1 MeV electron fluence calculated for 0.0335 gm/cm^2 shielding by this rough method is 6.81E13*e/cm^2-yr. A similar detailed machine calculation (to be discussed) employing much smaller energy increments yielded an equivalent 1 MeV electron fluence of 5.57E13 e/cm^2-yr. This difference is entirely due to the use of smaller energy increments in a machine calculation. The accuracy of the manual calculation can be improved by this procedure, but additional values of $\Phi(E_1)$ must be obtained by interpolation. It should be noted that this equivalent fluence is the front radiation contribution only. The back contribution must be calculated

---

*Throughtout this section, the floating point notation will be used to represent exponential quantities. 6.81E13 = 6.81 x 10^{13}

Table 6.2 Manual Calculation of Equivalent Fluence (Trapped Protons) (P_{max}, V_{oc})
Circular Orbit 835 km (450 n mi), 90 Degree Inclination

Energy Increment E_1 (MeV)	E_2 (MeV)	Integral Energy Spectrum* $\Phi(>E_1)$ (p/cm^2-day)	Difference Spectrum $\Phi(>E_1)-\Phi(>E_2)$ (p/cm^2-day)	Shielding Thickness 0.0335 gm/cm^2 D(E,6)	Shielding Thickness 0.0335 gm/cm^2 Equiv. Fluence (p/cm^2-day)	Shielding Thickness 0.0671 gm/cm^2 D(E,12)	Shielding Thickness 0.0671 gm/cm^2 Equiv. Fluence (p/cm^2-day)	Shielding Thickness 0.1675 gm/cm^2 D(E,30)	Shielding Thickness 0.1675 gm/cm^2 Equiv. Fluence (p/cm^2-day)
4	6	6.96E7	2.72E7	1.25E0	3.400E7				
6	8	4.24E7	1.12E7	1.27E0	1.420E7	9.80E-1	1.100E7		
8	10	3.12E7	0.61E7	8.27E-1	.505E7	9.53E-1	.580E7		
10	15	2.51E7	0.77E7	5.23E-1	.402E7	5.70E-1	.439E7	6.30E-1	.485E7
15	20	1.74E7	0.37E7	4.37E-1	.162E7	4.35E-1	.161E7	4.30E-1	.159E7
20	30	1.37E7	0.37E7	4.00E-1	.148E7	4.00E-1	.148E7	3.86E-1	.143E7
30	50	1.00E7	1.89E6	3.63E-1	.069E7	3.55E-1	.067E7	3.50E-1	.066E7
50	70	8.11E6	1.37E6	3.00E-1	.041E7	3.00E-1	.041E7	3.00E-1	.041E7
70	100	6.74E6	1.62E6	2.35E-1	.038E7	2.35E-1	.038E7	2.35E-1	.038E7
100	150	5.12E7	1.84E6	1.50E-1	.028E7	1.50E-1	.028E7	1.50E-1	.028E7
150		3.28E6							
Equivalent 10 MeV protons/cm^2-day					6.213E7		2.602E7		.9600E7
days/year					X 365		X 365		X 365
Equivalent 10 MeV protons/cm^2-year					2.27E10		9.50E9		3.50E9
Equivalent 1 MeV electrons/10 MeV proton					X 3E3		X 3E3		X 3E3
Equivalent 1 MeV electrons/cm^2-year					6.81E13		2.85E12		1.05E12
Equivalent 1 MeV electrons, P_{max}, V_{oc} (Machine Calculation) e/cm^2-yr					5.57E13		2.55E12		9.64E11

*References 6.2, 6.3

separately and added to the front contribution. It should be noted that the particle flux is not reduced by a factor of ½ to allow for the assumed infinite rear shielding. This factor is allowed for in the determination of D(E,t). In Table 6.3, the above calculation is repeated using D(E,t) values based on I_{sc}. The procedure and problems are identical to those previously discussed.

In Tables 6.4 and 6.5, the trapped proton contributions of equivalent 1 MeV electron fluence are calculated by manual methods for a circular earth orbit of 4650 km (2500 n mi) altitude and 90° inclination. Such an orbit penetrates the region with the most intense trapped proton flux. As in the previous case, the major equivalent fluence calculations occur in the lower proton energy increments, and protons of energies greater than 30 MeV can be ignored without significant error. In this and the previous example, proton energies below 4 MeV have been omitted because they are "cut off" by the lightest shielding considered [i.e., $D(<4,6) = 0$]. The calculated equivalent fluences for this orbit are approximately one thousand times greater than found at the lower altitude previously considered. In the circular orbit of 4650 km (2500 n mi) altitude, 90° inclination, there is also a relatively high flux of trapped electrons. The rough evaluation of this contribution to the equivalent fluence is shown in Table 6.6. The values of $\Phi(<E_1)$ shown are taken from integrated orbit tables from maps AE4 and AE5.[6.5] The values of D(E,t) are taken from Table 4.1. The calculation procedure for trapped electrons is exactly the same as that for trapped protons, with the exception that one equivalent fluence value will describe the variation of the solar cell parameters I_{sc}, P_{max} and V_{oc}. As in the case of the trapped proton evaluations, the major equivalent fluence contributions occur in a few lower energy increments. For cover glass shielding of 0.0335 gm/cm^2 (0.006 in fused silica), an equivalent fluence of 3.14E13 equivalent 1 MeV electrons/cm^2-yr is determined by these rough methods. A detailed machine calculation of this value indicates 1.99E13 equivalent 1 MeV electrons/cm^2-yr. Although this fluence is large enough to produce significant solar cell degradation, if considered separately, it is only one-thousandth of the previously calculated trapped proton equivalent fluence contribution for this orbit. On this basis, it is reasonable to ignore the trapped electron contribution to equivalent fluence in this orbit [4650 km (2500 n mi), 90°].

Table 6.3. Manual Calculation of Equivalent Fluence (Trapped Protons) (I_{sc})
Circular Orbit 835 km (450 n mi) 90 Degree Inclination

Energy Increment E_1 (MeV)	E_2 (MeV)	Integral Energy Spectrum $\Phi(>E_1)$ (p/cm^2-day)	Difference Spectrum $\Phi(>E_1)-\Phi(>E_2)$ (p/cm^2-day)	Shielding Thickness 0.0335 gm/cm^2 D(E,6)	Shielding Thickness 0.0335 gm/cm^2 Equiv. Fluence (p/cm^2-day)	Shielding Thickness 0.0671 gm/cm^2 D(E,12)	Shielding Thickness 0.0671 gm/cm^2 Equiv. Fluence (p/cm^2-day)	Shielding Thickness 0.1675 gm/cm^2 D(E,30)	Shielding Thickness 0.1675 gm/cm^2 Equiv. Fluence (p/cm^2-day)
4	6	6.96E7	2.72E7	4.75E-1	1.290E7				
6	8	4.24E7	1.12E7	5.55E-1	0.622E7	3.60E-1	0.403E7		
8	10	3.12E7	0.61E7	4.65E-1	.284E7	4.47E-1	0.273E7		
10	15	2.51E7	0.77E7	3.85E-1	.296E7	3.80E-1	0.292E7	2.95E-1	0.227E7
15	20	1.74E7	0.37E7	3.85E-1	.142E7	3.65E-1	0.135E7	3.17E-1	0.117E7
20	30	1.37E7	0.37E7	3.84E-1	.142E7	3.75E-1	0.139E7	3.45E-1	0.128E7
30	50	1.00E7	1.89E6	3.50E-1	.061E7	3.50E-1	0.066E7	3.40E-1	0.064E7
50	70	8.11E6	1.37E6	3.00E-1	.041E7	3.00E-1	0.041E7	3.00E-1	0.041E7
70	100	6.74E6	1.62E6	2.35E-1	.038E7	2.35E-1	0.038E7	2.35E-1	0.038E7
100	150	5.12E6	1.84E6	1.50E-1	.028E7	1.50E-1	0.028E7	1.50E-1	0.028E7
150		3.28E6							
Equivalent 10 MeV protons/cm^2-day					2.944E7		1.415E7		.643E7
days/year					x 365		x 365		x 365
Equivalent 10 MeV protons/cm^2-year					1.07E10		5.16E9		2.34E9
Equivalent 1 MeV electrons/10 MeV proton					x 3E3		x 3E3		x 3E3
Equivalent 1 MeV electrons/cm^2-year					3.21E13		1.55E13		7.03E12
Equivalent 1 MeV electron fluence, I_{sc} (Machine Calculation) e/cm^2-yr					2.71E13		1.43E13		6.73E12

Table 6.4 Manual Calculation of Equivalent Fluence (Trapped Protons) (I_{sc})
Circular Orbit 4650 km (2500 n mi), 90 Degree Inclination

Energy Increment E_1	E_2 (MeV)	Integral Energy Spectrum* $\phi(>E_1)$ (p/cm^2-day)	Difference Spectrum $\phi(>E_1)-\phi(>E_2)$ (p/cm^2-day)	Shielding Thickness 0.0335 gm/cm^2 D(E,6)	Equiv. Fluence (p/cm^2-day)	Shielding Thickness 0.0671 gm/cm^2 D(E,12)	Equiv. Fluence (p/cm^2-day)	Shielding Thickness 0.1675 gm/cm^2 D(E,30)	Equiv. Fluence (p/cm^2-day)
4	6	5.10E10	3.320E10	4.75E-1	1.580E10				
6	8	1.78E10	.835E10	5.55E-1	.464E10	3.60E-1	.300E10		
8	10	8.45E9	.370E10	4.65E-1	.172E10	4.47E-1	.166E10		
10	15	4.75E9	.308E10	3.85E-1	.119E10	3.80E-1	.117E10	2.95E-1	.091E10
15	20	1.75E9	.087E10	3.85E-1	.034E10	3.65E-1	.032E10	3.17E-1	.028E10
20	30	7.98E8	.0515E10	3.84E-1	.020E10	3.75E-1	.019E10	3.45E-1	.018E10
30	50	2.83E8	.0059E10	3.50E-1	.002E10	3.50E-1	.002E10	3.40E-1	.002E10
50	70	2.24E8	.0050E10	3.00E-1	.002E10	3.00E-1	.002E10	3.00E-1	.002E10
70	100	1.74E8	.0055E10	2.35E-1	.001E10	2.35E-1	.001E10	2.35E-1	.001E10
100	150	1.19E8	.0055E10	1.50E-1	.001E10	1.50E-1	.001E10	1.50E-1	.001E10
150		6.37E7							

Equivalent 10 MeV protons/cm^2-day	2.395E10	.640E10	.143E10
days/year	x365	x365	x365
Equivalent 10 MeV protons/cm^2-year	8.72E12	2.34E12	5.22E11
Equivalent 1 MeV electrons/10 MeV proton	x3E3	x3E3	x 3E3
Equivalent 1 MeV electrons/cm^2-year	2.62E16	7.00E15	1.56E15
Equivalent 1 MeV electrons, I_{sc} (Machine Calculation) e/cm^2-yr	1.84E16	5.82E15	1.16E15

*References 6.2, 6.3

Table 6.5 Manual Calculation of Equivalent Fluence (Trapped Protons) (P_{max}, V_{oc})
Circular Orbit 4650 km (2500 n mi), 90 Degree Inclination

Energy Increment E_1	E_2 (MeV)	Integral Energy Spectrum* $\phi(>E_1)$ (p/cm^2-day)	Difference Spectrum $\phi(>E_1)-\phi(>E_2)$ (p/cm^2-day)	Shielding Thickness 0.0335 gm/cm^2 D(E,6)	Shielding Thickness 0.0335 gm/cm^2 Equiv. Fluence (p/cm^2-day)	Shielding Thickness 0.0671 gm/cm^2 D(E,12)	Shielding Thickness 0.0671 gm/cm^2 Equiv. Fluence (p/cm^2-day)	Shielding Thickness 0.1675 gm/cm^2 D(E,30)	Shielding Thickness 0.1675 gm/cm^2 Equiv. Fluence (p/cm^2-day)
4	6	5.10E10	3.32E10	1.25E0	4.150E10				
6	8	1.78E10	0.835E10	1.27E0	1.060E10	9.80E-1	0.820E10		
8	10	8.45E9	0.370E10	8.27E-1	0.305E10	9.53E-1	0.352E10		
10	15	4.75E9	0.308E10	5.23E-1	0.161E10	5.70E-1	0.176E10	6.30E-1	0.194E10
15	20	1.67E9	0.087E10	4.37E-1	0.038E10	4.35E-1	0.038E10	4.30E-1	0.037E10
20	30	7.98E8	0.0515E10	4.00E-1	0.021E10	4.00E-1	0.021E10	3.86E-1	0.020E10
30	50	2.83E8	0.0059E10	3.63E-1	0.002E10	3.55E-1	0.002E10	3.50E-1	0.002E10
50	70	2.24E8	0.0050E10	3.00E-1	0.002E10	3.00E-1	0.002E10	3.00E-1	0.002E10
70	100	1.74E8	0.0055E10	2.35E-1	0.001E10	2.35E-1	0.001E10	2.35E-1	0.001E10
100	150	1.19E8	0.0055E10	1.50E-1	0.001E10	1.50E-1	0.001E10	1.50E-1	0.001E10
150		6.37E7							
Equivalent 10 MeV protons/cm^2-day					5.741E10		1.413E10		2.57E9
days/year					x365		x365		x365
Equivalent 10 MeV protons/cm^2-year					2.09E13		5.16E12		9.38E13
Equivalent 1 MeV electrons/10 MeV proton					x3E3		x3E3		x3E3
Equivalent 1 MeV electrons/cm^2-year					6.27E16		1.55E16		2.82E15
Equivalent 1 MeV electron fluence, P_{max},V_{oc}, (Machine Calculation) e/cm^2-year					4.35E16		1.27E16		2.09E15

*References 6.2, 6.3

Table 6.6. Manual Calculation of Equivalent Fluence (Trapped Electrons) *Circular Orbit 4650 km (2500 n mi), 90 Degree Inclination*

Energy Increment E_1 (MeV)	E_2 (MeV)	Integral Energy Spectrum* $\Phi(>E_1)$ (e/cm^2-day)	Difference Spectrum $\Phi(>E_1)-\Phi(>E_2)$ (e/cm^2-day)	Shielding Thickness 0.0335 gm/cm^2 D(E,6)	Shielding Thickness 0.0335 gm/cm^2 Equiv. Fluence (e/cm^2-day)	Shielding Thickness 0.0671 gm/cm^2 D(E,12)	Shielding Thickness 0.0671 gm/cm^2 Equiv. Fluence (e/cm^2-day)	Shielding Thickness 0.1675 gm/cm^2 D(E,30)	Shielding Thickness 0.1675 gm/cm^2 Equiv. Fluence (e/cm^2-day)
.05	.25	.714E13	55.3E11	1.0E-4	.055E10				
.25	.50	.161E13	14.4E11	3.0E-2	4.330E10	1.0E-2	1.4400E10		
.50	.75	.170E12	1.307E11	1.3E-1	1.690E10	8.3E-2	1.0848E10		
.75	1.00	.493E11	.251E11	2.6E-1	0.659E10	1.9E-1	.4770E10		
1.00	1.25	.242E11	.102E11	4.5E-1	0.459E10	3.5E-1	.3580E10	1.9E-1	0.194E10
1.25	1.50	.140E11	.0556E11	6.5E-1	0.361E10	5.4E-1	.300E10	3.2E-1	0.178E10
1.50	1.75	.844E10	.0329E11	8.8E-1	0.289E10	7.5E-1	.247E10	5.0E-1	0.165E10
1.75	2.00	.515E10	.0195E11	1.1E0	0.214E10	9.6E-1	.187E10	6.8E-1	0.133E10
2.00	2.25	.320E10	.0127E11	1.4E0	0.178E10	1.2E0	.152E10	9.0E-1	0.114E10
2.25	2.50	.193E10	.0076E11	1.6E0	0.122E10	1.4E0	.106E10	1.1E0	0.084E10
2.50	2.75	.117E10	.0050E11	1.9E0	0.095E10	1.7E0	.08540	1.3E0	0.065E10
2.75	3.00	.667E9	.0028E11	2.1E0	0.059E10	1.9E0	.053E10	1.5E0	0.042E10
3.00	3.25	.384E9	.0022E11	2.4E0	0.053E10	2.2E0	.048E10	1.7E0	0.037E10
3.25	3.50	.166E9	.0009E11	2.6E0	0.023E10	2.4E0	.021E10	2.0E0	0.018E10
3.50	3.75	.742E8	.0005E11	2.8E0	.014E10	2.6E0	.013E10	2.2E0	0.011E10
3.75	4.00	.259E8	.0002E11	3.1E0	.006E10	2.8E0	.006E10	2.4E0	0.005E10
4.00	4.25	.911E7	.0001E11	3.3E0	.003E10	3.2E0	.003E10	2.7E0	0.003E10
4.25	4.50	.190E7							
4.50	4.75	.340E6							
4.75	5.00								
5.00									
Equivalent 1 MeV electrons/cm^2-day					8.60E10		4.581E10		1.049E10
days/year					x 365		x 365		x 365
Equivalent 1 MeV electron fluence (Manual Calculation) e/cm^2-yr					3.14E13		1.67E13		3.82E12
Equivalent 1 MeV electron fluence (Machine Calculation) e/cm^2-yr					1.99E13		9.77E12		3.14E12

*Reference 6.5

At altitudes greater than 4650 km, the trapped proton contribution to the equivalent fluence decreases rapidly and the trapped electron contribution becomes more significant. At synchronous or geostationary altitude, the trapped proton contribution can be neglected. An example of a rough calculation of equivalent fluence for three different shielding materials for synchronous (35,900 km, 19400 n mi) altitude and 0° inclination is shown in Table 6.7. The rough calculated equivalent 1 MeV electron fluence for cells with 0.0335 gm/cm^2 of shielding is 4.17E13 e/cm^2-yr. Detailed machine calculations of this quantity indicate 2.54E13 equivalent 1 MeV electrons/cm^2-yr. The reason for the higher value found by the rough manual calculation is again related to the size of energy increments in the lower energy range and the rapidly changing values of D(E,t) in these ranges.

The calculation of absorbed dose in shielding materials is very similar in outline to the equivalent fluence calculation. This procedure is described mathematically in equation (6.2.1). In Table 6.8 a rough calculation of cover material dose is shown for three different depths in a fused silica cover glass. The rough calculated absorbed doses are quite close to the values calculated by detailed machine methods. The same procedure can be used for calculation of the absorbed dose deposited by trapped protons. The I(E,t) values in Figures 4.2 and 4.5 and Tables 4.2 and 4.5 may be used for this purpose. Although the dose contributed by trapped protons is often very high in the surface layers of shielding, this is usually not a significant contribution to the average absorbed dose in the shielding.

6.4 Computer Calculated Equivalent Fluence

The aforementioned rough calculations can be improved in accuracy and speed with the aid of computer processing. Although the quantity computed is exactly the same as before, the selection of difference flux and the corresponding damage coefficient can be programmed to achieve higher accuracy and more consistent results. The increased accuracy of calculated fluence is achieved mainly by use of finer energy increments for a given environment.

Table 6.7. Manual Calculation of Equivalent Fluence (Trapped Electrons) Circular Orbit 35,900 km (19,400 n mi), 0 Degree Inclination

Energy Increment E_1 (MeV)	E_2 (MeV)	Integral Energy Spectrum* $\Phi(>E_1)$ (e/cm^2-day)	Difference Spectrum $\Phi(>E_1)-\Phi(>E_2)$ (e/cm^2-day)	Shielding Thickness 0.0335 gm/cm^2 D(E,6)	Shielding Thickness 0.0335 gm/cm^2 Equiv. Fluence (e/cm^2-day)	Shielding Thickness 0.0671 gm/cm^2 D(E,12)	Shielding Thickness 0.0671 gm/cm^2 Equiv. Fluence (e/cm^2-day)	Shielding Thickness 0.1675 gm/cm^2 D(E,30)	Shielding Thickness 0.1675 gm/cm^2 Equiv. Fluence (e/cm^2-day)
.05	.25	3.97E12	25.90E11	1.0E-4	.0259E10				
.25	.50	1.38E12	9.60E11	3.0E-2	2.880E10	1.0E-2	0.960E10		
.50	.75	4.20E11	2.90E11	1.3E-1	3.770E10	8.3E-2	2.410E10		
.75	1.00	1.30E11	.902E11	2.6E-1	2.34E10	1.9E-1	1.710E10		
1.00	1.25	3.98E10	.274E11	4.5E-1	1.23E10	3.5E-1	0.960E10	1.9E-1	0.521E10
1.25	1.50	1.24E10	.0868E11	6.5E-1	.564E10	5.4E-1	0.304E10	3.2E-1	0.278E10
1.50	1.75	3.82E9	.0260E11	8.8E-1	.185E10	7.5E-1	.195E10	5.0E-1	0.130E10
1.75	2.00	1.22E9	.0085E11	1.1E0	.094E10	9.6E-1	.082E10	6.8E-1	0.058E10
2.00	2.25	3.69E8	.0025E11	1.4E0	.035E10	1.2E0	.030E10	9.0E-1	0.022E10
2.25	2.50	1.19E8	.0008E11	1.6E0	.014E10	1.4E0	.011E10	1.1E0	0.009E10
2.50	2.75	3.65E7	.0003E11	1.9E0	.006E10	1.7E0	.005E10	1.3E0	0.004E10
2.75	3.00	1.13E7	.0001E1	2.1E0	.002E10	1.9E0	.002E10	1.5E0	0.002E10
3.00	3.25	3.46E6		2.4E0		2.2E0		1.7E0	
3.25	3.50	1.36E6		2.6E0		2.4E0		2.0E0	
3.50	3.75	3.80E5		2.8E0		2.6E0		2.2E0	
3.75	4.00	8.45E4		3.1E0		2.8E0		2.4E0	
4.00	4.25	3.28E4		3.3E0		3.2E0		2.7E0	
Equivalent 1 MeV electrons/cm^2-day					11.145E10		6.669E10		1.024E10
days/year					x 365		x 365		x 365
Equivalent 1 MeV electrons/cm^2-year					4.17E13		2.44E13		3.74E12
Equivalent 1 MeV electron (Machine Calculation) e/cm^2-yr					2.54E13		1.35E13		2.81E12

*Reference 6.4

Table 6.8. Manual Calculation of Absorbed Dose (Trapped Electrons)
Circular Orbit 35,900 km (19,400 n mi), 0 Degree Inclination

Energy Increment E_1 (MeV)	E_2 (MeV)	Integral Energy Spectrum* $\Phi(>E_1)$ (e/cm^2-day)	Difference Spectrum $\Phi(>E_1)-\Phi(>E_2)$ (e/cm^2-day)	Depth in Shield 0.0055 gm/cm^2 I(E,1)	Depth in Shield 0.0055 gm/cm^2 Absorbed Dose (rad/day)	Depth in Shield 0.0168 gm/cm^2 I(E,3)	Depth in Shield 0.0168 gm/cm^2 Absorbed Dose (rad/day)	Depth in Shield 0.0335 gm/cm^2 I(E,6)	Depth in Shield 0.0335 gm/cm^2 Absorbed Dose (rad/day)
.05	.25	3.97E12	25.90E11	2.40E-8	6.22E4	1.90E-8	4.93E4	2.0E-9	.518E4
.25	.50	1.38E12	9.60E11	1.44E-8	1.39E4	1.42E-8	1.36E4	1.34E-8	1.29E4
.50	.75	4.20E11	2.90E11	1.26E-8	0.365E4	1.24E-8	0.360E4	1.21E-8	0.351E4
.75	1.00	1.30E11	.902E11	1.22E-8	0.110E4	1.20E-8	0.108E4	1.17E-8	0.106E4
1.00	1.25	3.98E10	.274E11	1.21E-8	0.033E4	1.19E-8	0.033E4	1.16E-8	0.032E4
1.25	1.50	1.24E10	.0868E11	1.21E-8	0.015E4	1.19E-8	0.012E4	1.16E-8	0.010E4
1.50	1.75	3.82E9	.0260E11	1.21E-8	0.093E4	1.19E-8	0.003E4	1.16E-8	0.003E4
1.75	2.00	1.22E9	.0085E11	1.21E-8	0.001E4	1.19E-8	0.001E4	1.16E-8	0.001E4
2.00	2.25	3.69E8	.0025E11	1.22E-8	0.000E4	1.21E-8	0.000E4	1.18E-8	0.000E4
2.25	2.50	1.19E8	.0008E11	1.23E-8		1.22E-8		1.19E-8	
2.50	2.75	3.65E7	.0003E11	1.23E-8		1.22E-8		1.20E-8	
2.75	3.00	1.13E7	.0001E11	1.24E-8		1.23E-8		1.21E-8	
3.00		3.46E6							
					8.137E4		6.807E4		2.31E4
					x 365		x 365		x 365
Absorbed Dose, Rad/yr (Manual Calculation)					2.97E7		2.48E7		8.45E6

*Reference 6.4

For circular orbits around the earth, Vette, et al.[6.1-6.9] have time integrated both electron and proton environments for convenient energy ranges, various altitudes, and for inclinations of 0°, 30°, and 90°. The average daily fluences are tabulated in references 6.1 through 6.9. Electron environment is taken from reference 6.5 in which both inner zone (AE-5) and outer zone (AE-4) electron models are integrated and tabulated.

For the trapped proton environment, three maps are utilized: AP5 (reference 6.1) for the energies from 0.4 to 4 MeV, AP6 (reference 6.2) for the energies from 4 to 30 MeV, and AP7 (reference 6.3) for the energies greater than 50 MeV. For a given altitude and inclination, an integral spectrum of the AP7 was extrapolated back to 30 MeV and the intensity was normalized to the AP6 in order to eliminate a discontinuity there. Similarly, the intensity at 4 MeV from the AP5 was normalized to that of the AP6. The AP1 data (reference 6.8) for the energies from 30 to 50 MeV was not utilized because it is obsolete data, with the spectrum not readily available and the energy interval covered being too small on a logarithmic scale to add any significant information.

Although lower energy proton fluxes are more damaging than higher energy proton fluxes, most of the low energy component described in the AP5 (reference 6.3) is eliminated by the cover glass. Thus, the most important portion of the energy spectrum from the standpoint of solar cell damage is in the neighborhood of a few MeV, and hence, a normalization to the AP6 is of physical and practical significance.

The assessment of solar-flare proton effects is complicated by several problems. They are:

a. The unpredictable nature of future solar flare proton fluxes and energy spectrums.

b. The undefinable nature of geomagnetic cutoff energy during a flare event, and hence, the evaluation of the near earth flare environment.

c. The uncertainty in the isotropy of flare fluxes.

A few assumptions and limitations must be imposed on the calculation of equivalent fluence to overcome the above problems. As for the first problem, the equivalent fluence is calculated from two alternate methods of estimating the flare environment. The first estimated future flare environment is based on reference 6.9 and is commonly used in connection with many military satellite systems. An alternate environment estimate is determined from a recently developed model. Thus, the reader can have a choice of selecting an appropriate environment to fit the circumstances on hand. The environment in reference 6.9 leads to a worst case degradation estimate, whereas that described by the proposed model is a probable estimate.

The magnetic cutoff energy varies with both altitude and latitude even during quiescent periods, and hence becomes time dependent for spacecraft moving with respect to the earth. Further complications are caused by the plasma disturbance and magnetic field regime sweeping through the earth, the magnitude of which depends in part on the size and location of flares on the solar disk. Therefore, it is impossible to generalize all these conditions; however, there are two (2) distinct cases in which certain assumptions are valid as previously discussed:

a. at high altitude and latitude, the geomagnetic field makes almost negligible contribution to the cutoff phenomena during the storm, and

b. at very low altitude and latitude, the Störmer's cutoff approximation may prevail.

The damage coefficient for omnidirectional flux is exclusively utilized with the following understanding:

a. If the solar flare proton flux is omnidirectional throughout the event, the equivalent fluence computed with use of the omnidirectional damage coefficient described in section 4.0 will not result in any error due to the directionality of proton flux.

b. If the flux is unidirectional throughout the event, though such an event is very rare, the computed equivalent fluence will be in error by a factor of two.

Therefore, the uncertainty in flux directionality can be removed by the use of omnidirectional damage coefficient with the provision that the estimate can be very reasonable for most of the events with a very small probability of a factor of two underestimate.

The annual equivalent fluences thus calculated by computer are tabulated in Tables 6.9 through 6.30. The contents of these tables are summarized in Table 6.31 to assist the readers in finding a table for appropriate environments and parameters.

The damage produced by back radiation is, for the first order assumption, regarded as the same in nature and magnitude as that produced by the front radiation. In this context, an equivalent fluence attributable to the back radiation can be added to the front contribution by estimating an effective shield thickness of back shielding. This bold assumption is not valid when higher order effects are considered. If a composite back shielding material is similar to the front cover glass, a correction factor for a stopping power due to atomic number Z is small (proportional to Z) and only a density correction is required for the estimate. This is done by shifting a curve of equivalent fluence vs. cover glass thickness by a density factor. If the Z is vastly different, the equivalent fluence should be recomputed based on effective damage coefficient for the new shielding material.

6.5 Solar Array Degradation

The process of calculating equivalent 1 MeV electron fluence reduces the space radiation environment to a laboratory electron environment for which solar cell degradation has been evaluated. When the damage equivalent fluence is known, the estimation of solar array degradation can be completed. Up to this stage in the process of estimation of array degradation, the variables of base resistivity and cell thickness have not entered into the calculation.

The necessary solar cell data and the equivalent fluence value allow the estimation of solar cell output parameters through use of the data in Figures 3.7 through 3.14.

EQUIV. 1 MEV ELECTRON FLUENCE FOR JSC - CIRCULAR ORBIT, INC = 0 DEGREE
DUE TO GEOMAG TRAPPED ELECTRONS, REF. AE4 AND AE5.

ALTITUDE		SHIELD THICKNESS, GM/CM2						
(N.M.)	(KM)	0.	1.68E-02	3.35E-02	6.71E-02	1.12E-01	1.68E-01	3.35E-01
1.50E+02	2.78E+02	0.	0.	0.	0.	0.	0.	0.
3.00E+02	5.56E+02	1.23E+08	1.09E+08	1.01E+08	8.78E+07	7.53E+07	6.37E+07	4.12E+07
4.50E+02	8.33E+02	3.54E+10	2.87E+10	2.50E+10	2.01E+10	1.59E+10	1.24E+10	6.67E+09
6.00E+02	1.11E+03	3.04E+12	2.42E+12	2.08E+12	1.64E+12	1.28E+12	9.78E+11	5.11E+11
8.00E+02	1.48E+03	5.05E+13	3.99E+13	3.43E+13	2.70E+13	2.09E+13	1.60E+13	8.34E+12
1.00E+03	1.85E+03	1.62E+14	1.27E+14	1.09E+14	8.48E+13	6.54E+13	4.99E+13	2.60E+13
1.25E+03	2.31E+03	3.09E+14	2.35E+14	1.99E+14	1.53E+14	1.17E+14	8.88E+13	4.62E+13
1.50E+03	2.78E+03	3.60E+14	2.60E+14	2.14E+14	1.60E+14	1.20E+14	9.03E+13	4.68E+13
1.75E+03	3.24E+03	3.41E+14	2.26E+14	1.79E+14	1.26E+14	9.12E+13	6.76E+13	3.48E+13
2.00E+03	3.70E+03	3.09E+14	1.83E+14	1.35E+14	8.60E+13	5.84E+13	4.20E+13	2.13E+13
2.25E+03	4.17E+03	2.93E+14	1.54E+14	1.05E+14	5.78E+13	3.52E+13	2.36E+13	1.15E+13
2.50E+03	4.63E+03	2.85E+14	1.39E+14	8.86E+13	4.23E+13	2.21E+13	1.33E+13	6.04E+12
2.75E+03	5.09E+03	2.71E+14	1.27E+14	7.76E+13	3.32E+13	1.45E+13	7.16E+12	3.02E+12
3.00E+03	5.56E+03	2.45E+14	1.11E+14	6.67E+13	2.68E+13	1.03E+13	4.13E+12	1.64E+12
3.50E+03	6.48E+03	1.83E+14	7.85E+13	4.56E+13	1.71E+13	5.67E+12	1.73E+12	6.25E+11
4.00E+03	7.41E+03	1.38E+14	5.64E+13	3.22E+13	1.17E+13	3.72E+12	1.03E+12	3.55E+11
4.50E+03	8.33E+03	1.09E+14	4.44E+13	2.58E+13	1.00E+13	3.46E+12	1.08E+12	3.66E+11
5.00E+03	9.26E+03	7.70E+13	3.38E+13	2.10E+13	9.57E+12	4.15E+12	1.83E+12	6.85E+11
5.50E+03	1.02E+04	5.54E+13	2.84E+13	1.98E+13	1.15E+13	6.72E+12	4.10E+12	1.81E+12
6.00E+03	1.11E+04	4.87E+13	3.02E+13	2.37E+13	1.66E+13	1.17E+13	8.40E+12	4.22E+12
7.00E+03	1.30E+04	6.46E+13	4.70E+13	3.90E+13	2.92E+13	2.18E+13	1.63E+13	8.53E+12
8.00E+03	1.48E+04	8.94E+13	6.58E+13	5.50E+13	4.18E+13	3.15E+13	2.38E+13	1.26E+13
9.00E+03	1.67E+04	1.24E+14	9.21E+13	7.69E+13	5.84E+13	4.41E+13	3.33E+13	1.79E+13
1.00E+04	1.85E+04	1.58E+14	1.19E+14	9.87E+13	7.39E+13	5.46E+13	4.03E+13	2.07E+13
1.10E+04	2.04E+04	1.72E+14	1.30E+14	1.08E+14	8.07E+13	5.91E+13	4.27E+13	2.10E+13
1.20E+04	2.22E+04	1.75E+14	1.31E+14	1.09E+14	8.12E+13	5.88E+13	4.20E+13	1.99E+13
1.30E+04	2.41E+04	1.56E+14	1.16E+14	9.56E+13	7.01E+13	5.00E+13	3.51E+13	1.61E+13
1.40E+04	2.59E+04	1.37E+14	1.01E+14	8.26E+13	5.98E+13	4.21E+13	2.91E+13	1.30E+13
1.50E+04	2.78E+04	1.19E+14	8.62E+13	7.02E+13	5.03E+13	3.50E+13	2.39E+13	1.05E+13
1.60E+04	2.96E+04	9.58E+13	6.75E+13	5.40E+13	3.77E+13	2.56E+13	1.71E+13	7.37E+12
1.70E+04	3.15E+04	7.62E+13	5.18E+13	4.07E+13	2.75E+13	1.81E+13	1.18E+13	4.99E+12
1.80E+04	3.33E+04	6.04E+13	3.97E+13	3.06E+13	2.03E+13	1.31E+13	8.35E+12	3.44E+12
1.94E+04	3.59E+04	6.35E+13	3.67E+13	2.55E+13	1.35E+13	6.46E+12	2.81E+12	8.61E+11

Table 6.9. Annual Equivalent 1 MeV Electron Fluence Due to Trapped Electrons, Circular Orbits, Inclination 0 Degree , Infinite Backshielding Assumed

EQUIV. 1 MEV ELECTRON FLUENCE FOR JSC - CIRCULAR ORIBT, INC = 30 DEGREE
DUE TO GEOMAG TRAPPED ELECTRONS, REF. AE4 AND AE5.

ALTITUDE		SHIELD THICKNESS, GM/CM2						
(N.M.)	(KM)	0.	1.68E-02	3.35E-02	6.71E-02	1.12E-01	1.68E-01	3.35E-01
1.50E+02	2.78E+02	6.96E+08	5.33E+08	4.53E+08	3.54E+08	2.74E+08	2.10E+08	1.12E+08
3.00E+02	5.56E+02	2.17E+11	1.53E+11	1.26E+11	9.50E+10	7.18E+10	5.43E+10	2.83E+10
4.50E+02	8.33E+02	2.03E+12	1.50E+12	1.26E+12	9.61E+11	7.33E+11	5.57E+11	2.90E+11
6.00E+02	1.11E+03	9.24E+12	6.98E+12	5.90E+12	4.55E+12	3.48E+12	2.65E+12	1.38E+12
8.00E+02	1.48E+03	3.66E+13	2.76E+13	2.33E+13	1.80E+13	1.38E+13	1.05E+13	5.45E+12
1.00E+03	1.85E+03	8.82E+13	6.59E+13	5.54E+13	4.24E+13	3.23E+13	2.45E+13	1.28E+13
1.25E+03	2.31E+03	1.49E+14	1.07E+14	8.89E+13	6.67E+13	5.03E+13	3.79E+13	1.97E+13
1.50E+03	2.78E+03	1.65E+14	1.11E+14	8.88E+13	6.39E+13	4.69E+13	3.49E+13	1.80E+13
1.75E+03	3.24E+03	1.61E+14	9.84E+13	7.46E+13	4.99E+13	3.49E+13	2.55E+13	1.30E+13
2.00E+03	3.70E+03	1.52E+14	8.33E+13	5.91E+13	3.55E+13	2.31E+13	1.62E+13	8.13E+12
2.25E+03	4.17E+03	1.44E+14	7.18E+13	4.73E+13	2.45E+13	1.40E+13	9.04E+12	4.35E+12
2.50E+03	4.63E+03	1.37E+14	6.40E+13	4.00E+13	1.84E+13	9.10E+12	5.18E+12	2.34E+12
2.75E+03	5.09E+03	1.28E+14	5.75E+13	3.48E+13	1.46E+13	6.17E+12	2.92E+12	1.23E+12
3.00E+03	5.56E+03	1.14E+14	5.01E+13	2.98E+13	1.20E+13	4.65E+12	1.93E+12	7.90E+11
3.50E+03	6.48E+03	8.74E+13	3.73E+13	2.20E+13	8.90E+12	3.49E+12	1.49E+12	6.50E+11
4.00E+03	7.41E+03	6.86E+13	2.97E+13	1.81E+13	8.12E+12	3.77E+12	1.99E+12	9.44E+11
4.50E+03	8.33E+03	5.67E+13	2.68E+13	1.76E+13	9.35E+12	5.21E+12	3.21E+12	1.57E+12
5.00E+03	9.26E+03	4.81E+13	2.64E+13	1.91E+13	1.19E+13	7.69E+12	5.21E+12	2.60E+12
5.50E+03	1.02E+04	4.66E+13	2.96E+13	2.32E+13	1.62E+13	1.14E+13	8.15E+12	4.13E+12
6.00E+03	1.11E+04	5.16E+13	3.59E+13	2.93E+13	2.16E+13	1.58E+13	1.16E+13	6.00E+12
7.00E+03	1.30E+04	7.05E+13	5.21E+13	4.33E+13	3.26E+13	2.43E+13	1.81E+13	9.37E+12
8.00E+03	1.48E+04	9.12E+13	6.77E+13	5.64E+13	4.25E+13	3.16E+13	2.35E+13	1.22E+13
9.00E+03	1.67E+04	1.11E+14	8.25E+13	6.86E+13	5.13E+13	3.80E+13	2.80E+13	1.43E+13
1.00E+04	1.85E+04	1.17E+14	8.78E+13	7.28E+13	5.41E+13	3.95E+13	2.86E+13	1.41E+13
1.10E+04	2.04E+04	1.19E+14	8.89E+13	7.37E+13	5.44E+13	3.93E+13	2.80E+13	1.34E+13
1.20E+04	2.22E+04	1.09E+14	8.08E+13	6.66E+13	4.88E+13	3.48E+13	2.45E+13	1.13E+13
1.30E+04	2.41E+04	9.51E+13	6.95E+13	5.69E+13	4.11E+13	2.90E+13	2.01E+13	9.06E+12
1.40E+04	2.59E+04	7.95E+13	5.71E+13	4.62E+13	3.30E+13	2.29E+13	1.56E+13	6.88E+12
1.50E+04	2.78E+04	6.54E+13	4.60E+13	3.69E+13	2.58E+13	1.76E+13	1.18E+13	5.13E+12
1.60E+04	2.96E+04	5.15E+13	3.50E+13	2.76E+13	1.88E+13	1.25E+13	8.23E+12	3.50E+12
1.70E+04	3.15E+04	3.99E+13	2.61E+13	2.02E+13	1.34E+13	8.64E+12	5.53E+12	2.31E+12
1.80E+04	3.33E+04	3.03E+13	1.90E+13	1.43E+13	9.20E+12	5.77E+12	3.61E+12	1.47E+12

Table 6.10. Annual Equivalent 1 MeV Electron Fluence Due to Trapped Electrons, Circular Orbits, Inclination 30 Degree, Infinite Backshielding Assumed

EQUIV. 1 MEV ELECTRON FLUENCE FOR JSC - CIRCULAR ORBIT, INC = 60 DEGREE
DUE TO GEOMAG TRAPPED ELECTRONS, REF. AE4 AND AE5.

ALTITUDE		SHIELD THICKNESS, GM/CM2						
(N.M.)	(KM)	0.	1.68E-02	3.35E-02	6.71E-02	1.12E-01	1.68E-01	3.35E-01
1.50E+02	2.78E+02	1.67E+11	1.21E+11	1.00E+11	7.45E+10	5.49E+10	4.03E+10	2.05E+10
3.00E+02	5.56E+02	4.57E+11	3.18E+11	2.59E+11	1.91E+11	1.41E+11	1.04E+11	5.31E+10
4.50E+02	8.33E+02	1.47E+12	1.04E+12	8.56E+11	6.41E+11	4.79E+11	3.59E+11	1.85E+11
6.00E+02	1.11E+03	4.98E+12	3.68E+12	3.08E+12	2.35E+12	1.79E+12	1.35E+12	7.02E+11
8.00E+02	1.48E+03	1.93E+13	1.45E+13	1.22E+13	9.39E+12	7.17E+12	5.45E+12	2.83E+12
1.00E+03	1.85E+03	4.70E+13	3.51E+13	2.95E+13	2.26E+13	1.72E+13	1.31E+13	6.79E+12
1.25E+03	2.31E+03	7.89E+13	5.71E+13	4.73E+13	3.56E+13	2.68E+13	2.02E+13	1.05E+13
1.50E+03	2.78E+03	8.64E+13	5.87E+13	4.71E+13	3.41E+13	2.51E+13	1.87E+13	9.68E+12
1.75E+03	3.24E+03	8.59E+13	5.32E+13	4.07E+13	2.75E+13	1.94E+13	1.42E+13	7.27E+12
2.00E+03	3.70E+03	8.26E+13	4.64E+13	3.34E+13	2.05E+13	1.35E+13	9.53E+12	4.80E+12
2.25E+03	4.17E+03	7.85E+13	4.04E+13	2.73E+13	1.49E+13	8.93E+12	5.93E+12	2.88E+12
2.50E+03	4.63E+03	7.62E+13	3.73E+13	2.42E+13	1.21E+13	6.59E+12	4.05E+12	1.90E+12
2.75E+03	5.09E+03	7.23E+13	3.45E+13	2.19E+13	1.04E+13	5.24E+12	3.00E+12	1.38E+12
3.00E+03	5.56E+03	6.57E+13	3.10E+13	1.96E+13	9.29E+12	4.61E+12	2.59E+12	1.20E+12
3.50E+03	6.48E+03	5.22E+13	2.49E+13	1.62E+13	8.16E+12	4.39E+12	2.65E+12	1.27E+12
4.00E+03	7.41E+03	4.41E+13	2.18E+13	1.47E+13	8.11E+12	4.75E+12	3.05E+12	1.48E+12
4.50E+03	8.33E+03	3.85E+13	2.06E+13	1.46E+13	8.85E+12	5.57E+12	3.72E+12	1.82E+12
5.00E+03	9.26E+03	3.42E+13	2.04E+13	1.54E+13	1.02E+13	6.88E+12	4.77E+12	2.35E+12
5.50E+03	1.02E+04	3.30E+13	2.17E+13	1.72E+13	1.22E+13	8.60E+12	6.14E+12	3.05E+12
6.00E+03	1.11E+04	3.43E+13	2.41E+13	1.96E+13	1.44E+13	1.05E+13	7.63E+12	3.86E+12
7.00E+03	1.30E+04	4.23E+13	3.11E+13	2.57E+13	1.92E+13	1.42E+13	1.04E+13	5.32E+12
8.00E+03	1.48E+04	5.06E+13	3.73E+13	3.10E+13	2.32E+13	1.71E+13	1.26E+13	6.45E+12
9.00E+03	1.67E+04	5.81E+13	4.31E+13	3.57E+13	2.66E+13	1.96E+13	1.44E+13	7.29E+12
1.00E+04	1.85E+04	6.02E+13	4.47E+13	3.70E+13	2.74E+13	1.99E+13	1.44E+13	7.09E+12
1.10E+04	2.04E+04	5.95E+13	4.42E+13	3.65E+13	2.68E+13	1.93E+13	1.38E+13	6.55E+12
1.20E+04	2.22E+04	5.56E+13	4.10E+13	3.38E+13	2.47E+13	1.76E+13	1.24E+13	5.72E+12
1.30E+04	2.41E+04	4.83E+13	3.51E+13	2.87E+13	2.07E+13	1.46E+13	1.01E+13	4.56E+12
1.40E+04	2.59E+04	4.00E+13	2.86E+13	2.31E+13	1.65E+13	1.14E+13	7.79E+12	3.44E+12
1.50E+04	2.78E+04	3.31E+13	2.32E+13	1.86E+13	1.30E+13	8.90E+12	5.99E+12	2.59E+12
1.60E+04	2.96E+04	2.59E+13	1.76E+13	1.39E+13	9.48E+12	6.31E+12	4.16E+12	1.77E+12
1.70E+04	3.15E+04	2.01E+13	1.32E+13	1.02E+13	6.74E+12	4.36E+12	2.80E+12	1.17E+12
1.80E+04	3.33E+04	1.53E+13	9.61E+12	7.28E+12	4.69E+12	2.95E+12	1.85E+12	7.55E+11

Table 6.11. Annual Equivalent 1 MeV Electron Fluence Due to Trapped Electrons, Circular Orbits, Inclination 60 Degree, Infinite Backshielding Assumed

EQUIV. 1 MEV ELECTRON FLUENCE FOR JSC - CIRCULAR ORBIT, INC = 90 DEGREE
DUE TO GEOMAG TRAPPED ELECTRONS, REF. AE4 AND AE5.

ALTITUDE		SHIELD THICKNESS, GM/CM2						
(N.M.)	(KM)	0.	1.68E-02	3.35E-02	6.71E-02	1.12E-01	1.68E-01	3.35E-01
1.50E+02	2.78E+02	1.67E+11	1.21E+11	1.00E+11	7.41E+10	5.43E+10	3.96E+10	1.99E+10
3.00E+02	5.56E+02	4.12E+11	2.89E+11	2.36E+11	1.74E+11	1.27E+11	9.34E+10	4.73E+10
4.50E+02	8.33E+02	1.24E+12	8.83E+11	7.28E+11	5.44E+11	4.06E+11	3.03E+11	1.56E+11
6.00E+02	1.11E+03	4.25E+12	3.15E+12	2.64E+12	2.02E+12	1.53E+12	1.16E+12	6.01E+11
8.00E+02	1.48E+03	1.64E+13	1.24E+13	1.04E+13	8.02E+12	6.13E+12	4.65E+12	2.42E+12
1.00E+03	1.85E+03	4.02E+13	3.00E+13	2.52E+13	1.93E+13	1.47E+13	1.12E+13	5.80E+12
1.25E+03	2.31E+03	6.74E+13	4.88E+13	4.04E+13	3.04E+13	2.29E+13	1.73E+13	8.98E+12
1.50E+03	2.78E+03	7.36E+13	5.00E+13	4.02E+13	2.91E+13	2.14E+13	1.60E+13	8.26E+12
1.75E+03	3.24E+03	7.28E+13	4.51E+13	3.45E+13	2.33E+13	1.65E+13	1.20E+13	6.16E+12
2.00E+03	3.70E+03	6.96E+13	3.90E+13	2.80E+13	1.71E+13	1.13E+13	7.95E+12	4.00E+12
2.25E+03	4.17E+03	6.60E+13	3.38E+13	2.27E+13	1.23E+13	7.30E+12	4.82E+12	2.34E+12
2.50E+03	4.63E+03	6.40E+13	3.10E+13	1.99E+13	9.77E+12	5.19E+12	3.14E+12	1.46E+12
2.75E+03	5.09E+03	6.02E+13	2.83E+13	1.78E+13	8.20E+12	3.98E+12	2.20E+12	9.98E+11
3.00E+03	5.56E+03	5.46E+13	2.53E+13	1.58E+13	7.21E+12	3.41E+12	1.83E+12	8.37E+11
3.50E+03	6.48E+03	4.24E+13	1.97E+13	1.25E+13	6.04E+12	3.08E+12	1.78E+12	8.45E+11
4.00E+03	7.41E+03	3.55E+13	1.70E+13	1.12E+13	5.93E+12	3.35E+12	2.10E+12	1.02E+12
4.50E+03	8.33E+03	3.07E+13	1.59E+13	1.11E+13	6.56E+12	4.04E+12	2.67E+12	1.31E+12
5.00E+03	9.26E+03	2.67E+13	1.56E+13	1.17E+13	7.60E+12	5.06E+12	3.49E+12	1.72E+12
5.50E+03	1.02E+04	2.59E+13	1.69E+13	1.34E+13	9.41E+12	6.63E+12	4.73E+12	2.36E+12
6.00E+03	1.11E+04	2.72E+13	1.91E+13	1.55E+13	1.14E+13	8.31E+12	6.06E+12	3.08E+12
7.00E+03	1.30E+04	3.41E+13	2.51E+13	2.08E+13	1.55E+13	1.15E+13	8.47E+12	4.34E+12
8.00E+03	1.48E+04	4.16E+13	3.08E+13	2.56E+13	1.91E+13	1.42E+13	1.05E+13	5.36E+12
9.00E+03	1.67E+04	4.82E+13	3.58E+13	2.97E+13	2.21E+13	1.63E+13	1.20E+13	6.10E+12
1.00E+04	1.85E+04	5.07E+13	3.78E+13	3.13E+13	2.32E+13	1.69E+13	1.22E+13	6.02E+12
1.10E+04	2.04E+04	4.93E+13	3.67E+13	3.03E+13	2.23E+13	1.61E+13	1.15E+13	5.47E+12
1.20E+04	2.22E+04	4.70E+13	3.47E+13	2.86E+13	2.09E+13	1.49E+13	1.05E+13	4.86E+12
1.30E+04	2.41E+04	4.10E+13	2.98E+13	2.44E+13	1.76E+13	1.24E+13	8.58E+12	3.88E+12
1.40E+04	2.59E+04	3.39E+13	2.43E+13	1.97E+13	1.40E+13	9.72E+12	6.63E+12	2.93E+12
1.50E+04	2.78E+04	2.82E+13	1.98E+13	1.59E+13	1.11E+13	7.61E+12	5.12E+12	2.22E+12
1.60E+04	2.96E+04	2.21E+13	1.50E+13	1.18E+13	8.10E+12	5.39E+12	3.55E+12	1.51E+12
1.70E+04	3.15E+04	1.72E+13	1.12E+13	8.69E+12	5.77E+12	3.73E+12	2.40E+12	1.00E+12
1.80E+04	3.33E+04	1.31E+13	8.21E+12	6.22E+12	4.01E+12	2.52E+12	1.59E+12	6.47E+11

Table 6.12. Annual Equivalent 1 MeV Electron Fluence Due to Trapped Electrons, Circular Orbits, Inclination 90 Degree, Infinite Backshielding Assumed

EQUIV. 1 MEV ELECTRON FLUENCE FOR JSC - CIRCULAR ORBIT, INC = 0 DEGREE
DUE TO GEOMAG TRAPPED PROTONS, REF. AP5, AP6, AND AP7.

ALTITUDE		SHIELD THICKNESS, GM/CM2						
(N.M.)	(KM)	0.	1.68E-02	3.35E-02	6.71E-02	1.12E-01	1.68E-01	3.35E-01
1.50E+02	2.78E+02	0.	0.	0.	0.	0.	0.	0.
3.00E+02	5.56E+02	1.74E+11	2.89E+10	1.76E+10	1.51E+10	1.35E+10	1.24E+10	1.05E+10
4.50E+02	8.33E+02	9.45E+13	1.60E+13	8.97E+12	6.60E+12	5.19E+12	4.35E+12	3.24E+12
6.00E+02	1.11E+03	9.30E+14	1.67E+14	9.21E+13	6.18E+13	4.50E+13	3.57E+13	2.38E+13
8.00E+02	1.48E+03	6.72E+15	1.28E+15	6.81E+14	4.17E+14	2.81E+14	2.11E+14	1.27E+14
1.00E+03	1.85E+03	2.27E+16	4.47E+15	2.34E+15	1.33E+15	8.49E+14	6.12E+14	3.42E+14
1.50E+03	2.78E+03	1.45E+17	3.03E+16	1.45E+16	6.60E+15	3.51E+15	2.21E+15	9.66E+14
2.00E+03	3.70E+03	5.64E+17	1.23E+17	5.31E+16	1.97E+16	8.82E+15	4.89E+15	1.69E+15
2.50E+03	4.63E+03	1.02E+18	2.23E+17	9.06E+16	2.92E+16	1.16E+16	5.91E+15	1.75E+15
3.00E+03	5.56E+03	1.06E+18	2.36E+17	9.06E+16	2.61E+16	9.39E+15	4.47E+15	1.17E+15
4.00E+03	7.41E+03	3.96E+18	1.39E+17	3.72E+16	1.20E+16	4.77E+15	2.45E+15	7.41E+14
5.00E+03	9.26E+03	8.61E+18	7.23E+16	1.19E+16	2.86E+15	8.94E+14	3.84E+14	8.61E+13
6.00E+03	1.11E+04	8.73E+18	2.40E+16	2.74E+15	5.37E+14	1.40E+14	5.34E+13	9.51E+12.
8.00E+03	1.48E+04	6.63E+18	1.71E+15	9.78E+13	1.54E+13	3.36E+12	1.12E+12	1.56E+11
1.00E+04	1.85E+04	2.57E+18	3.93E+13	1.04E+12	1.48E+11	2.98E+10	9.33E+09	1.17E+09
1.20E+04	2.22E+04	3.03E+18	1.40E+11	1.39E+08	1.58E+05	5.37E+02	1.10E+01	8.94E-03
1.40E+04	2.59E+04	1.09E+19	1.49E+07	6.54E+03	3.48E+00	6.15E-03	6.48E-05	0.
1.60E+04	2.96E+04	1.79E+19	9.09E+05	1.51E+02	3.30E-02	0.	0.	0.
1.80E+04	3.33E+04	8.22E+18	6.06E+05	1.12E+02	2.68E-02	0.	0.	0.

Table 6.13. Annual Equivalent 1 MeV Electron Fluence for J_{sc} Due to Trapped Protons, Circular Orbits, Inclination 0 Degree, Infinite Backshielding Assumed

EQUIV. 1 MEV ELECTRON FLUENCE FOR JSC - CIRCULAR ORBIT, INC = 30 DEGREE
DUE TO GEOMAG TRAPPED PROTONS, REF. AP5, AP6, AND AP7.

ALTITUDE		SHIELD THICKNESS, GM/CM2						
(N.M.)	(KM)	0.	1.68E-02	3.35E-02	6.71E-02	1.12E-01	1.68E-01	3.35E-01
1.50E+02	2.78E+02	2.18E+12	3.60E+11	2.15E+11	1.79E+11	1.57E+11	1.42E+11	1.19E+11
3.00E+02	5.56E+02	7.32E+13	1.31E+13	7.26E+12	4.95E+12	3.69E+12	2.98E+12	2.08E+12
4.50E+02	8.33E+02	4.50E+14	8.49E+13	4.53E+13	2.80E+13	1.92E+13	1.47E+13	9.24E+12
6.00E+02	1.11E+03	1.64E+15	3.18E+14	1.66E+14	9.57E+13	6.24E+13	4.62E+13	2.74E+13
8.00E+02	1.48E+03	6.45E+15	1.29E+15	6.57E+14	3.57E+14	2.24E+14	1.60E+14	8.97E+13
1.00E+03	1.85E+03	1.82E+16	3.69E+15	1.84E+15	9.36E+14	5.55E+14	3.81E+14	1.98E+14
1.50E+03	2.78E+03	1.04E+17	2.12E+16	9.69E+15	4.05E+15	2.02E+15	1.21E+15	4.95E+14
2.00E+03	3.70E+03	3.15E+17	6.63E+16	2.67E+16	9.51E+15	4.11E+15	2.23E+15	7.47E+14
2.50E+03	4.63E+03	5.31E+17	1.02E+17	4.05E+16	1.28E+16	5.04E+15	2.54E+15	7.44E+14
3.00E+03	5.56E+03	6.24E+17	1.01E+17	3.78E+16	1.09E+16	3.99E+15	1.92E+15	5.13E+14
4.00E+03	7.41E+03	2.71E+18	5.97E+16	1.49E+16	4.65E+15	1.80E+15	9.09E+14	2.69E+14
5.00E+03	9.26E+03	4.83E+18	2.93E+16	4.62E+15	1.09E+15	3.39E+14	1.45E+14	3.24E+13
6.00E+03	1.11E+04	4.11E+18	8.88E+15	9.81E+14	1.92E+14	5.04E+13	1.92E+13	3.42E+12
8.00E+03	1.48E+04	2.77E+18	6.21E+14	3.48E+13	5.49E+12	1.20E+12	3.99E+11	5.58E+10
1.00E+04	1.85E+04	1.19E+18	1.60E+13	4.29E+11	6.09E+10	1.22E+10	3.81E+09	4.77E+08
1.20E+04	2.22E+04	1.05E+18	5.61E+10	6.18E+07	7.68E+04	2.83E+02	6.12E+00	5.40E-03
1.40E+04	2.59E+04	5.25E+18	5.91E+06	2.68E+03	1.47E+00	2.67E-03	2.85E-05	0.
1.60E+04	2.96E+04	7.86E+18	3.90E+05	6.54E+01	1.42E-02	0.	0.	0.
1.80E+04	3.33E+04	3.24E+18	2.29E+05	4.17E+01	9.81E-03	0.	0.	0.

Table 6.14. Annual Equivalent 1 MeV Electron Fluence for J_{SC} Due to Trapped Protons, Circular Orbits, Inclination 30 Degree, Infinite Backshielding Assumed

EQUIV. 1 MEV ELECTRON FLUENCE FOR JSC - CIRCULAR ORBIT, INC = 60 DEGREE
DUE TO GEOMAG TRAPPED PROTONS, REF. AP5, AP6, AND AP7.

ALTITUDE		SHIELD THICKNESS, GM/CM2						
(N.M.)	(KM)	0.	1.68E-02	3.35E-02	6.71E-02	1.12E-01	1.68E-01	3.35E-01
1.50E+02	2.78E+02	2.78E+13	2.19E+12	1.02E+12	4.80E+11	2.98E+11	2.25E+11	1.49E+11
3.00E+02	5.56E+02	1.82E+14	1.80E+13	8.76E+12	4.44E+12	2.77E+12	2.06E+12	1.28E+12
4.50E+02	8.33E+02	6.24E+14	7.17E+13	3.54E+13	1.82E+13	1.13E+13	8.25E+12	4.89E+12
6.00E+02	1.11E+03	1.68E+15	2.11E+14	1.05E+14	5.46E+13	3.39E+13	2.45E+13	1.41E+13
8.00E+02	1.48E+03	5.79E+15	7.59E+14	3.78E+14	1.96E+14	1.20E+14	8.49E+13	4.68E+13
1.00E+03	1.85E+03	1.45E+16	2.03E+15	1.00E+15	4.98E+14	2.92E+14	1.99E+14	1.03E+14
1.50E+03	2.78E+03	6.96E+16	1.06E+16	4.83E+15	2.02E+15	1.00E+15	6.06E+14	2.48E+14
2.00E+03	3.70E+03	1.99E+17	3.30E+16	1.39E+16	4.98E+15	2.16E+15	1.17E+15	3.93E+14
2.50E+03	4.63E+03	3.21E+17	5.37E+16	2.14E+16	6.78E+15	2.65E+15	1.34E+15	3.96E+14
3.00E+03	5.56E+03	3.51E+17	5.31E+16	1.98E+16	5.76E+15	2.10E+15	1.01E+15	2.68E+14
4.00E+03	7.41E+03	1.36E+18	3.09E+16	7.86E+15	2.45E+15	9.54E+14	4.83E+14	1.43E+14
5.00E+03	9.26E+03	2.38E+18	1.51E+16	2.41E+15	5.76E+14	1.79E+14	7.71E+13	1.72E+13
6.00E+03	1.11E+04	2.07E+18	4.71E+15	5.31E+14	1.04E+14	2.74E+13	1.04E+13	1.86E+12
8.00E+03	1.48E+04	1.43E+18	3.33E+14	1.90E+13	3.03E+12	7.08E+11	2.74E+11	9.15E+10
1.00E+04	1.85E+04	6.12E+17	8.85E+12	2.36E+11	3.33E+10	6.63E+09	2.08E+09	2.58E+08
1.20E+04	2.22E+04	5.52E+17	3.12E+10	3.42E+07	4.29E+04	1.58E+02	3.42E+00	3.03E-03
1.40E+04	2.59E+04	2.65E+18	3.36E+06	1.55E+03	8.67E-01	1.57E-03	0.	0.
1.60E+04	2.96E+04	4.02E+18	2.08E+05	3.51E+01	7.71E-03	0.	0.	0.
1.80E+04	3.33E+04	1.70E+18	1.90E+06	4.77E+03	1.28E+01	8.97E-02	2.92E-03	0.

Table 6.15. Annual Equivalent 1 MeV Electron Fluence for J_{sc} Due to Trapped Protons, Circular Orbits, Inclination 60 Degree, Infinite Backshielding Assumed

EQUIV. 1 MEV ELECTRON FLUENCE FOR JSC - CIRCULAR ORBIT, INC = 90 DEGREE
DUE TO GEOMAG TRAPPED PROTONS, REF. AP5, AP6, AND AP7.

ALTITUDE		SHIELD THICKNESS, GM/CM2						
(N.M.)	(KM)	0.	1.68E-02	3.35E-02	6.71E-02	1.12E-01	1.68E-01	3.35E-01
1.50E+02	2.78E+02	1.48E+13	1.60E+12	7.56E+11	3.60E+11	2.23E+11	1.70E+11	1.13E+11
3.00E+02	5.56E+02	1.20E+14	1.33E+13	6.54E+12	3.39E+12	2.17E+12	1.63E+12	1.02E+12
4.50E+02	8.33E+02	4.44E+14	5.40E+13	2.71E+13	1.44E+13	9.15E+12	6.72E+12	3.99E+12
6.00E+02	1.11E+03	1.25E+15	1.68E+14	8.46E+13	4.53E+13	2.84E+13	2.06E+13	1.20E+13
8.00E+02	1.48E+03	4.29E+15	6.27E+14	3.15E+14	1.66E+14	1.02E+14	7.20E+13	3.99E+13
1.00E+03	1.85E+03	1.11E+16	1.71E+15	8.46E+14	4.26E+14	2.49E+14	1.71E+14	8.82E+13
1.50E+03	2.78E+03	5.46E+16	8.94E+15	4.08E+15	1.71E+15	8.55E+14	5.19E+14	2.12E+14
2.00E+03	3.70E+03	1.63E+17	2.83E+16	1.20E+16	4.26E+15	1.85E+15	1.01E+15	3.39E+14
2.50E+03	4.63E+03	2.64E+17	4.59E+16	1.84E+16	5.82E+15	2.28E+15	1.15E+15	3.39E+14
3.00E+03	5.56E+03	2.82E+17	4.50E+16	1.70E+16	4.95E+15	1.80E+15	8.64E+14	2.30E+14
4.00E+03	7.41E+03	1.14E+18	2.65E+16	6.72E+15	2.11E+15	8.19E+14	4.14E+14	1.23E+14
5.00E+03	9.26E+03	2.00E+18	1.30E+16	2.08E+15	4.95E+14	1.54E+14	6.63E+13	1.48E+13
6.00E+03	1.11E+04	1.77E+18	4.05E+15	4.56E+14	8.94E+13	2.35E+13	8.94E+12	1.60E+12
8.00E+03	1.48E+04	1.23E+18	2.88E+14	1.63E+13	2.57E+12	5.61E+11	1.87E+11	2.62E+10
1.00E+04	1.85E+04	5.13E+17	7.38E+12	2.00E+11	2.83E+10	5.64E+09	1.76E+09	2.19E+08
1.20E+04	2.22E+04	4.77E+17	2.68E+10	2.95E+07	3.66E+04	1.34E+02	2.89E+00	2.56E-03
1.40E+04	2.59E+04	2.25E+18	2.93E+06	1.36E+03	7.56E-01	1.37E-03	0.	0.
1.60E+04	2.96E+04	3.45E+18	2.87E+06	6.81E+03	1.72E+01	1.16E-01	3.69E-03	0.
1.80E+04	3.33E+04	1.45E+18	1.63E+06	4.08E+03	1.09E+01	7.62E-02	2.48E-03	0.

Table 6.16. Annual Equivalent 1 MeV Electron Fluence for J_{sc} Due to Trapped Protons, Circular Orbits, Inclination 90 Degree, Infinite Backshielding Assumed

EQUIV. 1 MEV ELECTRON FLUENCE FOR VOC AND PMAX - CIRCULAR ORBIT,INC=0 DEGREE
DUE TO GEOMAG TRAPPED PROTONS, REF. AP5, AP6, AND AP7.

ALTITUDE		SHIELD THICKNESS, GM/CM2						
(N.M.)	(KM)	0.	1.68E-02	3.35E-02	6.71E-02	1.12E-01	1.68E-01	3.35E-01
1.50E+02	2.78E+02	0.	0.	0.	0.	0.	0.	0.
3.00E+02	5.56E+02	8.16E+11	5.46E+10	2.41E+10	1.89E+10	1.59E+10	1.41E+10	1.16E+10
4.50E+02	8.33E+02	4.47E+14	3.36E+13	1.50E+13	9.78E+12	6.99E+12	5.52E+12	3.78E+12
6.00E+02	1.11E+03	4.29E+15	3.63E+14	1.67E+14	9.93E+13	6.54E+13	4.83E+13	2.90E+13
8.00E+02	1.48E+03	3.12E+16	2.87E+15	1.32E+15	7.11E+14	4.32E+14	3.00E+14	1.61E+14
1.00E+03	1.85E+03	1.04E+17	1.03E+16	4.71E+15	2.36E+15	1.35E+15	8.97E+14	4.47E+14
1.50E+03	2.78E+03	6.72E+17	7.35E+16	3.21E+16	1.30E+16	6.18E+15	3.57E+15	1.37E+15
2.00E+03	3.70E+03	2.58E+18	3.06E+17	1.24E+17	4.14E+16	1.66E+16	8.49E+15	2.58E+15
2.50E+03	4.63E+03	4.68E+18	5.67E+17	2.19E+17	6.36E+16	2.27E+16	1.06E+16	2.77E+15
3.00E+03	5.56E+03	4.83E+18	6.06E+17	2.23E+17	5.82E+16	1.90E+16	8.28E+15	1.90E+15
4.00E+03	7.41E+03	6.33E+19	3.72E+17	9.00E+16	2.61E+16	9.36E+15	4.41E+15	1.16E+15
5.00E+03	9.26E+03	4.14E+20	2.02E+17	3.00E+16	6.60E+15	1.87E+15	7.38E+14	1.44E+14
6.00E+03	1.11E+04	9.15E+20	6.90E+16	7.08E+15	1.27E+15	3.06E+14	1.06E+14	1.66E+13
8.00E+03	1.48E+04	3.09E+21	5.13E+15	2.58E+14	3.75E+13	7.56E+12	2.31E+12	2.83E+11
1.00E+04	1.85E+04	5.07E+21	1.23E+14	2.76E+12	3.66E+11	6.78E+10	1.96E+10	2.16E+09
1.20E+04	2.22E+04	6.54E+22	4.56E+11	5.31E+08	4.92E+05	1.61E+03	2.90E+01	2.21E-02
1.40E+04	2.59E+04	7.83E+24	4.92E+07	2.75E+04	1.13E+01	1.90E-02	1.80E-04	0.
1.60E+04	2.96E+04	3.48E+25	3.03E+06	7.29E+02	1.13E-01	1.42E-05	0.	0.
1.80E+04	3.33E+04	1.43E+25	2.02E+06	5.31E+02	9.15E-02	1.22E-05	0.	0.

Table 6.17. Annual Equivalent 1 MeV Electron Fluence for V_{oc} and P_{max} Due to Trapped Protons, Circular Orbits, Inclination 0 Degree, Infinite Backshielding Assumed

EQUIV. 1 MEV ELECTRON FLUENCE FOR VOC AND PMAX - CIRCULAR ORBIT,INC=30 DEGREE
DUE TO GEOMAG TRAPPED PROTONS, REF. AP5, AP6, AND AP7.

ALTITUDE		SHIELD THICKNESS, GM/CM2						
(N.M.)	(KM)	0.	1.68E-02	3.35E-02	6.71E-02	1.12E-01	1.68E-01	3.35E-01
1.50E+02	2.78E+02	1.03E+13	6.99E+11	3.09E+11	2.31E+11	1.88E+11	1.65E+11	1.32E+11
3.00E+02	5.56E+02	3.42E+14	2.83E+13	1.29E+13	7.71E+12	5.19E+12	3.93E+12	2.48E+12
4.50E+02	8.33E+02	2.09E+15	1.90E+14	8.73E+13	4.71E+13	2.88E+13	2.04E+13	1.15E+13
6.00E+02	1.11E+03	7.50E+15	7.32E+14	3.30E+14	1.66E+14	9.69E+13	6.60E+13	3.48E+13
8.00E+02	1.48E+03	2.99E+16	2.99E+15	1.35E+15	6.42E+14	3.57E+14	2.36E+14	1.17E+14
1.00E+03	1.85E+03	8.46E+16	8.70E+15	3.90E+15	1.74E+15	9.15E+14	5.79E+14	2.65E+14
1.50E+03	2.78E+03	5.04E+17	5.22E+16	2.20E+16	8.16E+15	3.63E+15	2.02E+15	7.17E+14
2.00E+03	3.70E+03	1.65E+18	1.68E+17	6.33E+16	2.02E+16	7.83E+15	3.90E+15	1.14E+15
2.50E+03	4.63E+03	2.93E+18	2.59E+17	9.84E+16	2.81E+16	9.93E+15	4.62E+15	1.18E+15
3.00E+03	5.56E+03	3.96E+18	2.59E+17	9.27E+16	2.44E+16	8.04E+15	3.54E+15	8.28E+14
4.00E+03	7.41E+03	7.35E+19	1.60E+17	3.63E+16	1.02E+16	3.54E+15	1.64E+15	4.23E+14
5.00E+03	9.26E+03	3.18E+20	8.22E+16	1.17E+16	2.53E+15	7.08E+14	2.79E+14	5.40E+13
6.00E+03	1.11E+04	5.49E+20	2.55E+16	2.53E+15	4.56E+14	1.09E+14	3.81E+13	5.97E+12
8.00E+03	1.48E+04	1.42E+21	1.86E+15	9.18E+13	1.34E+13	2.70E+12	8.25E+11	1.01E+11
1.00E+04	1.85E+04	2.62E+21	4.98E+13	1.14E+12	1.51E+11	2.78E+10	8.01E+09	8.79E+08
1.20E+04	2.22E+04	2.20E+22	1.83E+11	2.33E+08	2.39E+05	8.43E+02	1.60E+01	1.34E-02
1.40E+04	2.59E+04	4.26E+24	1.95E+07	1.12E+04	4.77E+00	8.25E-03	7.95E-05	0.
1.60E+04	2.96E+04	1.55E+25	1.30E+06	3.15E+02	4.89E-02	0.	0.	0.
1.80E+04	3.33E+04	5.67E+24	7.62E+05	1.98E+02	3.36E-02	0.	0.	0.

Table 6.18. Annual Equivalent 1 MeV Electron Fluence for V_{oc} and P_{max} Due to Trapped Protons, Circular Orbits, Inclination 30 Degree, Infinite Backshielding Assumed

EQUIV. 1 MEV ELECTRON FLUENCE FOR VOC AND PMAX - CIRCULAR ORBIT,INC=60 DEGREE
DUE TO GEOMAG TRAPPED PROTONS, REF. AP5, AP6, AND AP7.

ALTITUDE		SHIELD THICKNESS, GM/CM2						
(N.M.)	(KM)	0.	1.68E-02	3.35E-02	6.71E-02	1.12E-01	1.68E-01	3.35E-01
1.50E+02	2.78E+02	5.82E+14	5.25E+12	2.19E+12	8.55E+11	4.47E+11	3.06E+11	1.78E+11
3.00E+02	5.56E+02	2.68E+15	4.26E+13	1.84E+13	7.89E+12	4.26E+12	2.89E+12	1.58E+12
4.50E+02	8.33E+02	7.02E+15	1.69E+14	7.35E+13	3.27E+13	1.78E+13	1.19E+13	6.18E+12
6.00E+02	1.11E+03	1.66E+16	4.95E+14	2.18E+14	9.84E+13	5.40E+13	3.57E+13	1.81E+13
8.00E+02	1.48E+03	5.40E+16	1.78E+15	7.89E+14	3.57E+14	1.93E+14	1.26E+14	6.12E+13
1.00E+03	1.85E+03	1.23E+17	4.83E+15	2.14E+15	9.33E+14	4.83E+14	3.03E+14	1.37E+14
1.50E+03	2.78E+03	5.61E+17	2.61E+16	1.10E+16	4.08E+15	1.81E+15	1.00E+15	3.60E+14
2.00E+03	3.70E+03	1.41E+18	8.28E+16	3.30E+16	1.06E+16	4.11E+15	2.05E+15	6.03E+14
2.50E+03	4.63E+03	2.16E+18	1.37E+17	5.16E+16	1.48E+16	5.22E+15	2.43E+15	6.27E+14
3.00E+03	5.56E+03	2.58E+18	1.36E+17	4.89E+16	1.28E+16	4.23E+15	1.86E+15	4.32E+14
4.00E+03	7.41E+03	3.69E+19	8.28E+16	1.90E+16	5.37E+15	1.88E+15	8.70E+14	2.25E+14
5.00E+03	9.26E+03	1.52E+20	4.26E+16	6.12E+15	1.33E+15	3.75E+14	1.48E+14	2.88E+13
6.00E+03	1.11E+04	2.64E+20	1.35E+16	1.37E+15	2.47E+14	5.94E+13	2.07E+13	3.24E+12
8.00E+03	1.48E+04	7.17E+20	1.00E+15	4.98E+13	7.35E+12	1.52E+12	5.01E+11	1.12E+11
1.00E+04	1.85E+04	1.27E+21	2.76E+13	6.27E+11	8.22E+10	1.51E+10	4.35E+09	4.77E+08
1.20E+04	2.22E+04	1.13E+22	1.01E+11	1.29E+08	1.33E+05	4.71E+02	8.97E+00	7.53E-03
1.40E+04	2.59E+04	2.05E+24	1.11E+07	6.48E+03	2.81E+00	4.89E-03	0.	0.
1.60E+04	2.96E+04	7.83E+24	6.93E+05	1.68E+02	2.65E-02	0.	0.	0.
1.80E+04	3.33E+04	2.98E+24	6.12E+06	1.66E+04	3.84E+01	2.60E-01	7.62E-03	0.

Table 6.19. Annual Equivalent 1 MeV Electron Fluence for V_{oc} and P_{max} Due to Trapped Protons, Circular Orbits, Inclination 60 Degree, Infinite Backshielding Assumed

EQLIV. 1 MEV ELECTRON FLUENCE FOR VOC AND PMAX - CIRCULAR ORBIT,INC=90 DEGREE
DUE TO GEOMAG TRAPPED PROTONS, REF. AP5, AP6, AND AP7.

ALTITUDE		SHIELD THICKNESS, GM/CM2						
(N.M.)	(KM)	0.	1.68E-02	3.35E-02	6.71E-02	1.12E-01	1.68E-01	3.35E-01
1.50E+02	2.78E+02	2.02E+14	3.84E+12	1.61E+12	6.36E+11	3.36E+11	2.30E+11	1.34E+11
3.00E+02	5.56E+02	1.49E+15	3.12E+13	1.35E+13	5.94E+12	3.30E+12	2.27E+12	1.26E+12
4.50E+02	8.33E+02	4.47E+15	1.27E+14	5.58E+13	2.55E+13	1.42E+13	9.63E+12	5.04E+12
6.00E+02	1.11E+03	1.11E+16	3.93E+14	1.74E+14	8.04E+13	4.47E+13	2.99E+13	1.53E+13
8.00E+02	1.48E+03	3.30E+16	1.47E+15	6.57E+14	3.00E+14	1.63E+14	1.06E+14	5.19E+13
1.00E+03	1.85E+03	8.16E+16	4.05E+15	1.80E+15	7.92E+14	4.14E+14	2.60E+14	1.18E+14
1.50E+03	2.78E+03	3.84E+17	2.20E+16	9.30E+15	3.45E+15	1.54E+15	8.55E+14	3.06E+14
2.00E+03	3.70E+03	1.06E+18	7.11E+16	2.83E+16	9.06E+15	3.54E+15	1.76E+15	5.19E+14
2.50E+03	4.63E+03	1.69E+18	1.17E+17	4.44E+16	1.27E+16	4.50E+15	2.09E+15	5.37E+14
3.00E+03	5.56E+03	1.93E+18	1.15E+17	4.20E+16	1.10E+16	3.63E+15	1.60E+15	3.72E+14
4.00E+03	7.41E+03	2.98E+19	7.11E+16	1.63E+16	4.62E+15	1.61E+15	7.47E+14	1.93E+14
5.00E+03	9.26E+03	1.23E+20	3.66E+16	5.25E+15	1.15E+15	3.21E+14	1.27E+14	2.48E+13
6.00E+03	1.11E+04	2.24E+20	1.16E+16	1.18E+15	2.13E+14	5.10E+13	1.78E+13	2.78E+12
8.00E+03	1.48E+04	6.18E+20	8.64E+14	4.29E+13	6.27E+12	1.26E+12	3.87E+11	4.74E+10
1.00E+04	1.85E+04	1.07E+21	2.30E+13	5.31E+11	6.99E+10	1.28E+10	3.69E+09	4.05E+08
1.20E+04	2.22E+04	9.75E+21	8.73E+10	1.11E+08	1.13E+05	3.99E+02	7.62E+00	6.33E-03
1.40E+04	2.59E+04	1.72E+24	9.66E+06	5.67E+03	2.45E+00	4.26E-03	0.	0.
1.60E+04	2.96E+04	6.69E+24	9.21E+06	2.38E+04	5.19E+01	3.36E-01	9.57E-03	0.
1.80E+04	3.33E+04	2.54E+24	5.22E+06	1.42E+04	3.24E+01	2.21E-01	6.45E-03	0.

Table 6.20. Annual Equivalent 1 MeV Electron Fluence for V_{oc} and P_{max} Due to Trapped Protons, Circular Orbits, Inclination 90 Degree, Infinite Backshielding Assumed

ABSORBED DOSE(RAD SI), CIRCULAR ORBIT, INC = 0 DEGREE
DUE TO GEOMAG TRAPPED ELECTRONS, REF. AE4 AND AE5.

ALTITUDE		SHIELD THICKNESS, GM/CM2						
(N.M.)	(KM)	6.15E-03	1.84E-02	3.69E-02	7.38E-02	1.23E-01	1.84E-01	3.69E-01
1.50E+02	2.78E+02	0.	0.	0.	0.	0.	0.	0.
3.00E+02	5.56E+02	3.19E+00	2.65E+00	2.27E+00	1.86E+00	1.48E+00	1.05E+00	5.39E-01
4.50E+02	8.33E+02	3.81E+03	2.44E+03	1.69E+03	1.08E+03	7.03E+02	4.32E+02	1.71E+02
6.00E+02	1.11E+03	3.92E+05	2.44E+05	1.66E+05	1.03E+05	6.45E+04	3.86E+04	1.45E+04
8.00E+02	1.48E+03	6.82E+06	4.24E+06	2.87E+06	1.76E+06	1.08E+06	6.39E+05	2.37E+05
1.00E+03	1.85E+03	2.44E+07	1.49E+07	9.95E+06	5.93E+06	3.51E+06	2.03E+06	7.44E+05
1.25E+03	2.31E+03	5.82E+07	3.42E+07	2.20E+07	1.24E+07	6.80E+06	3.78E+06	1.33E+06
1.50E+03	2.78E+03	9.55E+07	5.33E+07	3.27E+07	1.69E+07	8.07E+06	4.15E+06	1.37E+06
1.75E+03	3.24E+03	1.33E+08	7.07E+07	4.15E+07	1.95E+07	7.67E+06	3.53E+06	1.05E+06
2.00E+03	3.70E+03	1.67E+08	8.65E+07	4.93E+07	2.15E+07	6.75E+06	2.72E+06	6.76E+05
2.25E+03	4.17E+03	1.98E+08	1.01E+08	5.68E+07	2.35E+07	6.15E+06	2.18E+06	4.21E+05
2.50E+03	4.63E+03	2.16E+08	1.10E+08	6.11E+07	2.47E+07	5.96E+06	1.93E+06	2.68E+05
2.75E+03	5.09E+03	2.19E+08	1.10E+08	6.06E+07	2.43E+07	5.89E+06	1.84E+06	1.62E+05
3.00E+03	5.56E+03	2.11E+08	1.03E+08	5.59E+07	2.20E+07	5.40E+06	1.65E+06	1.02E+05
3.50E+03	6.48E+03	1.83E+08	8.48E+07	4.36E+07	1.61E+07	3.79E+06	1.12E+06	4.79E+04
4.00E+03	7.41E+03	1.58E+08	6.89E+07	3.36E+07	1.17E+07	2.66E+06	7.71E+05	3.02E+04
4.50E+03	8.33E+03	1.31E+08	5.47E+07	2.57E+07	8.69E+06	2.19E+06	6.74E+05	3.19E+04
5.00E+03	9.26E+03	8.75E+07	3.60E+07	1.68E+07	5.79E+06	1.75E+06	6.07E+05	4.83E+04
5.50E+03	1.02E+04	5.18E+07	2.12E+07	9.90E+06	3.60E+06	1.38E+06	5.67E+05	8.59E+04
6.00E+03	1.11E+04	3.24E+07	1.33E+07	6.22E+06	2.41E+06	1.16E+06	5.63E+05	1.39E+05
7.00E+03	1.30E+04	1.75E+07	9.30E+06	5.50E+06	2.84E+06	1.56E+06	8.35E+05	2.51E+05
8.00E+03	1.48E+04	2.36E+07	1.24E+07	7.26E+06	3.73E+06	2.06E+06	1.12E+06	3.61E+05
9.00E+03	1.67E+04	2.89E+07	1.61E+07	9.87E+06	5.30E+06	2.90E+06	1.57E+06	4.95E+05
1.00E+04	1.85E+04	2.80E+07	1.74E+07	1.17E+07	6.99E+06	4.07E+06	2.24E+06	6.62E+05
1.10E+04	2.04E+04	2.91E+07	1.80E+07	1.21E+07	7.37E+06	4.59E+06	2.61E+06	7.62E+05
1.20E+04	2.22E+04	2.99E+07	1.82E+07	1.21E+07	7.38E+06	4.77E+06	2.76E+06	7.93E+05
1.30E+04	2.41E+04	2.85E+07	1.72E+07	1.13E+07	6.85E+06	4.41E+06	2.52E+06	6.97E+05
1.40E+04	2.59E+04	2.70E+07	1.61E+07	1.05E+07	6.27E+06	3.97E+06	2.25E+06	6.03E+05
1.50E+04	2.78E+04	2.58E+07	1.50E+07	9.64E+06	5.61E+06	3.48E+06	1.95E+06	5.11E+05
1.60E+04	2.96E+04	2.44E+07	1.39E+07	8.73E+06	4.90E+06	2.91E+06	1.57E+06	3.74E+05
1.70E+04	3.15E+04	2.30E+07	1.28E+07	7.85E+06	4.23E+06	2.37E+06	1.22E+06	2.65E+05
1.80E+04	3.33E+04	2.16E+07	1.16E+07	6.92E+06	3.54E+06	1.86E+06	9.26E+05	1.94E+05
1.94E+04	3.59E+04	2.77E+07	1.59E+07	9.92E+06	5.10E+06	2.26E+06	9.59E+05	9.02E+04

Table 6.21. Annual Absorbed Dose Due to Trapped Electrons, Circular Orbits, Inclination 0 Degree, Infinite Backshielding Assumed

ABSORBED DOSE(RAD SI), CIRCULAR ORBIT, INC = 30 DEGREE
CUE TO GEOMAG TRAPPED ELECTRONS, REF. AE4 AND AE5.

ALTITUDE		SHIELD THICKNESS, GM/CM2						
(N.M.)	(KM)	6.15E-03	1.84E-02	3.69E-02	7.38E-02	1.23E-01	1.84E-01	3.69E-01
1.50E+02	2.78E+02	1.47E+02	7.97E+01	4.82E+01	2.58E+01	1.45E+01	8.25E+00	3.04E+00
3.00E+02	5.56E+02	7.87E+04	3.82E+04	2.09E+04	9.57E+03	4.59E+03	2.39E+03	8.14E+02
4.50E+02	8.33E+02	5.52E+05	2.87E+05	1.66E+05	8.33E+04	4.35E+04	2.37E+04	8.34E+03
6.00E+02	1.11E+03	2.05E+06	1.12E+06	6.82E+05	3.63E+05	1.99E+05	1.11E+05	3.97E+04
8.00E+02	1.48E+03	7.90E+06	4.38E+06	2.69E+06	1.44E+06	7.91E+05	4.40E+05	1.57E+05
1.00E+03	1.85E+03	2.06E+07	1.13E+07	6.87E+06	3.62E+06	1.92E+06	1.05E+06	3.68E+05
1.25E+03	2.31E+03	4.27E+07	2.28E+07	1.35E+07	6.74E+06	3.27E+06	1.70E+06	5.73E+05
1.50E+03	2.78E+03	6.48E+07	3.33E+07	1.90E+07	8.76E+06	3.64E+06	1.73E+06	5.37E+05
1.75E+03	3.24E+03	8.58E+07	4.29E+07	2.38E+07	1.02E+07	3.51E+06	1.49E+06	4.02E+05
2.00E+03	3.70E+03	1.01E+08	4.98E+07	2.71E+07	1.11E+07	3.21E+06	1.21E+06	2.68E+05
2.25E+03	4.17E+03	1.14E+08	5.54E+07	2.98E+07	1.17E+07	2.98E+06	1.01E+06	1.65E+05
2.50E+03	4.63E+03	1.17E+08	5.64E+07	3.01E+07	1.17E+07	2.82E+06	8.99E+05	1.06E+05
2.75E+03	5.09E+03	1.16E+08	5.52E+07	2.91E+07	1.11E+07	2.68E+06	8.27E+05	6.64E+04
3.00E+03	5.56E+03	1.09E+08	5.09E+07	2.64E+07	9.88E+06	2.39E+06	7.29E+05	4.58E+04
3.50E+03	6.48E+03	9.36E+07	4.14E+07	2.05E+07	7.30E+06	1.76E+06	5.35E+05	3.28E+04
4.00E+03	7.41E+03	7.62E+07	3.25E+07	1.56E+07	5.39E+06	1.37E+06	4.37E+05	3.84E+04
4.50E+03	8.33E+03	5.85E+07	2.45E+07	1.16E+07	4.07E+06	1.23E+06	4.40E+05	5.79E+04
5.00E+03	9.26E+03	3.89E+07	1.66E+07	8.00E+06	3.02E+06	1.14E+06	4.77E+05	9.03E+04
5.50E+03	1.02E+04	2.62E+07	1.16E+07	5.86E+06	2.44E+06	1.14E+06	5.50E+05	1.35E+05
6.00E+03	1.11E+04	1.97E+07	9.41E+06	5.06E+06	2.35E+06	1.25E+06	6.54E+05	1.87E+05
7.00E+03	1.30E+04	1.66E+07	9.19E+06	5.63E+06	3.04E+06	1.72E+06	9.42E+05	2.86E+05
8.00E+03	1.48E+04	2.02E+07	1.14E+07	7.11E+06	3.92E+06	2.24E+06	1.23E+06	3.76E+05
9.00E+03	1.67E+04	2.18E+07	1.29E+07	8.41E+06	4.84E+06	2.81E+06	1.55E+06	4.60E+05
1.00E+04	1.85E+04	2.12E+07	1.29E+07	8.62E+06	5.16E+06	3.13E+06	1.76E+06	5.06E+05
1.10E+04	2.04E+04	2.15E+07	1.30E+07	8.64E+06	5.20E+06	3.27E+06	1.86E+06	5.26E+05
1.20E+04	2.22E+04	2.09E+07	1.24E+07	8.13E+06	4.84E+06	3.06E+06	1.74E+06	4.81E+05
1.30E+04	2.41E+04	1.99E+07	1.16E+07	7.50E+06	4.38E+06	2.74E+06	1.54E+06	4.11E+05
1.40E+04	2.59E+04	1.86E+07	1.07E+07	6.73E+06	3.83E+06	2.33E+06	1.29E+06	3.30E+05
1.50E+04	2.78E+04	1.74E+07	9.75E+06	6.02E+06	3.31E+06	1.95E+06	1.05E+06	2.57E+05
1.60E+04	2.96E+04	1.63E+07	8.83E+06	5.29E+06	2.79E+06	1.56E+06	8.13E+05	1.83E+05
1.70E+04	3.15E+04	1.51E+07	7.92E+06	4.61E+06	2.31E+06	1.22E+06	6.11E+05	1.27E+05
1.80E+04	3.33E+04	1.39E+07	7.00E+06	3.92E+06	1.86E+06	9.14E+05	4.39E+05	8.55E+04

Table 6.22. Annual Absorbed Dose Due to Trapped Electrons, Circular Orbits, Inclination 30 Degree, Infinite Backshielding Assumed

ABSORBED DOSE(RAD SI), CIRCULAR ORBIT, INC = 60 DEGREE.
DUE TO GEOMAG TRAPPED ELECTRONS, REF. AE4 AND AE5.

ALTITUDE		SHIELD THICKNESS GM/CM2						
(N.M.)	(KM)	6.15E-03	1.84E-02	3.69E-02	7.38E-02	1.23E-01	1.84E-01	3.69E-01
1.50E+02	2.78E+02	4.45E+04	2.37E+04	1.41E+04	7.36E+03	4.15E+03	2.26E+03	6.69E+02
3.00E+02	5.56E+02	1.70E+05	8.27E+04	4.51E+04	2.10E+04	1.07E+04	5.60E+03	1.68E+03
4.50E+02	8.33E+02	5.14E+05	2.51E+05	1.38E+05	6.47E+04	3.28E+04	1.73E+04	5.58E+03
6.00E+02	1.11E+03	1.34E+06	6.96E+05	4.04E+05	2.04E+05	1.09E+05	5.96E+04	2.05E+04
8.00E+02	1.48E+03	4.47E+06	2.42E+06	1.45E+06	7.64E+05	4.18E+05	2.32E+05	8.19E+04
1.00E+03	1.85E+03	1.13E+07	6.11E+06	3.67E+06	1.92E+06	1.02E+06	5.61E+05	1.96E+05
1.25E+03	2.31E+03	2.25E+07	1.20E+07	7.06E+06	3.53E+06	1.74E+06	9.09E+05	3.06E+05
1.50E+03	2.78E+03	3.30E+07	1.69E+07	9.64E+06	4.48E+06	1.92E+06	9.26E+05	2.88E+05
1.75E+03	3.24E+03	4.40E+07	2.20E+07	1.22E+07	5.30E+06	1.89E+06	8.18E+05	2.23E+05
2.00E+03	3.70E+03	5.28E+07	2.61E+07	1.43E+07	5.89E+06	1.77E+06	6.89E+05	1.58E+05
2.25E+03	4.17E+03	5.84E+07	2.86E+07	1.55E+07	6.19E+06	1.65E+06	5.83E+05	1.06E+05
2.50E+03	4.63E+03	6.11E+07	2.97E+07	1.60E+07	6.29E+06	1.62E+06	5.44E+05	7.82E+04
2.75E+03	5.09E+03	6.07E+07	2.91E+07	1.55E+07	6.05E+06	1.57E+06	5.17E+05	5.98E+04
3.00E+03	5.56E+03	5.72E+07	2.70E+07	1.41E+07	5.44E+06	1.44E+06	4.76E+05	5.12E+04
3.50E+03	6.48E+03	4.79E+07	2.16E+07	1.09E+07	4.07E+06	1.13E+06	3.87E+05	4.95E+04
4.00E+03	7.41E+03	4.05E+07	1.77E+07	8.67E+06	3.18E+06	9.60E+05	3.53E+05	5.56E+04
4.50E+03	8.33E+03	3.19E+07	1.38E+07	6.74E+06	2.54E+06	8.92E+05	3.60E+05	6.70E+04
5.00E+03	9.26E+03	2.21E+07	9.81E+06	4.92E+06	2.00E+06	8.47E+05	3.84E+05	8.45E+04
5.50E+03	1.02E+04	1.54E+07	7.20E+06	3.78E+06	1.68E+06	8.35E+05	4.17E+05	1.06E+05
6.00E+03	1.11E+04	1.19E+07	5.87E+06	3.26E+06	1.58E+06	8.61E+05	4.56E+05	1.28E+05
7.00E+03	1.30E+04	9.84E+06	5.52E+06	3.42E+06	1.87E+06	1.06E+06	5.80E+05	1.71E+05
8.00E+03	1.48E+04	1.13E+07	6.42E+06	4.01E+06	2.21E+06	1.27E+06	6.96E+05	2.08E+05
9.00E+03	1.67E+04	1.20E+07	7.05E+06	4.52E+06	2.58E+06	1.49E+06	8.19E+05	2.40E+05
1.00E+04	1.85E+04	1.16E+07	6.94E+06	4.55E+06	2.68E+06	1.61E+06	8.98E+05	2.56E+05
1.10E+04	2.04E+04	1.15E+07	6.85E+06	4.46E+06	2.64E+06	1.64E+06	9.23E+05	2.59E+05
1.20E+04	2.22E+04	1.12E+07	6.56E+06	4.23E+06	2.48E+06	1.56E+06	8.84E+05	2.43E+05
1.30E+04	2.41E+04	1.06E+07	6.10E+06	3.88E+06	2.24E+06	1.39E+06	7.77E+05	2.06E+05
1.40E+04	2.59E+04	9.72E+06	5.50E+06	3.44E+06	1.93E+06	1.17E+06	6.44E+05	1.65E+05
1.50E+04	2.78E+04	9.11E+06	5.03E+06	3.07E+06	1.67E+06	9.82E+05	5.29E+05	1.30E+05
1.60E+04	2.96E+04	8.33E+06	4.48E+06	2.67E+06	1.40E+06	7.84E+05	4.08E+05	9.24E+04
1.70E+04	3.15E+04	7.71E+06	4.01E+06	2.32E+06	1.16E+06	6.15E+05	3.08E+05	6.39E+04
1.80E+04	3.33E+04	7.04E+06	3.53E+06	1.97E+06	9.30E+05	4.61E+05	2.22E+05	4.38E+04

Table 6.23. Annual Absorbed Dose Due to Trapped Electrons, Circular Orbits, Inclination 60 Degree, Infinite Backshielding Assumed

.ABSORBED DOSE(RAD SI), CIRCULAR ORBIT, INC = 90 DEGREE
DUE TO GEOMAG TRAPPED ELECTRONS, REF. AE4 AND AE5.

ALTITUDE		SHIELD THICKNESS, GM/CM2						
(N.M.)	(KM)	6.15E-03	1.84E-02	3.69E-02	7.38E-02	1.23E-01	1.84E-01	3.69E-01
1.50E+02	2.78E+02	4.14E+04	2.28E+04	1.39E+04	7.47E+03	4.26E+03	2.32E+03	6.75E+02
3.00E+02	5.56E+02	1.42E+05	7.08E+04	3.95E+04	1.90E+04	9.94E+03	5.22E+03	1.55E+03
4.50E+02	8.33E+02	4.13E+05	2.06E+05	1.15E+05	5.49E+04	2.82E+04	1.49E+04	4.77E+03
6.00E+02	1.11E+03	1.09E+06	5.75E+05	3.38E+05	1.73E+05	9.34E+04	5.12E+04	1.76E+04
8.00E+02	1.48E+03	3.73E+06	2.04E+06	1.23E+06	6.52E+05	3.58E+05	1.99E+05	7.02E+04
1.00E+03	1.85E+03	9.51E+06	5.18E+06	3.12E+06	1.64E+06	8.77E+05	4.81E+05	1.68E+05
1.25E+03	2.31E+03	1.90E+07	1.01E+07	6.00E+06	3.01E+06	1.48E+06	7.77E+05	2.62E+05
1.50E+03	2.78E+03	2.77E+07	1.43E+07	8.19E+06	3.82E+06	1.63E+06	7.89E+05	2.46E+05
1.75E+03	3.24E+03	3.72E+07	1.86E+07	1.04E+07	4.50E+06	1.60E+06	6.94E+05	1.89E+05
2.00E+03	3.70E+03	4.48E+07	2.21E+07	1.21E+07	4.98E+06	1.49E+06	5.77E+05	1.31E+05
2.25E+03	4.17E+03	4.96E+07	2.43E+07	1.31E+07	5.23E+06	1.38E+06	4.85E+05	8.67E+04
2.50E+03	4.63E+03	5.20E+07	2.53E+07	1.36E+07	5.34E+06	1.35E+06	4.47E+05	6.15E+04
2.75E+03	5.09E+03	5.16E+07	2.47E+07	1.31E+07	5.10E+06	1.30E+06	4.21E+05	4.49E+04
3.00E+03	5.56E+03	4.87E+07	2.29E+07	1.20E+07	4.58E+06	1.19E+06	3.84E+05	3.71E+04
3.50E+03	6.48E+03	4.04E+07	1.82E+07	9.15E+06	3.38E+06	9.05E+05	3.02E+05	3.38E+04
4.00E+03	7.41E+03	3.43E+07	1.49E+07	7.26E+06	2.62E+06	7.56E+05	2.68E+05	3.83E+04
4.50E+03	8.33E+03	2.69E+07	1.16E+07	5.60E+06	2.07E+06	6.99E+05	2.74E+05	4.79E+04
5.00E+03	9.26E+03	1.84E+07	8.08E+06	4.01E+06	1.59E+06	6.53E+05	2.90E+05	6.16E+04
5.50E+03	1.02E+04	1.27E+07	5.86E+06	3.05E+06	1.33E+06	6.53E+05	3.23E+05	8.13E+04
6.00E+03	1.11E+04	9.67E+06	4.74E+06	2.61E+06	1.25E+06	6.77E+05	3.57E+05	1.01E+05
7.00E+03	1.30E+04	7.91E+06	4.43E+06	2.74E+06	1.50E+06	8.53E+05	4.66E+05	1.38E+05
8.00E+03	1.48E+04	9.34E+06	5.27E+06	3.28E+06	1.81E+06	1.04E+06	5.72E+05	1.71E+05
9.00E+03	1.67E+04	9.90E+06	5.81E+06	3.73E+06	2.13E+06	1.23E+06	6.77E+05	1.99E+05
1.00E+04	1.85E+04	9.55E+06	5.77E+06	3.81E+06	2.25E+06	1.36E+06	7.58E+05	2.16E+05
1.10E+04	2.04E+04	9.37E+06	5.60E+06	3.67E+06	2.18E+06	1.36E+06	7.65E+05	2.15E+05
1.20E+04	2.22E+04	9.33E+06	5.49E+06	3.55E+06	2.09E+06	1.32E+06	7.48E+05	2.06E+05
1.30E+04	2.41E+04	8.84E+06	5.13E+06	3.27E+06	1.90E+06	1.18E+06	6.60E+05	1.75E+05
1.40E+04	2.59E+04	8.15E+06	4.63E+06	2.90E+06	1.64E+06	9.93E+05	5.47E+05	1.40E+05
1.50E+04	2.78E+04	7.67E+06	4.25E+06	2.60E+06	1.42E+06	8.36E+05	4.51E+05	1.11E+05
1.60E+04	2.96E+04	7.04E+06	3.80E+06	2.27E+06	1.19E+06	6.69E+05	3.48E+05	7.89E+04
1.70E+04	3.15E+04	6.52E+06	3.40E+06	1.97E+06	9.88E+05	5.24E+05	2.62E+05	5.48E+04
1.80E+04	3.33E+04	5.96E+06	2.99E+06	1.67E+06	7.93E+05	3.93E+05	1.90E+05	3.74E+04

Table 6.24. Annual Absorbed Dose Due to Trapped Electrons, Circular Orbits, Inclination 90 Degree, Infinite Backshielding Assumed

ABSORBED DOSE(RAD SI), CIRCULAR ORBIT, INC = 0 DEGREE
DUE TO GEOMAG TRAPPED PROTONS, REF. AP5, AP6, AND AP7.

ALTITUDE		SHIELD THICKNESS, GM/CM2						
(N.M.)	(KM)	6.15E-03	1.84E-02	3.69E-02	7.38E-02	1.23E-01	1.84E-01	3.69E-01
1.50E+02	2.78E+02	0.	0.	0.	0.	0.	0.	0.
3.00E+02	5.56E+02	2.78E+01	6.73E+00	2.50E+00	1.92E+00	1.60E+00	1.42E+00	1.17E+00
4.50E+02	8.33E+02	1.55E+04	4.12E+03	1.60E+03	1.02E+03	7.24E+02	5.60E+02	3.58E+02
6.00E+02	1.11E+03	1.56E+05	4.40E+04	1.79E+04	1.04E+04	6.87E+03	4.97E+03	2.79E+03
8.00E+02	1.48E+03	1.14E+06	3.42E+05	1.40E+05	7.42E+04	4.55E+04	3.11E+04	1.55E+04
1.00E+03	1.85E+03	3.90E+06	1.21E+06	4.95E+05	2.45E+05	1.42E+05	9.34E+04	4.33E+04
1.50E+03	2.78E+03	2.53E+07	8.32E+06	3.26E+06	1.29E+06	6.32E+05	3.65E+05	1.30E+05
2.00E+03	3.70E+03	9.95E+07	3.38E+07	1.23E+07	3.95E+06	1.64E+06	8.37E+05	2.36E+05
2.50E+03	4.63E+03	1.79E+08	6.16E+07	2.12E+07	5.89E+06	2.19E+06	1.03E+06	2.48E+05
3.00E+03	5.56E+03	1.89E+08	6.53E+07	2.14E+07	5.28E+06	1.79E+06	7.82E+05	1.66E+05
4.00E+03	7.41E+03	4.05E+08	4.60E+07	8.73E+06	2.42E+06	9.00E+05	4.23E+05	1.04E+05
5.00E+03	9.26E+03	5.14E+08	2.69E+07	2.83E+06	5.79E+05	1.71E+05	6.75E+04	1.24E+04
6.00E+03	1.11E+04	3.29E+08	9.62E+06	6.59E+05	1.08E+05	2.69E+04	9.39E+03	1.37E+03
8.00E+03	1.48E+04	8.25E+07	7.71E+05	2.38E+04	3.10E+03	6.42E+02	1.96E+02	2.23E+01
1.00E+04	1.85E+04	7.37E+06	1.97E+04	2.54E+02	2.98E+01	5.68E+00	1.63E+00	1.66E-01
1.20E+04	2.22E+04	3.06E+05	7.75E+01	3.89E-02	2.91E-05	9.37E-08	1.59E-09	8.14E-13
1.40E+04	2.59E+04	2.33E+03	8.47E-03	1.84E-06	6.35E-10	1.07E-12	8.36E-15	0.
1.60E+04	2.96E+04	5.97E+02	5.27E-04	4.31E-08	6.00E-12	1.15E-17	0.	0.
1.80E+04	3.33E+04	3.41E+02	3.51E-04	3.18E-08	4.86E-12	9.89E-18	0.	0.

Table 6.25. Annual Absorbed Dose Due to Trapped Protons, Circular Orbits, Inclination 0 Degree, Infinite Backshielding Assumed

ABSORBED DOSE(RAD SI), CIRCULAR ORBIT, INC = 30 DEGREE
DUE TO GEOMAG TRAPPED PROTONS, REF. AP5, AP6, AND AP7.

ALTITUDE		SHIELD THICKNESS, GM/CM2						
(N.M.)	(KM)	6.15E-03	1.84E-02	3.69E-02	7.38E-02	1.23E-01	1.84E-01	3.69E-01
1.50E+02	2.78E+02	3.51E+02	8.57E+01	3.19E+01	2.34E+01	1.89E+01	1.63E+01	1.29E+01
3.00E+02	5.56E+02	1.22E+04	3.42E+03	1.38E+03	8.06E+02	5.41E+02	4.01E+02	2.37E+02
4.50E+02	8.33E+02	7.60E+04	2.26E+04	9.21E+03	4.88E+03	3.02E+03	2.10E+03	1.10E+03
6.00E+02	1.11E+03	2.80E+05	8.58E+04	3.46E+04	1.72E+04	1.01E+04	6.82E+03	3.34E+03
8.00E+02	1.48E+03	1.10E+06	3.48E+05	1.41E+05	6.59E+04	3.74E+04	2.44E+04	1.11E+04
1.00E+03	1.85E+03	3.12E+06	1.00E+06	4.00E+05	1.76E+05	9.50E+04	5.95E+04	2.53E+04
1.50E+03	2.78E+03	1.77E+07	5.82E+06	2.21E+06	7.98E+05	3.67E+05	2.03E+05	6.68E+04
2.00E+03	3.70E+03	5.24E+07	1.87E+07	6.21E+06	1.91E+06	7.68E+05	3.83E+05	1.04E+05
2.50E+03	4.63E+03	8.64E+07	2.82E+07	9.53E+06	2.59E+06	9.52E+05	4.42E+05	1.05E+05
3.00E+03	5.56E+03	9.49E+07	2.82E+07	8.90E+06	2.22E+06	7.59E+05	3.35E+05	7.27E+04
4.00E+03	7.41E+03	2.17E+08	2.01E+07	3.50E+06	9.35E+05	3.40E+05	1.57E+05	3.78E+04
5.00E+03	9.26E+03	2.43E+08	1.10E+07	1.10E+06	2.22E+05	6.46E+04	2.55E+04	4.67E+03
6.00E+03	1.11E+04	1.34E+08	3.57E+06	2.36E+05	3.88E+04	9.66E+03	3.37E+03	4.94E+02
8.00E+03	1.48E+04	3.16E+07	2.81E+05	8.47E+03	1.11E+03	2.29E+02	7.00E+01	8.00E+00
1.00E+04	1.85E+04	3.02E+06	7.97E+03	1.05E+02	1.22E+01	2.33E+00	6.67E-01	6.78E-02
1.20E+04	2.22E+04	1.10E+05	3.10E+01	1.72E-02	1.42E-05	4.94E-08	8.81E-10	4.94E-13
1.40E+04	2.59E+04	8.99E+02	3.35E-03	7.55E-07	2.68E-10	4.63E-13	3.68E-15	0.
1.60E+04	2.96E+04	2.56E+02	2.27E-04	1.86E-08	2.58E-12	0.	0.	0.
1.80E+04	3.33E+04	1.32E+02	1.33E-04	1.18E-08	1.78E-12	0.	0.	0.

Table 6.26. Annual Absorbed Dose Due to Trapped Protons, Circular Orbits, Inclination 30 Degree, Infinite Backshielding Assumed

ABSORBED DOSE(RAD SI), CIRCULAR ORBIT, INC = 60 DEGREE
DUE TO GEOMAG TRAPPED PROTONS, REF. AP5, AP6, AND AP7.

ALTITUDE		SHIELD THICKNESS, GM/CM2						
(N.M.)	(KM)	6.15E-03	1.84E-02	3.69E-02	7.38E-02	1.23E-01	1.84E-01	3.69E-01
1.50E+02	2.78E+02	2.44E+03	5.88E+02	2.18E+02	8.36E+01	4.52E+01	3.08E+01	1.73E+01
3.00E+02	5.56E+02	1.86E+04	4.84E+03	1.86E+03	7.89E+02	4.39E+02	2.94E+02	1.50E+02
4.50E+02	8.33E+02	7.24E+04	1.94E+04	7.53E+03	3.29E+03	1.84E+03	1.22E+03	5.90E+02
6.00E+02	1.11E+03	2.07E+05	5.71E+04	2.24E+04	9.99E+03	5.60E+03	3.66E+03	1.73E+03
8.00E+02	1.48E+03	7.30E+05	2.06E+05	8.13E+04	3.63E+04	2.01E+04	1.30E+04	5.83E+03
1.00E+03	1.85E+03	1.91E+06	5.52E+05	2.19E+05	9.43E+04	5.02E+04	3.12E+04	1.30E+04
1.50E+03	2.78E+03	9.51E+06	2.92E+06	1.10E+06	3.97E+05	1.83E+05	1.01E+05	3.35E+04
2.00E+03	3.70E+03	2.89E+07	9.11E+06	3.24E+06	9.98E+05	4.03E+05	2.02E+05	5.49E+04
2.50E+03	4.63E+03	4.75E+07	1.50E+07	5.01E+06	1.37E+06	5.02E+05	2.34E+05	5.57E+04
3.00E+03	5.56E+03	5.05E+07	1.49E+07	4.68E+06	1.17E+06	3.99E+05	1.76E+05	3.81E+04
4.00E+03	7.41E+03	1.09E+08	1.03E+07	1.84E+06	4.95E+05	1.80E+05	8.35E+04	2.01E+04
5.00E+03	9.26E+03	1.22E+08	5.67E+06	5.77E+05	1.17E+05	3.42E+04	1.35E+04	2.49E+03
6.00E+03	1.11E+04	6.91E+07	1.89E+06	1.28E+05	2.11E+04	5.24E+03	1.83E+03	2.68E+02
8.00E+03	1.48E+04	1.67E+07	1.51E+05	4.61E+03	6.05E+02	1.29E+02	4.23E+01	9.00E+00
1.00E+04	1.85E+04	1.65E+06	4.41E+03	5.77E+01	6.68E+00	1.27E+00	3.62E-01	3.67E-02
1.20E+04	2.22E+04	6.03E+04	1.71E+01	9.57E-03	7.88E-06	2.76E-08	4.92E-10	2.77E-13
1.40E+04	2.59E+04	4.95E+02	1.91E-03	4.38E-07	1.59E-10	2.72E-13	0.	0.
1.60E+04	2.96E+04	1.35E+02	1.21E-04	9.98E-09	1.40E-12	0.	0.	0.
1.80E+04	3.33E+04	6.93E+01	1.02E-03	1.32E-06	2.37E-09	1.58E-11	4.29E-13	0.

Table 6.27. Annual Absorbed Dose Due to Trapped Protons, Circular Orbits, Inclination 60 Degree, Infinite Backshielding Assumed

ABSORBED DOSE(RAD SI), CIRCULAR ORBIT, INC = 90 DEGREE
DUE TO GEOMAG TRAPPED PROTONS, REF. AP5, AP6, AND AP7.

ALTITUDE		SHIELD THICKNESS, GM/CM2						
(N.M.)	(KM)	6.15E-03	1.84E-02	3.69E-02	7.38E-02	1.23E-01	1.84E-01	3.69E-01
1.50E+02	2.78E+02	1.58E+03	4.30E+02	1.61E+02	6.22E+01	3.39E+01	2.31E+01	1.31E+01
3.00E+02	5.56E+02	1.33E+04	3.57E+03	1.38E+03	5.99E+02	3.41E+02	2.32E+02	1.20E+02
4.50E+02	8.33E+02	5.38E+04	1.46E+04	5.74E+03	2.59E+03	1.48E+03	9.86E+02	4.81E+02
6.00E+02	1.11E+03	1.61E+05	4.54E+04	1.80E+04	8.21E+03	4.67E+03	3.08E+03	1.46E+03
8.00E+02	1.48E+03	5.89E+05	1.70E+05	6.78E+04	3.06E+04	1.70E+04	1.10E+04	4.95E+03
1.00E+03	1.85E+03	1.56E+06	4.65E+05	1.85E+05	8.01E+04	4.28E+04	2.67E+04	1.13E+04
1.50E+03	2.78E+03	7.87E+06	2.46E+06	9.31E+05	3.37E+05	1.56E+05	8.63E+04	2.86E+04
2.00E+03	3.70E+03	2.45E+07	7.83E+06	2.78E+06	8.56E+05	3.46E+05	1.73E+05	4.71E+04
2.50E+03	4.63E+03	4.01E+07	1.27E+07	4.31E+06	1.17E+06	4.31E+05	2.00E+05	4.78E+04
3.00E+03	5.56E+03	4.15E+07	1.25E+07	4.02E+06	1.00E+06	3.42E+05	1.51E+05	3.27E+04
4.00E+03	7.41E+03	9.27E+07	8.87E+06	1.58E+06	4.25E+05	1.55E+05	7.17E+04	1.73E+04
5.00E+03	9.26E+03	1.04E+08	4.90E+06	4.97E+05	1.00E+05	2.94E+04	1.16E+04	2.14E+03
6.00E+03	1.11E+04	5.94E+07	1.62E+06	1.10E+05	1.81E+04	4.50E+03	1.57E+03	2.30E+02
8.00E+03	1.48E+04	1.43E+07	1.30E+05	3.96E+03	5.18E+02	1.07E+02	3.28E+01	3.74E+00
1.00E+04	1.85E+04	1.37E+06	3.68E+03	4.89E+01	5.69E+00	1.08E+00	3.08E-01	3.11E-02
1.20E+04	2.22E+04	5.21E+04	1.48E+01	8.22E-03	6.74E-06	2.34E-08	4.17E-10	2.33E-13
1.40E+04	2.59E+04	4.31E+02	1.66E-03	3.82E-07	1.38E-10	2.37E-13	0.	0.
1.60E+04	2.96E+04	1.16E+02	1.54E-03	1.88E-06	3.21E-09	2.04E-11	5.38E-13	0.
1.80E+04	3.33E+04	5.96E+01	8.70E-04	1.12E-06	2.02E-09	1.34E-11	3.63E-13	0.

Table 6.28. Annual Absorbed Dose Due to Trapped Protons, Circular Orbits, Inclination 90 Degree, Infinite Backshielding Assumed

TABLE 6.29 PREDICTED EQUIVALENT 1 MEV ELECTRON FLUENCE FOR SOLAR FLARE PROTONS, BASED ON REFERENCE 6.9

Years	Cell Parameter	Annual Equivalent 1 MeV Electron Fluence, Various Shielding (gm/cm^2)					
		0.0168	0.0335	0.0671	0.1115	0.1675	0.3350
1975-1977	J_{sc}	2.9E13	1.7E13	8.7E12	5.3E12	3.7E12	1.9E12
	V_{oc} and P_{max}	6.7E13	3.4E13	1.6E13	8.6E12	5.5E12	2.6E12
1978-1979	J_{sc}	1.5E14	1.3E14	4.4E13	2.6E13	1.8E13	9.7E12
	V_{oc} and P_{max}	3.3E14	1.7E14	8.0E13	4.3E13	2.7E13	1.3E13
1980-1982	J_{sc}	2.9E14	1.7E14	8.7E13	5.3E13	3.7E13	1.9E13
	V_{oc} and P_{max}	6.7E14	3.4E14	1.6E14	8.6E13	5.5E13	2.6E13
1983-1984	J_{sc}	1.5E14	1.3E14	4.4E13	2.6E13	1.8E13	9.7E12
	V_{oc} and P_{max}	3.3E14	1.7E14	8.0E13	4.3E13	2.7E13	1.3E13
1985-1987	J_{sc}	2.9E13	1.7E13	8.7E12	5.3E12	3.7E12	1.9E12
	V_{oc} and P_{max}	6.7E13	3.4E13	1.6E13	8.6E12	5.5E12	2.6E12

TABLE 6.30 EQUIVALENT 1 MEV ELECTRON FLUENCE FOR SOLAR FLARE PROTONS, BASED ON TADA MODEL

Years	Cell Parameters	Annual Equivalent 1 MeV Electron Fluence, Various Shielding (gm/cm^2) 0.0168	0.0335	0.0671	0.1115	0.1675	0.3350
1966	J_{sc}	3.2E11	2.5E11	1.8E11	1.4E11	1.1E11	7.0E10
	V_{oc} and P_{max}	6.0E11	4.2E11	2.9E11	2.0E11	1.5E11	9.0E10
1967	J_{sc}	1.1E12	8.2E11	5.9E11	4.4E11	3.4E11	2.1E11
	V_{oc} and P_{max}	2.1E12	1.4E12	9.4E11	6.4E11	4.8E11	2.7E11
1968	J_{sc}	4.1E12	2.6E12	1.5E12	9.5E11	6.4E11	2.9E11
	V_{oc} and P_{max}	8.9E12	5.3E12	2.8E12	1.6E12	1.0E12	4.1E11
1969	J_{sc}	8.7E12	5.6E12	3.3E12	2.0E12	1.4E12	6.1E11
	V_{oc} and P_{max}	1.9E13	1.1E13	6.0E12	3.4E12	2.2E12	8.8E11
1970	J_{sc}	5.7E12	4.3E12	3.1E12	2.3E12	1.8E12	1.1E12
	V_{oc} and P_{max}	1.1E13	7.5E12	4.9E12	3.4E12	2.5E12	1.4E12
1971	J_{sc}	5.4E12	4.0E12	2.8E12	2.0E12	1.5E12	8.9E11
	V_{oc} and P_{max}	1.1E13	7.2E12	4.6E12	3.0E12	2.2E12	1.2E12
1972	J_{sc}	9.2E12	5.9E12	3.5E12	2.1E12	1.4E12	6.4E11
	V_{oc} and P_{max}	2.0E13	1.2E13	6.4E12	3.6E11	2.3E11	9.3E11
1976	J_{sc}	6.2E11	4.0E11	2.3E11	1.4E11	9.6E10	4.3E10
	V_{oc} and P_{max}	1.3E12	8.0E11	4.3E11	2.4E11	1.5E11	6.2E10
1977	J_{sc}	4.3E11	3.5E11	2.8E11	2.3E11	1.9E11	1.4E11
	V_{oc} and P_{max}	7.3E11	5 6E11	4.1E11	3.1E11	2.5E11	1.7E11
1978	J_{sc}	2.8E12	1.8E12	1.1E12	6.5E11	4.4E11	2.0E11
	V_{oc} and P_{max}	6.1E12	3.7E12	2.0E12	1.1E12	7.0E11	2.8E11
1979	J_{sc}	4.8E12	2.9E12	1.6E12	9.7E11	6.2E11	2.6E11
	V_{oc} and P_{max}	1.1E13	6.1E12	3.1E12	1.7E12	1.0E12	3.8E11
1980	J_{sc}	4.9E12	3.4E12	2.2E12	1.5E12	1.1E12	5.7E11
	V_{oc} and P_{max}	9.9E12	6.4E12	3.8E12	2.4E12	1.6E12	7.8E11
1981	J_{sc}	3.1E12	2.4E12	1.7E12	1.3E12	1.0E12	6.4E11
	V_{oc} and P_{max}	5.8E12	4.1E12	2.7E12	1.9E12	1.4E12	8.2E11
1982	J_{sc}	2.6E12	1.8E12	1.2E12	8.0E11	5.8E11	3.1E11
	V_{oc} and P_{max}	5.3E12	3.4E12	2.0E12	1.3E12	8.7E11	4.2E11

Table 6.31. Summary of Tabulated Data in Tables 6.9 Through 6.30

Environment	Reference	Orbital Parameters	I_{sc}, Equivalent Fluence for Various Shielding Thicknesses	V_{oc}, P_{max}; Equivalent Fluence for Various Shielding Thicknesses	Absorbed Dose at Various Depths
Trapped Electrons	AE4, AE5[6.5] AE3[6.4]	Circular Orbits, Various Altitudes;			
		Inclination 0°	Table 6.9	Table 6.9 data applies	Table 6.21
		Inclination 30°	Table 6.10	Table 6.10 data applies	Table 6.22
		Inclination 60°	Table 6.11	Table 6.11 data applies	Table 6.23
		Inclination 90°	Table 6.12	Table 6.12 data applies	Table 6.24
Trapped Protons	AP5[6.1] AP6[6.2] AP7[6.3]	Circular Orbits, Various Altitudes;			
		Inclination 0°	Table 6.13	Table 6.17	Table 6.25
		Inclination 30°	Table 6.14	Table 6.18	Table 6.26
		Inclination 60°	Table 6.15	Table 6.19	Table 6.27
		Inclination 90°	Table 6.16	Table 6.28	Table 6.28
Solar Flare Protons	NASA TM X53865[6.9]	Free Space, 1 AU	Table 6.29	Table 6.29	
	Tada Model (Chapter 5)	Free Space, 1 AU	Table 6.30	Table 6.30	

The previously calculated equivalent fluence data for synchronous orbit will be used in the following example to illustrate the degradation of a solar array:

Solar Cell	10 ohm-cm resistivity 0.0305 cm (0.012 in.) thick
Cover Glass	0.015 cm (0.006 in.) thick 0.0335 gm/cm^2 fused silica, antireflecting coating, blue filter
Backshielding	Infinite
Equivalent 1 MeV Electron Fluence	
Trapped Electrons	2.55E13
Trapped Protons	0
Total	2.55E13 e/cm^2-yr

Solar Cell Output

		Absolute	Relative
At 0 Months	Equivalent Fluence, 0		
I_{sc}		36.7 mA/cm^2	1.00
V_{oc}		0.552 V	1.00
P_{max}		14.8 mW/cm^2	1.00
V_{mp}		0.433 V	1.00
At 4 Months	Equivalent Fluence, 8.50E12 e/cm^2		
I_{sc}		36.2 mA/cm^2	0.986
V_{oc}		0.548 V	0.992
P_{max}		14.7 mW/cm^2	0.994
V_{mp}		0.432 V	0.998
At 1 Year	Equivalent Fluence, 2.55E13 e/cm^2		
I_{sc}		35.7 mA/cm^2	0.975
V_{oc}		0.543 V	0.984
P_{max}		14.2 mW/cm^2	0.960
V_{mp}		0.430 V	0.994

	Absolute	Relative
At 3 Years	Equivalent Fluence, 7.65E13 e/cm^2	
I_{sc}	34.9 mA/cm^2	0.950
V_{oc}	0.535 V	0.970
P_{max}	13.4 mW/cm^2	0.905
V_{mp}	0.426 V	0.985

The effects of cover glass transmission loss due to radiation darkening have been omitted from this estimate. The average absorbed dose due to trapped electronics in this orbit is approximately 10^7 rad per year. The data in Figure 3.23 indicate that such a dose would cause a transmission loss of about 0.5% reflected in solar cell I_{sc} or P_{max}. The effects of solar flares on solar cell degradation have been omitted in this example. Adhesive darkening due to ultraviolet illumination has been omitted from this calculation. An additional factor which also must be included is the reflection loss due to glassing of solar cells with silicon monoxide anti-reflection coatings. With conventional state of the art cover glasses and solar cells, glassing may cause a 4 to 6% initial decrease in short circuit current. As discussed in Chapter 1, cells with improved anti-reflection coatings exhibit significantly reduced glassing or reflection loss.

REFERENCES

6.1 J. H. King, "Models of Trapped Radiation Environment, Vol. IV, Low Energy Protons," NASA SP-3024, 1967.

6.2 J. P. Lavine and J. I. Vette, "Models of the Trapped Radiation Environment, Vol. V, Inner Belt Protons," NASA SP-3024, 1970.

6.3 J. P. Lavine and J. I. Vette, "Model of the Trapped Radiation Environment, Vol. VI, High Energy Protons," NASA SP-3024, 1970.

6.4 J. I. Vette and A. B. Lucero, "Models of Trapped Radiation Environment, Vol. III, Electrons at Synchronous Altitudes," NASA SP-3024.

6.5 G. W. Singley and J. I. Vette, "The AE-4 Model of the Outer Radiation Zone Electron Environment," NASA, NSSDC 72-06, 1972.

6.6 M. J. Teague and J. I. Vette, "The Inner Zone Electron Model AE-5," NASA NSSDC 72-10, 1972.

6.7 G. W. Singley and J. I. Vette, "A Model Environment for Outer Zone Electrons," NASA, NSSDC 72-13, 1972.

6.8 J. I. Vette, "Models of the Trapped Radiation Environment, Vol. I, Inner Zone Protons and Electrons," NASA SP-3024, 1966.

6.9 D. K. Weidner, "Natural Space Environment Criteria for 1975-1985," NASA Space Stations, NASA TM X53865, August 1969, Second Edition, 10 August 1970.

CHAPTER 7

7.0 FLIGHT DATA

Considering the number of satellites in orbit, there is a very limited amount of array performance data available. A very large percentage of satellites are placed in low altitude earth orbits (less than 400 km) which experience very little degradation from trapped radiation. Of the satellites in orbits above 400 km, very few are instrumented to sense and telemeter electrical quantities which directly reflect basic solar-cell performance parameters. Flight data from prior to 1963 often involve p-n solar cells or n-p solar cells with much lower efficiency and poorer radiation hardness than that of currently available commercial cells. There are two sources of more recent solar cell performance flight data. These include a few solar cell flight experiments specifically designed to evaluate solar cell degradation. Such experiments have been flown on the ATS-1,[7.1] LES-6[7.2] and ATS-5[7.3] satellites. An alternative approach to the evaluation of solar cells in a space radiation environment is a general analysis of an entire satellite solar array. An example of this type of analysis was reported for IDSCS satellites.[7.4] Most of the available flight data are from satellites in synchronous orbit, however, a limited amount of data are available for lower earth orbits.

The data in Table 7.1, relating to solar array performance in a synchronous orbit, were collected by L. A. Gibson of the Aerospace Corporation.[7.5] All the solar cells used in these satellites have 10 ohm-cm base resistivity and cover glass shielding varying from 0.015 cm (0.006 in) microsheet to 0.076 cm (0.030 in) fused silica. No information was reported regarding cell thickness or backshielding. The reported degradation in power in most cases is between 2 to 6 percent after one year. The power loss estimated in Section 6.6 on the basis of trapped electrons alone was 4 percent per year for cells with 0.015 cm microsheet shielding. Considering that solar flare proton contributions to equivalent fluence and cover material darkening were omitted in this

TABLE 7.1 SYNCHRONOUS ORBIT SOLAR CELL ARRAY DEGRADATION

	TACSAT I	DSP	IDSCS	NATO A/NATO B	INTELSAT 3	INTELSAT 4	ATS-5
Contractor	HAC	TRW	Philco-Ford	Philco-Ford	TRW	HAC	HAC
Launch	9 Feb 69	6 Nov 70	16 Jun 66 18 Jan 67	A: 21 Nov 69 B: 20 Mar 70	3B: 18 Dec 68 3C: 5 Feb 69 3D: 21 May 69	∿Feb 71	12 Aug 69
Configuration	Drum	Drum & Paddles	24-sided Polygon	Drum	Drum	Drum	Drum
Design Life, yrs.	3	3	5	5	3	7	
Coverslide Thickness, mils	12	6	20	6	12	12	30
Coverslide Material	Fused Silica	Micro-sheet	Fused Silica	Fused Silica	Fused Silica	Fused Silica	Fused Silica
Solar Cell Resistivity, ohm-cm	10	10	10	10	10	10	10
Solar Cell Array:							
Time, years	3	1	5	2 1	1	0.7	1.7
Power Degradation, %	∿6	∿5	∿17-22	∿4 ∿2	∿6	∿3	∿4

calculation, there is reasonably good agreement between satellite performance and the predictions. The omission of solar flare equivalent fluence contributions appears justified, as flare activity was relatively low during the time period of the subject flight data.[7.5] The poor performance of IDSCS satellite solar arrays resulted from excessive ultraviolet degradation transmission loss in the cover glass adhesive due to the use of an improper primer.

Although degradations due to solar flares are often estimated and projected over long satellite missions, the flare events are discrete and their effects occur as rather abrupt degradations. An excellent example of this behavior is shown in Figure 7.1 for two satellites in synchronous orbits during the flare events of August 1972. The analysis was provided by H. Riess of TRW.[7.6] The solid line in Figure 7.1 is based on solar cell degradation predictions based on trapped electrons at synchronous altitude. The data indicate that the flares produced an abrupt 2% loss in maximum array current (i.e., short circuit current) in both satellites. It also can be observed that 5 months after the flare, the flight 3 array current had recovered to within nearly 1 percent of the value predicted without solar flares. This indicates that considerable annealing of flare radiation damage occurs after termination of the event. The behavior of a group of test cells on the ATS-5 satellite, during the August 1972 flare events, is shown in Figure 7.2. These cells degraded 0.2 percent in V_{oc}, 2.3 percent in I_{sc}, and 3.5 percent in P_{max} during the above period.[7.7]

A limited amount of flight data are also available from satellite solar arrays operated in circular orbits at lower altitudes. Data from several such satellites are tabulated in Table 7.2[7.8-7.10] In these orbits the equivalent fluence contribution is mainly from trapped protons. Two of the orbits, ERS 6 and Explorer 38, pass through regions in which the trapped proton flux is extremely large. The equivalent 1 MeV electron fluences are shown for each orbit. These were determined from Tables 6.16 and 6.19 with the assumption that: only trapped proton radiation contributed to the equivalent fluence, that infinite backshielding existed, and cover material darkening losses were negligible.

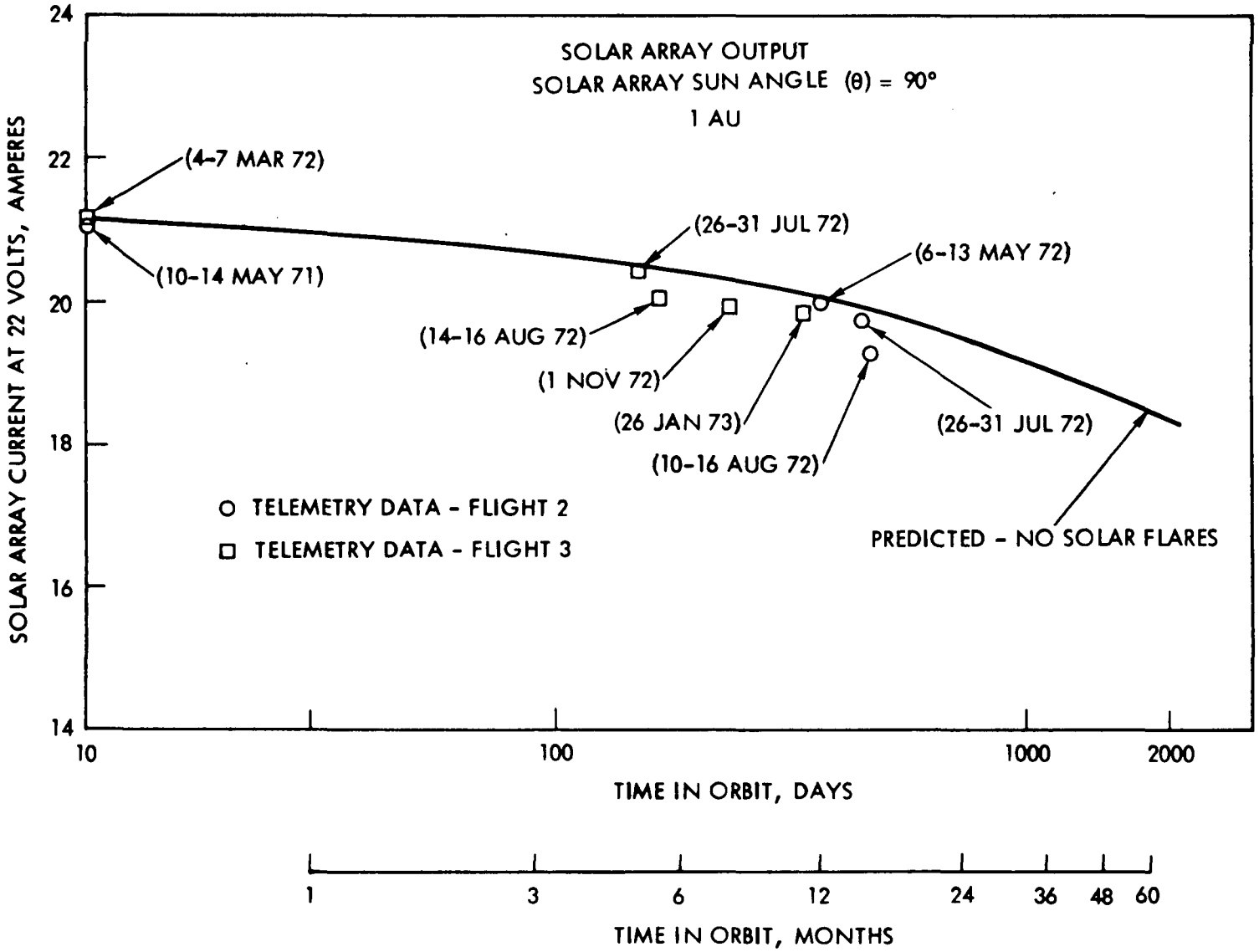

Figure 7.1 Performance of Two Satellite Solar Arrays in Synchronous Orbit During the August 1972 Solar Flares

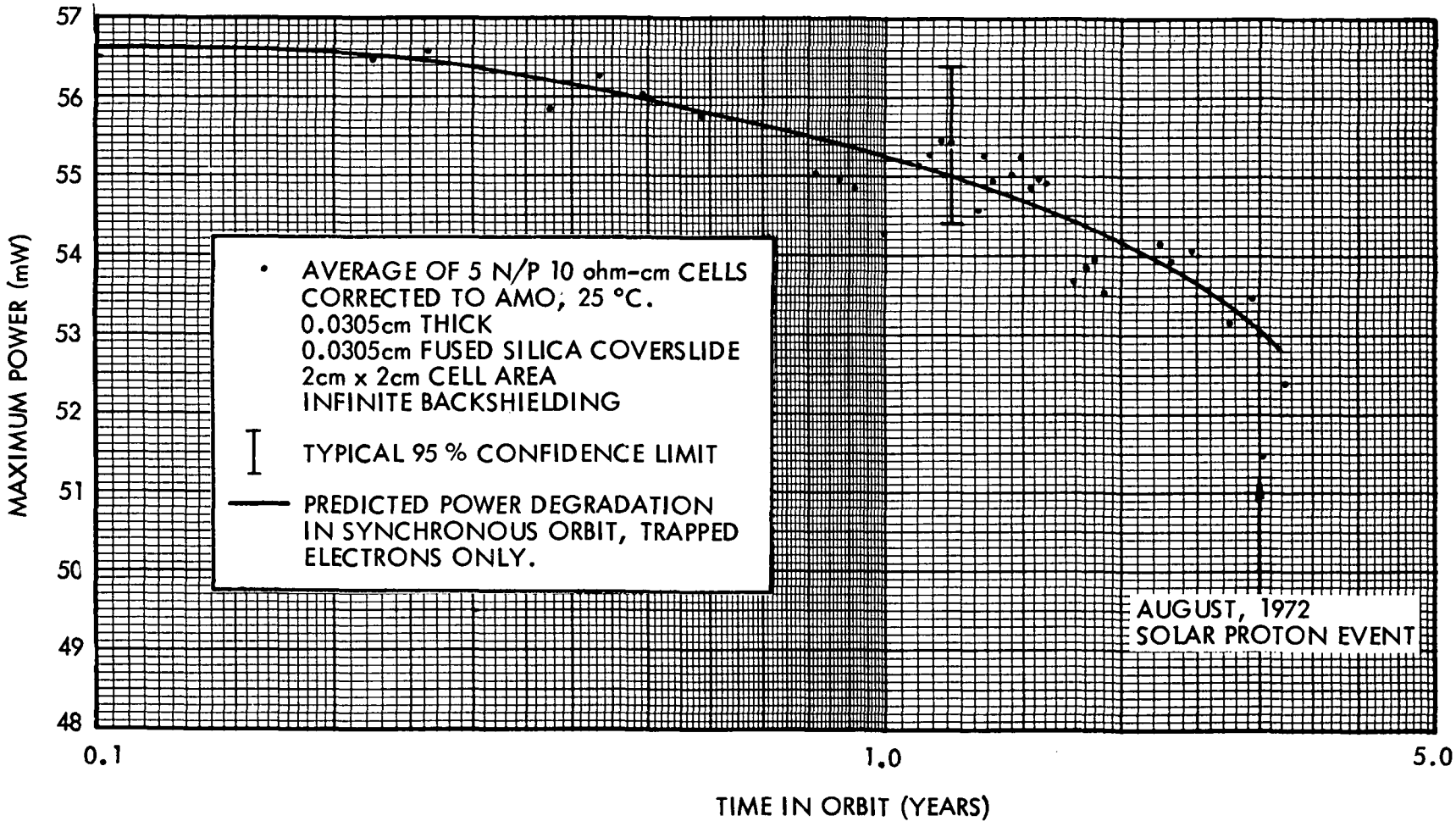

Figure 7.2 Degradation of Solar Cell Maximum Power Versus Time in Synchronous Orbit, ATS-5 Experimental Cells [7.7]

TABLE 7.2 SOLAR CELL ARRAY DEGRADATION, VARIOUS CIRCULAR ORBITS

Satellite Launch Date	Orbit Altitude, Inclination	Cells & Shielding Data	Equivalent 1MeV Electron Fluence (Assuming trapped radiation only & infinite back shielding)	Predicted (from equivalent fluence)	Observed
OGO4 28 July 1967	930 km (500 nmi) 86°	N/P 10 ohm-cm 0.015 cm microsheet	5.6×10^{13} e/cm^2-yr	$\frac{I_{sc}}{I_{sco}}$ = 0.96 @ 1 yr	0.96 @ 1 yr
1963-38C [7.8] 28 Sept 1963	1110 km (600 nmi) 90°	N/P 10 ohm-cm 0.015 cm microsheet	1.7×10^{14} e/cm^2-yr	$\frac{I_{sc}}{I_{sco}}$ = 0.95 @ 6 mo.	0.95 @ 6 mo.
ERS 6 [7.9] 1963-14C 9 May 1963	4170 km (2250 nmi) 90°	N/P 1 ohm-cm 0.051 cm fused silica	4.0×10^{15} e/cm^2-yr	$\frac{I_{sc}}{I_{sco}}$ = 0.74 @ 6 mo.	0.70 @ 6 mo.
Explorer 38 [7.10] (RAE 1) 4 July 1968	6700 km (3600 nmi) 60°	N/P 10 ohm-cm 0.0473 cm solar cells 0.102 cm fused silica	1.2×10^{15} e/cm^2-yr	$\frac{P_{max}}{P_{maxo}}$ = 0.75 @ 1 yr = 0.70 @ 2 yr = 0.62 @ 4.5 yr	0.72 @ 1 yr 0.65 @ 2 yr 0.55 @ 4.5 yr

The equivalent fluence values were used to estimate solar cell parameter changes from data in Figures 3.7 through 3.14. The predicted changes are shown in Table 7.2 along with observed parameter changes from flight data. The predicted degradations are in reasonable agreement with observed values.

The results of experiments on ERS 6 included several observations which have important consequences in array degradation predictions.[7.10] The cells of this satellite were observed to degrade in short circuit current at a rate of 5.5 ± 0.2 mA/cm^2-decade. This value compares well with those reported in Section 3.3 for laboratory proton irradiations in the 10 MeV energy range. Since the above rates are higher than those normally found for 1 MeV electron irradiations, it would be more accurate to use experimental proton degradation data for proton dominated orbits if such data were available. It was also observed that cells with adhesively-attached cover glass shields degraded at the same rate as those with mechanically-attached (no adhesive) shielding. It was concluded that adhesive darkening effects were less than the experimental error or negligible. The data also indicated that transmission loss in cover glass is not an important factor in array degradation.

In general, many factors can make array performance degrade to outputs lower than predicted. One of the most common causes is the effect of low energy protons on small unshielded areas of the solar cell. Another problem which has caused serious difficulties is the failure of cell interconnections, particularly in the case of solderless solar cells.

Gibson concluded that an initial 2 percent transmission loss, due to ultraviolet darkening of cover glass adhesive when added to the solar cell degradations, would account for the power degradation observed on most satellites reported in Table 7.1.[7.5] In the LES-6 experiments, Sarles and Stanley concluded that an initial 4 to 10 percent loss was caused by cover slide material darkening.[7.2]

REFERENCES

7.1 R. C. Waddel, "Solar Cell Radiation Damage on Synchronous Satellite ATS-1," Conf. Record of the Seventh Photovoltaic Specialists Conf., IEEE, p. 195, 1968.

7.2 F. W. Sarles, Jr. and A. G. Stanley, "Further Observed Degradation on the LES-6 Synchronous Solar Cell Experiment," Conf. Record of the Ninth IEEE Photovoltaic Specialists Conf., p. 331, 1972.

7.3 B. E. Anspaugh, "ATS-5 Solar Cell Experiment After 699 Days in Synchronous Orbit," op. cit., p. 308, 1972.

7.4 W. T. Picciano, R. A. Reitman and R. J. Grant, "Solar Cell and Coverslide Degradations at Near-Synchronous Altitude," Conf. Record of the Eighth IEEE Photovoltaic Specialists Conf., p.221, 1970.

7.5 L. A. Gibson, "Solar Cell Array Degradation at Synchronous Orbit," Aerospace Corp., 8 Aug. 1972.

7.6 H. Riess, private communication.

7.7 B. E. Anspaugh, private communication.

7.8 R. E. Fischell, "Solar Cell Power Systems for APL Satellites," Conf. Record of the Sixth Photovoltaic Specialists Conf., IEEE, Vol. II, p. 32, 1967.

7.9 J. M. Denney, "Final Flight Report, Tetrahedral Research Satellites," Vol. II, TRW Systems Report No. 8655-6006-RU-00, 15 Feb. 1964.

7.10 H. Burke, private communication.

Areal Density	Fused Silica 2.2 g/cm^3		Microsheet 2.5 g/cm^3		Aluminum 2.7 g/cm^3	
g/cm^2	cm	in	cm	in	cm	in
0.0168	.00764	.003	0.00672	0.00265	.00622	0.00245
0.0335	.0152	.006	0.0134	0.00528	.0124	0.00488
0.0671	.0305	.012	0.0268	0.0106	.0248	0.00976
0.112	.0509	.020	0.0448	0.0176	.0415	0.0163
0.168	.0764	.030	0.0672	0.0264	.0622	0.0245
0.335	.1520	.060	0.1340	0.0528	.124	0.0488

Table A Shielding Thickness Conversions

TABLE B CONSTANTS, PROPERTIES, AND VALUES

SILICON

Atomic Weight	28.09
Density	2.33 (g/cm^3)
Crystal Structure	Diamond, 8 atoms/unit cell
Lattice Constant	5.43×10^{-10} m, 5.43 (Å)
Atomic Radius	1.18×10^{-10} m, 1.18 (Å)
Atomic Density	5.00×10^{22} (cm^{-3})
Energy Gap @ 300K	1.78×10^{-19} (J), 1.11 (eV)
Energy Gap @ 0 K	1.91×10^{-19} (J), 1.21 (eV)
Electron Mobility (intrinsic) @ 300K, μ_n	1350 ($cm^2/V\ s$)
Hole Mobility (intrinsic) @ 300K, μ_p	480 ($cm^2/V\ s$)
Electron Diffusion Constant (intrinsic) @ 300K, D_n	35 (cm^2/s)
Hole Diffusion Constant (intrinsic) @ 300K, D_p	12 (cm^2/s)
n_i @ 300K	1.5×10^{10} (cm^{-3})
Dielectric Constant	11.7
Specific Heat, C_p @ 300K	0.7 (J/g K)
Thermal Conductivity @ 300K	1.5 (W/cm K)
Coefficient of Thermal Expansion, $\frac{\Delta L}{L \Delta T}$	2.5×10^{-6} (K^{-1})
Debye Temperature	658 (K)
Activation Energy, Self Diffusion	7.7×10^{-19} (J), 4.8 (eV)
Energy of Ionization	5.76×10^{-19} (J), 3.6 (eV)
Energy of Sublimation	7.80×10^{-19} (J), 4.9 (eV)
Elastic Moduli	
C_{11}	1.674×10^{11} (N/m^2)
C_{12}	0.652×10^{11} (N/m^2)
C_{44}	0.796×10^{11} (N/m^2)
Index of Refraction	3.5-4.0
Mohs' Hardness	7

TABLE B-continued

SILICON-continued

Solar Absorptance	0.8
Hemispherical Emittance	0.3

QUARTZ GLASS (FUSED SILICA)

Molecular Weight	60.8
Density	2.2 (g/cm^3)
Energy Gap	12.8×10^{-19} (J), ~ 8 (eV)
Dielectric Constant	3.5-3.9
Index of Refraction	1.46-1.51
Specific Heat, C_p	1 (J/g K)
Thermal Conductivity	0.014 (W/cm K)
Coefficient of Thermal Expansion, $\frac{\Delta L}{L \Delta T}$	0.55×10^{-6} (K^{-1})
Mohs' Hardness	4.9
Young's Modulus	7.16×10^{10} (N/m^2)
Rigidity Modulus	3.10×10^{10} (N/m^2)
Poisson's Ratio	0.16
Solar Absorptance	0.01
Hemispherical Emittance	0.78
Solar Absorptance (on array)	0.75-0.85
Hemispherical Emittance (on array)	0.78-0.80

SILICONE ELASTOMERS (TYPICAL)

Density	1.1 (g/cm^3)
Index of Refraction	1.41
Coefficient of Thermal Expansion, $\frac{\Delta L}{L \Delta T}$	300×10^{-6} (K^{-1})
Thermal Conductivity @ 300K	.0017 (W/cm K)
Specific Heat @ 300K	1.0 (J/g K)
Bond Thickness Between Cover Glass and Solar Cell	75-150 (μm)

TABLE B-continued

CONSTANTS

Boltzmann's Constant, k	1.38×10^{-23} (J/K), 8.62×10^{-5} (eV/K)
Planck's Constant, h	6.63×10^{-34} (J s)
Speed of Light, c	2.998×10^{8} (m/s)
Electron Charge, e	1.602×10^{-19} (C)
Permittivity of Free Space, ε_o	8.86×10^{-12} (F/m)
Permiability of Free Space, μ_o	12.6×10^{-7} (H/m)
Electron Rest Mass, m_e	9.11×10^{-31} (kg)
Proton Rest Mass, m_p	1.67×10^{-27} (kg)
Avagadro's Number	6.022×10^{23} (g-mole^{-1})

SILICON SOLAR CELL DATA

Active Area of 2 cm by 2 cm Solar Cell	3.8 (cm^{-2})
Series Resistance, R_s	0.2-0.5 (ohm)
Shunt Resistance, R_{sh}	> 1000 (ohm)